ProQuest LLC.
789 East Eisenhower Parkway
P.O. Box 1346
Ann Arbor, MI 48106 – 1346

To my wife, Jean, for her help and patience.

To my children, Neil and Andrew, for keeping no distraught.

THE COLD ROLLING AND PRIMARY RECRYSTALLISATION TEXTURES OF AUSTENITIC STAINLESS STEELS

by

Malcolm John Dickson

M.Sc.,B.Sc.(Hons), A.C.T.(Birm)Hons., A.I.M.,M.Inst.P.

A thesis submitted for the Degree of
Doctor of Philosophy (C.N.A.A.), June 1971.

FOREWORD

The research described was carried out during the period September 1968 to June 1971 in the Department of Metallurgy, Sheffield Polytechnic, where the author has been a Lecturer in Physical Metallurgy since September 1967. Part of the work was done at B.I.S.R.A. Laboratories.

The author has been working on preferred orientation in polycrystalline materials since 1965 and has previously been awarded the degree of M.Sc. for a thesis submitted to the University of Aston in Birmingham. The present volume is an extension of previous studies.

During the period of research the following post-graduate lecture courses were attended

"The crystallography of martensite transformations" by R.M.Wood.

"Electron metallography and electron diffraction" by P.L.James and A.Wirth.

"Applications of X-ray diffraction" by M.J.Dickson and R.P.Stratton.

The results and theories presented in this thesis are original, except where due reference is made to previous work.

M.J.Dickson,

June, 1971.

CONTENTS.

SUMMARY.

A critical review has been made of available literature on the cold rolling and primary recrystallisation textures of f.c.c. and b.c.c. metals and alloys, with later reference to recent work on stainless steels.

Using laboratory and commercial alloys a study has been made of factors influencing the cold rolling and primary recrystallisation textures of stainless steels. Preferred orientations have been assessed by X-ray determination of pole figures. The work is supplemented by other techniques - quantitative phase analysis of austenite and martensite, determination of diffraction line profiles, hardness measurements, optical and electron metallography, qualitative identification of carbide phases.

The high purity alloys (18%Cr 10%Ni, 18%Cr 12%Ni, 18%Cr 14%Ni, 18%Cr 12%Ni 7%Co and 18%Cr 25%Ni) were examined with particular reference to the rôle of the martensite transformation in developing primary recrystallisation textures. The first four alloys are metastable, the amountof martensite formed after 90-95% cold rolling increasing from ~5% for 18%Cr 14%Ni or 18%Cr 12%Ni 7%Co steels to ~86% for 18%Cr 10%Ni steel, and textures of both α' martensite and the remaining austenite are the same for each steel. Principal components of the martensite texture are $\{112\}\langle\bar{1}10\rangle$ and $\{111\}\langle\bar{1}\bar{1}2\rangle$, with a minor component $\{001\}\langle\bar{1}10\rangle$. The austenite exhibits a normal f.c.c. alloy type texture, $\{110\}\langle\bar{1}12\rangle$ + a minor $\{110\}\langle001\rangle$ component. The 18%Cr 10%Ni steel recrystallises to mainly $\{230\}\langle3,\bar{2},14\rangle$ and $\{6,10,1\}\langle5\bar{3}1\rangle$ orientations with considerable spread remaining in the region of $\{6,8,17\}\langle\bar{5}\bar{7}5\rangle$ (which is close to $\{225\}\langle\bar{5}\bar{3}3\rangle$). The other steels recrystallise to a $\{225\}\langle\bar{5}\bar{3}3\rangle$ texture.

In the metastable alloys, factors influencing development of the annealing textures are the relative amounts of α' and γ formed by cold rolling, recovery in both phases, $\alpha' \rightarrow \gamma$ shear

transformation, variant selectivity during the transformation and, finally, competitive growth of favourably oriented nuclei.

It is shown that recovery occurs in both phases, its effect being to sharpen textures about the principal components. During the $\alpha' \rightarrow \gamma$ transformation, further texture sharpening can occur through preferential selection of variants of the Kurdjumov-Sachs orientation relationship. The texture of 18%Cr 10%Ni steel after annealing for $\frac{1}{2}$ hour at 500 °C or 600 °C conforms to that predicted by transformation from principal α' rolling texture components. All groups of orientations originating from $\{112\}\langle\bar{1}10\rangle_{\alpha'}$ and $\{111\}\langle\bar{1}\bar{1}2\rangle_{\alpha'}$ are present in the transformed texture, but one group of orientations from $\{001\}\langle\bar{1}10\rangle_{\alpha'}$ is missing. This can only be accounted for by assuming that the eight variants compricing this component do not operate.

Subsequent development of the recrystallisation textures depends largely on the amounts of α' and γ formed during rolling. This is attributed to differences in density of nuclei formed within the range of γ cold rolling texture orientations and within the range of orientations derived from the martensite. Geometrical relationships between the nuclei and various ranges of matrix components are compared in terms of θ, the angle of misfit between <111> poles of nucleus and matrix, and ϕ, the rotation about this almost common <111> pole. Although the observed recrystallisation textures are generally considered to result from oriented growth, it is also shown that the transformation can provide suitable nuclei spontaneously, so that nucleation cannot be considered entirely random.

Unstabilised commercial steels (RF310, FST(L) and FSL(L)) recrystallise in a similar manner to laboratory alloys of equivalent metastability. Precipitation of carbides occurs during annealing but the particles are almost completely re-dissolved at 900 °C. Variations in carbide distribution prior to cold rolling, arising either from different compositions or

from different rates of cooling from the solution treatment temperature, have no significant effect on subsequent cold rolling and annealing textures.

In contrast, carbide-stabilised commercial steels (FCB, SF347,FDP,FMB and FMBTi) form their recrystallisation textures largely by retention of the γ cold rolling texture and/or retention of the γ texture immediately after transformation from the martensite. Much of the precipitation which occurs during annealing remains until the end of recrystallisation. Retention of the textures is attributed to restriction of grain boundary mobility by precipitate particles so that grains with high angle boundaries do not grow in preference to others, at least not to the same extent as they would in the absence of such precipitation.

Initial solution treatment of stabilised steels is important, as it controls the stability of the matrix prior to cold rolling. In the metastable range, observed effects of solution treatment on annealing textures are indirect, being related to the relative amounts of austenite and martensite after rolling.

PART I

A REVIEW OF LITERATURE

1. Introduction.

During plastic deformation of polycrystalline aggregates individual grains rotate, so that certain crystallographic directions become aligned with the principal directions of strain in the metal. The rotation takes place gradually as deformation proceeds, and the final orientation is approached when certain planes and directions become symmetrically aligned with respect to thedirection of working. The preferred orientation or texture produced depends on

a) variables in the material, such as crystal structure, metal, solute content, second phases present, initial grain size and initial texture.

b) process variables such as the stress system, amount of defomation, temperature of deformation and strain rate.

Preferred orientation may be retained during annealing and the final texture will be characteristic of the deformation texture, temperature and time of annealing, rates of heating and cooling, and annealing atmosphere.

Retention of a texture in polycrystalline aggregates imparts various degrees of anisotropy to the physical and mechanical properties. Although this anisotropy is similar to that found in single crystals, there is no simple correlation with properties because of the interactions between the grains in polycrystals.

There are two common ways of defining textures in metal sheets, pole figures or ideal orientations. A complete description of a texture is provided by a normal pole figure, in which the three-dimensional distribution of orientations is represented on a two-dimensional figure. This figure is similar to a stereographic projection of a single crystal, but differs in that the specimen is now a polycrystalline aggregate, so that only one set of crystallographic planes are projected but from many crystals. A preferred orientation thus gives rise to regions of high pole density on the projection with a scatter about these principal

orientations. It is usual in the construction of the pole figures to use the rolling plane as the basic circle and to plot the rolling direction at the top and bottom of the figure. An equivalent description is provided by the use of two inverse pole figures. Unlike the normal pole figure, these express the distribution of all crystallographic planes or directions with respect to some reference plane or direction in the sheet. Two figures are necessary to define completely the preferred orientation. An alternative, but less complete, description of a texture is to specify one or more discrete orientations $\{hkl\}\langle uvw\rangle$, where the $\{hkl\}$ planes are parallel to the rolling plane and the $\langle uvw\rangle$ directions parallel to the rolling direction. The two types of description are related in that a pole figure could theoretically be described in terms of an infinite number of such ideal orientations. For quantitative analysis a numerical description of the texture is often required, and for this a small number of ideal orientations is usually sufficient, although care must be taken in the interpretation. Apart from this, single orientations are most useful as labels for different types of textures. More often than not, the two descriptions are used in conjunction with each other, and pole figures are usually labelled with a number of ideal orientations.

A comprehensive review of texture development in metals and alloys generally was made by Dillamore and Roberts[1] in 1965. These authors considered virtually all data available to that date and gave a critical appraisal of, inter alia, theories of texture formation. However, since then, further results and ideas have emerged and some aspects of their review must now be considered out of date, although the work remains valuable as a standard reference and summary. Also, at that time, little work had been done on stainless steels, the subject of this thesis. The present review is consequently directed towards an up-to-date summary of texture theories for f.c.c. and b.c.c. materials, and previous work on stainless steels, being most relevant, is presented as a

seperate section. Textures developed on annealing are considered only in relation to those formed during primary recrystallisation.

2. F.C.C. Metals and Alloys.

2.1. Rolling Textures.

Room temperature rolling textures observed in f.c.c. metals and alloys after 90% reduction are of two general types. All the common pure metals, with the exception of silver, exhibit a texture which can be described as $\{135\}\langle 1\bar{2}1\rangle$, an orientation which represents the central region of a spread between $\{110\}\langle\bar{1}12\rangle$ and $\{112\}\langle\bar{1}\bar{1}1\rangle$. Silver and f.c.c. alloys containing certain amounts of solute show a texture described as $\{110\}\langle\bar{1}12\rangle$, with a minor $\{110\}\langle 001\rangle$ component. As the amount of solute is increased the $\{135\}\langle 1\bar{2}1\rangle$ texture changes gradually to $\{110\}\langle\bar{1}12\rangle$, but the extent of the transition is dependent on the nature of the solute present[2-7].

The texture characteristic of a particular metal or alloy may also be modified by raising or lowering the temperature of rolling, for example the $\{110\}\langle\bar{1}12\rangle$ texture changes to $\{123\}\langle 1\bar{2}1\rangle$ as the rolling temperature is raised[8-12]; conversely, rolling below room temperature favours a transition from $\{135\}\langle 1\bar{2}1\rangle$ to $\{110\}\langle\bar{1}12\rangle$[13,14]. In either case the temperature range over which transition occurs is characteristic of the particular metal or alloy.

The effects of alloying and change in temperature are qualitatively additive, in that transition to $\{110\}\langle\bar{1}12\rangle$ by alloying may be counteracted by a rise in rolling temperature[4].

A fundamental factor governing transition in texture is the decrease of stacking fault energy associated with alloying. Smallman and Green[15] studied the relationship in copper-aluminium and copper-germanium alloys, and Haessner[16] observed a similar correlation in cobalt-nickel alloys. Smallman and Green[15] concluded that the $\{110\}\langle\bar{1}12\rangle$ texture is characteristic of any pure metal or alloy having a stacking fault energy of about 35 ergs $cm.^{-2}$ or less, rolled at a temperature below about 0·25Tm (Tm= absolute melting point). As the atomic misfit and valency

difference between solute and solvent increases the critical value of stacking fault energy is reached at a progressively smaller addition of solute. These authors further established that the $\{110\}\langle\bar{1}12\rangle$ texture can be characteristic of a metal of stacking fault energy higher than 35 ergs cm.$^{-2}$ provided that it is rolled at a temperature below about 0·2Tm. In materials of very low stacking fault energy the texture tends to be stable at temperatures up to 0·5Tm.

2.2 Theories of Rolling Textures.

Most of the theories have adopted a single crystal approach to explain development of polycrystalline rolling textures. These assume that each individual grain in the polycrystal deforms as if it were an unconstrained single crystal, and the sequence of rotations of a few chosen orientations is assumed to represent the material as a whole. Slip, for instance, is envisaged to take place on one or two systems only. This oversimplified picture is far from reality, since a fundamental feature of polycrystalline deformation is that, in order to maintain grain boundary continuity, each grain is deformed into a shape that is dictated by the deformation of its neighbours. To achieve this unrestricted change of shape of a grain requires slip to take place on at least five slip systems. Theories which adopt the latter approach generally assume that the strain is homogeneously distributed so that the strain undergone by one individual grain is the same as that experienced by the material as a whole. A difficulty arises in this approach, however, because the magnitude and sense of crystal rotation is dependent on the choice of slip systems and such theories are not generally capable of making firm, unambiguous predictions about development of textures. Later theories adopting the single crystal model have overcome the problem by postulating that multiple slip is confined either to specific grains or to specific regions of grains i.e. the grain boundaries. An obvious advantage of these theories is that definite predictions can be made about the textures.

Calnan and Clews[17] had criticised earlier theories on the grounds that they did not explain the way in which the most favourable slip system or systems withstood resolved shear stresses which were greater than the critical resolved shear stress, until those on less favourable systems reached the critical value and multiple slip occured. Their approach was therefore based on the absence of cracks at grain boundaries which, in general, requires operation of at least five slip systems, and to account for this they introduced the concept of an effective stress. As the applied stress rises until it reaches the value at which slip would occur in a single crystal, the direction of effective tensile/compressive stress is envisaged to move in a direction so that when resolved on the most favourable system it is always below the critical value. This movement thus takes the effective stress axis to one of three positions, $\langle 110 \rangle$, $\langle 111 \rangle$ or $\langle 100 \rangle$, where there are, respectively, four, six, or eight systems available for multiple slip. However, for these orientations, symmetry of slip systems would not allow rotation of the grain relative to the applied stress axis. They then assumed that development of preferred orientation might be confined to surface grains, which are relatively unconstrained, and other grains for which large constraints would be necessary to prevent single or duplex slip. Thus the development of texture was accounted for by applying a single crystal treatment, and for rolling textures they assumed the end orientations to be those which mutually satisfy the simultaneous requirements of tension and compression axes. For f.c.c. crystals, Calnan and Clews predicted a spread from $\{110\}\langle \bar{1}12 \rangle$ to $\{311\}\langle \bar{1}12 \rangle$ together with the orientations $\{110\}\langle 111 \rangle$ and $\{110\}\langle 001 \rangle$. Since their analysis was based solely on primary and conjugate slip rotations, it could not account for differences within the range of f.c.c. rolling textures. However, the concept which they introduced and their method of accounting for multiple slip represent an important contribution in the history of texture theories.

Current theories regarding the development of alloy and

pure metal textures are due mainly to Wassermann[18], Haessner[19], Smallman and Green[15], and Dillamore and Roberts[20].

Wassermann[18] assumed that all metals tend first to form the pure metal texture, which he described as two limited fibre textures centred on the orientations $\{110\}\langle\bar{1}12\rangle$ and $\{112\}\langle\bar{1}\bar{1}1\rangle$. He showed that mechanical twinning would transform material in the $\{112\}\langle\bar{1}\bar{1}1\rangle$ orientation to $\{255\}\langle\bar{5}11\rangle$, which subsequently rotated, by slip processes, to $\{110\}\langle001\rangle$. It was argued that the strain accompanying twinning of the $\{110\}\langle\bar{1}12\rangle$ component is less compatible with the overall required strain than that associated with twinning of the $\{112\}\langle\bar{1}\bar{1}1\rangle$ component. Twinning merely limits the spread about the $\{110\}\langle\bar{1}12\rangle$ orientation. This theory is in agreement with the observation that metals of low stacking fault energy may deform by mechanical twinning[21]. A deficit is its failure to account satisfactorily for the mode of formation of the pure metal texture.

Haessner[19] also considered that mechanical twinning would aid formation of the $\{110\}\langle\bar{1}12\rangle$ texture and would cause formation of a $\{110\}\langle001\rangle$ component. His theory assumes that the $\{110\}\langle\bar{1}12\rangle$ texture is the end point of "normal" slip rotations (i.e. primary and duplex slip). He attributed the pure metal texture to the onset of non-octahedral slip, and for the case of mixed proportions of cubic slip and octahedral slip he suggested the range of orientations $\{110\}\langle\bar{1}12\rangle$ - $\{135\}\langle\bar{2}\bar{1}1\rangle$ - $\{112\}\langle\bar{1}\bar{1}1\rangle$ to explain the texture. Other workers[22,23] have also proposed cubic slip to account for development of the pure metal texture. Haessner[19] explained the dependence of cubic slip on stacking fault energy by pointing out that the wider the separation of the partial dislocations, the less likely will it be possible for dislocations dissociated in a $\{111\}$ plane to lie on a $\{100\}$ plane.

The theories described so far have all assumed that the

final texture in rolling will be a combination of the end orientations for simple tension and compression. A better approximation to the stress system during rolling was that adopted by Dillamore and Roberts[20]. Using a biaxial stress analysis, they determined the slip systems that would operate under combined stresses. A further refinement in their theory was to assume that the textures are developed as a consequence of deformation on two main systems, with multiple slip maintaining grain boundary continuity but not contributing significantly to texture development. The basis for this was experimental evidence which shows that multiple slip starts at grain boundaries and then spreads into the body of the grains[24]. Dillamore and Roberts[20] determined the end point of rotations for all possible initial grain orientations and found that most orientations rotate to $\{110\}\langle\bar{1}12\rangle$, although some move initially towards $\{110\}\langle001\rangle$. They pointed out that the alloy texture could therefore be completely explained solely on the basis of primary and duplex slip, without invoking twinning, as suggested by Haessner[16] and Wassermann[18].

Smallman and Green[15] and Dillamore and Roberts[20] attributed formation of the alloy texture to primary and conjugate slip processes, and considered the subsequent rotation to the pure metal texture to be caused by the onset of cross-slip. A reasonable amount of cross-slip was said to produce a final texture of the form $\{135\}\langle\bar{2}\bar{1}1\rangle$ or $\{146\}\langle\bar{2}\bar{1}1\rangle$, and a very large amount of cross-slip, such as that found in aluminium, was said to cause rotation to the texture $\{112\}\langle\bar{1}\bar{1}1\rangle$. Dependence of cross-slip on stacking fault energy clearly indicates correlation of texture and stacking fault energy. The temperature dependence of the texture was explained on the basis of thermal activation of cross-slip.

Haessner[16] had previously dismissed the possibility of cross-slip as a factor contibutory to texture development, on the grounds that the internal stresses present during rolling are generally greater than τ_{III}, the stress associated with

stage III work hardening in single crystals, so that cross-slip should always be possible during rolling of polycrystalline metals. Dillamore and Roberts[20] disagreed with this hypothesis, on the grounds that the amount of cross-slip required to contribute significantly to texture development would be relatively large and would therefore correspond to higher stresses than those required to initiate cross-slip. However, since cubic slip is geometrically equivalent to equal proportions of primary and cross-slip, it appeared at this stage that the textures observed could equally well be explained by the theory of Haessner or that of Dillamore and Roberts. The latter presented experimental evidence in the form of $\{111\}$ pole figures of super-purity aluminium and silver. These, they claimed, showed that whereas in silver texture development was solely towards $\{110\}\langle\bar{1}12\rangle$, in aluminium development was initially towards $\{110\}\langle\bar{1}12\rangle$ but later towards $\{112\}\langle\bar{1}\bar{1}1\rangle$. However, the evidence in the pole figures was questionable and their deductions were not entirely satisfactory.

The situation has been remedied by similar results from Hu et al.[25] and Butler and Green[26]. For a series of copper-aluminium alloys the pole figures of Butler and Green[26] showed, quite convincingly, that both metals and alloys tend first towards the pure metal texture, but with increasing reduction the alloys deviate towards $\{110\}\langle\bar{1}12\rangle$. The lower the stacking fault energy, the lower was the % reduction at which this change occurred, a finding which is consistent with the dependence of twinning on stacking fault energy. They concluded that both metals and alloys, irrespective of stacking fault energy, first undergo primary and duplex slip, followed by cross-slip, to develop a pure metal texture, but that at higher reductions the alloy texture is formed due to twinning.

A basic difficulty in accounting for multiple slip in theories of texture formation has been the inability, in general, to define precisely the systems which are required to operate.

A crystal of arbitrary orientation may achieve any imposed shape change by shear on five independent slip systems[27], but, as shown by Bishop Hill[28], for cubic crystals the five systems are to be chosen from sets of either six or eight, and the magnitude and sense of crystal rotation is dependent on the choice of systems. If all six or eight systems operate there is no rotation of the crystal. Further consideration of the problem by Dillamore, Butler and Green[29] has shown that for crystals having <110> or <111> transverse directions only four systems are necessary to produce the shape change imposed by rolling. Obviously, under such conditions there is no ambiguity in the choice of systems or in the relative activity on these systems. They plotted $d\theta/dE$ as the instantaneous rate of rotation in radians per unit natural longitudinal strain (Figures 1 and 2). In figure 1 $d\theta/dE$ is plotted for orientations having a $[\bar{1}10]$ transverse direction. A positive value of $d\theta/dE$ indicates that the rotation is such as to increase θ, while negative $d\theta/dE$ decreases θ. A stable orientation is shown by zero $d\theta/dE$ and a negative slope of the curve of $d\theta/dE$ vs. θ, while a metastable orientation has zero $d\theta/dE$ and a positive slope. Thus, for f.c.c. crystals having a $[\bar{1}10]$ transverse direction the stable orientations are $(110)[001]$ and $8\frac{1}{2}°$ from $(112)[\bar{1}\bar{1}1]$ or $\sim(4,4,11)\ [\bar{1}\bar{1},\bar{1}\bar{1},8]$. Figure 2 shows that for f.c.c. crystals having a $[\bar{1}\bar{1}1]$ transverse direction the stable orientations are both of the type $\{110\}\langle\bar{1}12\rangle$ Rotations predicted from these graphs were in good agreement with experimental results of Hu and Cline[30]. The analysis of Dillamore, Butler and Green[29], like that of Wassermann[18], predicts that the initial stages of texture development should always be towards a pure metal texture, since orientations having <110> and <111> transverse directions rotate equally rapidly towards the stable positions.

A reasonable explanation now seems to be available for experimentally observed differences in texture intensities, i.e. a significantly greater volume of material is associated with

the main components of the pure metal texture, where extensive cross-slip is available, than in the alloy texture. Also, aluminium, which can cross-slip more easily than say copper, exhibits an even more well developed texture. Although cross-slip does not affect the rotation of orientations having a <110> or <111> transverse direction, for arbitrary orientations it can be important. Groves and Kelly[31] indicated that when cross-slip occurs freely the von Mises condition requiring five independent slip systems is modified so that an arbitrary strain can be imposed if the crystal has three non-coplanar, non-perpendicular slip directions. Under these conditions, Chin and Mammel[32] have shown that there is no ambiguity in choice of shears thus giving a unique sense of rotation. Dillamore, Butler and Green[29] have then assumed that the net rate of rotation will be more rapid for a unique sense of rotation, and explain the observed differences in intensity on this basis.

An important feature of the f.c.c. alloy texture, not previously mentioned, and which most theories have tended to disregard, is the spread of minor orientations which includes a measurable density of {111} planes parallel to the rolling plane. Both Dillamore and Roberts[1] and Hu et al.[25] have suggested stacking-fault formation as the cause of this. Extensive faulting parallel to {111} planes would cause deformation to be confined to the {111} planes which are fault planes. In any grain the stress system initially favours faulting on one plane only, giving one slip plane with three independent slip systems per grain. A {111} texture will result from deformation in such a manner. Although formation of stacking-faults is a prerequisite of any mechanistic model of twin nucleation, Dillamore, Butler and Green[29] suggested that it cannot in itself lead to the drastic reorientation required to produce a {111} component. Also, as indicated by figure 1, normal slip rotations cause rapid depletion of components of the type {111} <$\bar{1}\bar{1}2$> and this is confirmed by experimental results[29]. However, Heye and Wassermann[33] have shown that in silver single

crystals a complex sequence of twinning, together with reversed shear, carries orientations having a <110> transverse direction to a variety of orientations including $\{111\}\langle\bar{1}\bar{1}2\rangle$. This seems the most likely explanation of the origin of this component.

The evidence to date now gives a fairly conclusive picture of the origin of f.c.c. rolling textures, i.e. the obvious features of texture transition are the result of mechanical twinning, while other differences within the range of textures are attributable to differences in ease of cross-slip. The analysis of rotations under cross-slip yet needs to be refined in order to explain why the end orientation should be $\sim\{4,4,11\}\langle\bar{1}1,\bar{1}1,8\rangle$ rather than $\{112\}\langle\bar{1}\bar{1}1\rangle$.

2.3 Primary Recrystallisation Textures

Deformation textures are a major factor in determining the nature of primary recrystallisation textures, but since different textures may be formed during various stages of annealing, relevant experimental observations are fewer than those relating to rolling textures. However, an attempt will be made to discuss results in general terms.

A rolling texture of the type $\{135\}\langle 1\bar{2}1\rangle$ usually recrystallises to the cube texture $\{100\}\langle 001\rangle$. This effect has been reported in copper[34-36], aluminium[37,38], nickel[39] and nickel-iron alloys[36,40]. The abundance of the cube texture depends on the annealing conditions and production variables, but to obtain it a pronounced rolling texture is generally required. In copper, after prior deformations of up to 50%, the recrystallisation texture is almost random; after 90% deformation the annealing texture resembles the deformation texture, and greater degrees of deformation produce a texture consisting of the cube orientation and its twins[34-36]. Fine grain in the starting material and a high annealing temperature tend to give a more perfect cube texture and to lower the density of twinning. For aluminium of 99.99% purity the recrystallisation textures are essentially the same as those of copper, but in aluminium it is more difficult

to produce entirely cube texture[37,38].

The effect of alloying is related to its effect on the deformation texture, but the amount of solute necessary completely to suppress cube texture is considerably less than that needed to cause transition to the alloy rolling texture[2,3]. In 70/30 brass[38] and in silver[41] rolled to 96% reduction at room temperature, the annealing texture is adaquately described by the indices $\{225\}<\bar{7}\bar{3}4>$ or near $\{113\}<\bar{2}\bar{1}1>$. In copper-zinc alloys[38] the $\{225\}<\bar{7}\bar{3}4>$ component originates as $\{214\}<\bar{5}\bar{2}3>$ in a 3% zinc alloy and with increasing zinc content it increases in intensity: at 6% zinc it rotates to $\sim\{427\}<\bar{4}\bar{2}3>$ and at 10% zinc to $\sim\{438\}<\bar{6}\bar{3}4>$[42]. (Other minor components accompany this transition). Similar annealing texture transitions occur in alloys of copper with aluminium[43], tin and germanium[2], and in nickel alloys containing molybdenum or cobalt[39]. The annealing textures of alloys of copper with phosphorus, arsenic and antimony (elements which are particularly effective in suppressing cube texture) are completely different: the major orientations are $\{227\}<77\bar{4}>$ and components related to $\{110\}<\bar{1}12>$ by a rotation about $<110>$[2,3]

There are various results from single crystal studies[1] which indicate that, in the absense of second phase effects, the geometrical relationship between the deformed and recrystallised grains is a rotation of $\sim\pm30°$-$40°$ about common $<111>$ poles. However, such rotations usually occur preferentially about certain $<111>$ directions rather that the full set of $<111>$ axes.

2.4 Theories of Primary Recrystallisation Textures.

Theoretical interpretations of recrystallisation textures in metals and alloys are not so widely applicable as those regarding deformation textures. In the past there have been two main, opposing theories of the mechanisms involved, namely, oriented nucleation and oriented growth.

Burgers and Louwerse[44] suggested that the new grains grow from small regions of certain orientations which are already present in the deformed matrix. The orientation of the recrystallised

grains is therefore determined by that of the original nuclei. However, in order to explain why recrystallisation textures are usually different from the rolling textures assumptions are necessary:-

a) that the oriented nuclei are too small to be detected when the rolling texture is determined,

b) that these nuclei are oriented more favourably for recrystallisation than those in the greater part of the matrix,

c) that after polygonisation has taken place within these nuclei, the polygonised nuclei are capable of growth.

Although this approach is capable of explaining certain observations, such as retention of the rolling texture in aluminium, it is not widely accepted. Moreover, in copper having a normal pure metal texture, electron microscope examination has shown that the individual crystal orientations describe completely the texture of the bulk material, but no evidence was found of cube-oriented grains.[45] Nucleation theories can account only for annealing textures of which the component orientations are represented in the deformation texture or are related to deformation components by comparatively slight rotations.

Barrett[46] and Beck[47] suggested that recrystallisation textures are determined by the preferential growth of nuclei having certain orientations. It is supposed that initially nuclei of varying orientations are formed but, since the rate of growth of a given nucleus depends on the difference of orientation between the matrix and the growing crystal, the nuclei having the fastest rates of growth will be those which are bounded by high angle boundaries. These nuclei, which give rise to the recrystallisation texture, will have orientations differing from the original by a rotation of approximately 45° about a <111> axis. This theory is well supported by the fact that recrystallisation textures of many metals and alloys are related to the deformation textures by simple rotational relationships. Also, Lucke[48] has shown the orientation relationship for maximum growth rate to be 40°

<111> rotations for the case of aluminium.

A general criticism of the oriented growth theory has been that the growth relationship is not sufficiently precise to account for the well defined recrystallisation textures which are obtained. However, Dillamore[43] has shown that in view of the restrictions on the growth of a nucleus to form part of the recrystallisation texture, the site at which nucleation occurs, and the range of orientations through which the nucleus must grow, the sharpness of the recrystallisation texture may be due to the conflicting conditions of growth into a multicomponent matrix. In his analysis of the relationship between deformation textures and annealing textures in f.c.c. metals it was suggested that the most probable sites for nucleation were grain boundaries and deformation band boundaries, and it was considered that the major components of the annealing texture arise from nuclei which are capable of growth, (a) into the orientations on either side of the boundary, (b) through the spread of these orientations, and (c) into the remaining two of the four symmetrical components of the deformation texture. He described the deformation texture using a number of ideal orientations between the limits $\{110\}\langle\bar{1}12\rangle$ and $\{112\}\langle\bar{1}\bar{1}1\rangle$ and assumed that a nucleus would be favoured for growth if it has a <111> pole within 10° of a <111> pole of the matrix and if the rotation about this pole is between 20° and 50°. For a deformation texture close to $\{110\}\langle\bar{1}12\rangle$ favourable nuclei are $\{4,9,17\}\langle 38\bar{5}\rangle$, $\{490\}\langle 001\rangle$ and $\{112\}\langle\bar{1}10\rangle$. However, the existence of a minor $\{110\}\langle 001\rangle$ component in the deformation texture acts to inhibit growth of $\{490\}\langle 001\rangle$ and $\{112\}\langle\bar{1}10\rangle$ nuclei, with the result that a spread around $\{4,9,17\}\langle 38\bar{5}\rangle$ emerges as the texture. This orientation is close to $\{113\}\langle\bar{2}\bar{1}1\rangle$. Deformation textures between $\{110\}\langle\bar{1}12\rangle$ +5° and $\{135\}\langle\bar{2}\bar{1}1\rangle$ yield no nucleus orientations suitable for growth into all four components of the deformation texture. There are a limited range of nuclei which can grow into only three components, and these are expected to compete with nuclei which can grow into only two components

but also into a wide spread about these components. A rather less well defined, diffuse annealing texture is expected. For deformation textures in the spread between $\{135\}\langle\bar{2}\bar{1}1\rangle$ and $\{236\}\langle\bar{7}\bar{3}4\rangle$, three favourable nuclei are considered. Of these $\{358\}\langle\bar{8}\bar{3}5\rangle$ is capable of growth only into three components of the matrix. The other nuclei, $\{110\}\langle001\rangle$ and $\{100\}\langle001\rangle$, are equally capable of growth into all four components of the deformation texture, but the misfit of $\{110\}\langle001\rangle$ is considerably greater than that of $\{100\}\langle001\rangle$, so that the latter is expected to dominate the annealing texture. A material which undergoes a very large amount of cross-slip during rolling was expected to give a texture whose centre of spread lies between $\{236\}\langle\bar{7}\bar{3}4\rangle$ and $\{112\}\langle\bar{1}\bar{1}1\rangle$. In this range there are no nuclei favoured for growth into three or four components, and orientations having extensive permitted growth ranges are expected to form the major annealing components. These are typified by $\{4,5,10,\}\langle\bar{1}5,\ \bar{8},10\rangle$, $\{551\}\langle\bar{1},\bar{1},10\rangle$ and $\{4,4,11\}\langle\bar{7}\bar{7}5\rangle$. The predictions were in good agreement with results obtained for aluminium, copper and some copper-aluminium alloys, but it must be stressed that the aluminium was of commercial quality.

Another criticism of the oriented growth theory has been the absence of some variants of the growth relationship. This argument cannot be applied to polycrystalline textures, and preferential selection of variants in single crystals is clearly possible from the work of Beck et al.[49-51], who showed that grain boundaries inedge orientation have higher mobility than those in screw orientation.

Although the oriented growth theory is more widely applicable in accounting for the textures observed, oriented nucleation is still a possible mechanism of formation of annealing textures. More generally, when oriented nucleation does occur, there will be further selection from the nuclei during competitive growth[52-54

2.5 Effect of Second Phases on Recrystallisation Textures.

Recrystallisation textures, being dependent on nucleation and grain growth, may in some cases be controlled by the presence of second phase particles.

In aluminium the relative proportions of cube texture and retained rolling texture are markedly dependent on processing variables and also on the purity of the metal. It is generally agreed that iron is the impurity element which has greatest effect on annealing textures, but opinions differ as to the mechanism by which it acts. Bunk and Esslinger[55] suggested that iron restricts recrystallisation to a cube texture by its effect on the rolling texture, but observations by Blade[56] indicate that small amounts of iron do not affect the rolling texture. A more likely explanation is that growth of the cube texture is restricted by precipitated particles[56-58].

Gokyu, Abe and Veyama[59] observed that recrystallisation textures in aluminium-copper alloys were dependent on the solution treatment prior to cold rolling, but that the rolling textures remained unaffected. Specimens which had not been solution treated recrystallised to $\{100\}<001>$ and $\{113\}<33\bar{2}>$, whereas solution treated specimens recrystallised to $\{110\}<001>$ and $\{110\}<\bar{1}10>$. These differences were attributed to the distribution of the precipitate during primary recrystallisation and the suppression of random nucleation around precipitated particles.

Mee and Sinclair[60] found that during the cold rolling of nickel-2½ vol.% thoria orientations of the type $\{hkl\}<001>$, and in particular $\{110\}<001>$, originating from the starting texture, were metastable, and that the degree of cold work required for their degeneration was a function of the initial milling and fabrication conditions. Heavy cold rolling produced a f.c.c. pure metal type of texture. In the recrystallisation texture a range of components was observed, including $\{100\}<001>$ and its twin orientation $\{122\}<\bar{2}\bar{1}2>$, $\{210\}<\bar{1}21>$, $\{359\}<\bar{3}01>$ and $\{445\}<\bar{1}2,7,4>$: the exact nature of the texture was dependent on the

particular alloy and on the degree of deformation. In an alloy in which the rolling texture after 91% reduction was mainly $\{110\}<001> + \{100\}<001>$, annealing for 1 hour at 1000°C produced a weak cube component and major orientations near $\{359\}<\bar{3}01>$ and $\{445\}<12,4,7>$. Annealing at 1400°C caused a decrease in the production of cube component, accompanied by strengthening of other components. This alloy possessed a banded structure of thoria particles. In other alloys, in which there was no banding, the rolling texture at 93% reduction was described in terms of components near $\{430\}<\bar{3},4,10>$ and $\{320\}<001>$, the former a normal f.c.c. rolling texture. After annealing at 1000°C the textures contained varying proportions of $\{100\}<001>$, $\{122\}<\bar{2}\bar{1}2>$ and $\{210\}<\bar{1}21>$ components. It was suggested that the $\{210\}<\bar{1}21>$ component could be the result of second-order twinning, or, alternatively, that the particular size spectrum and dispersion of thoria particles obtained in these alloys had impeded the nucleation and growth of cube-oriented grains.

3 B.C.C. Metals and Alloys.

3.1 Rolling Textures.

Taking a comprehensive view of the range of b.c.c. metals and alloys for which data is available, the rolling textures of polycrystals have frequently been described as the orientation $\{001\}<\bar{1}10>$ lying at the centre of the textural spread, with the remainder of the texture allotted to spread around $\{112\}<\bar{1}10>$, $\{111\}<\bar{1}10>$ and $\{111\}<\bar{1}\bar{1}2>$. ~~However,~~ The basis for this description has been the results of, inter alia, Barrett and Levenson[61] who found that single crystals of iron which developed these orientations seemed to be stable after heavy deformations. However, the $\{112\}<\bar{1}10>$ component is always present in the texture but the $\{111\}<\bar{1}\bar{1}2>$ and $\{111\}<\bar{1}10>$ components have been reported only in certain cases[1]. The tendency of some workers to use $\{111\}<\bar{1}10>$ in describing part of the texture is not completely justified, since the largest angle used to describe the spread about $\{001\}<\bar{1}\bar{1}0>$ only just includes $\{111\}<\bar{1}10>$. A preferred

description of the texture is in terms of the three major components, $\{112\}\langle\bar{1}10\rangle$, $\{001\}\langle\bar{1}10\rangle$ and $\{111\}\langle\bar{1}\bar{1}2\rangle$, with spread towards a minor $\{111\}\langle\bar{1}10\rangle$ component.

Further results obtained using single crystals have emphasised the importance of amount of deformation in distinguishing between stable and metastable orientations, and in relation to polycrystalline textures developed using >80% reduction the $\{111\}\langle\bar{1}\bar{1}2\rangle$ orientation can no longer be considered truly stable since at higher reductions the texture may deviate from this orientation. This is well illustrated by the results of Hu and Cline[62] for an iron-2%aluminium single crystal of initial orientation $\{111\}\langle\bar{1}\bar{1}2\rangle$, which rotated towards $\{332\}\langle\bar{1}\bar{1}3\rangle$ during a 70% reduction. This is equivalent to taking a crystal of different orientation and deforming it to (say) 90% reduction to form the $\{111\}\langle\bar{1}\bar{1}2\rangle$ orientation, and then superimposing an additional 7% reduction to give an overall reduction of 97%. An important implication here is that during the cold-rolling of polycrystals, experimental conditions might preclude such high reductions being obtained, and that consequently $\{111\}\langle\bar{1}\bar{1}2\rangle$ will remain as an important component of the texture.

Development of the polycrystalline texture is largely by development and subsequent breaking up of the $\{112\}\langle\bar{1}10\rangle$ component[1]

3.2 Theories of Rolling Textures.

The situation with regard to theoretical interpretation of b.c.c. rolling textures still leaves some doubt as to a complete explanation of their development.

For b.c.c. metals, Calnan and Clews[17] found that the end orientations were little effected by the choice of type of slip system i.e. whether $\{110\}\langle\bar{1}11\rangle$, $\{112\}\langle\bar{1}\bar{1}1\rangle$ or $\{123\}\langle\bar{1}\bar{1}1\rangle$. Major components of the texture were predicted as $\{111\}\langle\bar{1}10\rangle$ and $\{001\}\langle\bar{1}10\rangle$, but these orientations alone are not in accord with observed textures.

Dillamore and Roberts[20] assumed the operative slip systems to be $\{110\}\langle\bar{1}11\rangle$ on the basis that the other two types of slip

are geometrically equivalent to different proportions of primary and cross-slip on $\{110\}\langle\bar{1}11\rangle$ systems. They concluded that under the influence of primary and conjugate slip most of the material will rotate to orientations of the type $\{112\}\langle\bar{1}10\rangle$, and that cross-slip would start after this orientation had been reached, and would cause rotation of $\{001\}$ towards the rolling plane. Equal amounts of primary and cross-slip would produce an $\{001\}\langle\bar{1}10\rangle$ end orientation. The predicted texture was thus $\{112\}\langle\bar{1}10\rangle + \{001\}\langle\bar{1}10\rangle$ as major components, with a spread between them. To back up their theory Dillamore and Roberts showed pole figures of 95% cold-rolled vanadium, which were described by their predictions. The $\{111\}\langle\bar{1}10\rangle$ orientation corresponded to regions of low intensity, a common observation for b.c.c. metals[63].

It appears that the $\{111\}\langle\bar{1}10\rangle$ component used by some workers to describe part of the texture has no great significance. The intensity of $\{111\}\langle\bar{1}\bar{1}2\rangle$, on the other hand, is strong when it occurs, leaving no doubt as to its importance in describing particular textures. However, neither of the above theories can account for its presence. In a later paper, Dillamore[64] suggested that it occured as a result of initial texture, and he proposed the following:

a) from a random orientation, a texture initially comprising mainly $\{112\}\langle\bar{1}10\rangle$ with a minor $\{001\}\langle\bar{1}10\rangle$ component would form, With increasing deformation the intensity of $\{001\}\langle\bar{1}10\rangle$ would increase at the expense of that of $\{112\}\langle\bar{1}10\rangle$.

b) from an initial $\{110\}\langle001\rangle$ or $\{111\}\langle\bar{1}\bar{1}2\rangle$ texture, the final texture would contain also $\{111\}\langle\bar{1}10\rangle$ and $\{111\}\langle\bar{1}\bar{1}2\rangle$.

However, Hancock and Roberts[65], using inverse pole figures, reported an important $\{111\}$ component from material initially having an almost random orientation. This throws considerable doubt on Dillamore's hypothesis, as does the total strain analysis of Dillamore, Butler and Green[29], which was also applied to b.c.c. crystals. (Figures 1 and 2) Thus, Figure 1 predicts stable orientations corresponding to (001) [110] and 8° 14′ from $(\bar{1}\bar{1}1)$ [112]

or $\sim(\bar{1}\bar{1},\bar{1}\bar{1},8)$ [4,4,11], while Figure 2 predicts orientations both of the type $\{112\}\langle\bar{1}10\rangle$. A theory is yet required which can account for this orientation near $\{111\}\langle\bar{1}\bar{1}2\rangle$.

Finally, from the previous discussion on theories of f.c.c. rolling textures, twinning might be expected to play some rôle in defining the final b.c.c. texture. No theory to date has attempted to account for this.

3.3 Primary Recrystallisation Textures

Because there are no major differences between the rolling textures of b.c.c. metals and alloys, it is to be expected that their recrystallisation textures should follow a similar trend. This, in fact, occurs although the number and relative amounts of the textural components depend to a large extent on temperature. Also, impurities can exert a significant effect on annealing textures. Indeed, conflicting results may well arise from this important but often overlooked variable, and in view of this only a selection of results will be referred to in this section.

Using 2·65% silicon-iron, Stablein and Möller[66] observed that for rolling reductions up to 73% a high carbon (0·052%) variety of the material gave a texture similar to the rolling texture for all annealing temperatures <1100 °C. For a lower carbon (0·011%) variety, the texture began to change above 800 °C to $\{110\}\langle001\rangle$. For 92% rolling reduction there was negligible difference between the two grades. At 500 °C the texture showed a $\{111\}\langle\bar{1}\bar{1}2\rangle$ component which was said not to be present in the rolling texture, and at higher temperatures, up to 1000 °C, this component became stronger. Similar effects have been noted by Koh and Dunn[67] and by Haessner and Weik[68].

In tantalum, with a deformation texture consisting mainly of the $\{001\}\langle\bar{1}10\rangle$, $\{112\}\langle\bar{1}10\rangle$ and $\{111\}\langle\bar{1}\bar{1}2\rangle$ orientations, both Müller[69] and Pugh and Hibbard[70] report that recrystallisation was to a texture similar to the rolling texture but without the $\{111\}\langle\bar{1}\bar{1}2\rangle$ component. With tungsten, Pugh[71] found a slight sharpening of the rolling texture but no change of orientations

for temperatures up to 1800°C, which corresponded to complete softening.

Since the polycrystalline textures invariably contain three main components, it is difficult to deduce rotational relationships between the deformed and recrystallised grains. Results of single crystal studies are particularly relevant here, more so because it is possible to discuss the results in general terms. For instance, the usual observation is that the recrystallisation textures in b.c.c. single crystals contain components derived from the deformed crystal by rotations of between 25° and 30° around common <110> poles[72-78]. Not all the variants of this relationship are found, however, and in particular, a single crystal having a (111) [$\bar{1}\bar{1}2$] deformation texture recrystallises to (110) [001][72,74,76].

There are some recrystallised orientations which are related to the deformed matrix by rotations about <100> poles. These rotations were observed for crystals having a (100) [011] deformation texture, which gave rise, on annealing, to components with {100} parallel to the rolling plane[72,74,79,80,81]. Abe et al.[81] have suggested that this texture may really be a result of secondary recrystallisation since in all cases the annealing was carried out at relatively high temperatures, while lower temperatures gave the <110> rotational relationships.

Evans, Bitcon and Hughes[82] considered the effect of some binary alloy additions on the annealing textures of high purity iron. Rolling textures remained unaffected and were of the type {112}<$\bar{1}$10> + {001}<$\bar{1}$10> + {111}<$\bar{1}\bar{1}$2>, but the subsequent recrystallisation textures after 5hrs at 700°C enabled the alloys to be divided into two groups. After 70% reduction the pure iron recrystallised to strong components near {111}<$\bar{1}\bar{1}$2> and {111}<$\bar{1}$10> together with a {100}<001> component of lower intensity. After 90% reduction the {111}<$\bar{1}\bar{1}$2> component was considerably stronger. The spread towards {111}<$\bar{1}$10> remained, but a {100}<012> component was now present. Iron-5% titanium showed similar textures but

after 70% reduction the $\{111\}\langle\bar{1}\bar{1}2\rangle$ component clearly dominated the texture, with $\{111\}\langle\bar{1}10\rangle$ and $\{100\}\langle001\rangle$ as minor components. After 90% reduction also, the $\{111\}\langle\bar{1}\bar{1}2\rangle$ component was of higher intensity, with $\{111\}\langle\bar{1}10\rangle$ and $\{100\}\langle012\rangle$ as minor components. Other alloys, which were assumed on the basis of plastic anisotropy measurements to exhibit similar behaviour, were those containing 0·02% carbon, 0·1% carbon and 0·05% phosphorus. By contrast the pole figures of iron-0·6% aluminium and iron-0·5% manganese were said to be typical of a group which included alloys containing 1·0% manganese, 1·0% nickel, 1·0% chromium, 0·25% copper and 1·0% copper. A rimming steel and mild steel were also included in this group. The recrystallisation texture of iron-0·6% aluminium after 59% reduction consisted of $\{110\}\langle001\rangle$ and $\{100\}\langle001\rangle$ components of equal intensity, with a very weak $\{111\}\langle\bar{1}\bar{1}2\rangle$ component. After 79% reduction, the $\langle001\rangle$ fibre texture was more complete, with $\{110\}\langle001\rangle$ near the centre of the spread, and the $\{111\}\langle\bar{1}\bar{1}2\rangle$ component was now much stronger. For 90% reduction the texture was quite diffuse by comparison with the previous alloys. The main components were $\{111\}\langle\bar{1}\bar{1}2\rangle$ and $\{100\}\langle001\rangle$, part of which was rotated around the sheet normal and tilted out of the plane of the sheet towards $\{115\}\langle\bar{1}\bar{1}0\rangle$. Iron-0·5% manganese behaved slightly differently. After 90% reduction, $\{110\}\langle001\rangle$ and $\{100\}\langle001\rangle$ were present together with $\{111\}\langle\bar{1}10\rangle$ and $\{111\}\langle\bar{1}\bar{1}2\rangle$. Summarising this work, the differences were largely in the much higher intensities of $\{111\}$ components for the first group of alloys. The authors noted that these alloys would have a strong tendency for segregation either of interstitial elements or phosphorus to dislocations or for substitutional elements to form very fine carbonitride particles, whereas the second group of alloys were either simple substitutional additions or ones that interact less strongly with interstitial impurities and thus tend to stay in solution.

3.4 Theories of Primary Recrystallisation Textures.

Theories of recrystallisation textures of f.c.c. materials have similarly been applied to b.c.c. materials. In recent years the respective rôles of oriented nucleation and oriented growth have been recognised as complementary rather than opposing.

The observed rotational relationships between deformed and recrystallised grains are well supported by the results of Lucke[48], who showed that for iron-3% silicon the orientation relationship for maximum growth rate is a $27^\circ\langle 110\rangle$ rotation.

Dillamore[64] has put forward a purely geometrical analysis based on oriented growth relationships to derive annealing texture orientations in b.c.c. metals from their deformation textures. This analysis is similar to that carried out for f.c.c. metals[43] and likewise considers probable nucleation sites for recrystallisation and the textural limitations on grains growing into a deformed matrix. It was assumed that two different deformation textures could be obtained according to the condition of the starting material, although this hypothesis now seems doubtful. (Section 3.2) However, this does not invalidate the recrystallisation theory as such, but the results implied by the analysis will obviously relate to the choice of orientations defining the deformation texture. Dillamore's analysis was based on $\langle 110\rangle$ rotations which simultaneously satisfy the growth relationship between growing grain and two components of the deformed matrix, and a range of 20° to 60° was permitted. For material initially having the $\{112\}\langle\bar{1}10\rangle$ - $\{001\}\langle\bar{1}10\rangle$ texture spread, recrystallisation is envisaged to commence as competition between the orientations $\{111\}\langle\bar{1}10\rangle$ and $\{554\}\langle\bar{2}\bar{2}5\rangle$ (which is close to $\{111\}\langle\bar{1}\bar{1}2\rangle$). Initially $\{111\}\langle\bar{1}10\rangle$ is said to have an advantage because of its greater probability of nucleation and its capacity for growth through the immediate orientation spread about its parent orientations, whereas $\{554\}\langle\bar{2}\bar{2}5\rangle$ is able to grow into a greater part of the deformation texture i.e. it is favourably oriented for growth into both of the $\{112\}\langle\bar{1}10\rangle$ deformation texture components and the

$\{001\}\langle\bar{1}10\rangle$ component. For a deformation texture consisting of the orientations $\{112\}\langle\bar{1}10\rangle$, $\{001\}\langle\bar{1}10\rangle$, $\{111\}\langle\bar{1}10\rangle$ and $\{111\}\langle\bar{1}\bar{1}2\rangle$, the $\{111\}\langle\bar{1}10\rangle$ and $\{554\}\langle\bar{2}\bar{2}5\rangle$ nuclei are inhibited by $\{111\}\langle\bar{1}10\rangle$ and $\{111\}\langle\bar{1}\bar{1}2\rangle$ components of the deformation texture, and the only orientation which is favoured by an ability to grow into components other than those in which it forms is $\{10, 8, 7\}\langle 13\bar{5}\rangle$.

Dillamore[64] further pointed out that in the early stages of recrystallisation the texture consisting of $\{112\}\langle\bar{1}10\rangle$ and $\{001\}\langle\bar{1}10\rangle$ orientations will also contain $\{111\}\langle\bar{1}10\rangle$ and $\{554\}\langle\bar{2}\bar{2}5\rangle$ as recrystallisation components, so that at this stage it approximates to his second type of deformation texture. Nuclei formed at boundaries between $(112)\,[1\bar{1}0]$ and $(11\bar{2})\,[1\bar{1}0]$ actually include a small proportion of $\{10,8,7\}\langle 13\bar{5}\rangle$ and these will be favoured for growth into $\{111\}\langle\bar{1}10\rangle$ oriented recrystallised grains. On this basis, high annealing temperatures or long annealing times at low temperatures were expected to give rise to similar recrystallisation textures from the two types of deformation texture.

Dillamore[64] suggested that the nucleation frequency of orientations having $\langle 110\rangle$ directions parallel to the rolling direction is high, since all grain boundaries between orientations in the spread about this $\langle 110\rangle$ direction are capable of nucleating such orientations. Therefore, at low temperatures and for short annealing times, i.e. when the growth rate is low, nucleatian probability will dominate formation of the texture. Thus, the low temperature, short-time annealing texture of b.c.c. metals was expected to consist of $\{hhl\}\langle 1\bar{1}0\rangle$ components with $\{111\}\langle 1\bar{1}0\rangle$ predominating. On the other hand, when the growth rate becomes dominant, orientations of lower nucleation frequency, but capable of rapid growth into a large volume fraction of material, would be the main components of the recrystallisation texture. These were predicted as $\{554\}\langle\bar{2}\bar{2}5\rangle$ and $\{10,8,7\}\langle 13\bar{5}\rangle$.

This attempt at rationalisation of annealing textures in

b.c.c. materials was well founded since both predictions agreed reasonably well with quoted experimental results, which included those of previous workers. However, it is possible that oriented nucleation could also be responsible in part for these recrystallisation textures, especially if one recognises that $\{111\}\langle\bar{1}\bar{1}2\rangle$ is a major component of the rolling texture, and that a small amount of $\{111\}\langle\bar{1}10\rangle$ is inevitably present as part of the textural spread. Hence, $\{111\}\langle\bar{1}\bar{1}2\rangle$ could become a major component of the recrystallisation texture simply by recrystallisation in situ, while $\{111\}\langle\bar{1}10\rangle$ grains can grow from the $\{112\}\langle\bar{1}10\rangle$-$\{001\}\langle\bar{1}10\rangle$ spread by oriented growth. That is not to say, however, that there are two separate processes operating, rather that the initial capacity for growth of $\{111\}\langle\bar{1}10\rangle$ is greater than that of $\{111\}\langle\bar{1}\bar{1}2\rangle$, whereas in the later stages of recrystallisation the growth rates may tend to equalise. This proposal may be compared with a re-interpretation of the experimental results of Dillamore, Smith and Watson[83]. Their pole figure of 70% cold-rolled iron was described in terms of four orientations, $\{112\}\langle\bar{1}10\rangle$, $\{001\}\langle\bar{1}10\rangle$, $\{111\}\langle\bar{1}\bar{1}2\rangle$ and $\{111\}\langle\bar{1}10\rangle$, but the latter clearly corresponded to regions of low intensity. After annealing for 15mins at 700°C, the peaks were centred on $\{111\}\langle\bar{1}\bar{1}2\rangle$ and $\{111\}\langle\bar{1}10\rangle$ orientations of equal intensity.

The work of Dillamore, Smith and Watson[83] was directed towards distinguishing between the possible mechanisms from electron microscope observations. However, the discrepancy in their interpretation of major orientations in the rolling texture has already been pointed out, and, in addition, in discussing development of the annealing texture they appear to have ignored completely the major component centred on $\{111\}\langle\bar{1}\bar{1}2\rangle$. Apart from this, they concluded that oriented grain boundary nucleation was responsible for retention of some $\{001\}\langle\bar{1}10\rangle$ component in the annealing texture, although the importance which they attached to this seems an oversight in view of the fact that $\{001\}\langle\bar{1}10\rangle$ corresponded to an area of very low intensity on the pole figure.

3.5 Effect of Second Phases on Recrystallisation Textures

Leslie[84] has compared textures in iron with those of an iron-0·8% copper alloy. Rolling textures remained unaltered, and there was no effect on the annealing texture, providing the copper was precipitated before cold rolling. If, however, rolling was carried out after solution treatment, and the copper was then precipitated (3hrs at 500°C) followed by annealing (5hrs at 700°C), the texture was of the type $\{001\}\langle\bar{1}10\rangle + \{112\}\langle\bar{1}10\rangle + \{111\}\langle\bar{1}\bar{1}2\rangle$ while the texture of iron after this treatment contained a much stronger $\{111\}\langle\bar{1}\bar{1}2\rangle$ component. This effect was attributed to a raising of the recrystallisation temperature by the presence of the precipitation.

The effect of aluminium nitride on recrystallisation textures in iron and steels has received considerable attention due to the commercial use of aluminium in the manufacture aluminium-killed steels. There is still some doubt, however, as to whether or not a true precipitate is involved.

Stickels[85] examined the recrystallisation behaviour of iron containing aluminium and nitrogen. He showed that if AlN was precipitated before rolling the recrystallisation textures were similar to those observed in aluminium-free iron, and consisted of a strong $\{111\}\langle\bar{1}\bar{1}2\rangle$ component with a minor $\{111\}\langle\bar{1}10\rangle$ component. On the other hand, if the material was supersaturated with respect to precipitation of AlN, a $\{111\}\langle\bar{1}10\rangle$ primary recrystallisation texture developed over a certain interval of isothermal annealing temperatures. This was always accompanied by a spread towards $\{111\}\langle\bar{1}\bar{1}2\rangle$ and $\{001\}\langle\bar{1}10\rangle$. Lowering the degree of supersaturation depressed the temperature interval in which a $\{111\}\langle\bar{1}10\rangle$ texture developed.

Dillamore, Smith and Watson[83] have compared the recrystallisation textures of aluminium-killed and rimming steel using texture parameters. They considered two treatments, either annealing directly for 15mins at 700°C, or an additional preheating for 24hrs at 450°C. The intensity of $\{111\}$ component was markedly

increased in the aluminium-killed steel by the low temperature treatment before annealing at 700°C, while in the rimming steel the $\{111\}$ component was slightly weakened. They gave an interpretation of the role of AlN based on the selective suppression of nuclei of certain orientations. It was considered that precipitation at grain boundaries would prevent grain boundary nucleation and reduce the intensity of $\{001\}\langle\bar{1}10\rangle$ component, while segregation to subgrain boundaries would inhibit the final stages of recovery. In this way normal subgrain growth is prevented and, since subsequent growth is proportional to the available driving force, orientations close to $\{111\}\langle\bar{1}10\rangle$ should be favoured. Although $\{110\}\langle\bar{1}10\rangle$ provides the highest driving force for growth, it was noted that there is only a small amount of material in this orientation and its growth range is limited. This explanation does not consider the $\{111\}\langle\bar{1}\bar{1}2\rangle$ component of the recrystallisation texture. When precipitation of AlN occurs after nucleation, it cannot be effective in this way. In fact, Borchers and Kim[86] have shown that such precipitation occurs in the new grain boundaries slowing down their motion and weakening the texture by removing the orientation-selective effects of the anisotropy of the driving force.

4. Austenitic Stainless Steels.

In any material sheet textures have a direct bearing on performance in operations which involve stretch forming and deep drawing. Choice of textures in annealed stock can actually lead to improvement in behaviour provided that the crystallographic directionality resulting from the texture matches the stress system which is applied during forming. It is with this in mind that attention is now focussed on stainless steels, which, until relatively recent times had received little thought. Indeed, as yet there is little or no published work on the ferritic alloys but since, in general, most b.c.c. metals and alloys have similar textures, it is expected that ferritic stainless steels will conform to the general pattern of behaviour. Current interest lies in the austenitic steels, and the variables which may be used to control cold rolling and primary recrystallisation textures in these alloys.

4.1 Stable Alloys.

Alloyed austenities remain stable provided that the Md temperature is below the temperature of working. For the purpose of classifying steels into stable or metastable alloys, an arbitrary, but practical, definition will be adopted whereby an austenite will be classed as stable at room temperature if no martensite is formed in it after cold rolling to 90% reduction.

Both rolling and annealing textures conform to the general behaviour of f.c.c. metals and alloys, with stacking fault energy being a controlling factor.

4.1.1 Rolling Textures.

For 18%Cr steels, complete stability at room temperature occurs for nickel contents $>\sim 14\%$[87]. Dickson and Green[87] have shown that an 18%Cr 14%Ni steel exhibits a normal $\{110\}<\bar{1}12>$ type of texture: steels of the 25%Cr 20%Ni variety should also exhibit this type of texture. Austenites having higher stacking fault energies, approaching that of copper, should exhibit the pure metal type of texture when rolled at room temperature, but there are no results to confirm this.

Goodman and Hu[11] confirmed the existence of a texture transition as a function of rolling temperature. Using an 18%Cr 10%Ni steel, they showed that the rolling texture changed gradually from $\{110\}\langle\bar{1}12\rangle$ to $\{110\}\langle\bar{1}12\rangle + \{112\}\langle\bar{1}\bar{1}1\rangle$ type as the temperature was raised from 200°C to 800°C.

4.1.2 Primary Recrystallisation Textures.

In high purity alloys the $\{110\}\langle\bar{1}12\rangle$ texture produced by cold rolling at room temperature recrystallises to $\{113\}\langle\bar{2}\bar{1}1\rangle$[87].

The transition in annealing textures has been followed in 18%Cr 10%Ni steel[88]. Annealing at 900°C, of strip rolled at 200-600°C to 90% reduction, produces orientations near $\{113\}\langle\bar{3}\bar{3}2\rangle$, $\{112\}\langle\bar{5}\bar{5}4\rangle$ and $\{123\}\langle\bar{1}\bar{1}1\rangle$, while strip rolled at 800°C exhibits predominantly cube texture, together with $\{122\}\langle\bar{2}\bar{1}2\rangle$ twins and a minor component near $\{530\}\langle001\rangle$.

4.2 Metastable Alloys.

These alloys are metastable in the sense that working progressively raises the Ms until it reaches the temperature of working. When this occurs, the strain-induced $\gamma \Rightarrow \alpha'$ transformation takes place during rolling, with subsequent formation of a duplex ~~temperature.~~ texture.

4.2.1 Rolling Textures.

Goodman and Hu[88], using 18%Cr 10%Ni steel, observed that after 90% reduction crystallites of each phase had assumed their normal end orientations. The austenite developed a typical f.c.c. alloy texture, viz. $\{110\}\langle\bar{1}12\rangle$ + a minor $\{110\}\langle001\rangle$ component, whereas the texture of the martensite consisted of a spread between the main orientations $\{111\}\langle\bar{1}\bar{1}2\rangle + \{112\}\langle\bar{1}10\rangle$ and a spread towards a minor $\{001\}\langle\bar{1}10\rangle$ component. The amount of martensite was estimated from pole figure intensities, as 70-80%, but no details were given as to how this estimation had been carried out.

The above textures have been confirmed in work reported by Dickson and Green[87]. In this case, phase analysis was carried out by an X-ray method described by Dickson[89], which extends the normal direct comparison method to account for preferred

orientation. The results[87] showed that the amount of martensite formed after 93% reduction was ~86%, ~33%, and ~4% for 18%Cr steels containing, respectively, 10%, 12% and 14%Ni. In all cases the texture of the austenite remained unchanged. The martensite texture of 18%Cr 10%Ni steel was similar to that reported by Goodman and Hu, but in the 18%Cr 12%Ni steel only the $\{111\}\langle\bar{1}\bar{1}2\rangle_{\alpha'}$ and $\{112\}\langle\bar{1}10\rangle_{\alpha'}$ components were observed. No texture was reported for the martensite in 18%Cr 14%Ni steel. Dickson and Green[87] attributed absence of the $\{001\}\langle\bar{1}10\rangle$ component in 18%Cr 12%Ni steel to delayed development of the b.c.c. texture.

It is interesting to compare relative intensities of martensite components in stainless steels with the intensities normally observed in b.c.c. metals and alloys. The $\{001\}\langle\bar{1}10\rangle$ component which normally dominates the texture is reduced to secondary importance in the α' texture. This difference arises because the martensite in stainless steels is formed gradually: prior deformation of the austensite, involving development of its own texture, will influence subsequent grain rotations in the transforned martensite.

4.2.2 Primary Recrystallisation Textures.

Goodman and Hu,[88] using 18%Cr 10%Ni steel, found that annealing for 1 hr. at 600°C increased the intensity of the $\{110\}\langle\bar{1}12\rangle_{\gamma}$ component, with appearance of a new orientation, $\sim\{230\}\langle 3\bar{2}1\rangle_{\gamma}$, and that simultaneously the intensity of the martensite texture decreased. At higher annealing temperatures this new orientation disappeared, leaving a $\{110\}\langle\bar{1}12\rangle_{\gamma}$ recrystallisation texture. These authors concluded that the transformation of $\alpha\rightarrow\gamma$ was by growth of crystallites of retained austenite, but they explained the presence of the orientation near $\{230\}\langle 3\bar{2}1\rangle$ by stating that it could be related, by a Kurdjumov-Sachs relationship, to the $\{111\}\langle\bar{1}\bar{1}2\rangle_{\alpha'}$ component of the rolling texture and was therefore derived from $\{111\}\langle\bar{1}\bar{1}2\rangle_{\alpha'}$ by a reverse martensite transformation.

It seems unlikely, however, that only one component of the martensite rolling texture should transform to austenite by a reverse martensite process.

A somewhat different annealing process occured in the 18%Cr 10%Ni steel examined by Dickson and Green[87]. After ½hr at 500°C new orientations appeared in the austenite, ~{230}<3$\bar{2}$1> and ~{112}<$\bar{1}\bar{1}$1>. The remainder of the texture consisted of a spread between {110}<$\bar{1}\bar{1}$2> and {110}<001>. The texture was essentially the same after ½hr at 600°C, but after ½hr at 700°C the intensity of ~{110}<$\bar{1}$12> and ~{230}<3$\bar{2}$1> components had increased and a further component appeared, ~{230}<3,$\bar{2}$,13>. At 800°C the intensity of this orientation increased, at the expense of the ~{110}<$\bar{1}$12> component. After ½hr at 900°C or 1hr at 1000°C, the texture could be described by two distributions of orientations, one being near {230}<3$\bar{2}$1> and containing {430}<$\bar{3}$40; the other near {230}<3,$\bar{2}$,13> and containing {430}<001>. Dickson and Green[87] concluded that formation of the annealing texture consisted of reverse transformation of all orientations in the martensite rolling texture, followed by recrystallisation in the austenite according to an oriented growth process.

4.3 Effect of Second Phases on Recrystallisation Textures.

With respect to rolling temperatures in the range 600-800°C, when the pure metal rolling texture is formed, Goodman and Hu[88] found that an important consideration was the distribution of carbide phases, which precipitate in the temperature range 500-800°C. After rolling at 600°C, transition was almost as complete as in specimens rolled at 800°C, but on annealing at 900°C cube texture was formed only in the strip which had been rolled at the higher temperature. Rolling at 600°C produced a fine dispersion of carbides, visible only by electron microscopy, whereas rolling at 800°C cause extensive precipitation of large particles which were optically visible. It was concluded that the finely dispersed carbides had impeded the growth of cube-oriented grains.

PART II

A STUDY OF FACTORS INFLUENCING THE COLD ROLLING AND PRIMARY RECRYSTALLISATION TEXTURES OF AUSTENITIC STAINLESS STEELS.

1. Introduction.

Previous results obtained for stainless steels still leave some doubt concerning development of textures in metastable alloys. For instance, the $\{111\}\langle\bar{1}\bar{1}2\rangle + \{112\}\langle\bar{1}10\rangle$ martensite rolling texture reported by Dickson and Green[87] for 18%Cr 12%Ni steel has not been confirmed, and it is not absolutely clear why the $\{001\}\langle\bar{1}10\rangle$ component should be missing. If this observation was significant, other changes might be expected to occur as the austenite stability is increased, but previously it was not possible to determine the texture of martensite in 18%Cr 14%Ni steel. Also, recrystallisation from the duplex rolling texture of metastable alloys is complicated by occurrence of the reverse martensite reaction. The process has not been analysed in detail and there remains disagreement between the results of Dickson and Green[87] and those of Goodman and Hu[88].

One of the aims of the present work was to resolve the above problems by re-examining the cold rolling and primary recrystallisation textures of high purity alloys. The experimental technique which has been used achieved much better resolution of diffracted radiation than was obtained previously, so that textures could be determined when as little as ~5% of a phase was present. Particular attention was given to the rôle of the martensite transformation and the overall development of primary recrystallisation textures.

A second aim of the experimental work was to compare textures of the high purity steels with those of some commercial alloys, which included carbide-stabilised varieties. Because of the higher carbon levels of commercial alloys in general, and the presence of NbC and TiC in stabilised steels, austenite stability as a function of composition can vary according to the type of heat treatment prior to cold rolling. Furthermore, morphology of undissolved carbides will be influenced by rate of cooling from the solution treatment temperature i.e. annealing would differ

the solution treatment temperature i.e. annealing would allow formation of some intergranular carbide phases which could affect subsequent recrystallisation behaviour, whereas quenching would tend to suppress this effect. To allow for these changes, two extremes of both solution treatment temperature and rate of cooling were studied as variables. The rôle of niobium, titanium and molybdenum in stabilised steels was analysed by comparison with unstabilised alloys.

Finally, the effect of increasing temperature of rolling is well established[11], but there has been no work carried out on the effect of sub-zero rolling, which would decrease austenite stability and might alter development of the martensite rolling texture. This variable has been studied using selected alloys only.

2. Materials.

Compositions of steels used are given in Tables 1 and 2. The 18/10, 18/12 and 18/14 alloys were supplied in the form of ½in. forged slabs which had been annealed for 1 hour at 1050°C. Other laboratory alloys, 18/12/Co and 18/25, were supplied as hot rolled ½in. strip. The commercial alloys were all received as ½in. strip in the hot rolled, softened and descaled condition.

3. Pickling.

To maintain a clean surface the laboratory alloys were first pickled in a boiling solution of 5% nitric acid/30% hydrochloric acid/65% water. During subsequent processing of all alloys pickling was carried out after every heat treatment.

4. Preliminary Treatments.

Some preliminary treatments were carried out to minimise the presence of initial texture. For the 18/10, 18/12 and 18/14 alloys these consisted of cold rolling ⅓30% followed by annealing for 1 hour at 1050°C, the sequence being repeated down to a thickness of 0·2in. The other steels were annealed for 1 hour at 1050°C and cold rolled to 0·2in.

5. Experimental Techniques.

5.1. Rolling and Annealing.

For the laboratory alloys and unstabilised commercial steels the following initial heat treatments were used :-

(a) 1 hour at 1050°C, furnace cooled.

(b) 1 hour at 1050°C, water quenched.

Additional treatments used for the carbide-stabilised steels were :-

(c) 15 minutes at 1300°C, furnace cooled.

(d) 15 minutes at 1300°C, water quenched.

Samples of 18/10, 18/12 and 18/14 steels were cold rolled to 95% reduction, with the material being reversed end-to-end between passes and oil lubrication to minimise surface friction.

The 95% reduction was achieved with difficulty, by repeatedly passing small pieces (2in)long) of 90% reduced material. For a strict definition of room temperature rolling, intermittent cooling of the strip was applied as necessary. During the rolling, specimens were cut from each strip after reductions given by $\log_e t_o/t_x$ = a multiple of 0·5, where t_o and t_x represent, respectively, initial and final thicknesses. Specimens of 90% and 95% cold rolled strip were annealed for $\frac{1}{2}$ hour at temperatures in the range 500-900°C.

The other alloys were cold rolled to 90% reduction, and annealed as above.

Selected alloys (18/10 and FCB)were rolled at approximately -196°C. This was achieved by cooling the strip in liquid nitrogen after every 6 passes up to 30% reduction, then after every 2 passes between 30% and 70%, and then after every single pass up to 90% reduction. The material was reversed end-to-end as before but no lubrication was used. Specimens were annealed as above.

5.2. Determination of Texture Parameters.

Samples having the initial heat treatments (defined in 5.1) were machined on one side only to a thickness of 0·15in., followed by grinding and etching for one minute in boiling 5% nitric acid/ 30% hydrochloric acid/65% water. To define these effective statting conditions, texture parameters were calculated from measurements obtained using a Philips X-ray generator and vertical diffractometer. Definition and significance of these parameters together with experimental details are discussed in the Appendix.

5.3. Determination of Pole Figures.

Quantitative pole figures were determined by the Schulz X-ray reflection method using a Siemens X-ray generator and texture gonionmeter.

The Siemens goniometer is a two-circle instrument which uses counter techniques for X-ray detection. The principal features may be seen in Figures 3(a) and 3(b). The primary X-ray beam passes through the aperture collimating slit system (1)and the horizontal slit (2) before irradiating the specimen (3) which is mounted on a rotation assembly (4) at the centre of the large vertical ring (5). When the vertical ring (5) is set at the appropriate Bragg angle, θ, to the primary X-ray beam, the diffracted beam passes through the counter tube collimating slits (6) and into the counter tube (7), which is set at an angle 2θ to the primary beam. The diffracted radiation received by the counter is derived solely from those lattice planes whose normals bisect the angle between incident and diffracted beams.

The whole rotation assembly (4) is shuttled to and fro a distance of 15mm. once every second and, with each shuttle action, a ratchet mechanism (8) rotates the specimen 1° about the normal to its surface. Thus a complete rotation of the specimen takes place in 6 minutes. At the same time, the vertical ring which carries the specimen rotation assembly is rotated by a second ratchet assembly (9) about the normal through the centre of the ring. The resultant tilt of the specimen is usually 5° in 6 minutes.

As a result of the shuttling of the specimen, an area approximately 15mm. square can be irradiated, thus reducing the chance of a non-representative selection of crystals being examined. The rotation and simultaneous tilting of the specimen is such that the normals to the reflecting planes can be plotted on a spiral path on a pole figure.

As the angle of tilt increases up to 50° the change in absorption of the X-ray beam is exactly cancelled by a change in the volume of diffracting material i.e. no correction is required for intensity values up to 50° from the centre of the pole figure. In practice, the slight loss of intensity between 50° and 70° is so small that it can be neglected, but above 70° serious defocussing of the Bragg reflection occurs. As a consequence, the peripheral regions of the pole figure cannot be determined withthe same accuracy. However, by allowing for the theoretical decrease in intensity[90], reasonable accuracy can be obtained in the range 70-85° from the rolling plane normal. Providing the measurements in this region are not used for comparison, they serve a useful purpose in completing the definition of texture.

{200} pole figures of the cold rolling and annealing textures were obtained using MoK_{α} radiation monitored by a scintillation counter. Specimen preparation involved grinding and etching to a section approximately midway between surface and centre of the strip.

The intensity contours on all pole figures have been labelled in multiples of the random level corresponding to a specimen with randomly oriented grain structure. To obtain this interval, it is necessary to measure both the zero and random levels of diffracted radiation. Zero level was assessed as the average of background levels obtained by offsetting the counter tube arm on either side of the 2θ position. The random level was checked by two methods, by using as "random" specimens those having the initial heat treatments, and by total integration of diffracted intensity over the whole area of the pole figure assuming the decrease after 70° to be linear.

Reproducibility of both zero and random levels was to within ± 5%, so that the accuracy of intensity contours is approximately ± 10%.

To provide supplementary information on textural changes during annealing, intensities of individual components have been assessed from point measurements taken from pole figure data. Such measurements must always be used with caution because the intensity at any point on a pole figure is a function of an effectively infinite number of individual crystal orientations. However, by careful choice of the pole positions of given orientations in a particular texture, reliable semi-quantitative measurements can be obtained which are at least proportional to the relative intensities of distributions centred on the orientations in question. Intensities of the following orientations have been assessed from measurements at positions indicated by $I(\alpha^\circ+\beta^\circ)$, where α is the angle from the rolling plane normal and β is the rotation about the rolling plane normal.

Component	Intensity Measurement
$\{112\}\langle\bar{1}10\rangle$	$2XI(35^\circ+90^\circ)$
$\{111\}\langle\bar{1}\bar{1}2\rangle$	$2 \times I(55^\circ)$
$\{001\}\langle\bar{1}10\rangle$	$I(0^\circ)$
$\{110\}\langle\bar{1}12\rangle$	$2 \times I(45^\circ + 55^\circ)$
$\{110\}\langle001\rangle$	$I(45^\circ + 90^\circ)$
$\{230\}\langle3,\bar{2},14\rangle$	$4 \times I(55^\circ+75^\circ)$
$\{6,8,17\}\langle\bar{5}\bar{7}5\rangle$	$4 \times I(65^\circ + 40^\circ)$
$\{6,10,1\}\langle\bar{5}\bar{3}1\rangle$	$4 \times I(60^\circ + 15^\circ)$
$\{225\}\langle\bar{5}\bar{3}3\rangle$	$2 \times I(30^\circ)$

5.4 Phase Analysis of Austenite and Martensite.

Phase analysis of the cold rolled and annealed specimens was carried out using the Philips X-ray generator and vertical diffractometer. Theory of the method and examples of calculations are given in the Appendix.

5.5 Determination of Diffraction Line Profiles.

Lattice re-arrangement during the early stages of annealing was studied from line profiles of selected Bragg reflections. The diffractometer was used, with a very slow scanning speed of $\frac{1}{8}^{\circ}$ per minute.

5.6 Vickers Hardness Measurements.

Vickers hardness measurements were made on the cold rolled and annealed specimens.

5.7 Optical and Electron Metallography.

Selected samples only were examined.

Optical metallography was carried out using the Vickers projection microscope. Specimen preparation involved polishing to 1μ followed by electrolytic etching in 10% oxalic acid at 2-4 volts using the specimen as anode and a stainless steel cathode.

Electron metallography was carried out using the Jeol 6A electron microscope. Specimens of rolled and annealed sheet were thinned to 0·010in. in boiling 30% hydrochloric acid/5% nitric acid/ 65% water, and then ground to grade 600 silicon carbide paper. Discs 3mm. in diameter were punched out and chemical thinning and polishing was done using a Polaron instrument. Thinning was carried out in 25%perchloric acid/75%methanol at 17 volts with a jet of electrolyte impinging on one side only to produce a dished shape. This was repeated for the other side. Subsequent polishing was done in a seperate cell using 10%perchloric acid/90%methanol at 5 volts until a hole was just visible. The region near the perforation was examined in transmission.

5.8 Identification of Carbide Extracts.

This was intended as a confirmatory examination of the carbide phases which occur in these steels rather than a detailed investigation of the effect of solution treatment and recrystallisation annealing. One sample only from selected alloys was examined. The phases were extracted electrolytically in 5% hydrochloric acid/95% water using a current density of $\sim$ 0·25 amps.in.$^{-2}$ Qualitative identication was made from diffractometer patterns.

6. Results.

6.1 Cold Rolling and Annealing Textures.

6.1.1 Laboratory Alloys.

Table 3 lists the texture parameters measured after preliminary rolling and annealing treatments. Deviations from the random level (=1) are marginal. These results show that each steel had an essentially random grain orientation prior to cold rolling, so that subsequent influence of initial texture as a variable can be dismissed.

Figure 4 shows the progress of martensite formation during rolling of 18/10, 18/12 and 18/14 alloys. Each steel shows first an "incubation period" during which the Ms is raised to room temperature. Maximum amount of martensite is formed by ~90% reduction: further rolling to 95% reduction should therefore merely sharpen the texture about the principal orientations. Measured intensities were actually slightly higher after 95% reduction but the difference was marginal, being only of the same order as differences between the full range of laboratory and commercial alloys after 90% reduction.

{200} pole figures are shown for the 18/10, 18/12 and 18/14 steels after 95% cold rolling. Because of experimental difficulties in achieving this reduction, other alloys have been examined after 90% reduction only.

18%Cr 10%Ni steel

Figures 5 and 6 show the {200} pole figures of 18%Cr 10%Ni steel after 95% cold rolling. The α' texture (Figure 5) really consists of two fibre components, i.e. a <111> fibre component normal to the rolling plane and an incomplete <110> fibre texture parallel to the rolling direction. In terms of ideal orientations, the principal components are $\{112\}\langle\bar{1}10\rangle_{\alpha'}$ and $\{111\}\langle\bar{1}\bar{1}2\rangle_{\alpha'}$. There is also spread towards a minor $\{001\}\langle\bar{1}10\rangle_{\alpha'}$ component. The austenite exhibits a normal f.c.c. alloy type of texture, viz $\{110\}\langle\bar{1}12\rangle$ + a minor $\{110\}\langle 001\rangle$ component. (Figure 6)

Physical changes taking place within the martensite during annealing are indicated by figures 7 and 8. Figure 7 compares the relative intensities of principal α' texture components. These measurements have been made using identical instrument settings, so that they are a function not only of textural changes but also of the amount of martensite present. The $\%\alpha'$ curve has been superimposed to demonstrate this effect. The essential feature of Figure 7 is the increase in intensity of all components after ½ hour at 500°C, when the amount of martensite has actually decreased slightly. This can only be related to the onset of recovery, causing sharpening of the α' texture. Further evidence of recovery within the martensite is provided by figure 8, which shows profiles of the 200 α' reflection. These curves were also obtained with identical instrument settings, so that the general decrease in line intensity results fromthe decreasing amount of martensite. A sriking feature is that recovery starts at ~500°C, but there is no evidence of recrystallisation within the martensite at 600°C. At 700°C, the amount of martensite is so small that recrystallisation cannot be entirely eliminated but the breadth of the line does suggest that the amount of recrystallisation, if any, is minimal.

Figures 9-12 show the $\{200\}\gamma$ pole figures after cold rolling and annealing. After annealing for ½ hour at 500°C, ~6%α' has transformed to γ(Figure 7) with a corresponding change in the austenite texture (Figure 9). One of the peak distributions is now centred on $\{110\}<001>$ with spread towards $\{110\}<\bar{1}12>$. For reasons which will become evident during the discussion, the orientations $\{110\}<\bar{5}57>$, $\{430\}<001>$ and $\{430\}<\bar{6},8,17>$ are also shown as belonging to this part of the texture. The other high intensity region in Figure 9 is not so clearly defined: it is centred on orientations close to $\{6,8,17\}<\bar{5}\bar{7}5>$ but includes considerable spread towards $\{430\}<\bar{3}40>$. Again, this will later be shown to be quite significant.

After annealing for ½ hour at 600°C only ~10%α' remains (Figure 7). The texture remains the same (Figure 10) but intensities

are significantly higher and the distribution of orientations is more clearly defined.

At 700°C the martensite has almost disappeared (Figure 7) and further textural changes are evident in the austenite. Figure 11 shows that after annealing for ½ hour at 700°C, in the region $\{110\}\langle\bar{1}12\rangle$ - $\{110\}\langle 001\rangle$, the distribution of intensity has changed and the general level of intensity has decreased. At the same time, in the region of $\{430\}\langle\bar{3}40\rangle$, the intensity has increased.

The positions of $\{230\}\langle 3,\bar{2},14\rangle$ and $\{6,10,1\}\langle 5\bar{3}1\rangle$ orientations are also indicated in figure 11, to show that they lie within the general spread of texture at this stage. The intensity of these components increases after annealing at 800°C, and after ½hour at 900°C (Figure 12) they emerge as major components of the recrystallisation texture. There still remains a considerable spread towards other orientations, particularly those of the type $\{6,8,17\}\langle\bar{5}\bar{7}5\rangle$.

Figure 13 compares intensities of important γ orientations during the annealing cycle and figure 14 shows the variation in profile of the 220γ reflection. The slight increase in line intensity at 500°C (Figure 14) could be partly due to a decrease in the amount of martensite: a positive deduction of the onset of recovery is therefore not possible. However, having identified recovery within the martensite at 500°C, it is reasonable to assume that it has also started in the austenite at this temperature. (This is further confirmed when the results for 18%Cr 12%Ni and 18%Cr 14%Ni steels are considered, since in these alloys textural changes in the austenite do not mask the effect of onset of recovery on line profile). Recovery within the austenite is certainly evident at 600°C and is associated with the very high intensities in figure 10. Returning to figure 13, we see that the initial increase in intensity of $\{110\}\langle 001\rangle$ and $\{110\}\langle\bar{1}12\rangle$ coincides with the transformation of $\alpha'\rightarrow\gamma$, with recovery taking place simultaneously in both phases. The intensities of $\{6,10,1\}\langle 5\bar{3}1\rangle$, $\{6,8,17\}\langle\bar{5}\bar{7}5\rangle$ and $\{230\}\langle 3,\bar{2},14\rangle$ components increase during the recovery range and continue to

increase up to 900°C. The intensities of $\{110\}\langle\bar{1}12\rangle$ and $\{110\}\langle 001\rangle$ decrease during recrystallisation.

18%Cr 12%Ni steel

Rolling textures of both α' and γ phases remain the same as the nickel content is increased within the composition range of metastable alloys. Figure 15 shows that the γ texture of 18%Cr 12%Ni steel is the same as that in 18%Cr 10%Ni steel. Figure 16 shows that the α' texture is also similar but its intensity is slightly lower than in the previous alloy.

The 18%Cr 12%Ni steel recrystallises to a $\{225\}\langle\bar{5}\bar{3}3\rangle$ texture. This is shown in the $\{200\}\gamma$ pole figure after annealing for ½ hour at 900°C (Figure 17). Changes taking place during annealing are shown in Figures 18 and 19. When the results of 18%Cr 14%Ni steel have been considered, it will be appreciated that the marked increase in intensity of $\{110\}\langle\bar{1}12\rangle$ and $\{110\}\langle 001\rangle$ rolling texture components of 18%Cr 12%Ni steel at 600°C (Figure 18) is due partly to recovery and partly to the large increase in amount of austenite at this temperature. The small but significant increase in intensity of $\{225\}\langle\bar{5}\bar{3}3\rangle$ at 600°C arises solely from the $\alpha'\rightarrow\gamma$ transformation. Pronounced textural changes take place at higher temperatures to establish the $\{225\}\langle\bar{5}\bar{3}3\rangle$ recrystallisation texture. These results are amplified by the $\{220\}\gamma$ line profiles (Figure 19), which show that recovery within the austenite starts at ~500°C, becomes much more pronounced at 600°C, but is followed by recrystallisation between 600°C and 700°C.

18%Cr 14%Ni steel

Rolling textures of 18%Cr 14%Ni steel (Figures 20 and21) are similar to those of 18%Cr 12%Ni steel.

The recrystallisation texture (Figure 22) is also similar but slightly better defined. There are, however, important differences when the changes during annealing are considered. At 600°C, the increase in intensity of $\{110\}\langle\bar{1}12\rangle$ and $\{110\}\langle 001\rangle$ (Figure 23) is due mainly to recovery, since the small amount of martensite which has transformed at this temperature would be insufficient

to account for this increase in texture intensity. Also, at this temperature, there is complete absence of intensity in the region of $\{225\}<\bar{5}\bar{3}3>$. Appearance of this orientation is delayed until recrystallisation occurs. (Figures 23 and 24)

18%Cr 12%Ni 7%Co steel

In terms of austenite stability this alloy is similar to 18%Cr 14%Ni steel. Accordingly the cold rolling and annealing textures are the same (Figures 25 and 26) and changes during annealing follow a similar trend (Figures 27 and 28).

18%Cr 25%Ni steel

This alloy is a fully stable austenite which exhibits the standard f.c.c. alloy texture on cold rolling (Figure 29) and the corresponding $\{225\}<\bar{5}\bar{3}3>$ recrystallisation texture after annealing (Figure 30). Changes during annealing (Figures 31 and 32)remain the same as in 18%Cr 14%Ni steel.

6.1.2 Commercial Alloys.

Table 4 lists the texture parameters measured after preliminary rolling and annealing treatments. In some cases deviations from the random level are marginally greater than for the laboratory alloys, but the differences are not significant. For practical purposes, each steel can be considered as having an essentially random structure prior to cold rolling and again subsequent influence of initial texture can be neglected.

Figure 33 shows the progress of martensite formation during rolling for a selection of the alloys. The trends are obviously the same as for laboratory alloys. A new feature is shown by the behaviour of FCB steel after annealing at 1050°C, i.e. complete transformation to α' martensite occurs during rolling.

Cold rolling textures are typified by the examples of pole figures shown in Figures 34-36. After initial heat treatment at 1050°C, the α' texture of FCB steel is different (Figure 34). The intensities of $\{112\}<\bar{1}10>$ and $\{111\}<\bar{1}\bar{1}2>$ components are now equal and the intensity of $\{001\}<\bar{1}10>$ has increased by comparison

with (say) the 18%Cr 10%Ni steel. However, if the initial heat treatment is at 1300°C, the texture (Figure 35) is similar to that of the laboratory alloys. Other commercial alloys exhibit α' rolling textures similar to Figure 35, and the full results are summarised in Table 5, as relative intensities of the principal components.

Austenite rolling textures of the commercial alloys are all of the f.c.c. alloy type, and are typified by the $\{200\}_\gamma$ pole figure of RF310 steel after annealing at 1050°C (Figure 36).

On the basis of recrystallisation behaviour the commercial steels fall into two groups. The unstabilised steels (RF310, FST(L) and FSL(L)) recrystallise in a manner similar to the laboratory alloys of equivalent metastability. On the other hand, the carbide-stabilised varieties (FCB, SF347, FDP, FMB and FMBTi) do not undergo the same re-orientation during annealing. Instead, the final re-crystallisation texture is formed largely by retention of the γ cold rolling texture and/or retention of the γ texture immediately after transformation from the martensite. Table 6 lists the $\%\alpha'$ after cold rolling and summarises the recrystallisation textures in terms of three ideal orientations, $\{225\}\langle\bar{5}\bar{3}3\rangle$, $\{110\}\langle\bar{1}12\rangle$ and $\{110\}\langle 001\rangle$. For some of the textures, this description is oversimplified but the relative intensities of these components throughout serve as a useful guide to differences between the various alloys and to the effect of different initial heat treatments applied to individual alloys. The $\{225\}\langle\bar{5}\bar{3}3\rangle$ orientation is very close to $\{6,8,17\}\langle\bar{5}\bar{7}5\rangle$ which was used to describe textures in 18%Cr 10%Ni steel. For simplicity, only the $\{225\}\langle\bar{5}\bar{3}3\rangle$ position is shown on pole figures of the commercial steels but it is recognised that the intensity measured in this position in some cases represents a wide spread of orientations which include those originating from the α' martensite texture by transformation.

RF310 steel.

This steel represents a fully stable austenite. The recrystallisation texture after annealing at 1050°C (Figure 37) is of the $\{225\}\langle\bar{5}\bar{3}3\rangle$ type. The transition is marginally less complete than in its laboratory counterpart, 18%Cr 25%Ni, since there still remains some spread of orientations in the region of the γ rolling texture. This point is also illustrated in Figure 38, where the intensities of $\{110\}\langle\bar{1}12\rangle$ and $\{110\}\langle 001\rangle$ remain at a higher level at 900°C. The mechanism of development of the recrystallisation texture is similar to the laboratory alloys, with recovery causing sharpening of the rolling texture at 600°C and giving way to recrystallisation by re-orientation at higher temperatures(Figures 38 and 39). Figure 40 shows that water quenching from 1050°C has negligible effect. Intensities of $\{225\}\langle\bar{5}\bar{3}3\rangle$, $\{110\}\langle\bar{1}12\rangle$ and $\{110\}\langle 001\rangle$ components are the same (Table 6).

FST(L) steel

This is a fairly stable alloy; only ~10%α' is formed during cold rolling (Table 6). Again the recrystallisation texture after annealing at 1050°C is of the $\{225\}\langle\bar{5}\bar{3}3\rangle$ type (Figure 41) and transition is less complete than for (say) the 18%Cr 14%Ni laboratory alloy. Mechanism of development of the recrystallisation texture remains the same (Figures 42 and 43) and water quenching from 1050°C has negligible effect (Figure 44 and Table 6).

FSL(L) steel

The composition of this alloy is similar to that of FST(L) steel. This is reflected in the results shown in Figures 45-48 and in the texture intensities given in Table 6 which establish a similar annealing behaviour.

FCB steel

After initial annealing at 1050°C, FCB steel completely transforms to α' martensite during rolling, and the ratio of principal α' texture components is different by comparison with more stable austenites (Table 5).

Changes taking place within the martensite during annealing are similar to those observed for 18%Cr 10%Ni steel. Figures 49 and 50 show that, during subsequent annealing at 500°C, the intensities of α' components are increased by recovery, but there is no evidence of recrystallisation within the martensite at 600°C. (Figure 50). At 700°C, the amount of martensite is again so small that recrystallisation cannot be entirely eliminated, but the breadth of the line still suggests that the amount of recrystallisation, if any, is minimal.(Parallel observations were made on other alloys to establish this as a general effect).

Figures 51-55 indicate changes taking place within the austenite during annealing. Figure 51 shows the $\{200\}\gamma$ pole figure after $\frac{1}{2}$ hour at 600°C, when there still remains ~12%martensite in the structure. This pole figure therefore represents the texture of austenite derived entirely from martensite. Description of the texture in terms of ideal orientations is the same as for the 18%Cr 10%Ni steel. The main differences are that the intensities of $\{110\}<001>$ and $\{110\}<\bar{1}12>$ type orientations are lower in FCB steel. Figure 52 shows that a large part of the texture at 600°C is retained at 900°C, notably the $\{110\}<001>$- $\{110\}<\bar{1}12>$ spread, but the intensity of $\{225\}<\bar{5}\bar{5}3>$ type components is now considerably lower and the spread towards $\{430\}<\bar{3}40>$ has disappeared. The decrease in intensity of $\{225\}<\bar{5}\bar{5}3>$ corresponds with increasing intensity of $\{110\}<001>$ (Figure 53). The 220γ line profiles (Figure 54) show that recrystallisation begins between 600°C and 700°C when this change occurs. However, the 220γ line intensity after $\frac{1}{2}$ hour at 700°C has increased whereas the corresponding series of line profiles for 18%Cr 10%Ni steel shows a decrease in intensity at this temperature. This suggests a different mechanism of recrystallisation in FCB steel.

Water quenching from 1050°C has negligible effect on the recrystallisation texture (Figure 55 and Table 6).

Annealing at 1300°C causes greater solution of carbon and alloying elements to produce a more stable austenite. During subsequent cold rolling only ~87%α' is formed (Table 6). The main changes in the corresponding recrystallisation texture (Figure 56) are a higher intensity of $\{225\}<\bar{5}\bar{3}3>$ and a lower intensity of $\{110\}<001>$.

Water quenching from 1300°C causes even greater solution of carbides, ~71%α' being formed during rolling. However, the recrystallisation texture remains essentially the same, as shown by the pole figure (Figure 57) and the intensities of principal texture components (Table 6). Figure 58 shows that the $\{225\}<\bar{5}\bar{3}3>$ orientation originates during the $\alpha \rightleftharpoons \gamma$ transformation, and after the transformation is complete there is no major change of texture.

SF347 steel

After annealing at 1050°C, SF347 steel transforms to ~85%α' during cold rolling (Table 6). The corresponding recrystallisation texture (Figure 59) consists largely of $\{225\}<\bar{5}\bar{3}3>$ with spread towards $\{110\}<\bar{1}12>$ and a minor $\{110\}<001>$ component. The texture is similar to FCB annealed at 1300°C. Similarity in behaviour is further confirmed when the intensities of principal γ components and the variation of 220γ line profile are considered (Figures 60 and 61). Water quenching causes only a slight decrease in the amount of martensite (Table 6) and the recrystallisation texture remains the same (Table 6 and Figure 62).

Annealing at 1300°C causes appreciable solution of carbides, since only ~35%α' is formed during rolling (Table 6). The recrystallisation texture is now quite different (Figure 63), consisting mainly of $\{110\}<\bar{1}12>$ with $\{225\}<\bar{5}\bar{3}3>$ and $\{110\}<001>$ both of lower intensity. Water quenching from 1300°C produces a similar texture (Table 6 and Figure 64). The stability of the austenite after initial treatment at 1300°C is approximately equivalent to the 18%Cr 12%Ni laboratory steel, but the mechanism of recrystallisation as shown by intensities of principal

components (Figure 65) is quite different. During the annealing cycle the $\{110\}\langle\bar{1}12\rangle$ + $\{110\}\langle001\rangle$ rolling texture orientations are not removed by re-orientation and remain as major components of the recrystallisation texture. The initial increase in intensity of $\{225\}\langle\bar{5}\bar{3}3\rangle$ arises from transformed martensite but in contrast to 18%Cr 12%Ni steel growth of this orientation is suppressed.

FDP steel

The trend of recrystallisation textures of the previous steel is repeated in the behaviour of FDP steel. After initial treatment at 1050°C, the results are similar.(Figures 66-69).

After treatment at 1300°C, only ~ 9%α' is formed during rolling (Table 6) and the main difference in annealing texture is the slightly higher intensity of $\{110\}\langle001\rangle$ (Table 6, Figures 70 and 71). Figure 72 shows that the γ rolling texture orientations are largely retained during recrystallisation.

FMB steel

This is a fairly stable steel, equivalent to the 18%Cr 14%Ni laboratory alloy. Only ~2%α' is formed during rolling of FMB (Table 6)

The recrystallisation texture after annealing at 1050°C (Figure 73) is essentially a retained γ cold rolling texture, consisting of $\{110\}\langle\bar{1}12\rangle$ + $\{110\}\langle001\rangle$ orientations. There is also a spread of low intensity towards $\{225\}\langle\bar{5}\bar{3}3\rangle$ which,of course, does not appear in the rolling texture. Figure 74 shows that this orientation appears between 700°C and 800°C, but growth is resricted such that the rolling texture orientations are retained with little loss of intensity. Figure 75 shows that recrystallisation occurs between 700°C and 800°C, but in contrast to (say) 18%Cr 14%Ni steel, the same orientations are largely retained.

Other treatments produce the same recrystallisation texture (Table 6, Figures 76-78).

FMBTi steel

This is the titanium bearing equivalent of FMB. The textures

and recrystallisation behaviour are the same (Figures 79-84).

6.1.3 Effect of Rolling at Lower Temperatures.

Figures 85-88 show the effect of rolling at ~-196°C on the textures of 18%Cr 10%Ni and FCB steels.

The 200 α' pole figure of 18%Cr 10%Ni steel rolled to 90% reduction (Figure 85) indicates that the relative intensities of $\{001\}\langle\bar{1}10\rangle$ and $\{111\}\langle\bar{1}\bar{1}2\rangle$ are increased (Also the amount of α' formed during rolling was increased to 100%). The recrystallisation behaviour, however, was similar to the sample rolled at room temperature.

More pronounced differences are exhibited by FCB steel. After initial annealing at 1050°C, the rolling texture at -196°C (Figure 86) shows a much greater increase in intensity of the $\{001\}\langle\bar{1}10\rangle$ component with a decrease in intensity of $\{111\}\langle\bar{1}\bar{1}2\rangle$. The subsequent recrystallisation texture is also different (Figure 87) The main component is now $\{110\}\langle\bar{1}12\rangle$ with $\{110\}\langle 001\rangle$ and $\{225\}\langle\bar{5}\bar{3}3\rangle$ at secondary intensity. Development of the texture is still largely by retention of the texture formed at lower temperatures (Figure88).

6.2 Hardness Curves.

Figures 89-96 show hardness curves for the commercial steels. In general, the observed variations in hardness confirm deductions made previously from line profiles. i.e. recovery occurs ~500°C and, with the exception of FMB and FMBTi steels, recrystallisation occurs over the range 600°C-900°C. Throughout the series of alloys the highest recrystallisation annealing treatment, ½ hour at 900°C is sufficient to produce essentially complete recrystallisation. (Hardness curves were also determined for the laboratory alloys but the results were similar to (say) RF310 commercial steel).

For the unstabilised alloys (Figures 89-91), rate of cooling from 1050°C again has little effect on hardness and there are no significant differences between the steels.

For the stabilised alloys (Figures 91-96), rate of cooling from 1050°C again has little effect. In some cases (FCB, SF347 and FMBTi) water quenching from 1300°C retains a higher hardness than

furnace cooling, but the difference is not great. The main effect of the stabilising elements is that a higher hardness is retained at 700°C by comparison with unstabilised alloys. This is most noticeable in FMB and FMBTi steels (Figures 95 and 96) where the alloys are still in the recovery stage at 700°C.

6.3 Metallographic Observations.

Table 7 gives grain sizes of the commercial steels measured after initial heat treatment and after subsequent cold rolling and annealing.(Measurements made on laboratory alloys were similar to results shown for the unstabilised steels). Initial grain sizes vary within a factor of 8 while those after cold rolling and annealing vary within a factor of 4. Although initial treatment at 1300°C promotes noticeable grain growth, after cold rolling and annealing the grain size is similar to that in other samples.

Useful comments on the optical metallography are limited to effects of the initial solution treatments. This is because subsequent cold rolling merely breaks up any existing distribution of undissolved particles with the result that only the quantity of undissolved phases, or conversely the extent of their solution in the matrix, remains as a variable to be considered in discussion.

The main effects are typified by the areas shown in Figures 97-99. For the unstabilised steels, furnace cooling from 1050°C left a fine network of grain boundary carbides (~0·5μ), whereas water quenching tended to suppress such precipitation leaving only the original undissolved carbides (~1-2μ) in the matrix (Figure 97). The amount of undissolved particles was much greater in RF310 than in FST(L) and FSL(L) steels.

The niobium and titanium stabilised steels (FCB, SF347 and FDP), in addition to some fine grain boundary carbides, showed more massive grain boundary networks (~1μ) after annealing at 1050°C (Figure 98), but solution treatment at 1300°C removed much of this. FMBTi steel behaved in a similar manner to these alloys.

FMB steel showed almost complete solution of large carbides

after all heat treatments e.g. Figure 99 shows the fine grain boundary particles produced during furnace cooling from 1050°C.

Table 8 gives the results of qualitative analysis of carbide extracts from selected alloys. For the unstabilised alloys, e.g. RF310, only $M_{23}C_6$ is involved. For the stabilised steels NbC, TiC and possibly Mo_2C can also occur.

It was the electron metallography which highlighted important differences between stabilised and unstabilised steels as regards precipitation and re-solution of precipitates during the annealing cycle. The observations are summarised by Figures 100-108, which show micrographs of thin foils taken from RF310, FCB and FMB steels.

Figure 100 indicates that recovery in RF310 steel is almost complete after ½ hour at 600°C. At 700°C, some precipitation occurs but this is more evident at 800°C. (Figure 101). At 900°C, however, most of this precipitate has re-dissolved leaving a matrix essentially free from fine precipitates (Figure 102).

Figures 103-105 consider a similar sequence for FCB steel. The area shown in Figure 103 has actually started to recrystallise at 600°C. Figure 104 shows some isolated fine particles at 700°C but precipitation is much more extensive at 800°C (Figure 105). After ½ hour at 900°C (Figure 106) precipitate particles (~0·1μ) are still present in the matrix.

A similar effect is demonstrated for FMB steel in Figures 107 and 108.

This retention of precipitate particles at 900°C by the stabilised steels is in complete contrast to the unstabilised steel which exhibits re-solution of particles at this temperature.

7. Discussion.

7.1 Rolling Textures.

Within the scope of the present work, there are no differences in cold rolling textures that could be attributed to differences in grain size or distribution of second phases. The comment about grain size is a general one since the observed variations would not be expected to have any effect, but the point is illustrated by the results for FMBTi steel where the initial grain size varies by a factor of 4 yet there are no real differences in the amounts of austenite and martensite or the textures of each phase. Initial texture has already been dismissed as a variable by ensuring an essentially random condition prior to cold rolling. Factors controlling the observed textures are therefore matrix (austenite) composition and temperature of rolling.

7.1.1 α' Martensite Rolling Textures.

During rolling at room temperature, except when the amount of martensite approaches 100%, relative intensities of principal components (Table 5) remain constant throughout the composition range of metastable alloys. It is interesting to compare the observed relative intensities of $\{112\}\langle\bar{1}10\rangle$, $\{111\}\langle\bar{1}\bar{1}2\rangle$ and $\{001\}\langle\bar{1}10\rangle$ components of the α' rolling texture with the intensities normally observed in b.c.c. rolling textures. The $\{001\}\langle\bar{1}10\rangle$ component usually dominates the rolling texture, but is reduced to secondary importance in the α' texture. This difference arises because the martensite in stainless steels is formed gradually: prior deformation of the austenite, involving development of its own texture, will influence subsequent grain rotations in the transformed martensite. Results for FCB steel rolled at room temperature, and 18%Cr 10%Ni and FCB steels rolled at $\sim -196^{\circ}C$, show that, if the martensite transformation is completed at an earlier stage of deformation, the final α' texture tends toward the normal b.c.c. type.

It was previously reported by Dickson and Green[87] that only $\{112\}\langle\bar{1}10\rangle$ and $\{111\}\langle\bar{1}\bar{1}2\rangle$ components were present in the

α' texture of 18%Cr 10%Ni steel, and they attributed absence of the $\{001\}\langle\bar{1}10\rangle$ component to delayed development of the b.c.c. rolling texture. This occurence, as shown by the present results, is certainly not general, and could have resulted from a small amount of initial texture, sufficient to alter significantly the sequence of texture development, since rolling was previously carried out directly after forging and annealing. In the present work, use of pretreatments to ensure a random starting condition has avoided this. Apart from this difference, other rolling textures reported by Dickson and Green[87] are confirmed by the present results.

7.1.2 Austenite Rolling Textures.

The austenite cold rolling textures of these alloys are controlled by the value of γ/Gb, and for the limited range of compositions only the variation of γ with composition needs to be considered. By working out the least squares fit of data from several workers Gallagher[91] has shown that $d\gamma/dNi \simeq 2{\cdot}6$ ergs. $cm.^{-2}$ $wt\%^{-1}$. Taking $\gamma 18/10 = 22$ ergs.cm^{-2}, this gives $\gamma 18/12 \simeq$ 27 ergs.cm^{-2} and $\gamma 18/14 \simeq 32$ ergs.cm^{-2}. Assuming $G = 7{\cdot}4 \times 10^{11}$ dynes.cm^{-2} and $a\gamma = 3{\cdot}59$ A° the corresponding values of γ/Gb are $1{\cdot}43 \times 10^{-3}$, $1{\cdot}76 \times 10^{-3}$ and $2{\cdot}09 \times 10^{-3}$ for the 18%Cr 10%Ni, 18%Cr 12%Ni and 18%Cr 14%Ni steels respectively. Silver, which is known to exhibit the f.c.c. alloy type of texture on rolling at room temperature, has $\gamma/Gb \simeq 3{\cdot}1 \times 10^{-3}$. It is not surprising, then, that the same texture is exhibited by the austenite ineach steel covering the range of metastability.

In the stable austenite range, 18%Cr 25%Ni steel also exhibits the alloy texture. From the same data $\gamma 18/25 \simeq 61$ ergs. cm^{-2} giving $\gamma/Gb \simeq 4 \times 10^{-3}$. At higher values of γ/Gb, approaching that of, say, copper ($\simeq 5{\cdot}3 \times 10^{-3}$), austenites should exhibit the pure metal type of texture when rolled at room temperature but there are no results to confirm this.

7.2 Primary Recrystallisation Textures of High Purity Iron-Chromium-Nickel Austenites.

Basically two different textures have been identified. The 18%Cr 10%Ni steel recrystallises to mainly $\{230\}<3,\bar{2},14>$ and $\{6,10,1\}<5\bar{3}1>$ orientations with considerable spread remaining in the region of $\{6,8,17\}<\bar{5}\bar{7}5>$, whereas 18%Cr 12%Ni, 18%Cr 14%Ni, 18%Cr 12%Ni 7%Co and 18%Cr 25%Ni steels recrystallise to a $\{225\}<\bar{5}\bar{3}3>$ texture. The obvious difference in rolling behaviour of the two sets of alloys is the much higher amount of martensite ($\sim$86%α') formed in 18%Cr 10%Ni steel than in 18%Cr 12%Ni steel ($\sim$32%α') and the other alloys.

7.2.1 Comparison with Previous Results.

The recrystallisation texture of 18%Cr 10%Ni steel was previously described (Dickson and Green[87]) as mainly $\{230\}<3,\bar{2},13>$ and $\{230\}<3\bar{2}1>$ components, which may be identified, respectively, with $\{230\}<3,\bar{2},14>$ and $\{6,10,1\}<5\bar{3}1>$ orientations used in the present work, these being a slightly better description of the peak positions. Similarly, the $\{225\}<\bar{5}\bar{3}3>$ texture of 18%Cr 12%Ni and 18%Cr 14%Ni steels was previously described[87] as $\{113\}<\bar{2}\bar{1}1>$. The results of Dickson and Green[87] are thus confirmed and those of Goodman and Hu[88] for 18%Cr 10%Ni steel remain anomalous.

7.2.2 Mechanism of Texture Development.

Formation of recrystallisation textures from the duplex ($\alpha'+\gamma$) rolling textures of metastable austenitic steels involves several stages. These are:-

1) recovery within the deformed austenite
2) recovery within the deformed martensite
3) formation of recrystallisation nuclei within the range of austenite rolling texture orientations
4) martensite to austenite shear transformation
5) variant selectivity during the transformation
6) recovery within the derived austenite
7) formation of recrystallisation nuclei within the range of transformed orientations

8) competitive growth of favourable orientations to form the final texture: this is influenced by the relative amounts of α' and γ formed during rolling.

Successive stages overlap, but the rôle of each can be discussed separately, in the general order of occurrence.

Recovery.

Recovery merely leads to sharpening of the existing texture about the principal orientations. This has been illustrated for both 18%Cr 10%Ni and 18%Cr 14%Ni extremes of the composition range of metastable alloys. Recovery within the martensite prior to transformation has an important bearing on the derived austenite texture. The effect is that, even with random selection of variants during the transformation, that part of the austenite texture derived from the martensite should be less diffuse. Continuation of recovery within the derived austenite leads to further texture sharpening before recrystallisation.

The Martensite Transformation.

The martensite transformation in stainless steels has been the subject of many research papers, and there has been much discussion on the reactions which seem possible, i.e. whether $\gamma \rightarrow \alpha'$ or $\gamma \rightarrow \varepsilon \rightarrow \alpha'$. It is generally considered that ε is a transition phase and that continuing deformation will transform it to α' martensite, so that the final product is the same in either case. The reverse transformation is simply $\alpha' \rightarrow \gamma$. In relation to development of polycrystalline textures it is the orientation relationships between γ and α' phases that are of interest rather than the mechanism of the transformation itself. Both the Kurdjumov-Sachs and Nishyama relationships have been reported,

the former $(111)_\gamma \parallel (110)_{\alpha'}$ and $[1\bar{1}0]_\gamma \parallel [1\bar{1}1]_{\alpha'}$

the latter $(111)_\gamma \parallel (110)_{\alpha'}$ and $[\bar{2}11]_\gamma \parallel [1\bar{1}0]_{\alpha'}$

The two orientations are related by a $5^\circ 16'$ rotation of the b.c.c. lattice about the $[110]_\alpha$ axis. Kelly and Nutting[92] and Venables[93] claimed to have identified the Kurdjumov-Sachs

relationship using electron diffraction patterns. A difficulty here is that the inaccuracy in orientation measurements based on this technique might amount to the difference between the two relationships, and it is now recognised that neither can be excluded by electron diffraction determination. Lagneborg[94] concluded that either could be involved. It is even possible that the actual relationships cannot be accounted for by parallelism between rational planes and directions. Accurate X-ray diffraction experiments by Breedis and Robertson[95] have shown that small but significant deviations from the Kurdjumov-Sachs relationship exist in a 16%Cr 12%Ni steel. They reported an orientation relationship where $(111)_\gamma$ is $0{\cdot}5^\circ$ from $(110)_{\alpha'}$ and $[1\bar{1}0]_\gamma$ is $0{\cdot}6^\circ$ from $[1\bar{1}1]_{\alpha'}$. Similar results were reported by Kelly[96] for 17%Cr 9%Ni steel. When relating transformation textures in polycrystals, differences of this order of magnitude may be ignored. Even the difference of $5^\circ 16'$ between the two relationships is itself sufficiently small to allow them to yield similar distributions of variant orientations after transformation. In view of this, and taking into account that the concensus of opinion and experimental results favours the Kurdjumov-Sachs relationship, the present discussion will be confined to interpretation of results in terms of this mechanism.

To interpret the γ texture immediately after reverse transformation, the martensite reaction will first be considered purely from a geometrical point of view, i.e. with complete random selection of variants. In any one crystal there are 24 possible variants of the Kurdjumov-Sachs relationship, giving rise to 24 new orientations from each parent orientation. These actually consist of 12 twin-related pairs, with both orientations of a pair having the same habit plane. The 24 orientations also fall into 3 groups of 8: within each group the orientations are relatively close together, the minimum and maximum angles between orientations being, respectively, 8° and 22°. Figures 109-111 show positions of the new orientations after transforming

from $\{001\}\langle\bar{1}10\rangle_{\alpha'}$, $\{111\}\langle\bar{1}\bar{1}2\rangle_{\alpha'}$ and $\{112\}\langle\bar{1}10\rangle_{\alpha'}$ starting orientations. Table 9 lists these orientations and describes the complete 24-variant solutions in terms of the 3 ideal orientations about which each group of 8 is positioned. The table also shows how the intensity changes as a result of transformation.

The $\{001\}\langle\bar{1}10\rangle_{\alpha'}$ component thus gives rise to one group of orientations centred on $\{100\}\langle 001\rangle_{\gamma}$ and two groups centred on twin-related $\{110\}\langle\bar{5}57\rangle_{\gamma}$ orientations (Figure 109).

The $\{111\}\langle\bar{1}\bar{1}2\rangle_{\alpha'}$ texture consists of two twin-related components, each of which gives rise to one group of orientations centred on $\{430\}\langle\bar{3}40\rangle_{\gamma}$ and two groups centred on twin-related $\{430\}\langle\bar{6},8,17\rangle_{\gamma}$ components. The combined effect (Figure 110) produces two twin-related $\{430\}\langle\bar{3}40\rangle_{\gamma}$ components and four components of the type $\{430\}\langle\bar{6},8,17\rangle_{\gamma}$.

Similarly, the $\{112\}\langle\bar{1}10\rangle_{\alpha'}$ texture consists of two twin-related components, each of which gives rise to one group of orientations centred on $\{430\}\langle 001\rangle_{\gamma}$ and two groups centred on $\{6,8,17\}\langle\bar{5}\bar{7}5\rangle_{\gamma}$, with the combined effect (Figure 111) of two $\{430\}\langle 001\rangle_{\gamma}$ components and four components of the type $\{6,8,17\}\langle\bar{5}\bar{7}5\rangle_{\gamma}$.

Figure 112 is a prediction of the resultant austenite texture in terms of these ideal orientations. Obviously this figure is not meant to be a full description of the texture, but if the previous analysis is valid these orientations should at least fall within the general spread of texture. Comparison with Figure 10 shows that, apart from the complete absence of intensity in the centre of the pole figure, the γ texture of 18%Cr 10%Ni steel after $\frac{1}{2}$ hour at 600°C conforms to the predictions. The group of orientations centred on $\{100\}\langle 001\rangle_{\gamma}$, and originating from $\{001\}\langle\bar{1}10\rangle_{\alpha'}$, is missing. This is direct evidence of preferential selection of Kurdjumov-Sachs variants, since it can only be accounted for by assuming that the eight variants comprising this component do not operate. Suppression of certain habit planes during

transformation has previously been reported by Bokros and Parker[97] and Borik and Richman[98]. Its effect is to produce a sharper transformation texture than would arise when random selection occurs. Thus, the texture shown in Figure 10 is sharper due to the absence of orientations close to $\{100\}\langle 001\rangle_\gamma$. The $\{001\}\langle \bar{1}10\rangle_{\alpha'}$ component has transformed only to orientations in the region of $\{110\}\langle \bar{5}57\rangle_\gamma$, which merge with the $\{110\}\langle \bar{1}12\rangle$-$\{110\}\langle 001\rangle$ spread.

Recrystallisation in the Austenite.

Subsequent recrystallisation in the austenite depends on the amounts of α and γ in the cold rolling texture. In the more stable alloys, which have only a small amount of α' in the rolling texture, nuclei forming within the range of γ rolling texture orientations are required to grow through a fairly limited range of matrix components in order to become part of the recrystallisation texture. In highly metastable alloys, however, the wider range of orientations of the b.c.c. rolling texture is transferred via the $\alpha \rightarrow \gamma$ transformation to the derived austenite texture. From Figure 10, there are two main distributions involved, but there is also a considerable spread of orientations between these high intensity areas. In order to become part of the recrystallisation texture, nuclei must grow through a much wider range of matrix components than in the former case. The process is still further complicated when some austenite remains in the rolling texture since nuclei from this range of orientations will compete with those from the derived austenite components which are already competing amongst themselves. Density of nuclei, being governed by the relative amounts of the various orientation distributions, is highly influential in governing the final form of the recrystallisation texture.

Various results from single crystal studies[1] indicate that, in the absence of second phase or other inhibiting effects, the geometrical relationship between deformed and recrystallised

grains in f.c.c. materials is a rotation of ~ 30-40° about common <111> poles, and Lücke[48] has shown the orientation relationship for maximum growth rate to be 40° <111> rotations for the case of aluminium. In accordance with these observations, and following the principles set out by Dillamore[43], it will be assumed that, in general, a nucleus will be favoured for growth if it has a <111> pole almost in common with the matrix into which it grows and if the rotation about this pole is ~40°. Tables 10-13 compare geometrical relationships of the principal recrystallisation components for different ranges of matrix components in terms of θ, the angle of misfit between <111> poles of nucleus and matrix, and ϕ, the rotation about this almost common <111> pole.

For a f.c.c. deformation texture of the $\{110\}<\bar{1}12>$ type, Dillamore[43] deduced that nuclei favourable for growth from grain boundaries or deformation band boundaries would be of the types $\{4,9,17\}<\bar{3}8\bar{5}>$, $\{490\}<001>$ and $\{112\}<\bar{1}10>$. The rolling texture also contains a minor $\{110\}<001>$ component, which, as shown by Figures 23 and 31 occupies about one quarter of the total volume. Both $\{112\}<\bar{1}10>$ and $\{490\}<001>$ nuclei are inhibited by this component,[43,99] so that nuclei of the $\{4,9,17\}<\bar{3}8\bar{5}>$ type should be preferred. The $\{225\}<\bar{5}\bar{3}3>$ orientation used to describe the recrystallisation textures lies close to this. Table 10 compares geometrical conditions for $\{225\}<\bar{5}\bar{3}3>$ nuclei growing into various matrix orientations. Nuclei of this type are favourable for growth into both components of the $\{110\}<\bar{1}12>$ texture and the $\{110\}<001>$ component, and should therefore form the recrystallisation texture of stable austenites having low values of γ/Gb. When a small amount of α' martensite is formed during cold rolling, as in the 18%Cr 14%Ni steel, $\{225\}<\bar{5}\bar{3}3>$ is confronted with other ranges of matrix orientations, which are also represented in Table 10. The $\{6,8,17\}<\bar{5}\bar{7}5>$ component is very close to $\{225\}<\bar{5}\bar{3}3>$ and therefore merely becomes part of the range of growing nuclei. Small amounts of this component will actually enhance development of the recrystallisation texture

by spontaneously providing suitable nuclei, and to this extent, nucleation of the recrystallisation texture can no longer be considered entirely random. Orientations such as $\{110\}<\bar{5}57>$ and $\{430\}<\bar{6},8,17>$ are close to $\{110\}<\bar{1}12>$, and may be considered as part of the spread around $\{110\}<\bar{1}12>$. Similarly $\{430\}<001>$ may be considered as part of the spread around $\{110\}<001>$. Matrix components such as these present no serious inhibiting effects, as shown by their geometrical relationships (Table 10); at least one out of two or two out of four matrix components remain favourable for $\{225\}<\bar{5}\bar{3}3>$ nuclei. However, the greater the deviation from the $\{110\}<\bar{1}12>$ - $\{110\}<001>$ spread, then the greater is the liklihood of inhibition occuring. Orientations of the $\{430\}<\bar{3}40>$ type will present the greatest inhibiting effect, due to a very large angle of misfit of both components with $\{225\}<\bar{5}\bar{3}3>$ (Table 10). For small amounts of α', the effect will be negligible, but increasing metastability will eventually restrict development of the $\{225\}<\bar{5}\bar{3}3>$ recrystallisation texture through the presence of $\{430\}<\bar{3}40>$ type matrix components and others. The present results show that at least 30% α' can be tolerated before this occurs.

For the opposite extreme of austenite stability, i.e. 18%Cr 10%Ni steel, the recrystallisation texture consists mainly of two groups of orientations, centred on $\{230\}<3,\bar{2},14>$ and $\{6,10,1\}<5\bar{3}1>$, with spread towards $\{6,8,17\}<\bar{5}\bar{7}5>$ type minor components. Nuclei of these orientations can originate entirely from the range of orientations produced by the $\alpha'\rightarrow\gamma$ shear transformation. Table 11 shows that conditions are highly favourable for $\{230\}<3,\bar{2},14>$ nuclei to grow into the $\{110\}<001>$ + $\{430\}<001>$ matrix distribution. Other orientations have at least one component which tends to inhibit growth by virtue of its mismatch with the matrix. Taking an overall view, $\{230\}<3,\bar{2},14>$ nuclei seem to be capable of absorbing or partially absorbing all orientations except those of the type $\{6,8,17\}<\bar{5}\bar{7}5>$. Table 12 shows that

nuclei of the type $\{6,10,1\}<5\bar{3}1>$ would tend to be inhibited by the $\{110\}<001> + \{430\}<001>$ spread. Apart from this, these nuclei also seem capable of absorbing or partially absorbing the matrix, with the exception of $\{6,8,17\}<\bar{5}\bar{7}5>$. Particular differences (Table 12) are that the two $\{110\}<\bar{1}12>$ components are now equally favourable, and growth into both of the $\{430\}<\bar{3}40>$ components is likely, although the angle of rotation is less favourable for one of them. Conditions governing growth of $\{6,8,17\}<\bar{5}\bar{7}5>$ nuclei are summarised in Table 13. This orientation is much less favourably oriented for the range of matrix components. In particular, $\{430\}<\bar{3}40>$ and $\{430\}<\bar{6},8,17>$ components will tend to inhibit growth. The $\{6,8,17\}<\bar{5}\bar{7}5>$ orientation is not easily absorbed by $\{230\}<3,\bar{2},14>$ (Table 11) or by $\{6,10,1\}<5\bar{3}1>$ (Table 12) so that the spread towards this orientation in the final texture (Figure 12) probably results from its retention by "recrystallisation in situ", i.e. subgrains growing until they reach a size attributable to recrystallised grains.

Nuclei arising from the small amount of austenite in 18%Cr 10%Ni steel will merely become part of the spread centred on $\{6,8,17\}<\bar{5}\bar{7}5>$ and therefore have no significant effect on the recrystallisation texture. Increasing amounts of austenite will increase the density of $\{225\}<\bar{5}\bar{3}3>$ nuclei until they eventually provide major competition with other growing nuclei. Transition to this type of recrystallisation texture will take place as the austenite stability increases.

Formation of the $\{230\}<3,\bar{2},14> + \{6,10,1\}<5\bar{3}1>$ recrystallisation texture cannot be interpreted unambiguously, and is more complicated than was considered by previously by Dickson and Green[87]. The fact that there are two main types of nuclei involved will in one sense help the growth process, i.e. grains unfavourably oriented for one nucleus might be favourably oriented for the other. In general, all that can be concluded is that recrystallisation takes place by growth competition between $\{230\}$

$\langle 3,\bar{2},14\rangle$ and $\{6,10,1\}\langle 5\bar{3}1\rangle$. From the present analysis, it is likely that the $\{110\}\langle 001\rangle$ + $\{430\}\langle 001\rangle$ spread disappears by growth of the $\{230\}\langle 3,\bar{2},14\rangle$ component. The low angle of misfit of the latter with the matrix will actually favour rapid growth at an early stage during recrystallisation. This probably accounts for a large part of the texture rearrangement which takes place between 600°C (Figure 10) and 700°C (Figure11) when the intensity of $\{110\}\langle 001\rangle$ has rapidly decreased. The $\{6,10,1\}$ $\langle 5\bar{3}1\rangle$ nuclei are more favourably oriented for growth into $\{110\}$ $\langle\bar{1}12\rangle$ and $\{430\}\langle\bar{3}40\rangle$ components, and probably account for the greater proportion of growth into this part of the matrix.

Relative Contributions.

Relative contributions of the various stages may be summarised as follows:-

Recovery is important in that it leads to sharpening of both α' and γ rolling textures. When large amounts of martensite are formed during rolling, its effect is more significant, i.e. texture sharpening produced in the martensite prior to reverse transformation will contribute to a less diffuse spread of orientations in the derived austenite than if recovery was delayed until after the transformation. The crystallographic nature of the $\alpha' \rightarrow \gamma$ transformation limits the spread of orientations which are present in the austenite immediately after transformation, and variant selectivity can contribute to texture sharpening at this stage by suppression of certain variants of the Kurdjumov-Sachs orientation relationship. As the alloy stability increases and less martensite is formed, the influence of the transformation becomes less important. Throughout the range of metastable austenites, oriented growth rather than oriented nucleation is largely responsible for development of recrystallisation textures. However, the $\alpha' \rightarrow \gamma$ transformation is capable of spontaneously producing suitably oriented nuclei and certainly in the 18%Cr 10%Ni alloy the mechanism should be partly considered as oriented nucleation.

7.3 Primary Recrystallisation Textures of Commercial Stainless Steels.

7.3.1 Unstabilised Steels.

The unstabilised steels (RF310, FST(L) and FSL(L)) recrystallise in a similar manner to the laboratory alloys of equivalent metastability (cf. Figures 22 and 41, Figures 30 and 37) Mode of development of the textures remains the same but some further deductions can now be made regarding the effects of initial solution treatment. For instance, furnace cooling allows formation of some fine intergranular carbides, probably of the type $(Cr,Fe)_{23}C_6$ but these have no significant effect on subsequent cold rolling and annealing behaviour because the network is broken up by the severe deformation. The same will apply to stringers of undissolved carbides and inclusions. The slightly different carbon contents of FST(L) and FSL(L) (Table 2) do not produce any noticeable difference in amount of undissolved carbides. By contrast, RF310 steel shows appreciable quantities of undissolved carbides after both annealed and water quenched conditions, yet recrystallisation textures are similar to the other steels (cf. Figures37 and 41), indicating that carbon in amounts up to 0·1% has little effect.

Precipitation of $(Cr, Fe)_{23} C_6$ during recrystallisation does not inhibit re-orientation, presumably because the particles are re-dissolved fairly readily under annealing conditions of increasing temperature (Figure 102). One can envisage a dynamic situation of precipitation and dissolution with dissolution being more or less complete during the later stages of annealing.

7.3.2 Stabilised Steels.

The carbide-stabilised steels (FCB, SF347, FDP, FMB and FMBTi) form their recrystallisation textures largely by retention of the γ cold rolling texture and/or retention of the γ texture immediately after transformation from the martensite(e.g. Figures 52,59,66 and 73). Initial solution treatment is important only in so far as it controls the stability of the matrix prior to

cold rolling i.e. solution of carbon and alloying elements promotes a more stable austenite. The observed effects of solution treatment on annealing textures are therefore indirect being related to the relative amounts of austenite and martensite after rolling. High solution treatment temperatures are required to show variation in textures through dissolution of NbC or TiC. In all alloys, initial distributions of undissolved particles are broken up during rolling.

The essential difference between the unstabilised and stabilised steels is that, in the stabilised alloys, precipitation occurs during annealing and much of it remains until the end of recrystallisation (Figures 106 and 108). The carbide phases which are involved are probably NbC, TiC, $(Cr,Fe,Mo)_{23}C_6$ and possibly Mo_2C.

The mechanism by which the textures are retained is most likely one of precipitate particles restricting grain boundary mobility so that grains with high angle boundaries do not grow in preference to others, at least not to the same extent as they would in the absence of precipitate particles. Inhibition of texture re-orientation in this manner is certainly not complete in these alloys. This is most clearly shown by the results for FMB and FMBTi steels which form only relatively small amounts of α' martensite during rolling. The recrystallisation textures (Figures 73 and 79) consist largely of retained $\{110\}\langle\bar{1}12\rangle$ + $\{110\}\langle 001\rangle$ austenite orientations but there is also spread towards the $\{225\}\langle\bar{5}\bar{3}3\rangle$ orientation which can arise in these alloys only by oriented growth from the rolling texture.

8. Some Implications of the Present Results.

A knowledge of the textures which may be obtained in a particular metal or alloy is important since it could lead to useful control of preferred orientation during fabrication. Current examples of this are:

(a) producing a "balanced" texture in copper and aluminium sheet, which minimises the amount of earing during subsequent pressing

operations,

(b) developing a high "through-thickness" strength in mild steel, leading to improved deep-drawability.

It is now well established that the rolling textures of stable f.c.c. metals and alloys are of two general types, referred to as the "pure metal" texture and the "alloy" texture, and that transition from one to the other may be effected by varying the stacking fault energy or by changing the rolling temperature. However, the annealing textures derived from these rolling textures are not commercially useful as a means of improving press-forming properties.

The textures which have been observed in austenitic stainless steels are of interest because the modifying influence of the $\gamma \rightleftharpoons \alpha'$ transformation in metastable alloys and/or carbide forming elements in stabilised steels now makes possible formation of annealing texture orientations which are not normally characteristic of a f.c.c. matrix.

The relation of the present results to sheet forming properties can be summarised as follows.

(i) A"new" range of recrystallisation textures are possible in carbide-stabilised steels which cover the range of metastable austenites. The texture can be varied, by control of matrix stability, to give required balance between the three main distributions centred on $\{110\}\langle\bar{1}12\rangle$, $\{110\}\langle001\rangle$ and $\{225\}\langle\bar{5}\bar{5}3\rangle$. Forming properties have yet to be examined but because a wide range of orientations is involved, the amount of earing associated with the mixed textures should be less than when single orientations are involved.

(ii) The results have emphasised the importance of solution treatment control applied to stabilised steels in the metastable range.i.e. large variations in annealing textures and associated properties can arise through use of different treatments.

(iii) In carbide-stabilised austenites which show little or no α'

during deformation, the $\{110\}\langle\bar{1}12\rangle\gamma$ rolling texture is retained during recrystallisation. This texture obtained in α brass by secondary recrystallisation is known to show slightly improved deep drawability compared with isotropic material, and might be used to advantage in this class of stainless steel.

9. Future Trends in Research.

Theories are still being refined in order to give complete account of all aspects of texture formation. Because of the difficulty of assessing the statistical nature of polycrystalline textures, future work might concentrate more on single crystal studies which yield unambiguous information for analysis.

There is much to be learned about the rôle played by impurities and second phases on both rolling and recrystallisation textures. The rôle of phase transformations, as distinct from precipitation of minor phases, has only just begun to be explored. In particular, the influence of the reversible $\gamma \rightleftharpoons \alpha'$ transformation in stainless steels is well established and future work on these alloys might concentrate on exploiting the transformation to develop new recrystallisation textures in a f.c.c. matrix.

The present work is being extended using the following approaches:-

(a) recrystallisation texture transition in high purity 18%Cr steels over the range 10-12%Ni.

(b) rolling texture transition in stable 18%Cr austenites as a function of nickel content

(c) rôle of carbide-stabilising elements in high purity austenites.

REFERENCES

1. I.L.Dillamore and W.T.Roberts — Met.Reviews 10(1965)271.
2. Y.C.Liu and R.H.Richman — Trans.Met.Soc.A.I.M.E. 218(1960)688.
3. R.H.RIchman and Y.C.Liu — Trans.Met.Soc.A.I.M.E. 221(1961)720.
4. R.E.Smallman — J.Inst.Metals 84 (1955-56)10.
5. A.Merlini and P.A.Beck — Trans.Amer.Min.Met.Eng. 203(1955)395.
6. M.Hatherley — J.Aust.Inst.Metals 8(1963)140.
7. F.Haessner — Z.Metallkunde 53(1962)403.
8. H.Hu and R.S.Cline — J.Appl.Physics 32(1961)760.
9. H.Hu R.S.Cline and S.R.Goodman — J.Appl.Physics 32(1961)1392.
10. H.HU and S.R.Goodman — Trans.Met.Soc.A.I.M.E. 227(1963)1454.
11. S.R.Goodman and H.Hu — Trans.A.I.M.E. 230(1964)1413.
12. D.Green — M.Met.Thesis,Univ.of Sheffield (1963).
13. H.Kueller — Oster.Akad.Wiss.Math.-Naturw. 7(1958)117.
14. H.Hu and S.R.Goodman — Trans.Met.Soc.A.I.M.E. 227(1963)627.
15. R.E.Smallman and D.Green — Acta Met. 12(1964)145.
16. F.Haessner — Z.Metallkunde 53(1962)403.
17. E.A.Calnan and C.J.B.Clews — Phil.Mag. 42(1951)616.
18. G.Wassermann — Z.Metallkunde 54(1963)61.
19. F.Haessner — Z.Metallkunde 54(1963)98.
20. I.L.Dillamore and W.T.Roberts — Acta Met. 12(1964)281.

21. P.R.Thornton and T.E.Mitchell — Phil.Mag. 7(1962)371.

22. E.A.Calnan — J.Inst.Metals 84(1955-56)503.

23. T.Ll.Richards and S.F.Pugh — J.Inst.Metals 88(1959-60)399.

24. L.Clareborough and A.Hargreaves — Progress in Metal Physics 8(1958)1.

25. H.Hu, R.S.Cline and S.R.Goodman — "Recrystallisation, Grain Growth and Textures", (1965)295. Metals Park, Ohio(Amer.Soc.Metals).

26. E.Butler and D.Green — University of Aston in Birmingham. Private Communication, June 1967.

27. R.vonMises — Z.angew.Math.Mech. 8(1928)161.

28. J.W.F.Bishop and R.Hill — Phil.Mag. 42(1951)414.

29. I.L.Dillamore, E.Butler and D.Green — Metal Science Journal 2(1968)161.

30. H.Hu and R.S.Cline — Trans.Met.Soc.A.I.M.E. 224(1962)784.

31. G.Groves and A.Kelly — Phil.Mag. 8(1963)877.

32. G.Y.Chin and L.Mammel — Trans.Met.Soc.A.I.M.E. 239(1967)1400.

33. W.Heye and G.Wassermann — Physica StatusSolidi 18(1966)107.

34. M.Cook and T.Ll.Richards — J.Inst.Metals 66(1940)1.

35. W.M.Baldwin — Trans.A.I.M.M.E. 166(1946)591.

36. E.Schmid and H.Thomas — Zeit.Physik 130(1951)293.

37. T.Ll.Richards and S.F.Pugh — J.Inst.Metals 88(1959-60)399.

38. P.Beck and H.Hu — J.Inst.Metals 4(1952)83.

39. K.Detert, P.Dersch and H.Migge — Z.Metallkunde 54(1963)263.

40. W.R.Seymour and D.Harker — Trans.A.I.M.M.E. 188(1950)1001.

41. H.Hu, R.S.Cline and S.R.Goodman — Trans.Met.Soc.A.I.M.E. 224(1962)96.

42. A.Merlini and P.A.Beck — Trans.A.I.M.M.E. 203(1955)395.

43. I.L.Dillamore — Acta Met. 12(1964)1005.

44. W.G.Burgers and P.C.Louwerse — Z.Physik 67(1931)607.

45. F.Haessner, U.Jakubowski and M.Wilkens — Physika Status Solidi 7(1964)701.

46. C.S.Barrett — Trans.A.I.M.M.E. 137(1950)128.

47. P.A.Beck — Trans.A.I.MM.E. 191(1951)475.

48. K.Lucke — Deutche Gesellschaft fur Metallkunde (1964)London

49. S.Kohara, M.N.Parthasarathi and P.A.Beck — Trans.Met.Soc.A.I.M.E. 212(1958)875.

50. S.Kohara, M.N.Parthasarathi and P.A.Beck — J.Appl.Physics 29(1958)1125.

51. M.N.Parthasarathi and P.A.Beck — "Proprietes des Joints de Grains" (1961):Paris (Presses Universitaires)

52. P.A.Beck — Advances in Physics 3(1954)245.

53. C.G.Dunn — Acta Met. 1(1953)163.

54. J.E.Burke — Trans.A.I.M.M.E. 194(1952)263.

55. W.Bunk and P.Esslinger — Z.Metallkunde 50(1959)278.

56. J.C.Blade — J.Inst.Metals 90(1961-2)374.

57. T.Amitani — Nippon Kinzoku Gakkai-Si 24(1960)765.

58. F.Haessner, G.Hasing and H.P.Stuwe — Z.Metallkunde 47(1956)743.

59. I.Gokyu, H.Abe and H.Veyama — Nippon Kinzoku Gakkai-Si 29(1965)515.

60. P.B.Hee and R.A.Sinclair — J.Inst.Metals 94(1966)319.

61. C.S.Barrett and L.H.Levenscn — Trans.A.I.M.M.E. 145(1941)281.

62. H.Hu and R.S.Cline — Trans.Met.Soc.A.I.M.E. 224(1962)784.

63. G.Wassermann and A.Greven — Texturen Metallischen Werkstoffe Springer Verlag. Berlin (1962).

64. I.L.Dillamore — Trans.Met.Soc.A.I.M.E. 233(1965)702.

65. P.C.Hancock and W.T.Roberts — J.I.S.I. 205(1967)547.

66. H.Stablein and H.Möller — Arch.Eisenhüttenwesen 29(1958)433.

67. P.K.Koh and C.G.Dunn — Trans.Met.Soc.A.I.M.E. 218(1960)65.

68. F.Haessner and H.Weik — Arch.Eisenhüttenwesen 27(1956)153.

69. H.Müller — Zeit.Metallkunde 49(1958)575.

70. J.W.Pugh and W.R.Hibbard — Trans.Amer.Soc.Metals 48(1956)526.

71. J.W.Pugh — Trans.Met.Soc.A.I.M.E. 212(1958)637.

72. N.Ujuye and R.Maddin — Ttans.A.I.M.M.E. 206(1956)1298.

73. C.G.Dunn — Acta Met.2(1954)173 .

74. H.Hu — Trans.Met.Soc.A.I.M.E. 221(1961)130.

75. C.G.Dunn — Trans.Amer.Inst.Min.Met.Eng. 200(1954)549.

76. C.G.Dunn and P.K.Koh — Trans.Amer.Inst.Min.Met.Eng. 206(1956)1017

77. H.Hu — Trans.Met.Soc.A.I.M.E. 215(1959)320.

78. B.F.Decker and D.Harker — J.Appl.Physics. 22(1951)900.

79. H.K.Chen and R.Maddin — Trans.Amer.Inst.Min.Met.Eng. 197(1953)300.

80. R.G.Aspden — Trans.Met.Soc.A.I.M.E. 227(1963)909.

81. H.Abe, M.Matsuo and K.Ito — Trans.Japan Inst.Metals 4(1963)28.

82. P.R.V.Evans, J.C.Bitcon and I.F.Hughes — J.I.S.I. 207(1969)331.

83. I.L.Dillamore, C.J.E.Smith and T.W.Watson — Metal Science Journal 1(1967)49.

84. W.C.Leslie — Trans.Met.Soc.A.I.M.E. 221(1961)752.

85. C.A.Stickels — Trans.Met.Soc.A.I.M.E. 236 (1966)1295.

86. H.Borchers and Z.Q.Kim — Arch.Eisenhüttenwesen 36(1965)311.

87. M.J.Dickson and D.Green — Mater.Sci.Eng. 4(1969)304.

88. S.R.Goodman and H.Hu — Trans.Met.Soc.A.I.M.E. 233(1965)103.

89. M.J.Dickson — J.Appl.Cryst. 2(1969)176.

90. — Texture-Goniometer, Siemens und Halske Aktiengesellschaft, Wernerwek für Messtechnik.

91. P.C.J.Gallagher — Metallurgical Trans. 1(1970)2303.

92. P.M.Kelly and J.Nutting — J.Iron and St.Inst. 197(1961)199.

93. J.A.Venables — Phil.Mag. 7(1962)35.

94. R.Lagneborg — Acta.Met. 12(1964)823.

95. J.F.Breedis and W.D.Robertson — Acta.Met. 10(1962)1077.

96. P.M.Kelly — Acta.Met. 13(1965)635.

97. J.C.Bokros and E.R.Parker — Acta.Met. 11(1963)1291.

98. F.Borik and R.H.Richman — Trans.Met.Soc.A.I.M.E. 239(1967)675.

99. P.A.Beck — Trans.A.I.M.M.E. 203(1955)1270.

ACKNOWLEDGEMENTS.

The following acknowledgements are made:-

D.Thacker, Deputy Principal, Sheffield Polytechnic.

-for help in initiating the work.

R.P.Stratton, College Supervisor and Director of Studies, Sheffield Polytechnic.

D.Dulieu, Industrial Supervisor, B.I.S.R.A.Laboratories.

-for their guidance and constructive criticisms during the preparation of the thesis.

A.Wirth, Sheffield Polytechnic,

-for help with the electron metallography.

D.Green, The University of Aston in Birmingham.

T.Ll.Richards, The University of Aston in Birmingham.

-for their encouragement and continuing interest in my career.

International Nickel Ltd.

B.I.S.R.A. Laboratories.

Samuel Fox & Company Ltd.

Firth Vickers Stainless Steels Ltd.

-for supply of materials.

TABLE I

Compositions of laboratory steels

Steel	C	Mn	Si	S	P	Cr	Ni	Co	N	Fe
18/10	0.026	0.1	0.2	0.005	0.005	18.2	10.0	-	0.012	Bal.
18/12	0.032	0.2	0.2	0.006	0.005	18.0	11.9	-	0.010	Bal.
18/14	0.017	0.1	0.2	0.005	0.005	18.3	14.0	-	0.011	Bal.
18/12/Co	0.008	0.2	0.2	0.005	0.005	18.1	12.2	7.0	0.010	Bal.
18/25	0.003	0.1	0.32	0.005	0.005	18.0	24.7	-	0.004	Bal.

TABLE 2

Compositions of commercial steels

Steel	C	Mn	Si	S	P	Cr	Ni	Ti	Nb	Mo	N	Fe
RF 310	0.10	1.64	0.56	0.016	0.018	24.64	21.53	-	-	-	0.030	Bal.
FST (L)	0.05	1.12	0.52	0.003	0.025	18.72	9.97	-	-	-	0.025	Bal.
FSL (L)	0.022	1.17	0.59	0.009	0.026	18.78	10.6	-	-	-	0.018	Bal.
FCB	0.04	0.70	0.48	0.012	0.013	18.25	9.62	-	0.83	-	0.032	Bal.
SF 347	0.04	1.55	0.76	0.025	0.029	18.09	9.68	-	0.72	-	0.027	Bal.
FDP	0.075	0.98	0.6	0.006	0.031	17.95	9.88	0.41	-	-	0.031	Bal.
FMB	0.05	1.48	0.35	0.010	0.021	17.06	11.50	-	-	2.80	0.025	Bal.
FMB Ti	0.035	1.54	0.35	0.008	0.024	17.45	12.00	0.42	-	2.59	0.020	Bal.

TABLE 3

Texture parameters of laboratory steels after preliminary rolling and annealing

Steel	Phkl						
	111	200	220	311	331	420	422
18/10	1.1	0.8	1.2	1.1	0.9	1.0	0.9
18/12	1.2	0.9	1.2	0.9	1.1	0.8	0.9
18/14	1.1	0.9	1.1	1.1	0.8	1.0	1.0
18/12/Co	1.2	0.9	1.1	1.3	0.9	0.8	0.8
18/25	1.1	1.0	1.1	1.2	0.8	0.9	0.9=

TABLE 4

Texture parameters of commercial steels after preliminary rolling and annealing

Steel	Heat Treatment	Phkl						
		111	200	220	311	331	420	422
RF 310	1hr 1050°C FC	1.1	1.2	1.0	0.9	0.8	1.3	0.7
	1hr 1050°C WQ	1.2	1.3	1.0	0.8	0.7	1.2	0.8
FST(L)	1hr 1050°C FC	1.3	1.2	1.1	0.7	0.9	1.1	0.7
	1hr 1050°C WQ	1.1	1.2	1.2	0.8	0.7	1.0	1.0
FSL(L)	1hr 1050°C FC	1.0	1.3	1.1	0.8	1.1	0.9	0.8
	1hr 1050°C WQ	1.3	1.2	1.2	0.9	0.9	0.8	0.7
FCB	1hr 1050°C FC	1.2	1.2	1.1	0.7	0.8	0.8	1.2
	1hr 1050°C WQ	1.0	1.1	1.3	0.8	1.1	0.7	1.0
	15min 1300°C FC	1.1	1.3	1.2	0.9	0.9	0.8	0.8
	15min 1300°C WQ	1.3	1.1	1.0	0.7	0.8	1.1	1.0
SF 347	1hr 1050°C FC	1.1	1.1	1.2	0.8	0.7	1.0	1.1
	1hr 1050°C WQ	1.3	1.2	1.0	0.7	0.9	1.1	0.8
	15min 1300°C FC	1.2	1.2	1.1	0.9	1.1	0.8	0.7
	15min 1300°C WQ	1.1	1.0	1.3	0.9	1.2	0.9	0.6
FDP	1hr 1050°C FC	1.3	1.0	1.2	1.0	1.1	0.7	0.7
	1hr 1050°C WQ	1.1	1.2	1.2	0.9	0.7	0.9	1.0
	15min 1300°C FC	1.1	1.0	1.1	1.0	0.8	0.9	1.1
	15min 1300°C WQ	1.3	1.1	1.1	0.7	1.2	0.8	0.8
FMB	1hr 1050°C FC	1.1	1.0	1.3	0.8	0.9	0.9	1.0
	1hr 1050°C WQ	1.0	0.9	1.4	0.7	1.2	0.9	0.9
	15min 1300°C FC	1.3	0.8	1.2	0.9	0.9	1.1	0.8
	15min 1300°C WQ	1.2	0.9	1.2	1.0	0.8	0.8	1.1
FMB Ti	1hr 1050°C FC	0.9	0.9	1.3	1.1	1.0	0.9	0.9
	1hr 1050°C WQ	1.1	0.7	1.2	0.9	1.0	1.2	0.9
	15min 1300°C FC	1.0	0.8	1.2	1.1	0.9	1.2	0.8
	15min 1300°C WQ	1.1	1.0	1.3	1.2	0.7	0.8	0.9

TABLE 5

Relative intensities of principal α' rolling texture components for the commercial alloys

Steel	Heat treatment	$\%\alpha'$	$2xI_{(35^\circ+90^\circ)}$	$2xI_{55^\circ}$	I_{0°	$\{112\}\langle\bar{1}10\rangle$ %	$\{111\}\langle\bar{1}\bar{1}2\rangle$ %	$\{001\}\langle\bar{1}$ %
FST (L)	1 hr 1050°C FC	11	6.6	4.0	1.5	54	33	12
	1 hr 1050°C WQ	10	6.2	3.0	1.5	58	28	14
FSL (L)	1 hr 1050°C FC	10	5.8	3.8	1.5	52	34	14
	1 hr 1050°C WQ	10	6.2	4.0	1.6	52	34	14
FCB	1 hr 1050°C FC	100	5.0	5.2	3.0	38	39	23
	1 hr 1050°C WQ	100	5.2	5.0	2.9	40	38	22
	15 min 1300°C FC	87	5.7	3.8	1.8	50	34	16
	15 min 1300°C WQ	71.5	6.6	4.0	1.5	54	33	13
SF 347	1 hr 1050°C FC	85	6.0	4.0	1.7	51	34	15
	1 hr 1050°C WQ	82	5.4	3.6	1.5	52	34	14
	15 min 1300°C FC	35	6.2	4.0	1.8	52	33	15
	15 min 1300°C WQ	30	5.2	2.6	1.5	56	28	16
FDP	1 hr 1050°C FC	84	6.1	4.2	1.8	50	35	15
	1 hr 1050°C WQ	75	5.6	3.8	1.5	51	35	14
	15 min 1300°C FC	9	6.3	4.1	1.7	52	34	14
	15 min 1300°C WQ	9	6.2	3.7	1.6	54	32	14

TABLE 6

Relative intensities of principal recrystallisation texture components for the commercial alloys

Steel	Heat Treatment	% α after cold rolling	$2xI_{30^\circ}$	$2xI_{(45^\circ \div 55^\circ)}$	$I_{(45^\circ \div 90^\circ)}$	$\{225\}\langle\bar{5}\bar{3}3\rangle$ %	$\{110\}\langle\bar{1}12\rangle$ %	$\{110\}\langle001$ %
RF 310	1hr 1050°C FC	0	7.8	2.0	1.0	72	19	9
	1hr 1050°C WQ	0	7.6	2.0	1.0	72	19	9
FST(L)	1hr 1050°C FC	11	6.0	2.8	1.2	60	28	12
	1hr 1050°C WQ	10	6.4	2.8	1.4	60	27	13
FSL(L)	1hr 1050°C FC	10	7.6	2.8	1.0	66	25	9
	1hr 1050°C WQ	10	7.0	2.9	1.0	64	27	9
FCB	1hr 1050°C FC	100	4.2	4.6	3.9	33	36	31
	1hr 1050°C WQ	100	4.4	5.1	4.2	32	37	31
	15min 1300°C FC	87	7.8	4.4	2.2	54	31	15
	15min 1300°C WQ	71.5	8.0	4.0	1.5	59	30	11
SF 347	1hr 1050°C FC	85	8.2	5.0	2.5	52	32	16
	1hr 1050°C WQ	82	7.6	4.8	2.4	51	33	16
	15min 1300°C FC	35	3.8	5.0	1.8	36	47	17
	15min 1300°C WQ	30	3.6	5.0	1.7	35	49	16
FDP	1hr 1050°C FC	84	8.0	5.0	2.5	52	32	16
	1hr 1050°C WQ	75	8.0	4.8	1.9	54	33	13
	15min 1300°C FC	9	4.0	5.0	2.4	35	44	21
	15min 1300°C WQ	9	4.2	5.0	2.5	36	43	21
FMB	1hr 1050°C FC	2	2.4	8.0	3.3	18	58	24
	1hr 1050°C WQ	2	2.4	8.4	3.0	17	61	22
	15min 1300°C FC	2	2.4	8.0	3.7	17	57	26
	15min 1300°C WQ	2	2.2	8.8	3.3	15	62	23
FMB Ti	1hr 1050°C FC	3	2.2	8.6	2.7	16	64	20
	1hr 1050°C WQ	3	2.2	8.0	2.7	17	62	21
	15min 1300°C FC	2	2.0	9.0	2.9	14	65	21
	15min 1300°C WQ	2	2.0	8.8	2.6	15	66	19

TABLE 7

Grain sizes of commercial steels.

Steel	Initial heat treatment	Average Grain diameter (mm)	Average Grain Diameter (mm) after 90% CR + ½ hr 900°C. AC.
RF 310	1 hr 1050°C. FC.	4×10^{-2}	3.5×10^{-3}
	1 hr 1050°C. WQ.	2.5 "	4.5 "
FST(L)	1 hr 1050°C. FC.	4.5 "	6.5 "
	1 hr 1050°C. WQ.	5.5 "	8.5 "
FSL(L)	1 hr 1050°C. FC.	5.5 "	10 "
	1 hr 1050°C. WQ.	6 "	13.5 "
FCB	1 hr 1050°C. FC	6.5 "	6.5 "
	1 hr 1050°C. WQ.	2.5 "	6 "
	15 min 1300°C. FC.	9 "	4.5 "
	15 min 1300°C. WQ.	12 "	5 "
SF 347	1 hr 1050°C. FC.	2.5 "	4.5 "
	1 hr 1050°C. WQ.	2 "	6.5 "
	15 min 1300°C. FC.	12 "	7 "
	15 min 1300°C. WQ.	9 "	4 "
FDP	1 hr 1050°C. FC.	5.5 "	5 "
	1 hr 1050°C. WQ.	2.5 "	4.5 "
	15 min 1300°C. FC.	15 "	4.5 "
	15 min 1300°C. WQ.	15 "	5.5 "
FMB	1 hr 1050°C. FC.	12.5 "	6 "
	1 hr 1050°C. WQ.	9 "	6 "
	15 min 1300°C. FC.	15 "	6.5 "
	15 min 1300°C. WQ.	15 "	6.5 "
FMB Ti	1 hr 1050°C. FC.	3 "	5 "
	1 hr 1050°C. WQ.	4 "	5 "
	15 min 1300°C. FC.	12 "	4.5 "
	15 min 1300°C. WQ.	12 "	5 "

TABLE 8

Carbide phases present in commercial steels.

Steel	Treatment	Carbide phases present
NF 310	1 hr 1050°C. FC, 90% CR + ½ hr 800°C. AC.	$M_{23}C_6$
FCB	"	$M_{23}C_6$ + NbC
SF 347	"	$M_{23}C_6$ + NbC
FDP	"	$M_{23}C_6$ + TiC
FHB	"	$M_{23}C_6$ + possibly Mo_2C
FHB Ti	"	$M_{23}C_6$ + TiC + possibly Mo_2C

Table 9

Ideal orientations after transformation from principal components of the α' rolling texture

Principal components of α' rolling texture	Components resulting from $\alpha' \rightarrow \gamma$	Intensities relative to original
$\{001\}\langle\bar{1}10\rangle$	$\{100\}\langle001\rangle$	1/3
	$\{110\}\langle\bar{5}57\rangle$	2/3
$\{111\}\langle\bar{1}\bar{1}2\rangle$	$\{430\}\langle\bar{3}40\rangle$	1/3
	$\{430\}\langle\bar{6},8,17\rangle$	2/3
$\{112\}\langle\bar{1}10\rangle$	$\{430\}\langle001\rangle$	1/3
	$\{6,8,17\}\langle\bar{5}\bar{7}5\rangle$	2/3

Table 10

Geometrical conditions governing growth of $\{225\}\langle\bar{5}\bar{3}3\rangle$ nuclei

Nucleus	Parent	θ°	ϕ°	Comments
$\{225\}\langle\bar{5}\bar{3}3\rangle$	$\{110\}\langle\bar{1}12\rangle$	14	42	Favourable
		10	26	
	$\{110\}\langle 001\rangle$	11	42	Favourable
	$\{110\}\langle\bar{5}57\rangle$	8	27	Favourable
		15	23	
	$\{430\}\langle 001\rangle$	9	41	Favourable
		16	55	
	$\{430\}\langle\bar{6},8,17\rangle$	10	37	Partially favourable
		16	50	
		10	19	
		29	37	
	$\{430\}\langle\bar{3}40\rangle$	23	37	Unfavourable
		23	40	
	$\{6,8,17\}\langle\bar{5}\bar{7}5\rangle$	3		Close to $\{225\}\langle\bar{5}\bar{3}3\rangle$
		7		
		5		
		4		

Table 11

Geometrical conditions governing growth of $\{230\}\langle 3,\bar{2},14\rangle$ nuclei

Nucleus	Parent	θ°	ϕ°	Comments
$\{230\}\langle 3,\bar{2},14\rangle$	$\{110\}\langle\bar{1}12\rangle$	3	20	Partially favourable
		20	39	
	$\{110\}\langle 001\rangle$	1	19	Favourable
	$\{110\}\langle\bar{5}57\rangle$	8	26	Favourable
		15	55	
	$\{430\}\langle 001\rangle$	7	25	Favourable
		7	25	
	$\{430\}\langle\bar{6},8,17\rangle$	7	24	Partially favourable
		10	40	
		7	16	
		24	29	
	$\{430\}\langle\bar{3}40\rangle$	5	44	Partially favourable
		28	55	
	$\{6,8,17\}\langle\bar{5}\bar{7}5\rangle$	12	55	Unfavourable
		15	38	
		15	38	
		18	60	

Table 12

Geometrical conditions governing growth of $\{6,10,1\}\langle 5\bar{3}1\rangle$ nuclei

Nucleus	Parent	θ°	ϕ°	Comments
$\{6,10,1\}\langle 5\bar{3}1\rangle$	$\{110\}\langle\bar{1}12\rangle$	12	40	Favourable
		12	38	
	$\{110\}\langle 001\rangle$	18	60	Unfavourable
	$\{110\}\langle\bar{5}57\rangle$	5	33	Partially favourable
		20	40	
	$\{430\}\langle 001\rangle$	13	43	Partially favourable
		26	47	
	$\{430\}\langle\bar{6},8,17\rangle$	10	47	Partially favourable
		3	41	
		22	45	
		26	53	
	$\{430\}\langle\bar{3}40\rangle$	14	25	Favourable
		7	12	
	$\{6,8,17\}\langle\bar{5}\bar{7}5\rangle$	12	45	Unfavourable
		19	52	
		25	43	
		35	72	

Table 13

Geometrical conditions governing growth of $\{6,8,17\}\langle\bar{5}\bar{7}5\rangle$ nuclei

Nucleus	Parent	θ°	ϕ°	Comments
$\{6,8,17\}\langle\bar{5}\bar{7}5\rangle$	$\{110\}\langle\bar{1}12\rangle$	12	28	Favourable
		12	28	
	$\{110\}\langle 001\rangle$	15	55	Favourable
	$\{110\}\langle\bar{5}\bar{5}7\rangle$	6	34	Favourable
		16	30	
	$\{430\}\langle 001\rangle$	10	46	Favourable
		16	48	
	$\{430\}\langle\bar{6},8,17\rangle$	10	31	Partially favourable
		15	44	
		18	34	
		31	44	
	$\{430\}\langle\bar{3}40\rangle$	18	39	Unfavourable
		24	41	

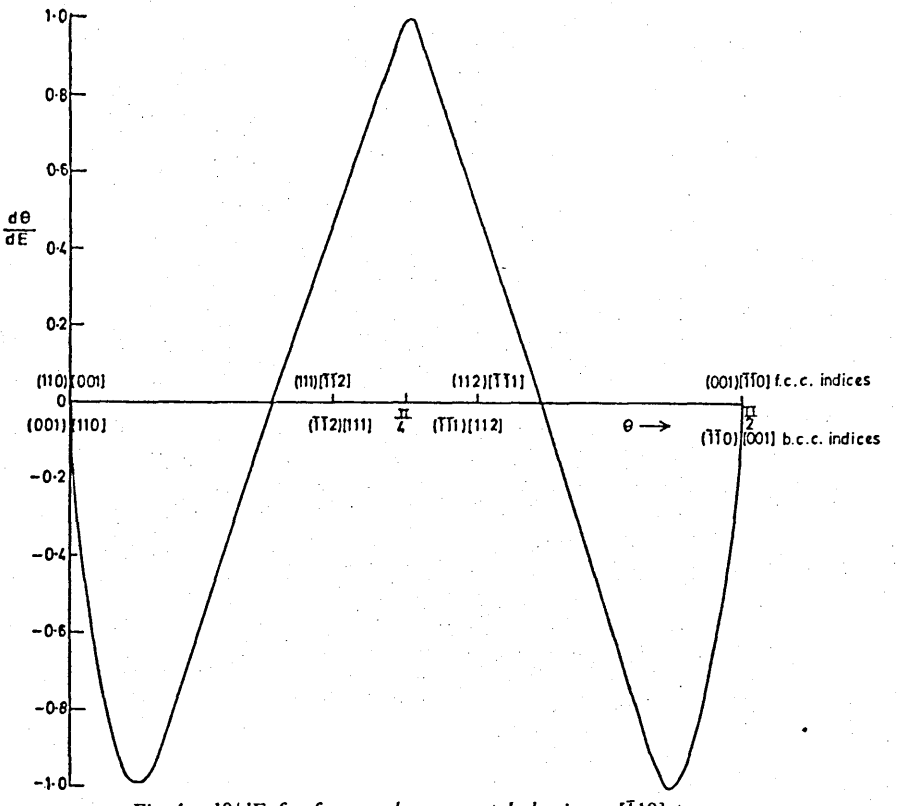

Fig. 1 dθ/dE *for f.c.c. or b.c.c. crystals having a* [1̄10] *transverse direction.*

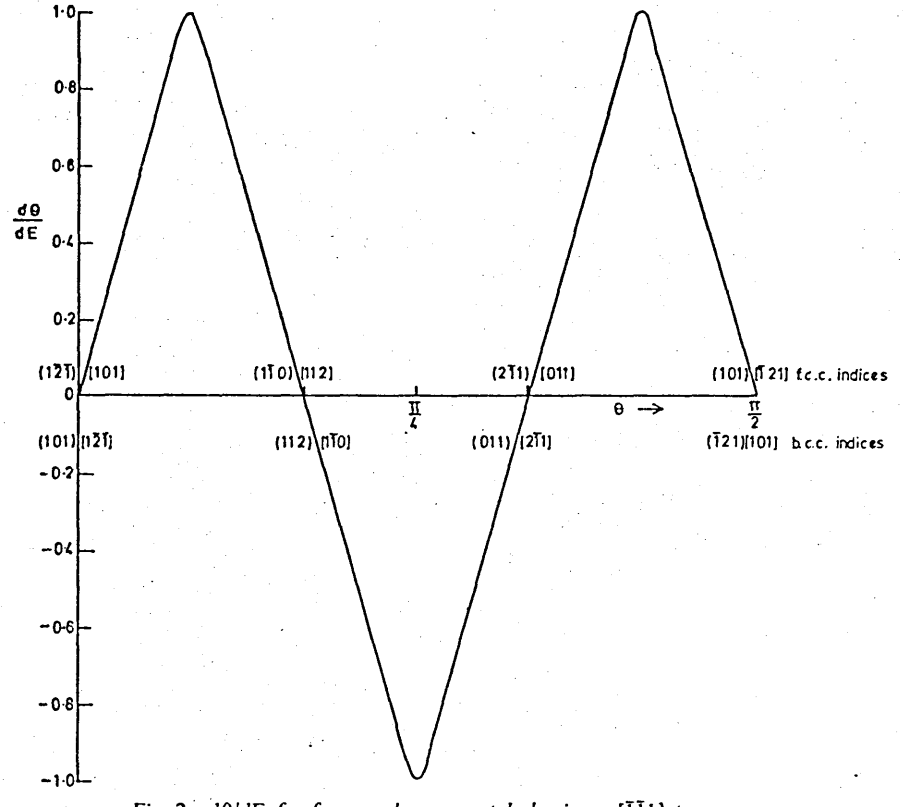

Fig. 2 dθ/dE *for f.c.c. or b.c.c. crystals having a* [1̄1̄1] *transverse direction.*

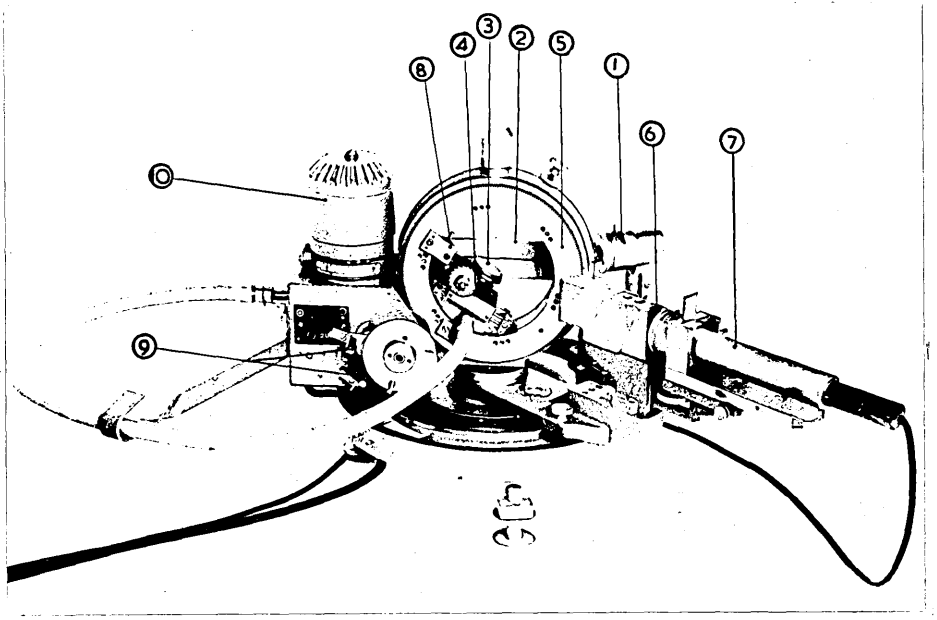

Figure 3(a) The Siemens texture goniometer.

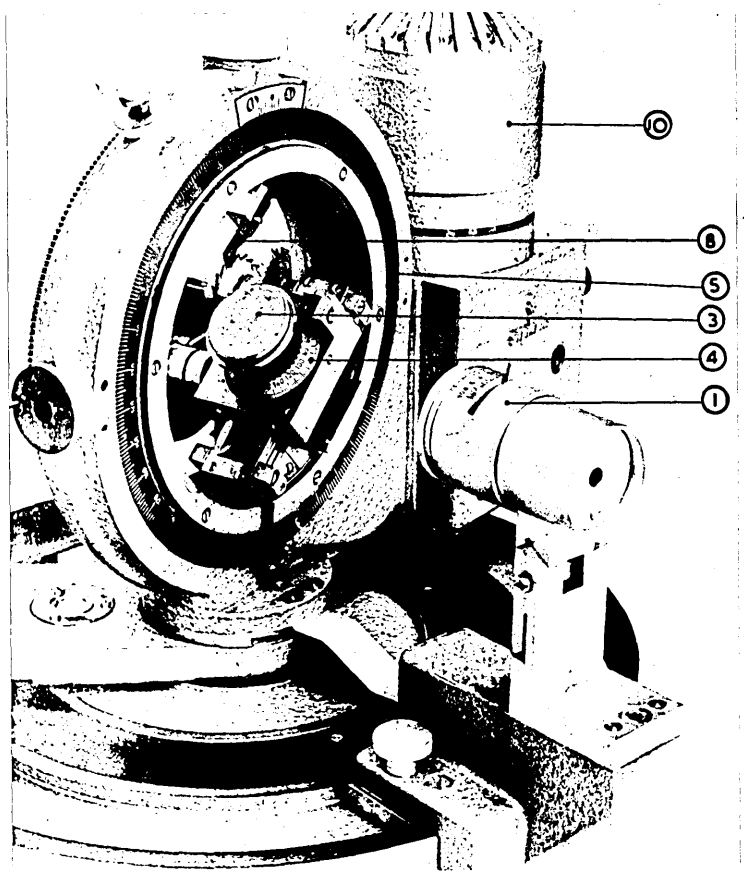

Figure 3(b) Close-up view of the goniometer with horizontal slit removed.

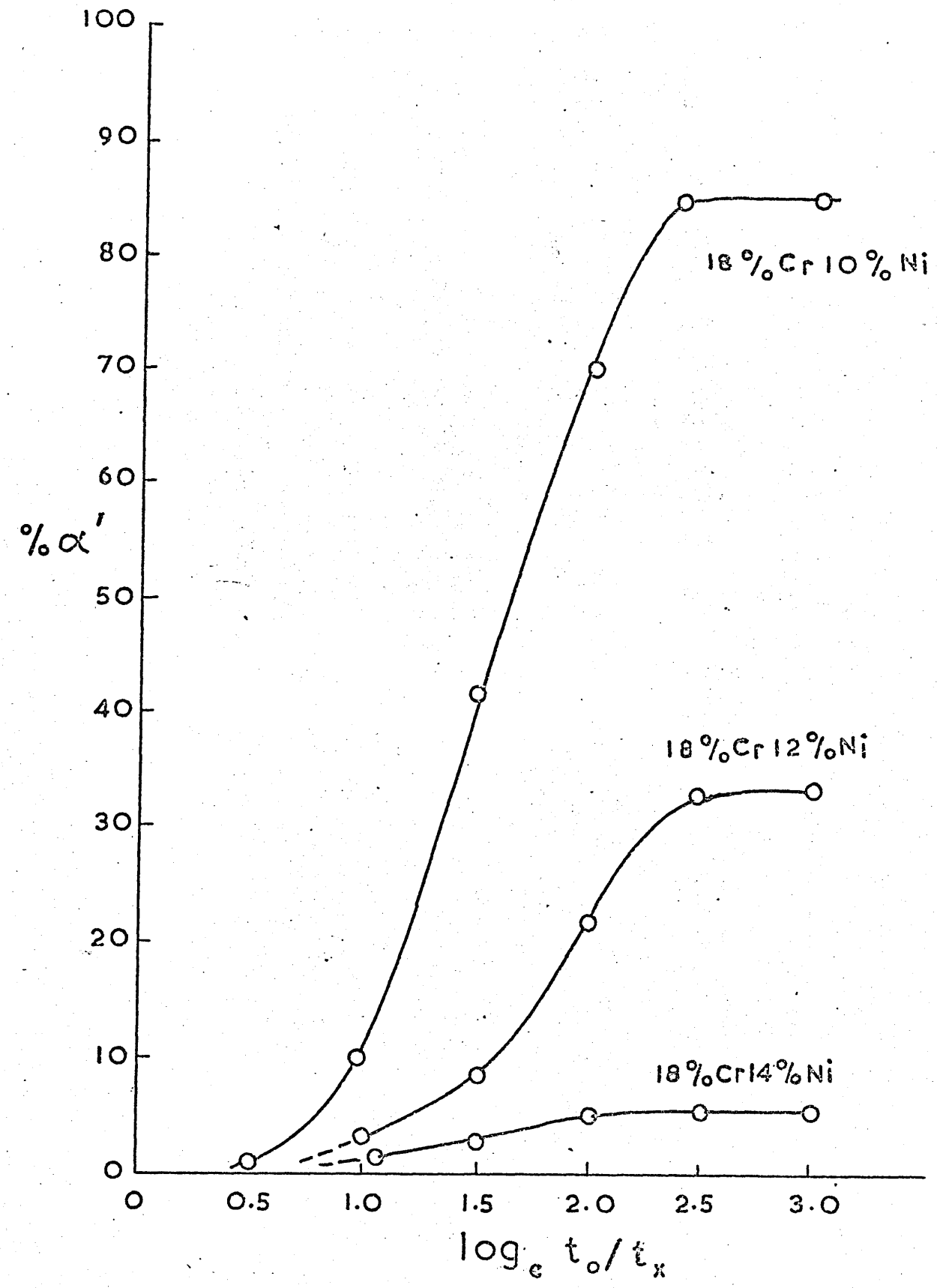

Figure 4.

Variation of % α' during cold rolling of 18%Cr steels containing 10%, 12% and 14% Ni.

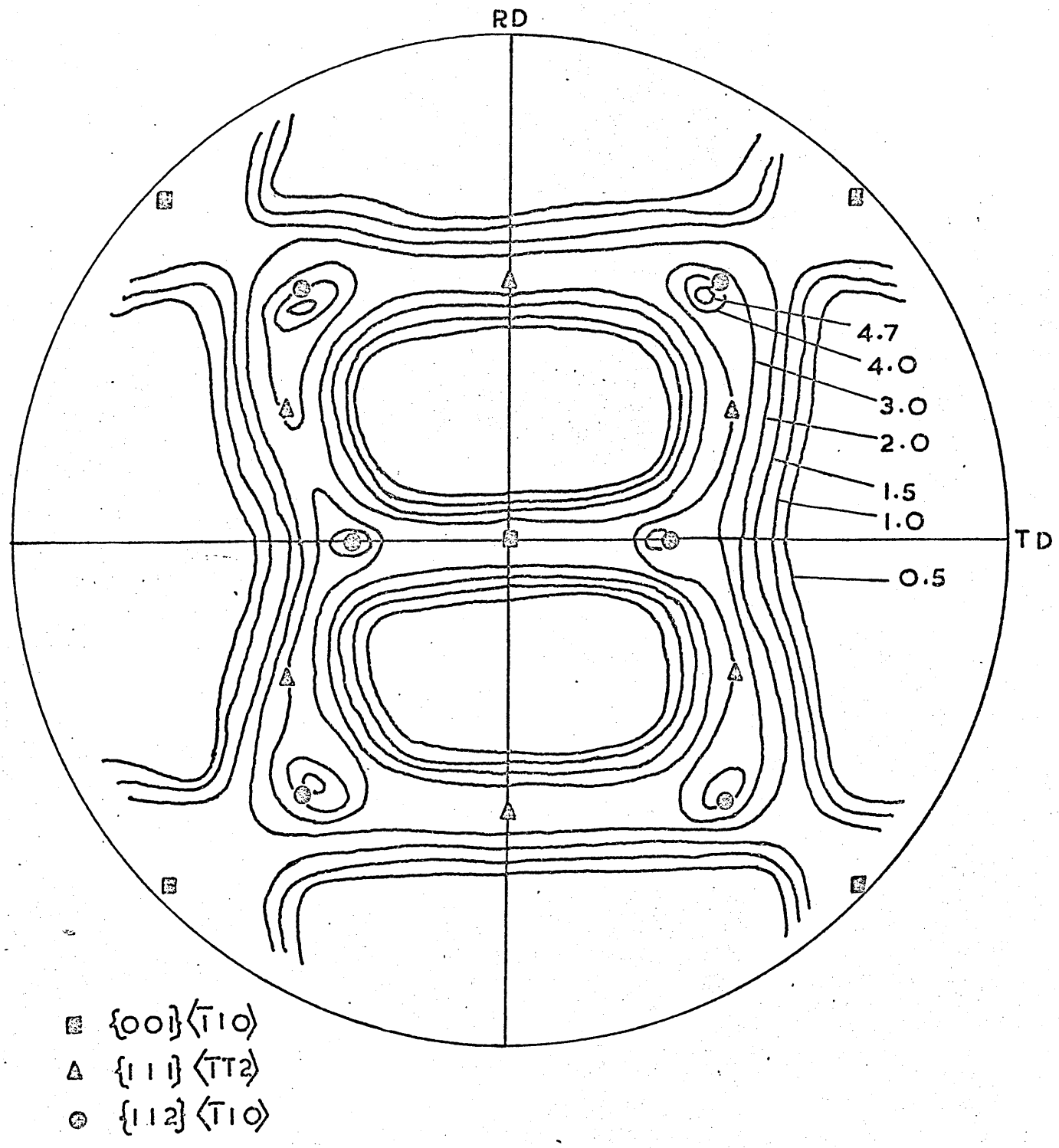

Figure 5.

{200}α' pole figure of 18%Cr 10%Ni steel.
1 hr 1050°C. FC , 95% cold rolled.

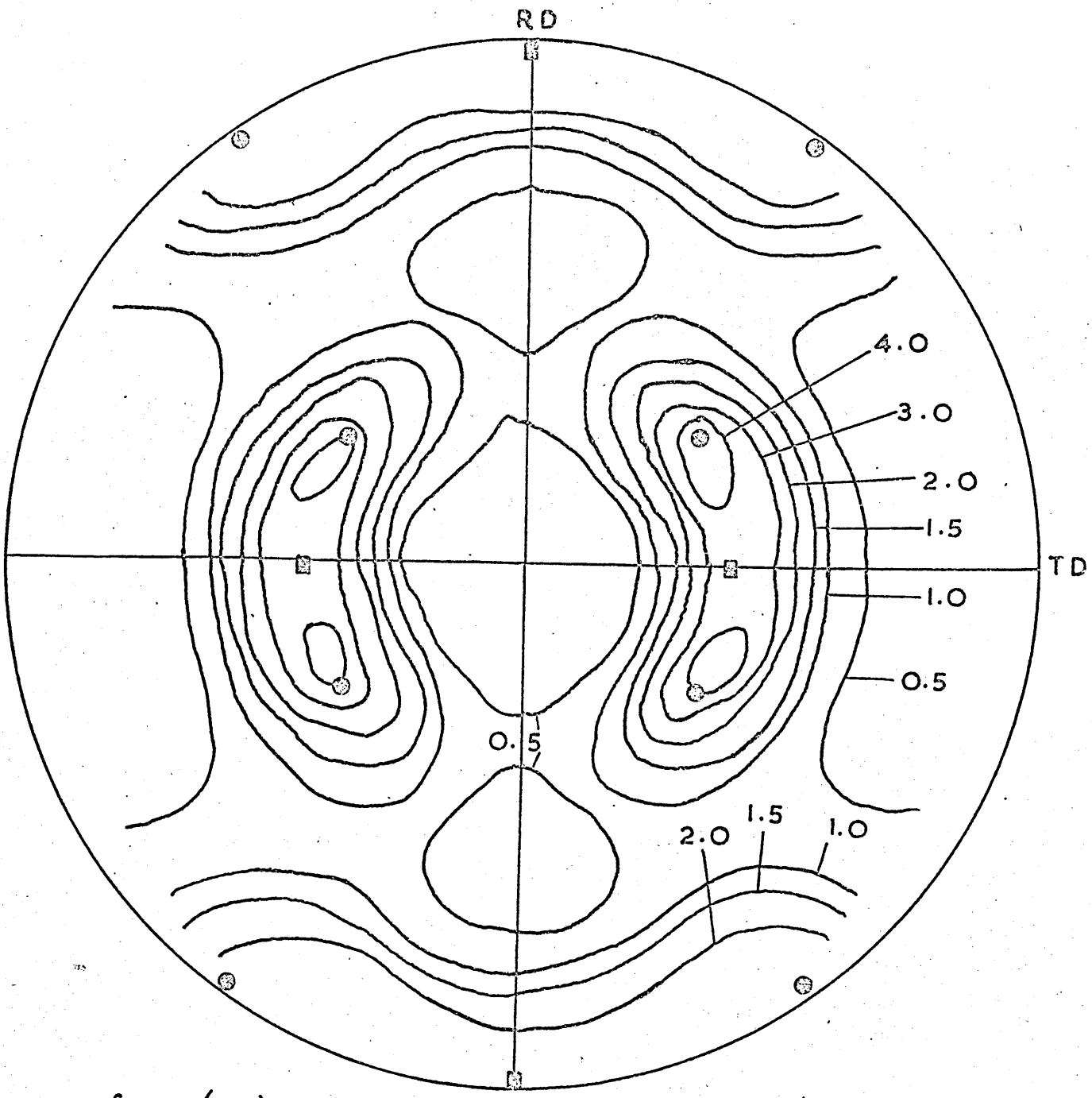

Figure 6.
{200}γ pole figure of 18%Cr 10%Ni steel.
1 hr 1050°C. FC, 95% cold rolled.

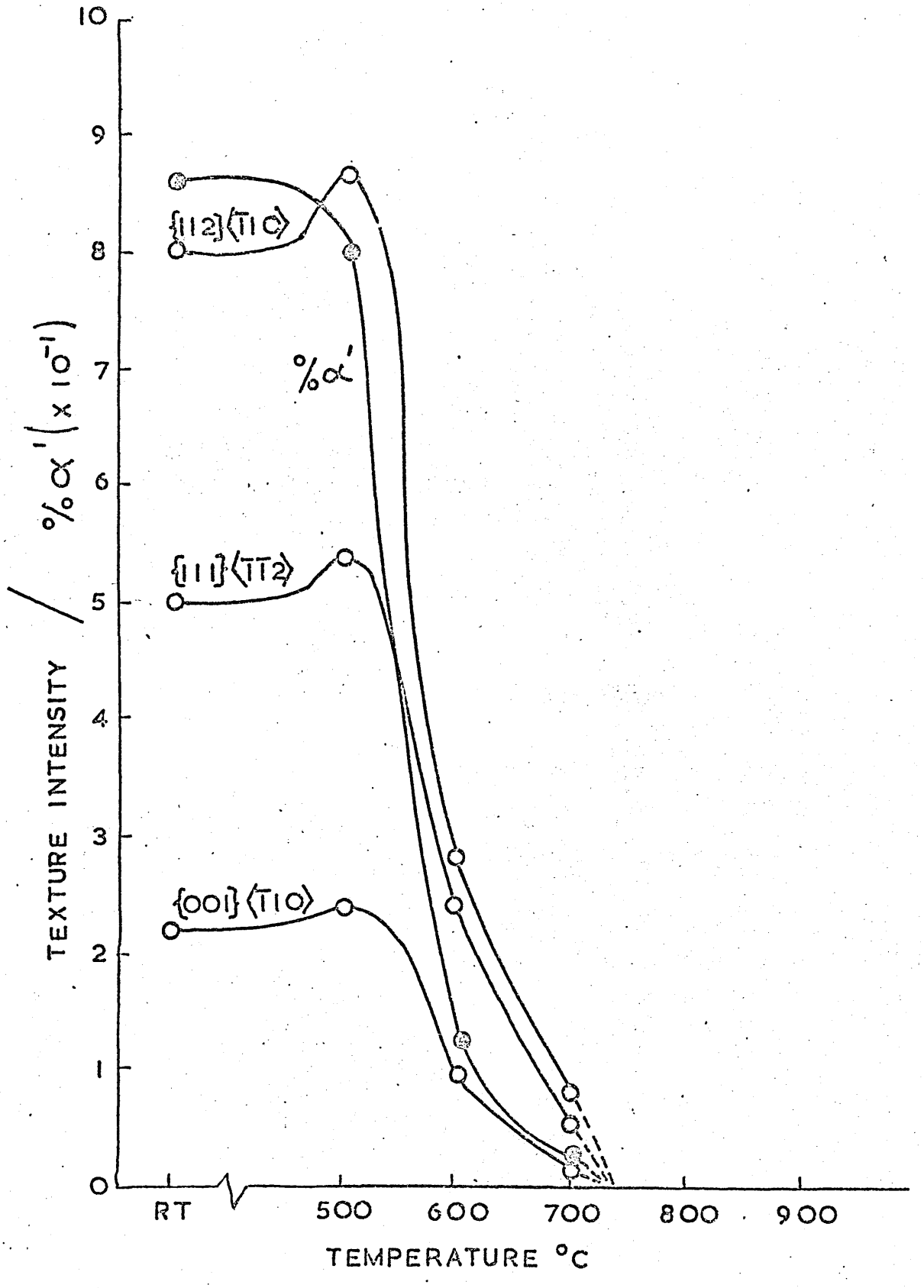

Figure 7.

Variation of % α' and intensities of α' texture components for 18%Cr 10%Ni steel.

1 hr 1050°C. FC, 95% cold rolled and annealed.

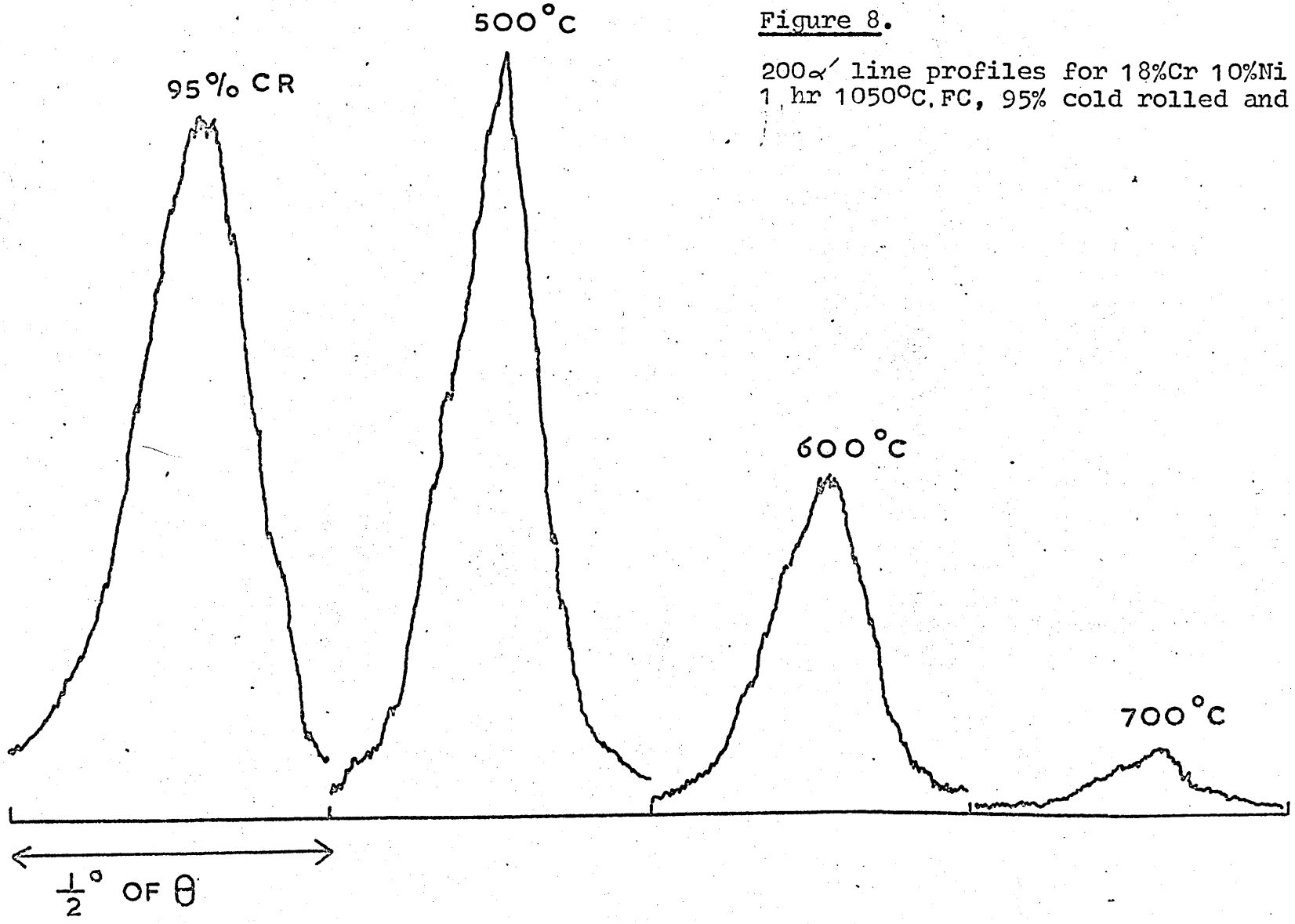

Figure 8.

200α' line profiles for 18%Cr 10%Ni steel. 1 hr 1050°C, FC, 95% cold rolled and annealed

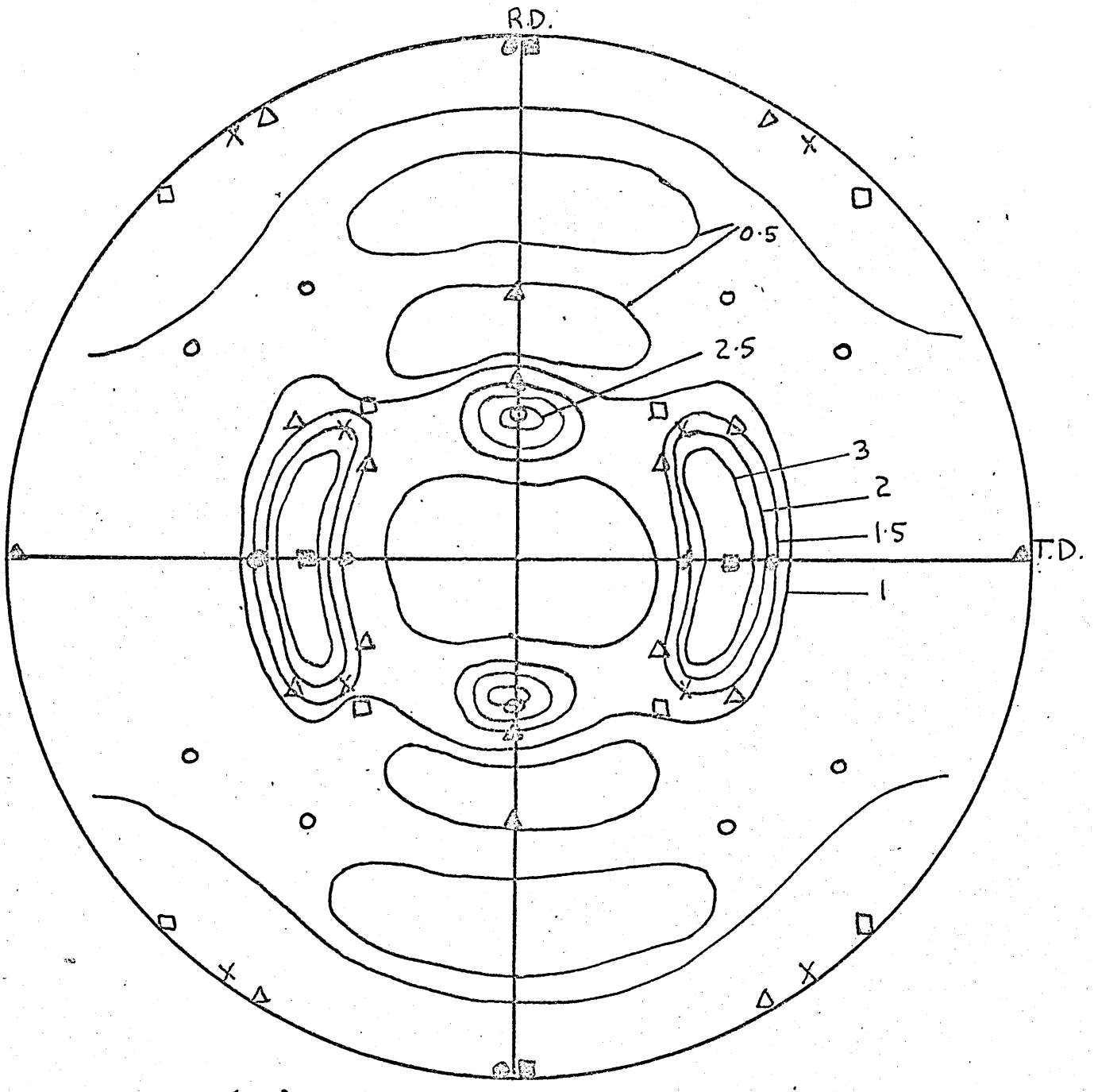

□ {110}<$\bar{5}$ 5 7>
△ {430}<$\bar{3}$ 40>
△ {430}<$\bar{6}$,8,17>
× {110}<$\bar{1}$12>
● {430}<001>
○ {6,8,17}<$\bar{5}$ 7 5>
▣ {110}<001>

Figure 9.
{200}γ pole figure of 18%Cr 10%Ni steel.
1 hr 1050°C. FC, 95% cold rolled + $\frac{1}{2}$hr 500°C. AC.

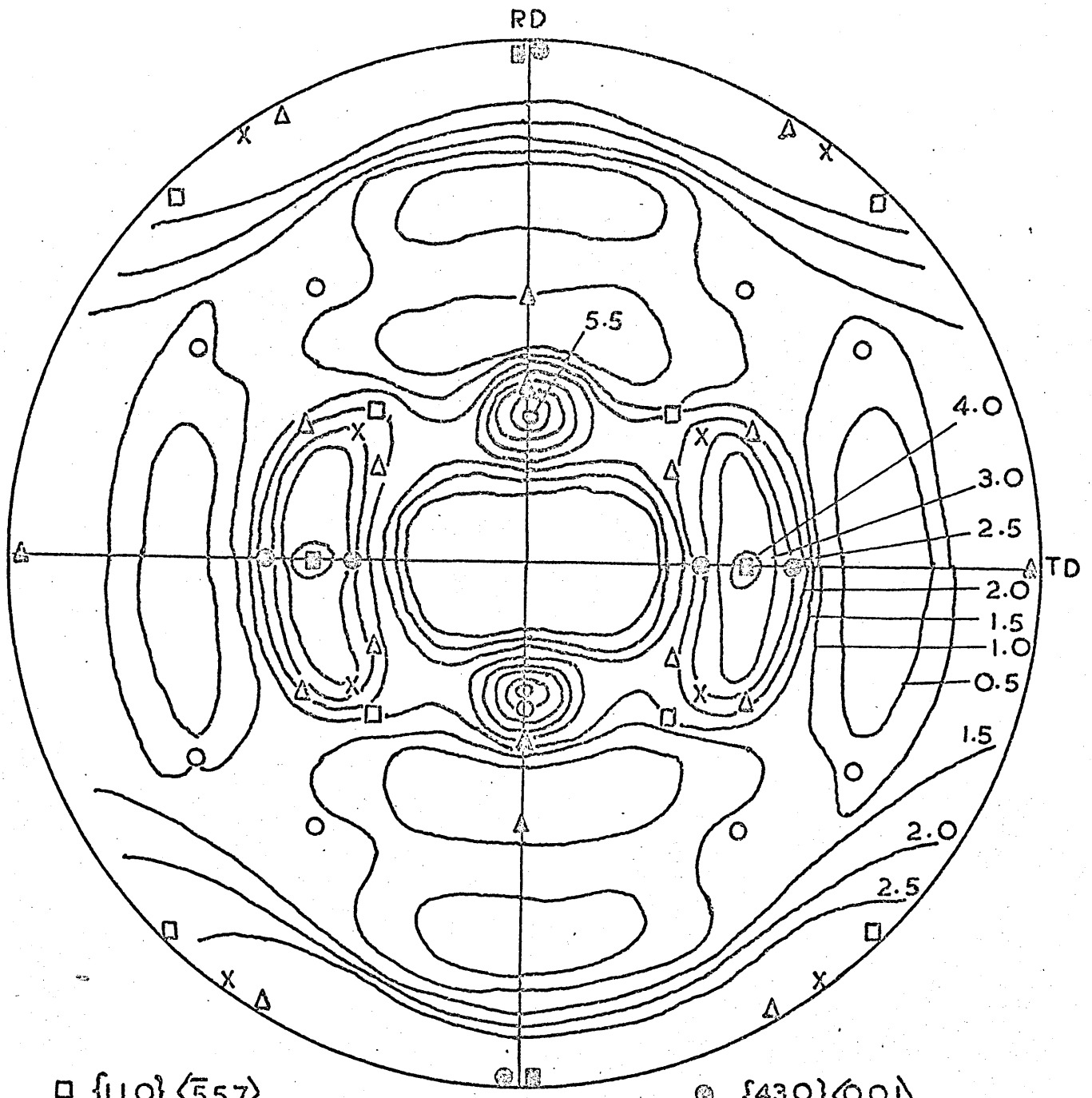

□ {110} ⟨$\bar{5}$57⟩
▲ {430} ⟨$\bar{3}$40⟩
△ {430} ⟨$\bar{6}$, 8, 17⟩
× {110} ⟨$\bar{1}$12⟩
◉ {430} ⟨001⟩
○ {6, 8, 17} ⟨$\bar{5}$75⟩
■ {110} ⟨001⟩

Figure 10.
{200}γ pole figure of 18%Cr 10%Ni steel.
1 hr 1050°C. FC, 95% cold rolled + $\frac{1}{2}$hr 600°C. AC.

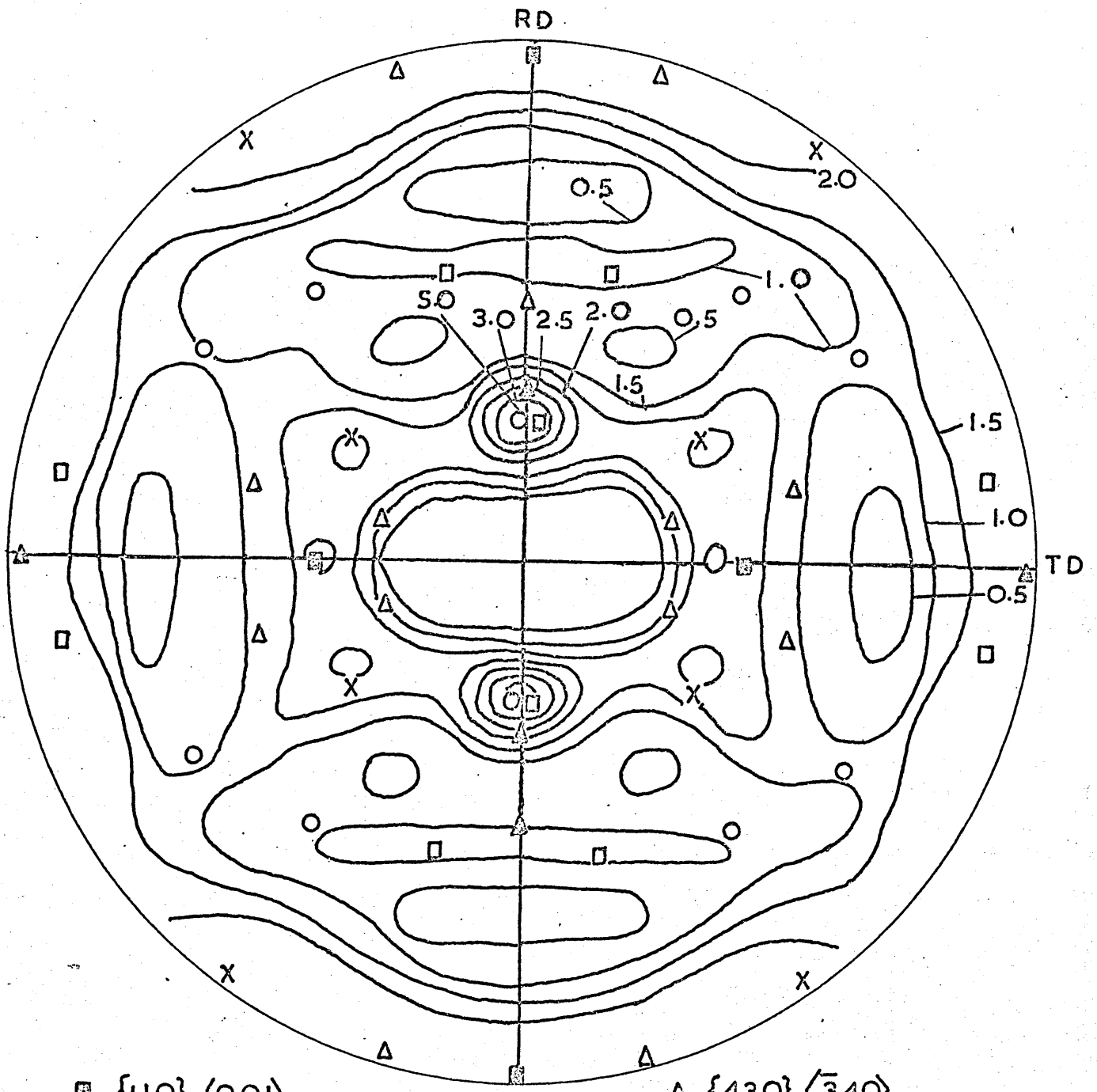

■ {110} ⟨001⟩
X {110} ⟨$\bar{1}$12⟩
○ {6,8,17} ⟨$\bar{5}\bar{7}$5⟩
▲ {430} ⟨$\bar{3}$40⟩
△ {230} ⟨3,$\bar{2}$,14⟩
□ {6,10,1} ⟨5$\bar{3}$1⟩

Figure 11.
{200}γ pole figure of 18%Cr 10%Ni steel.
1 hr 1050°C. FC, 95% cold rolled + ½hr 700°C. AC.

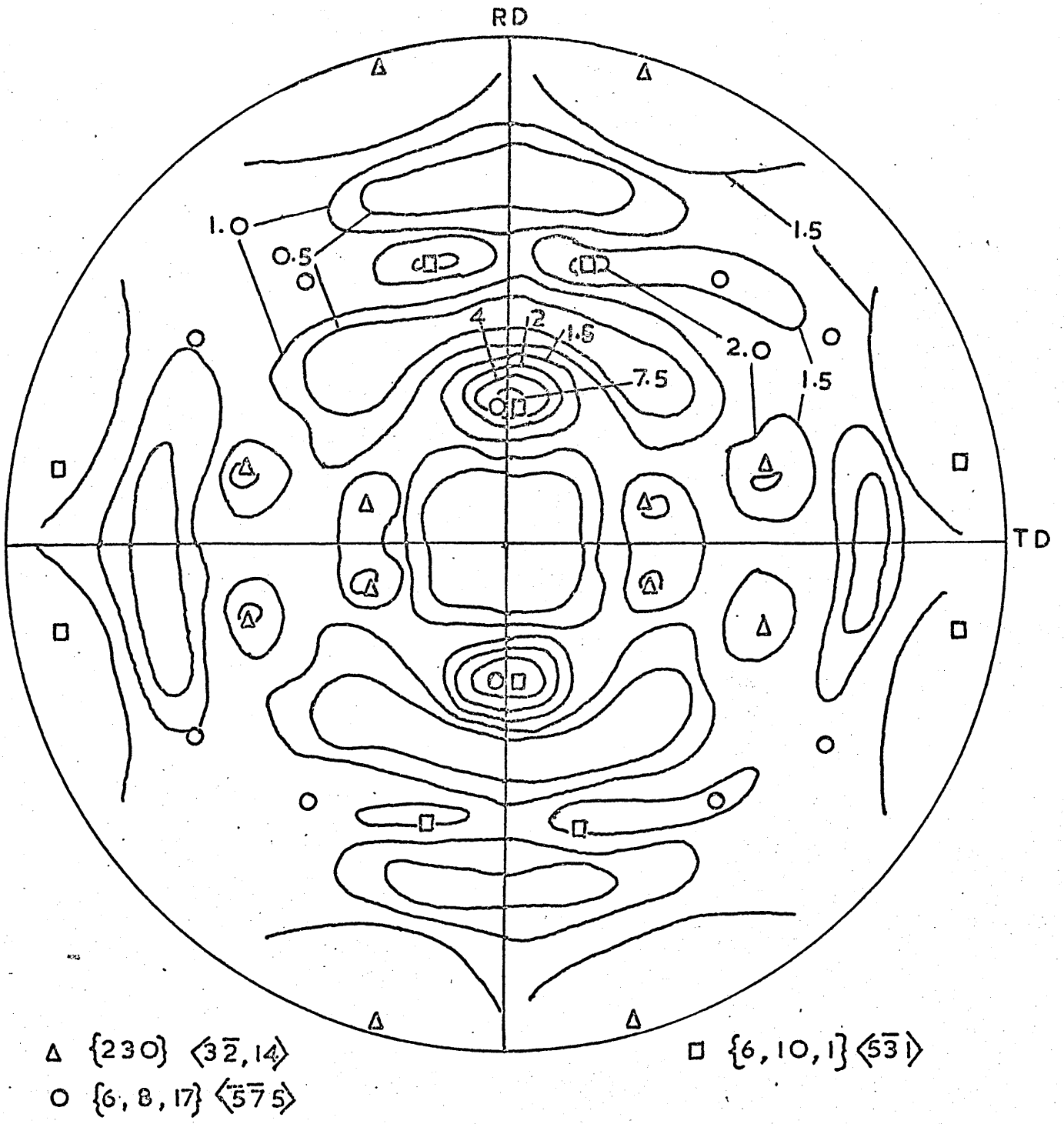

Figure 12.

{200}γ pole figure of 18%Cr 10%Ni steel.

1 hr 1050°C. FC, 95% cold rolled + ½hr 900°C. AC.

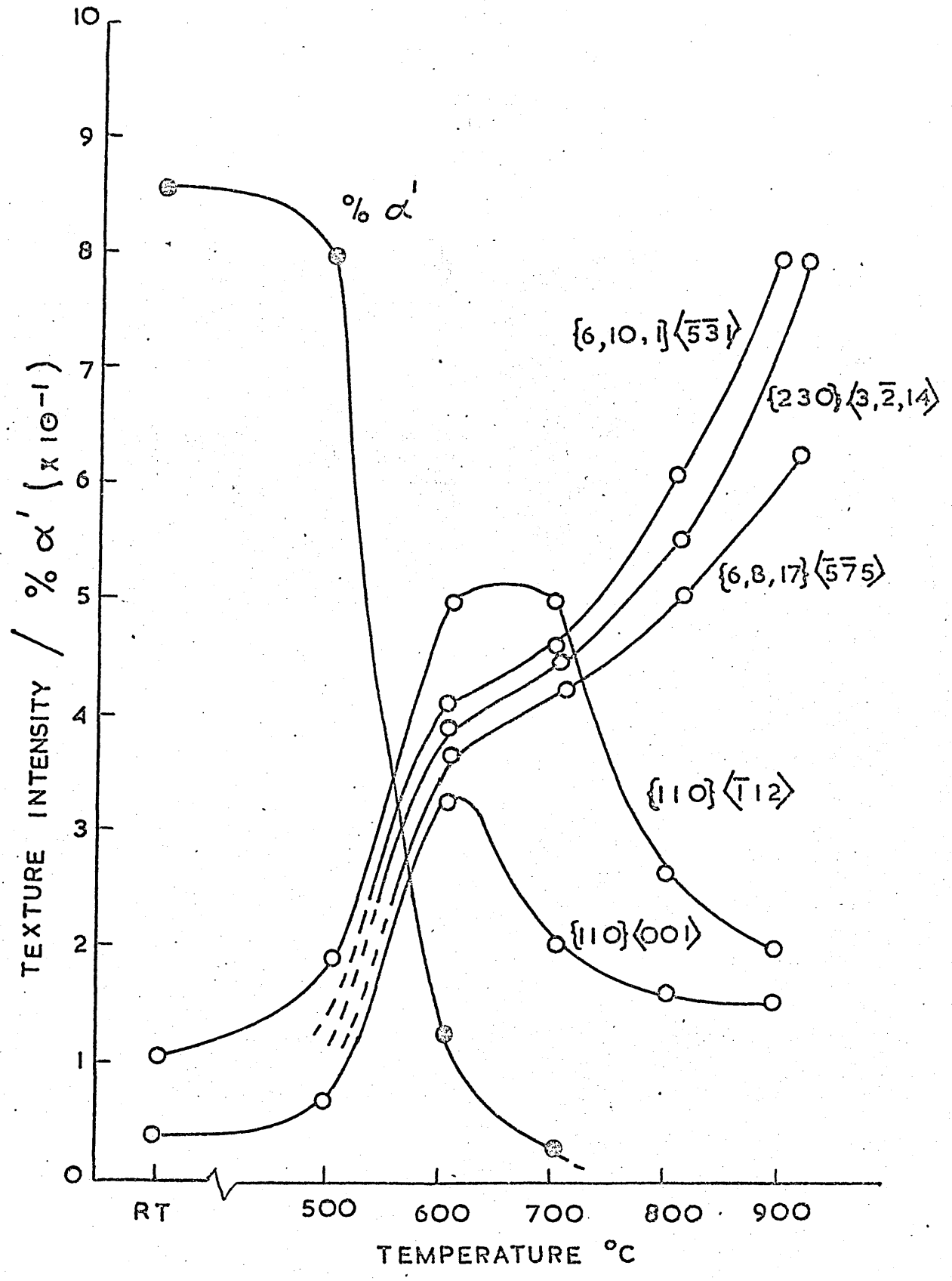

Figure 13.

Variation of % α' and intensities of γ texture components for 18%Cr 10%Ni steel.

1 hr 1050°C. FC, 95% cold rolled and annealed.

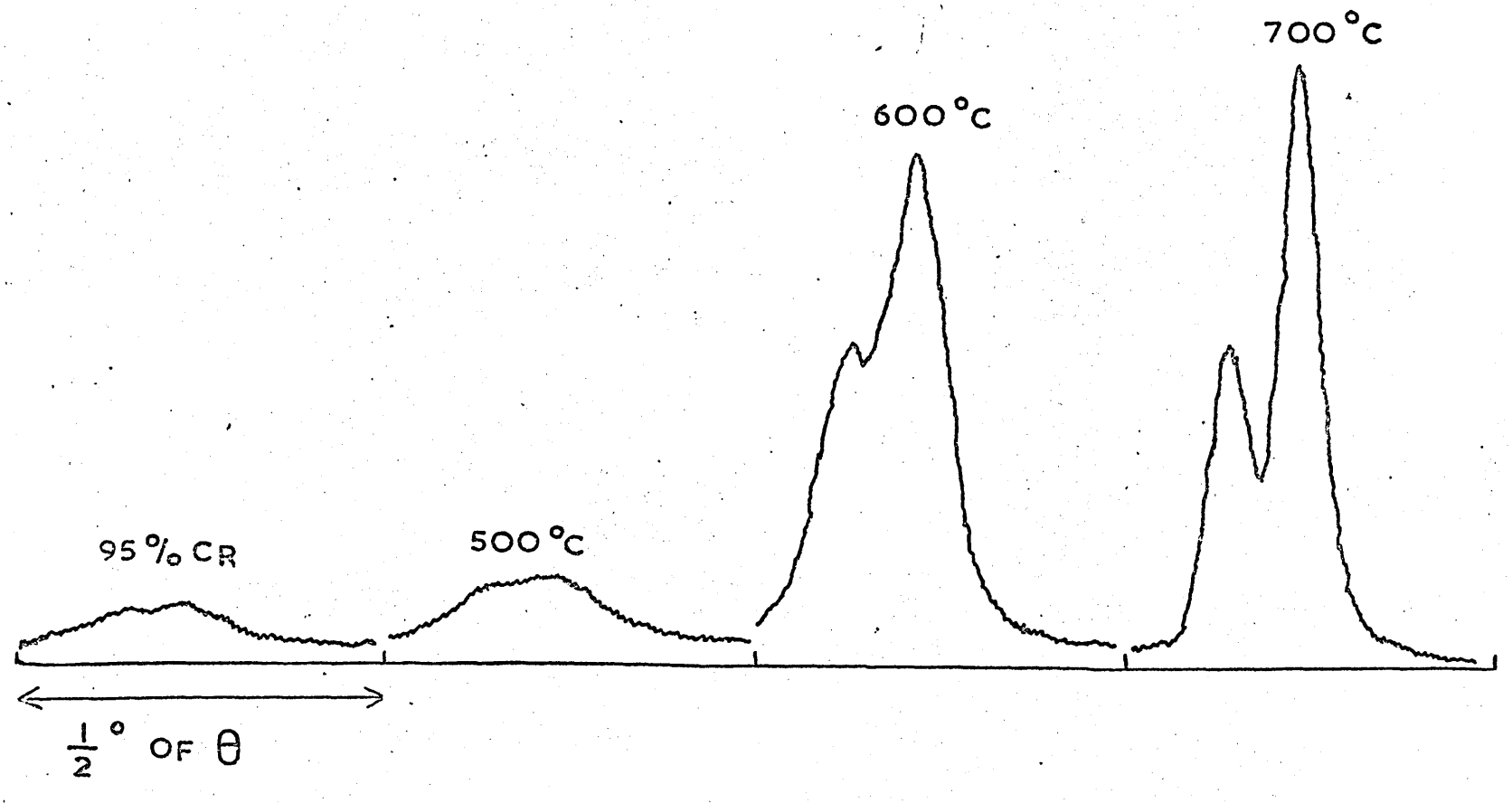

Figure 14.
220γ line profiles for 18%Cr 10%Ni steel.
1 hr 1050°C, FC, 95% cold rolled and annealed.

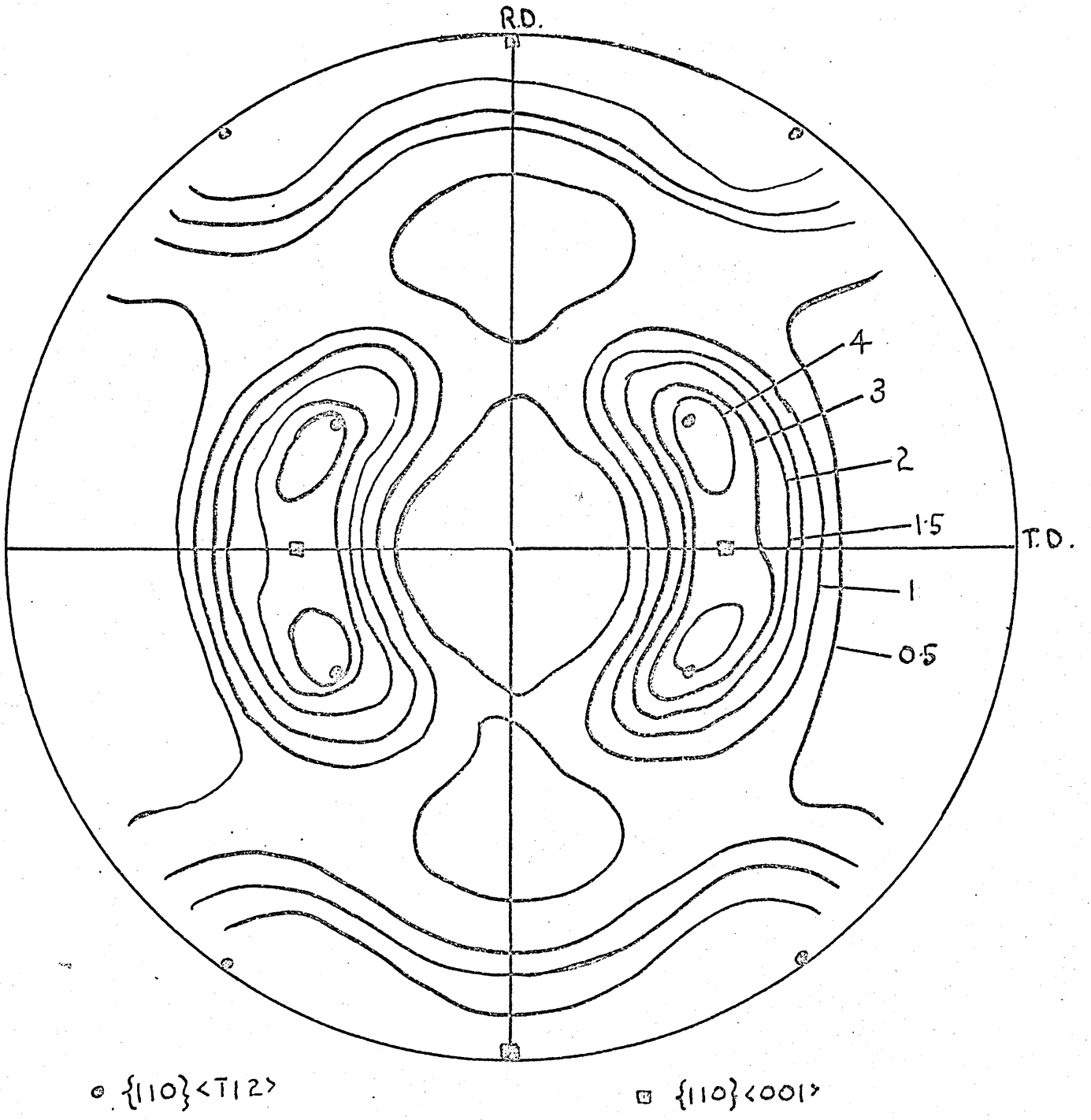

Figure 15.
{200}γ pole figure of 18%Cr 12%Ni steel.
1 hr 1050°C. FC, 95% cold rolled.

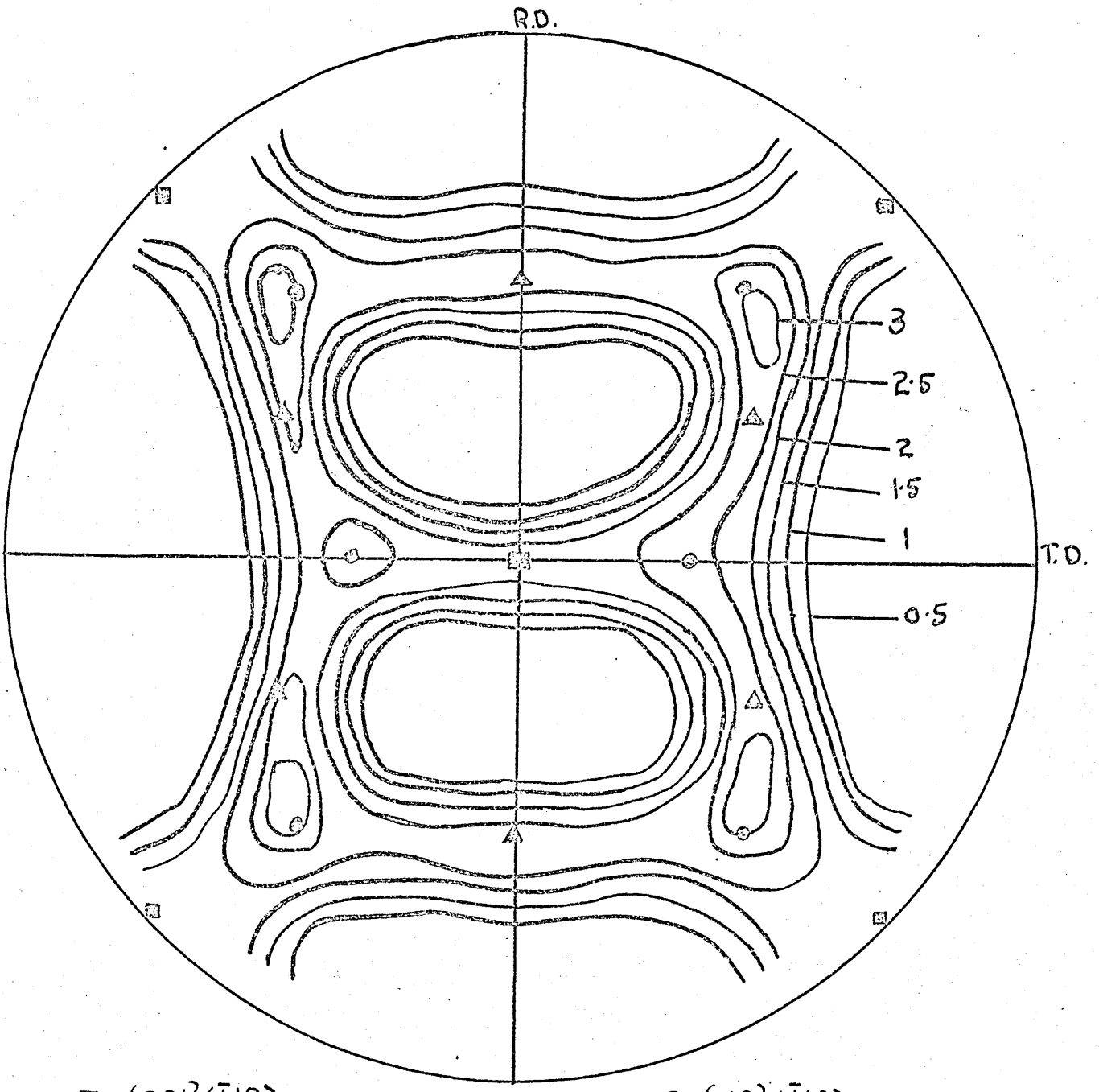

■ {001}<T10>

● {112}<T10>

△ {111}<TT2>

Figure 16.
{200}$_{\alpha'}$ pole figure of 18%Cr 12%Ni steel.
1 hr 1050°C. FC, 95% cold rolled.

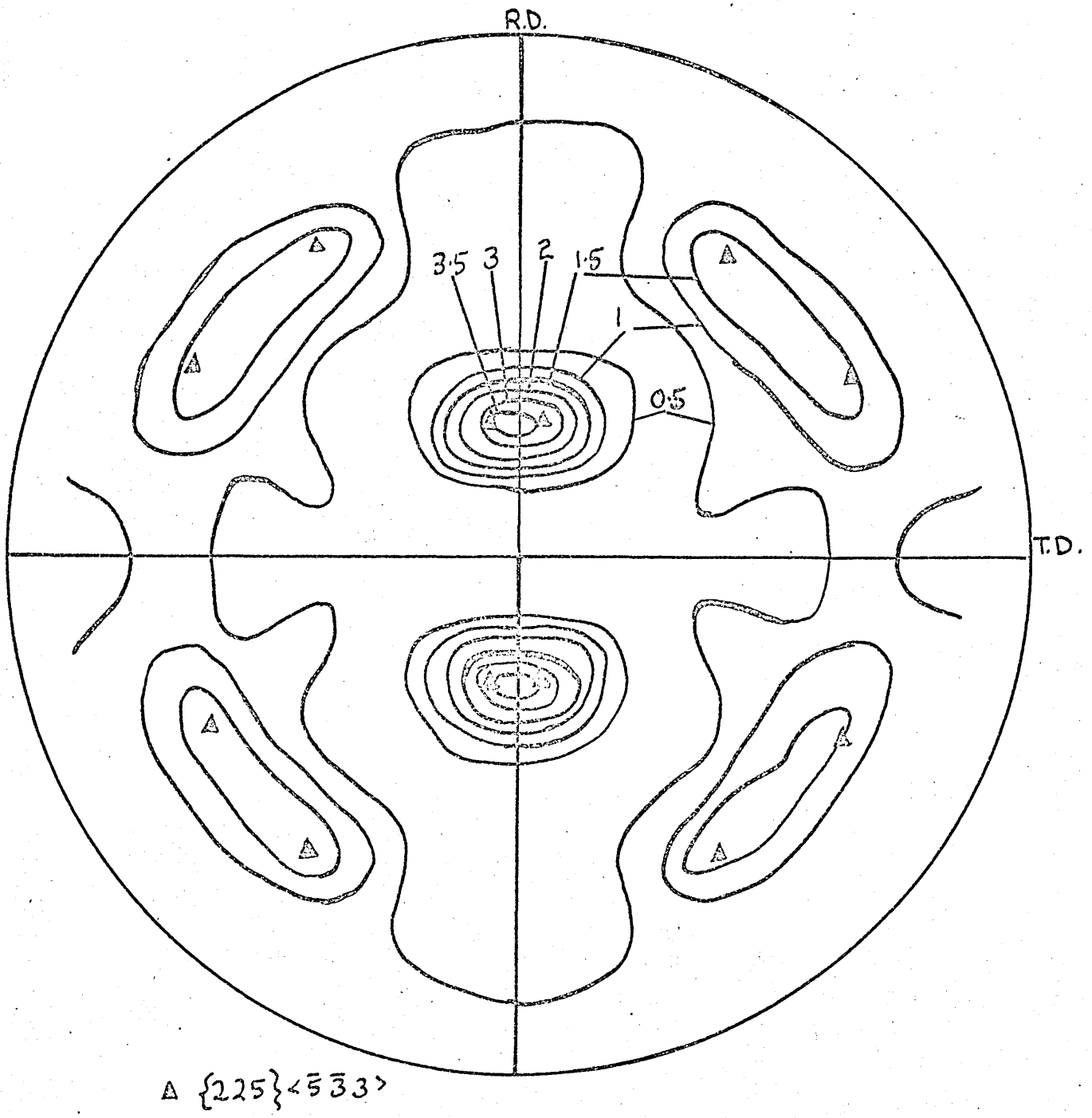

Figure 17.
{200}γ pole figure of 18%Cr 12%Ni steel.
1 hr 1050°C. FC, 95% cold rolled + ½hr 900°C. AC.

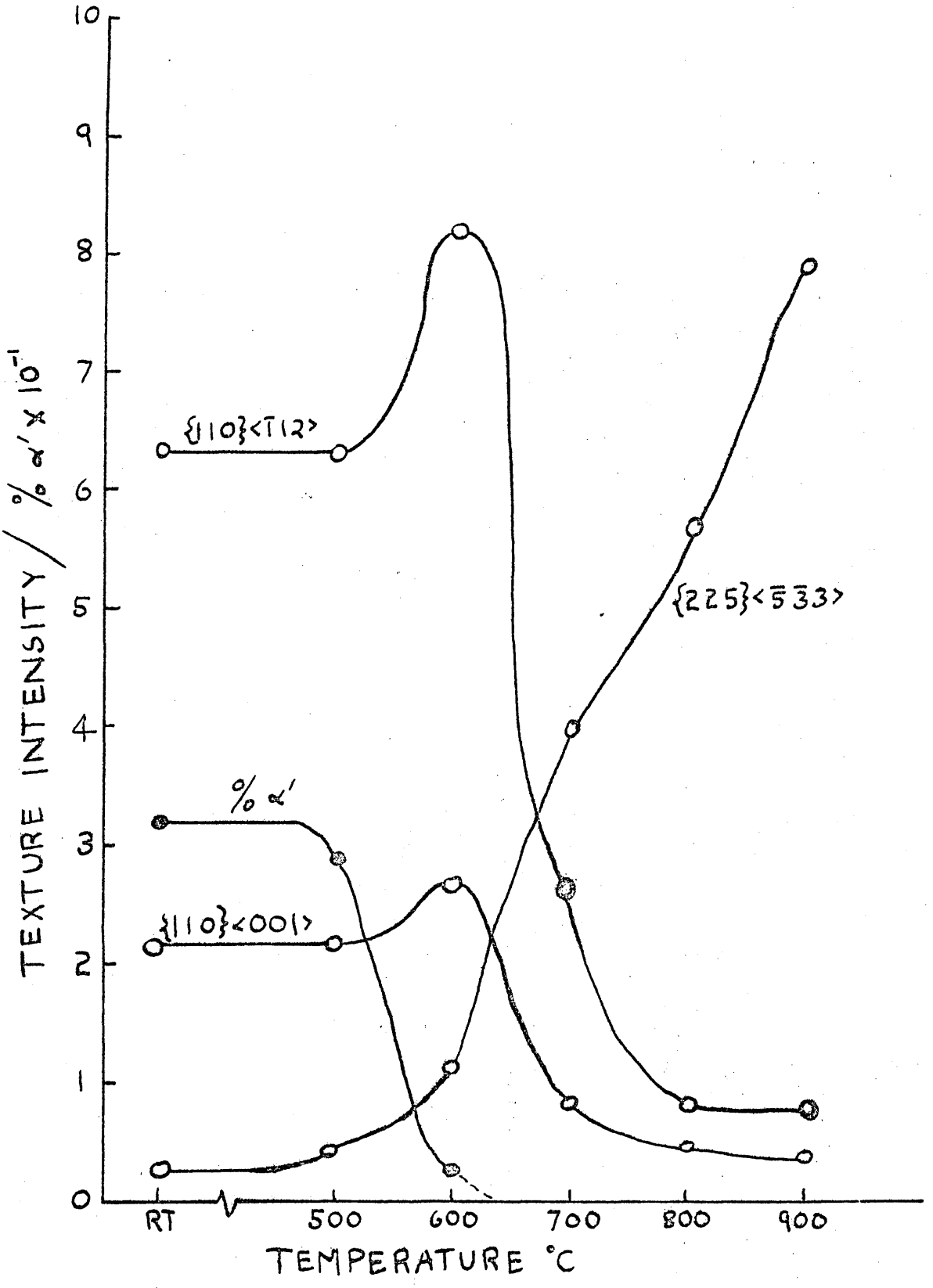

Figure 18.

Variation of % α' and intensities of γ texture components for 18%Cr 12%Ni steel.

1 hr 1050°C FC, 95% cold rolled and annealed.

Figure 19.

220γ line profiles for 18%Cr 12%Ni steel.
1 hr 1050°C. FC, 95% cold rolled and annealed.

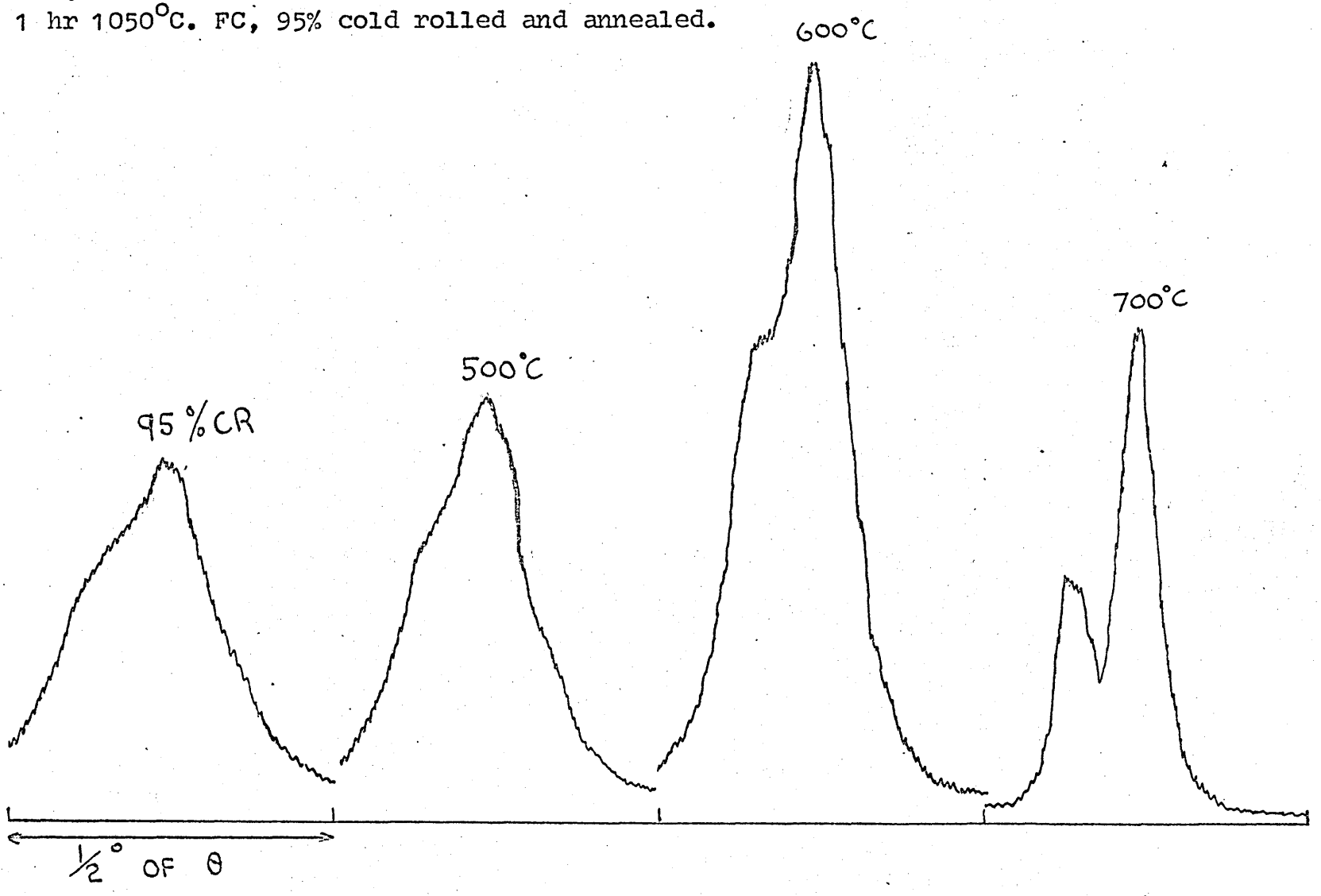

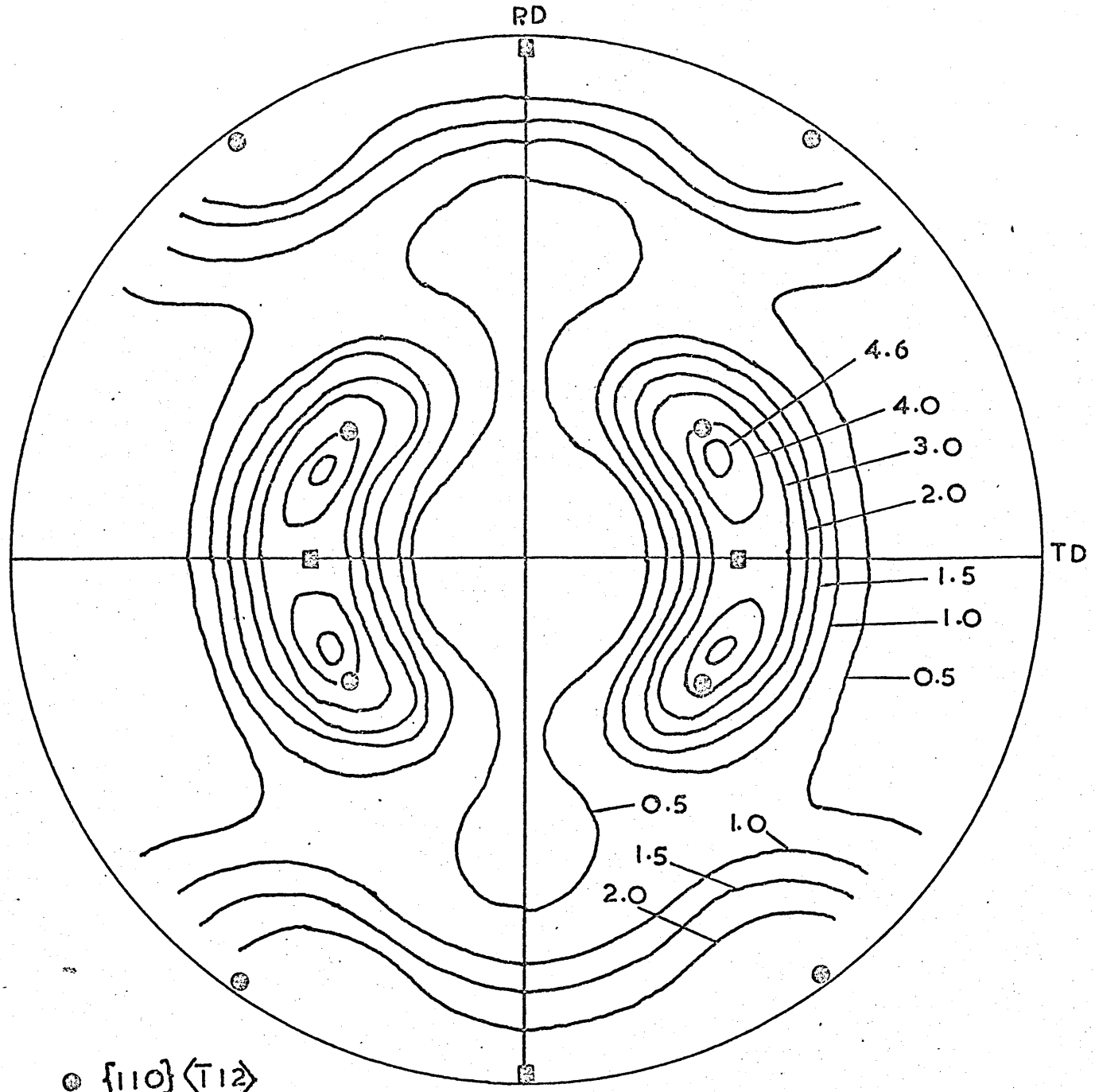

Figure 20.
{200}γ pole figure of 18%Cr 14%Ni steel.
1 hr 1050°C. FC, 95% cold rolled.

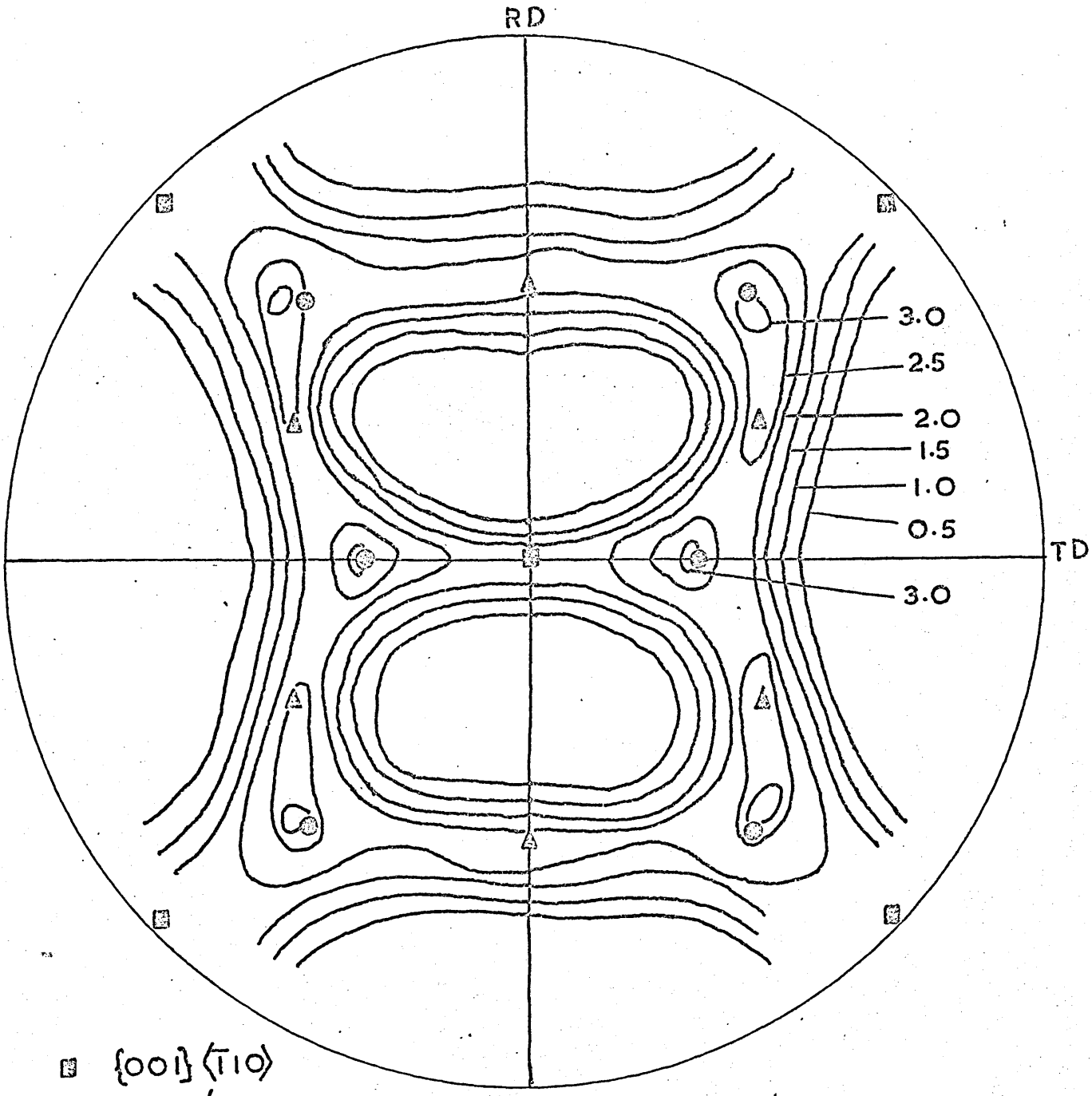

Figure 21.
{200}$_{\alpha'}$ pole figure of 18%Cr 14%Ni steel.
1 hr 1050°C. FC, 95% cold rolled.

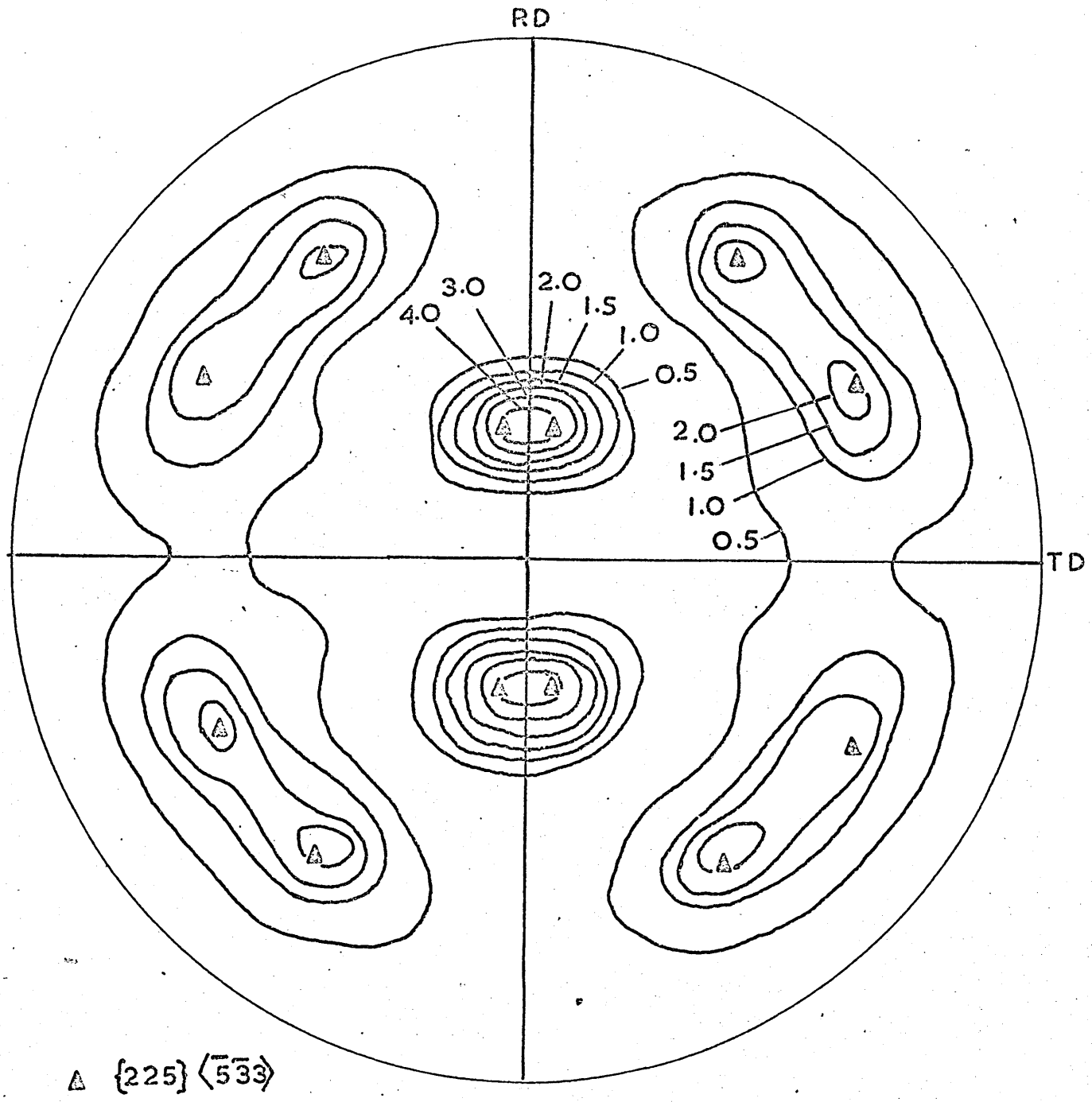

Figure 22.
{200}γ pole figure of 18%Cr 14%Ni steel.
1 hr 1050°C. FC, 95% cold rolled + ½hr 900°C. AC.

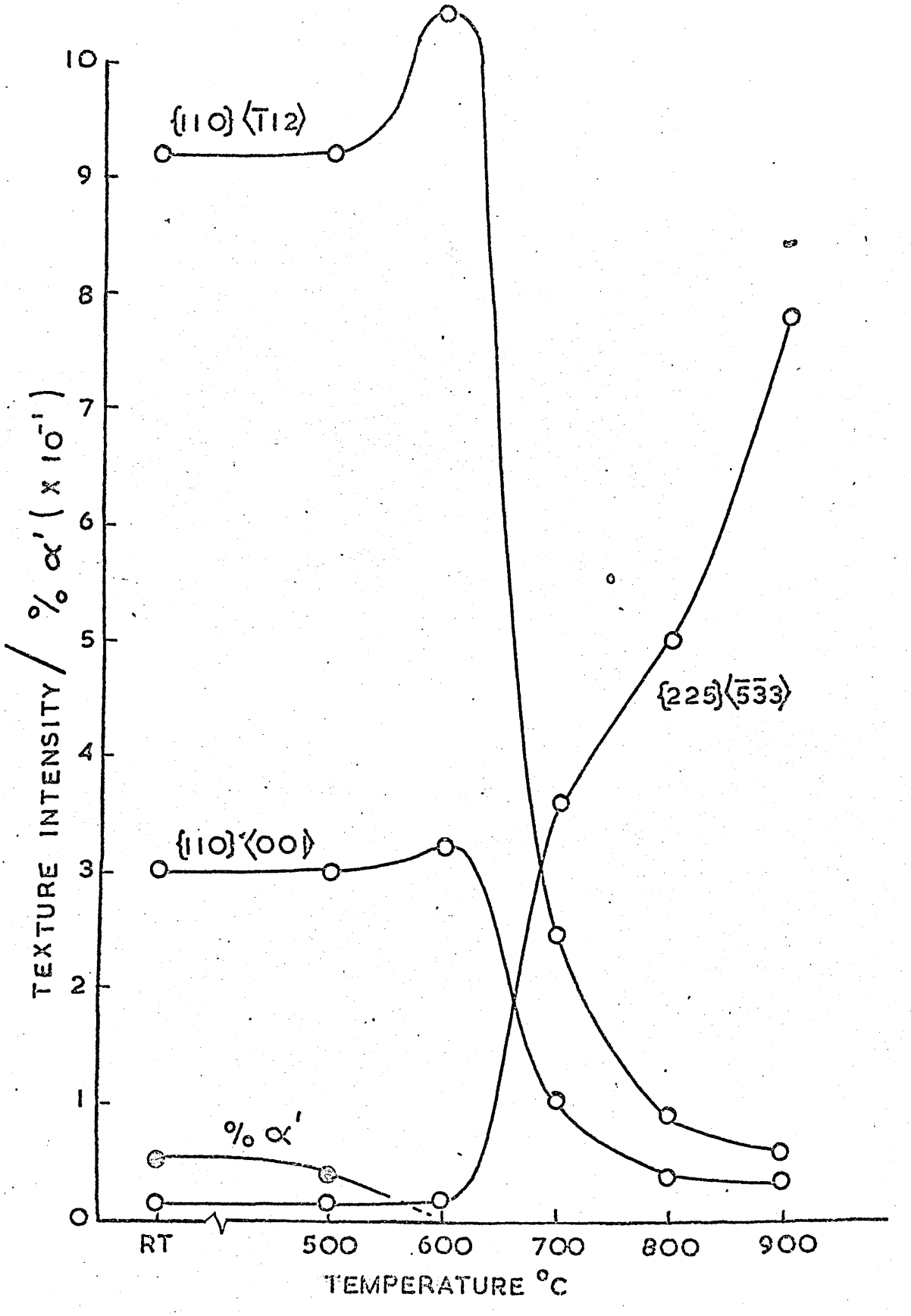

Figure 23.

Variation of % α' and intensities of γ texture components for 18%Cr 14%Ni steel.

1 hr 1050°C. FC, 95% cold rolled and annealed.

Figure 24.

220γ line profiles for 18%Cr 14%Ni steel.

1 hr 1050°C. FC, 95% cold rolled and annealed.

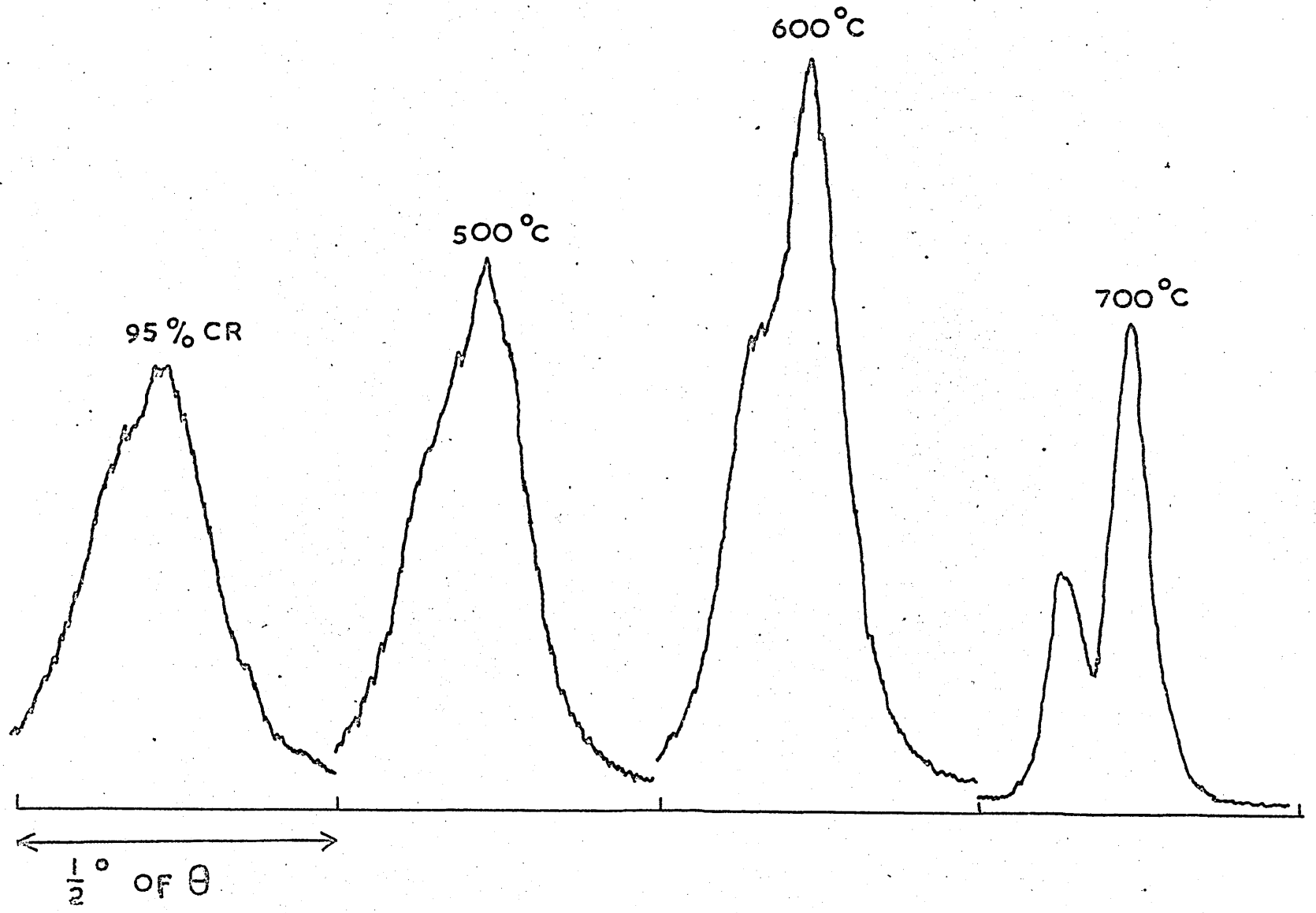

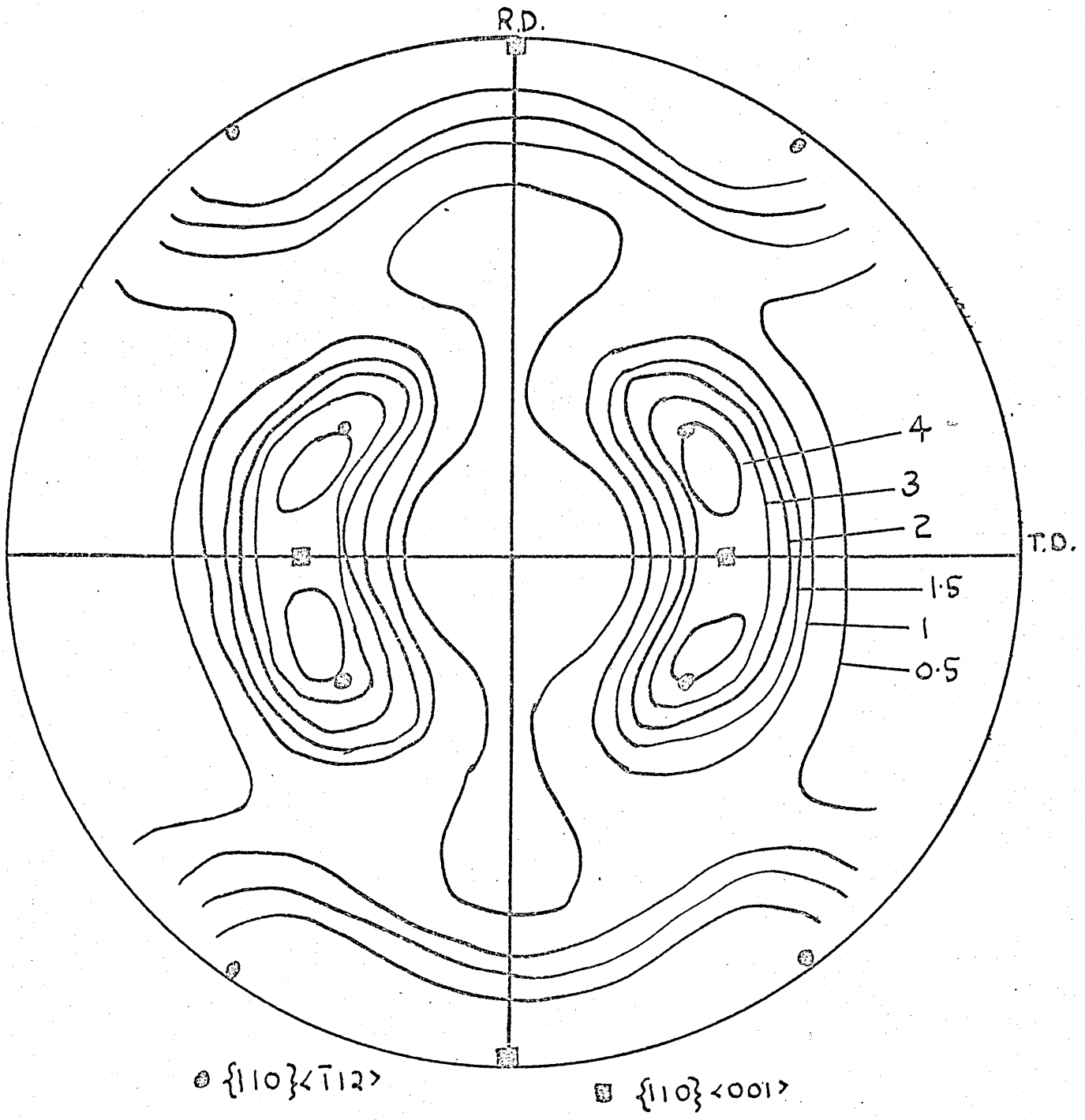

Figure 25.
{200}γ pole figure of 18%Cr 12%Ni 7%Co steel.
1 hr 1050°C. FC, 90% cold rolled.

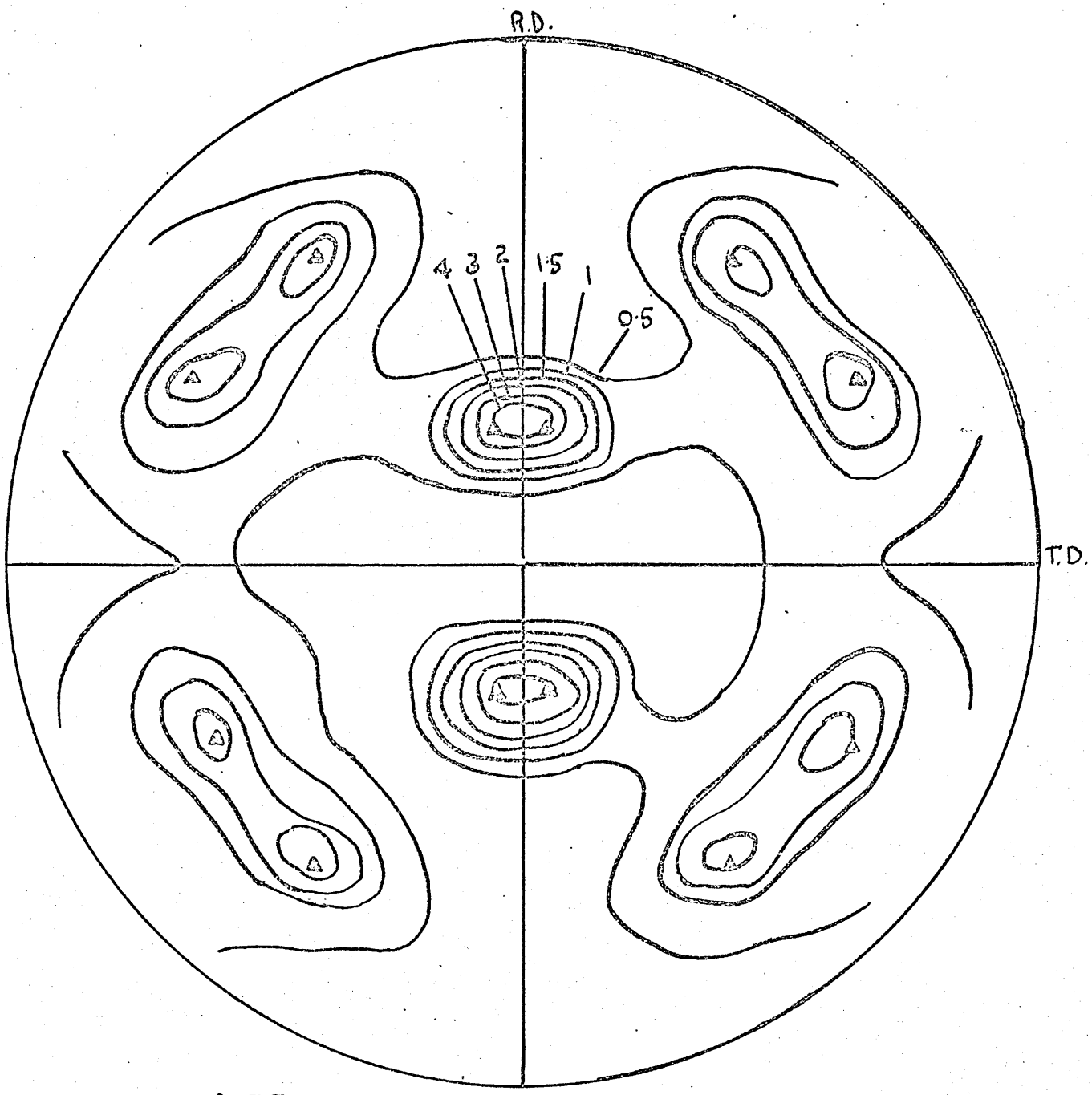

Figure 26.
{200}γ pole figure of 18%Cr 12%Ni 7%Co steel.
1 hr 1050°C. FC, 90% cold rolled + ½hr 900°C. AC.

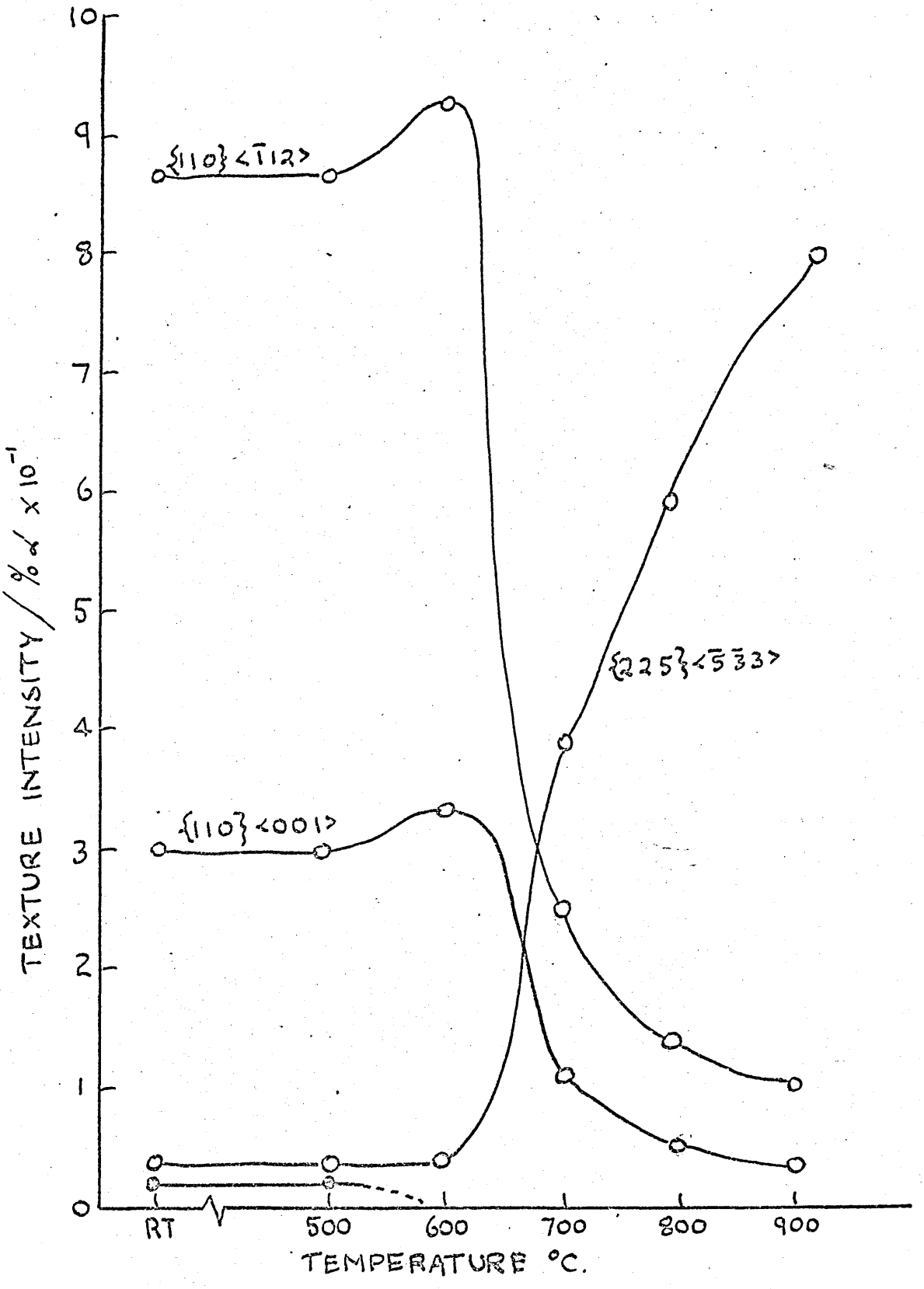

Figure 27.

Variation of % α' and intensities of γ texture components for 18%Cr 12%Ni 7%Co steel.

1 hr 1050°C. FC, 90% cold rolled and annealed.

Figure 28.

220γ line profiles for 18%Cr 12%Ni 7%Co steel.
1 hr 1050°C. FC, 90% cold rolled and annealed.

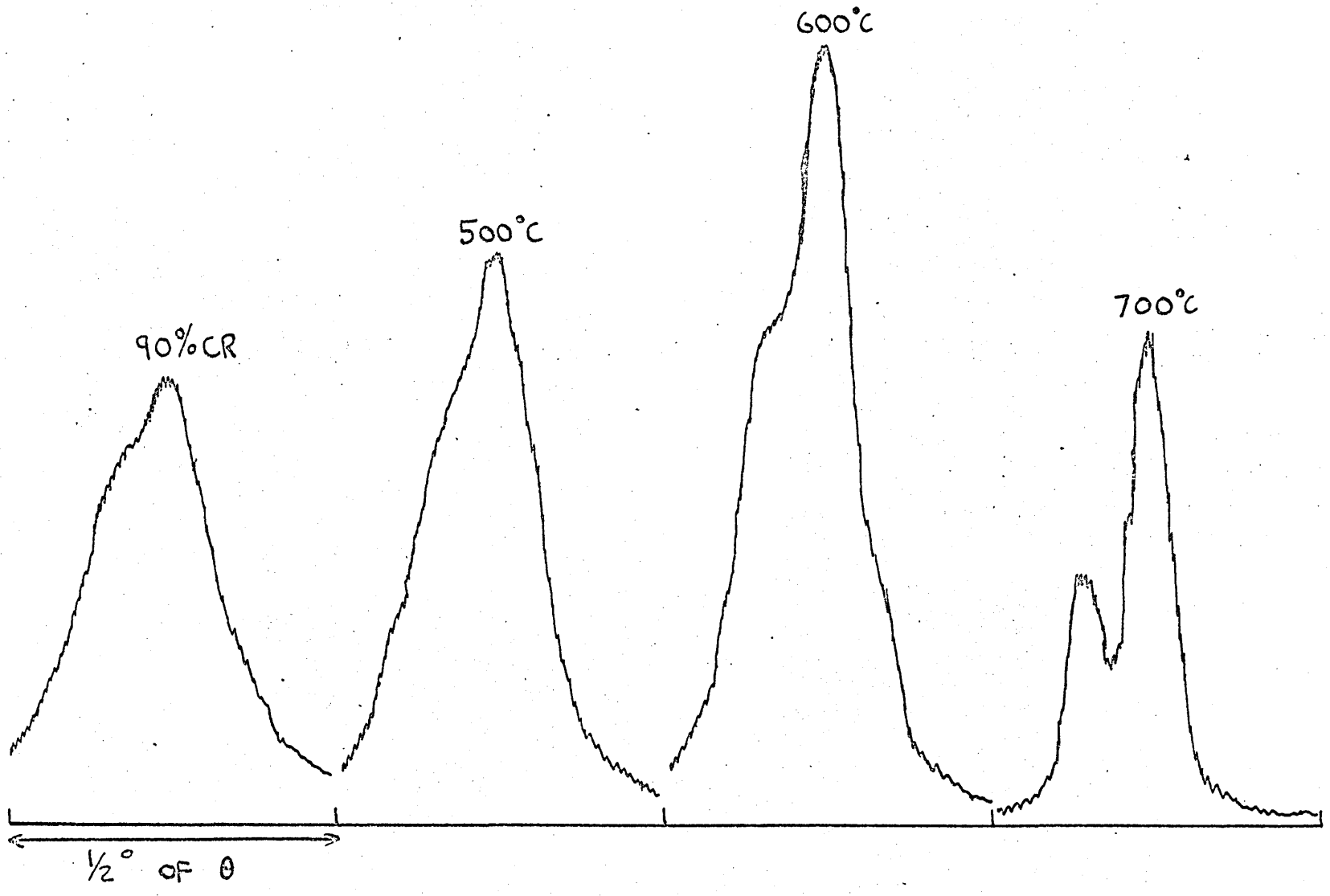

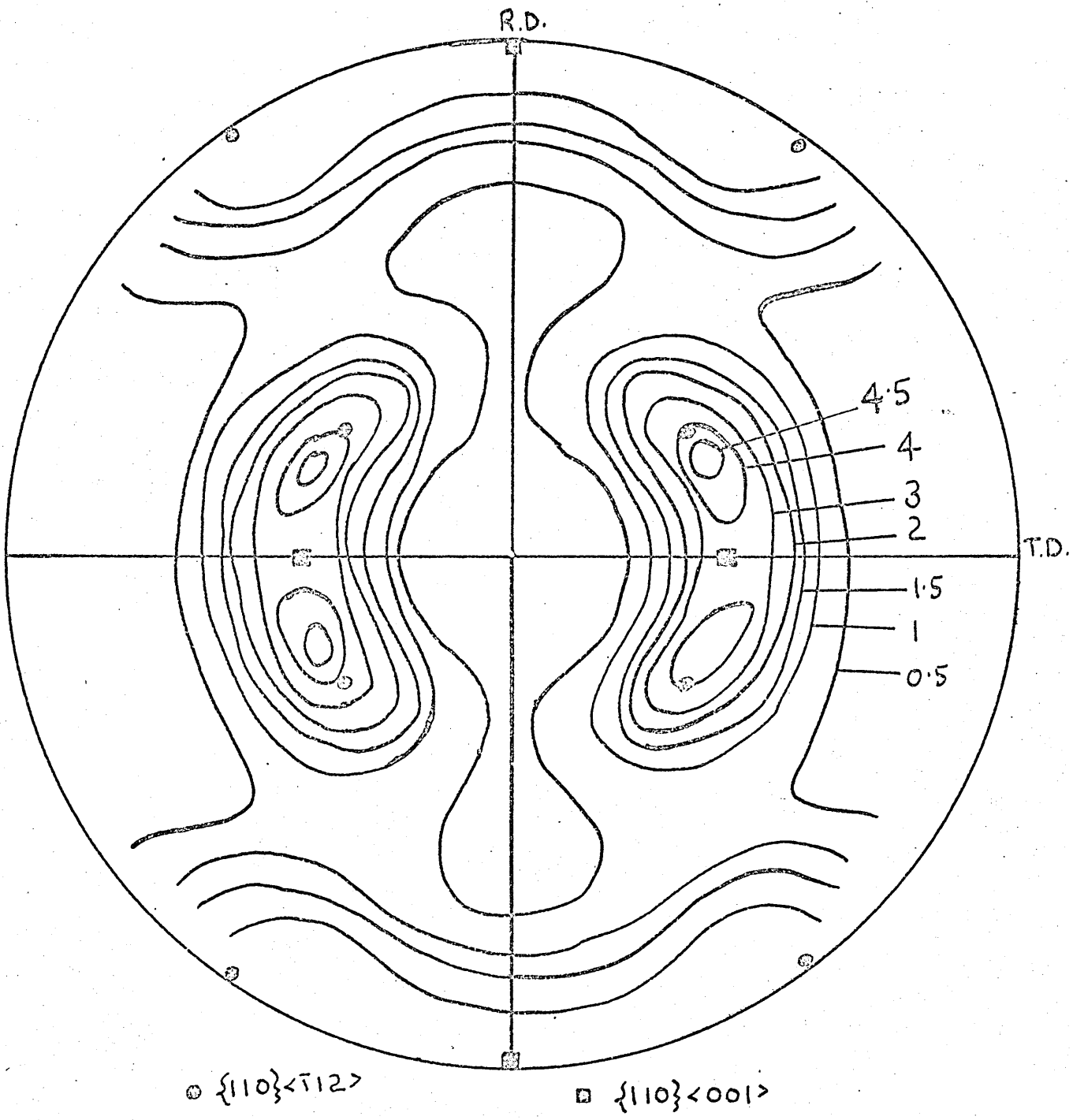

Figure 29.
{200}γ pole figure of 18%Cr 25%Ni steel.
1 hr 1050°C. FC, 90% cold rolled.

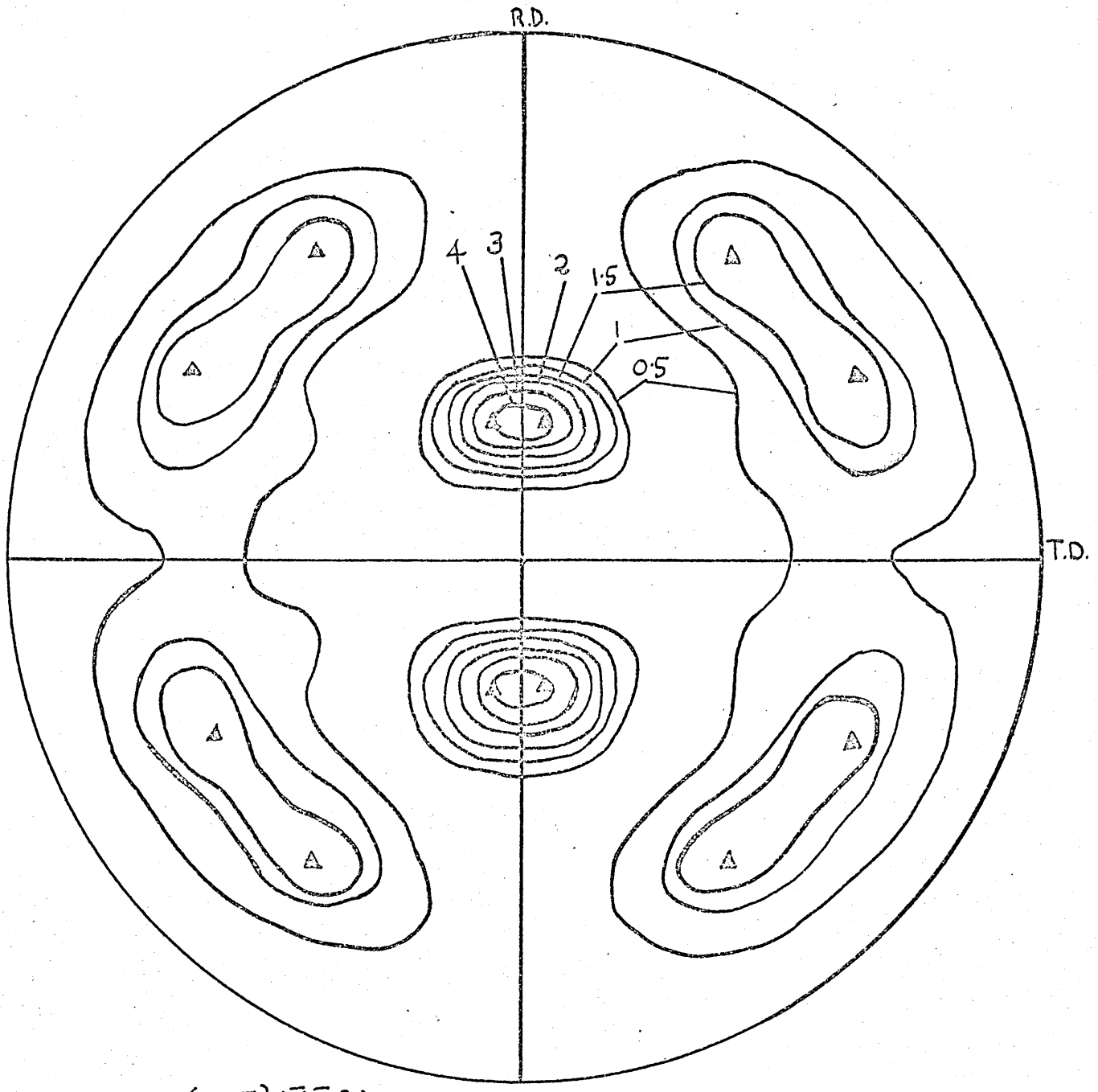

Figure 30.

{200}γ pole figure of 18%Cr 25%Ni steel.

1 hr 1050°C. FC, 90% cold rolled + ½hr 900°C. AC.

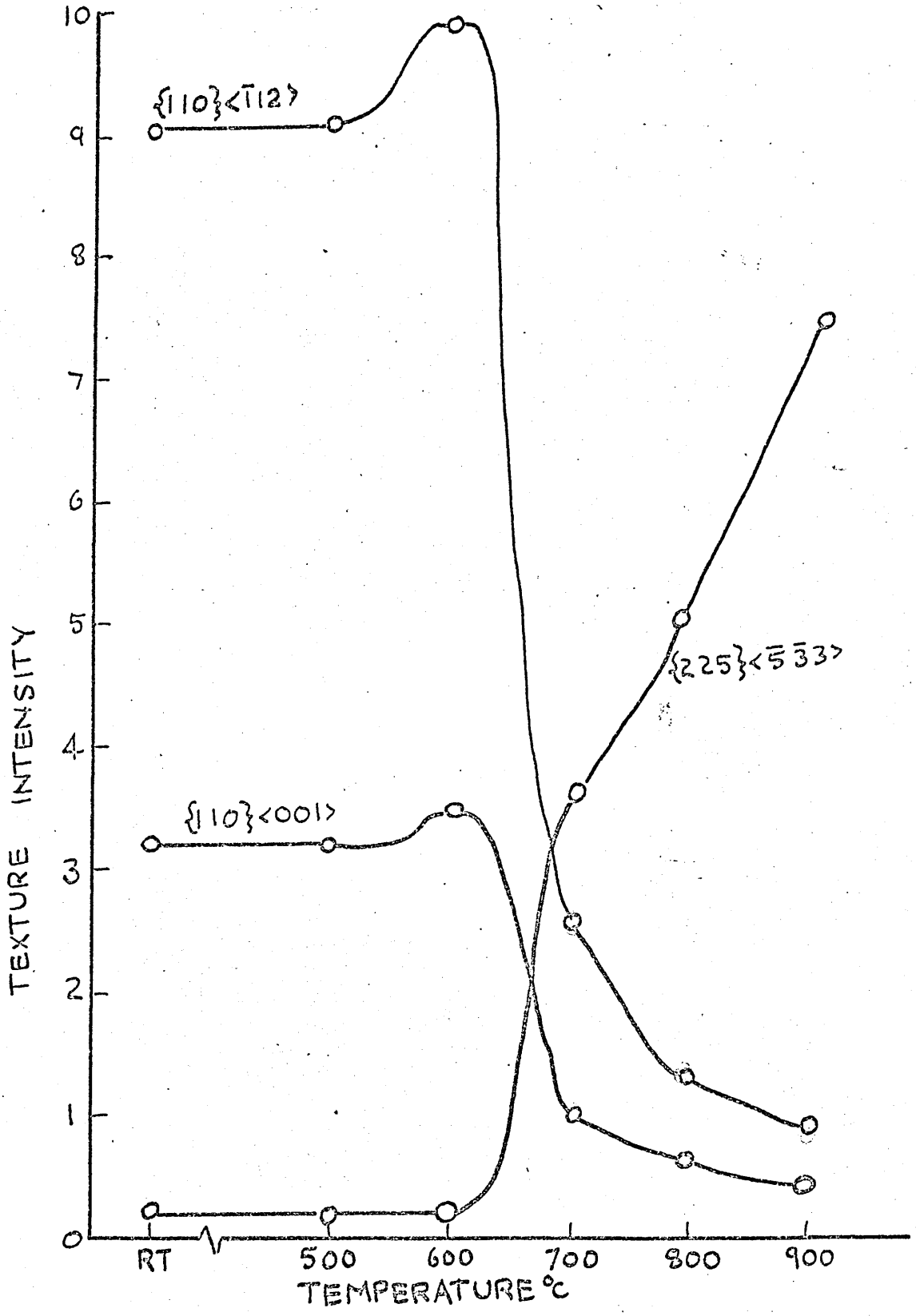

Figure 31.

Variation of intensities of γ texture components for 18%Cr 25%Ni steel.

1 hr 1050°C. FC, 90% cold rolled and annealed.

Figure 32.

220γ line profiles for 18%Cr 25%Ni steel.

1 hr 1050°C. FC, 90% cold rolled and annealed.

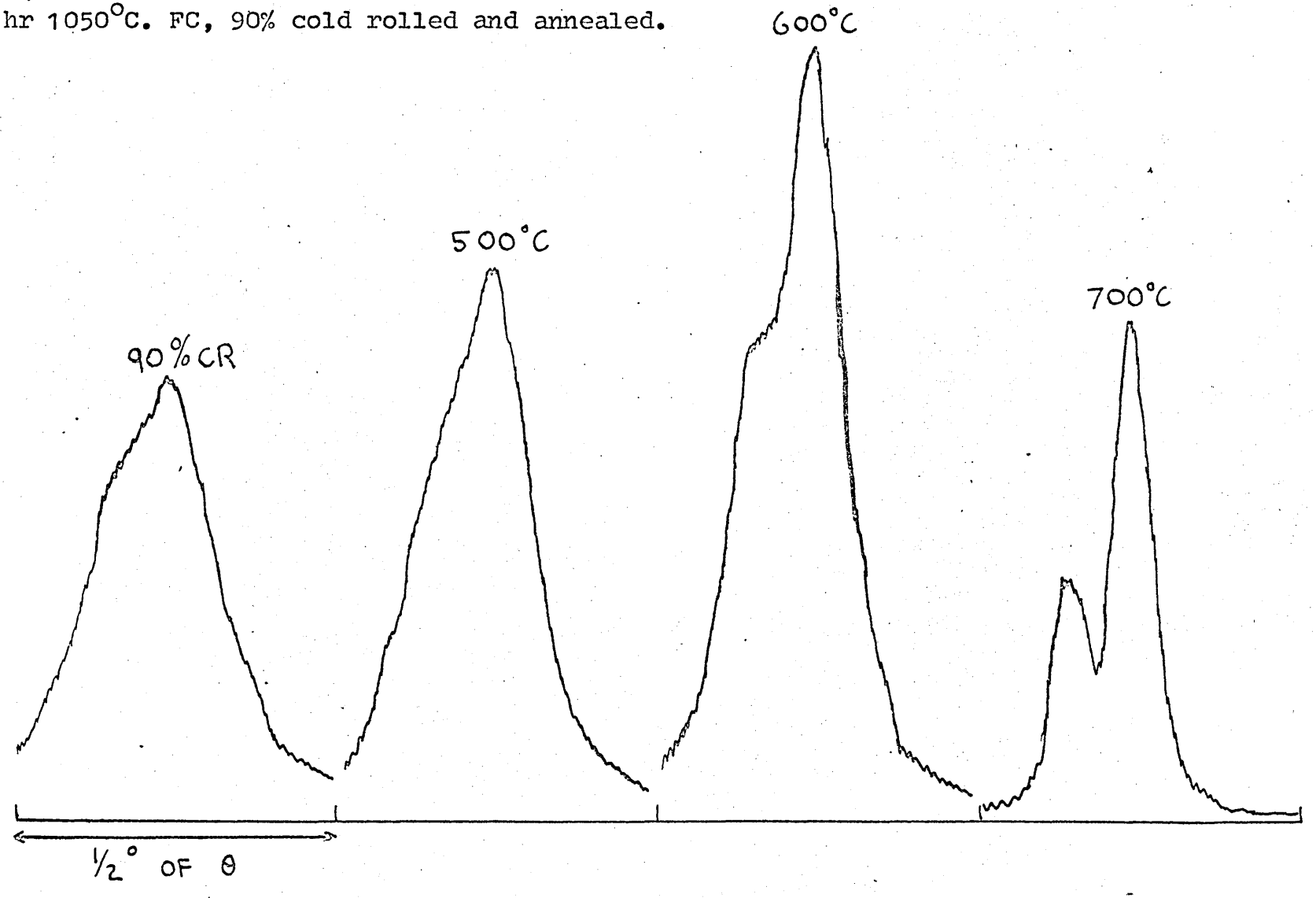

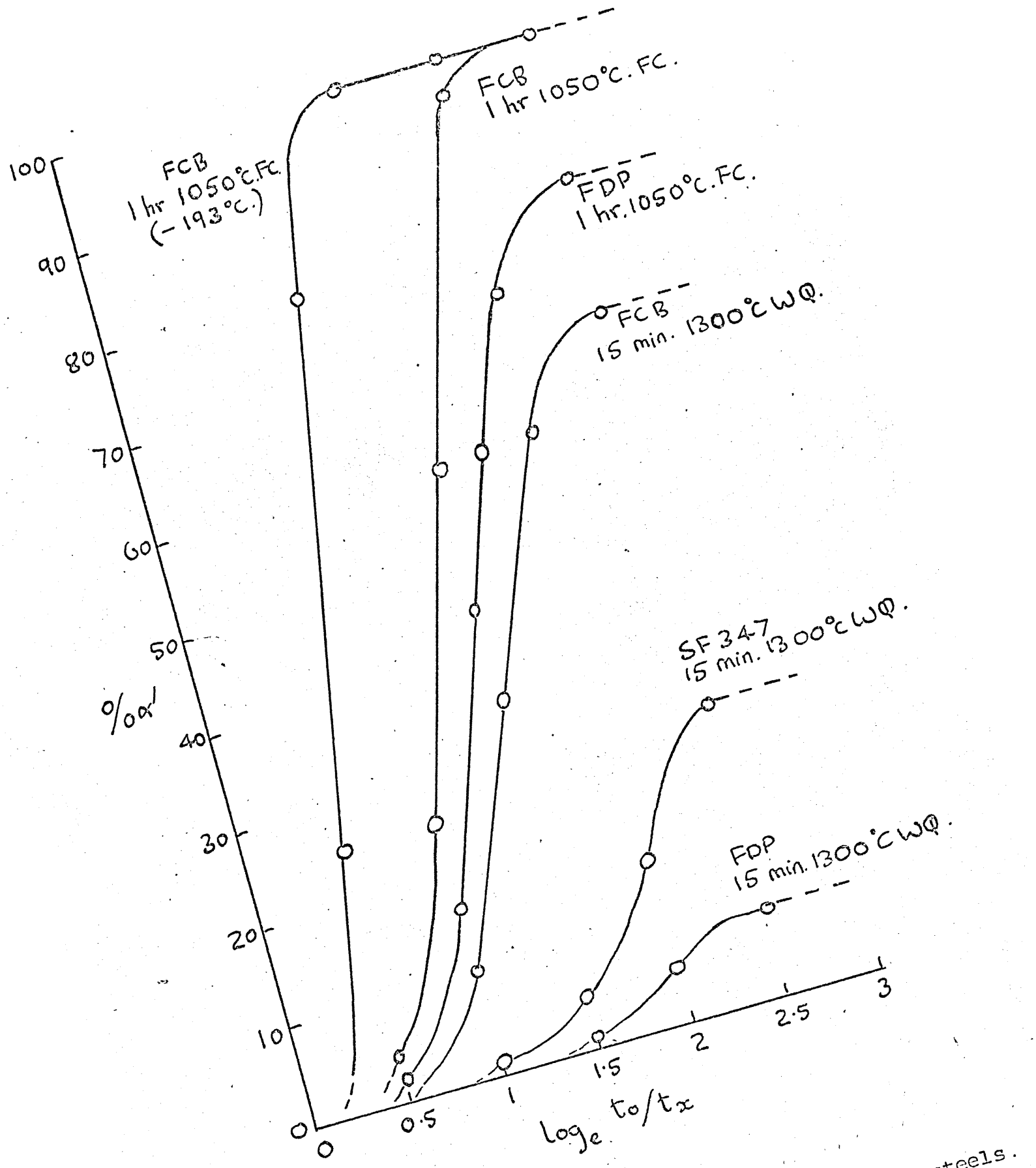

Figure 33

Variation of % α' during cold rolling of commercial steels.

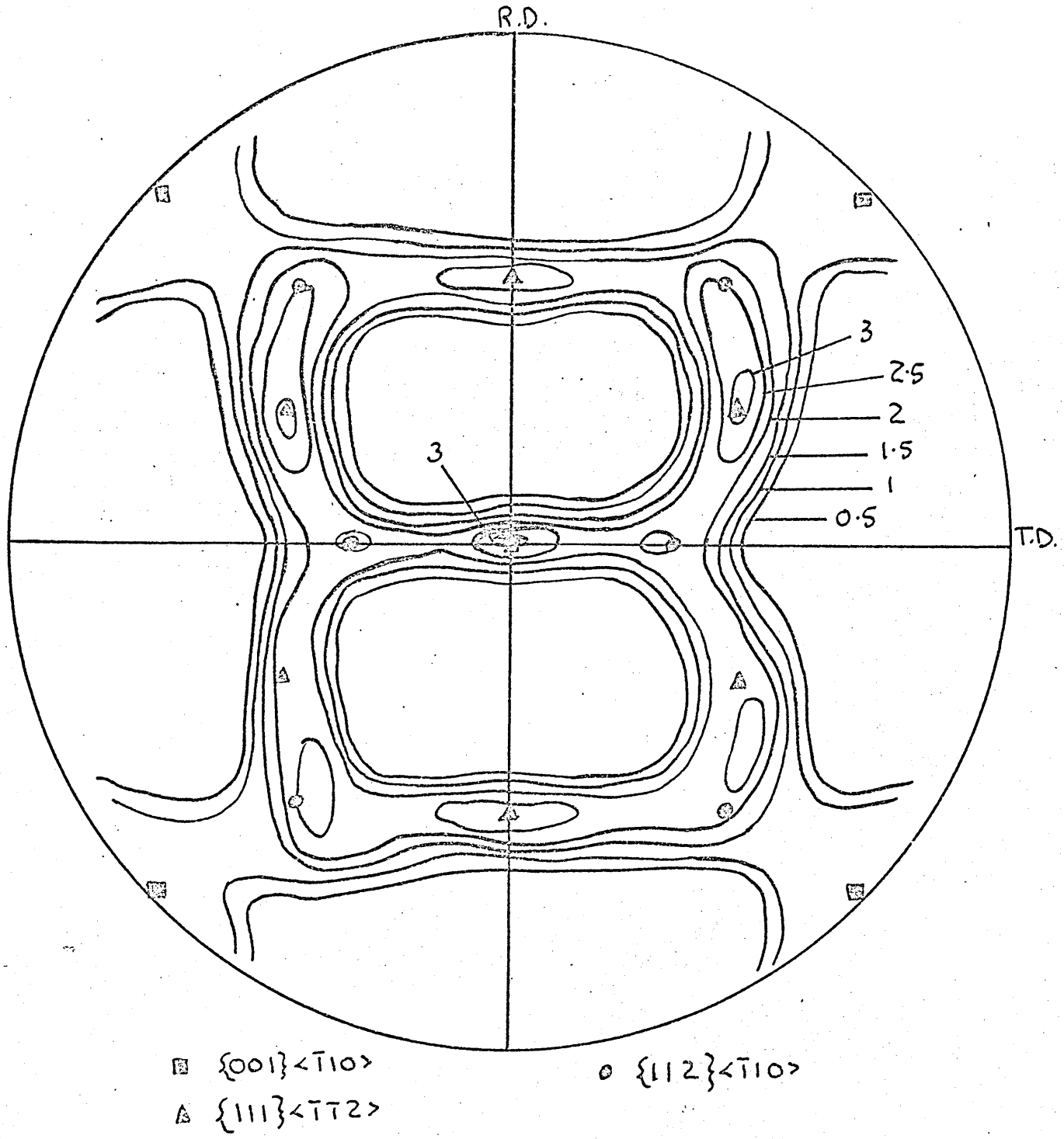

Figure 34

{200}α' pole figure of FCB steel.
1hr 1050^{o}C.FC, 90% cold rolled.

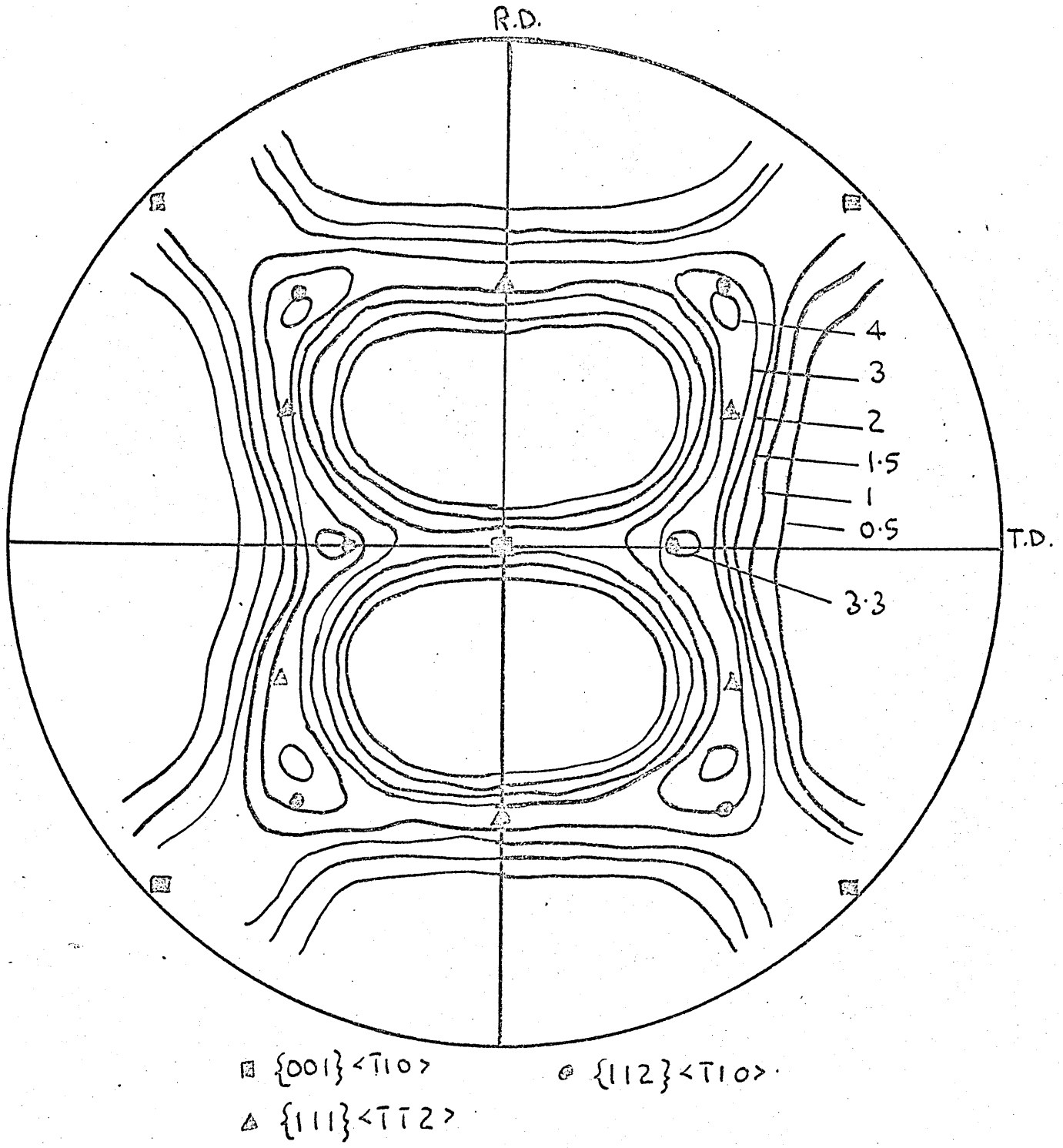

Figure 35

{200}α' pole figure of FCB steel.
15 min. 1300°C WQ, 90% cold rolled.

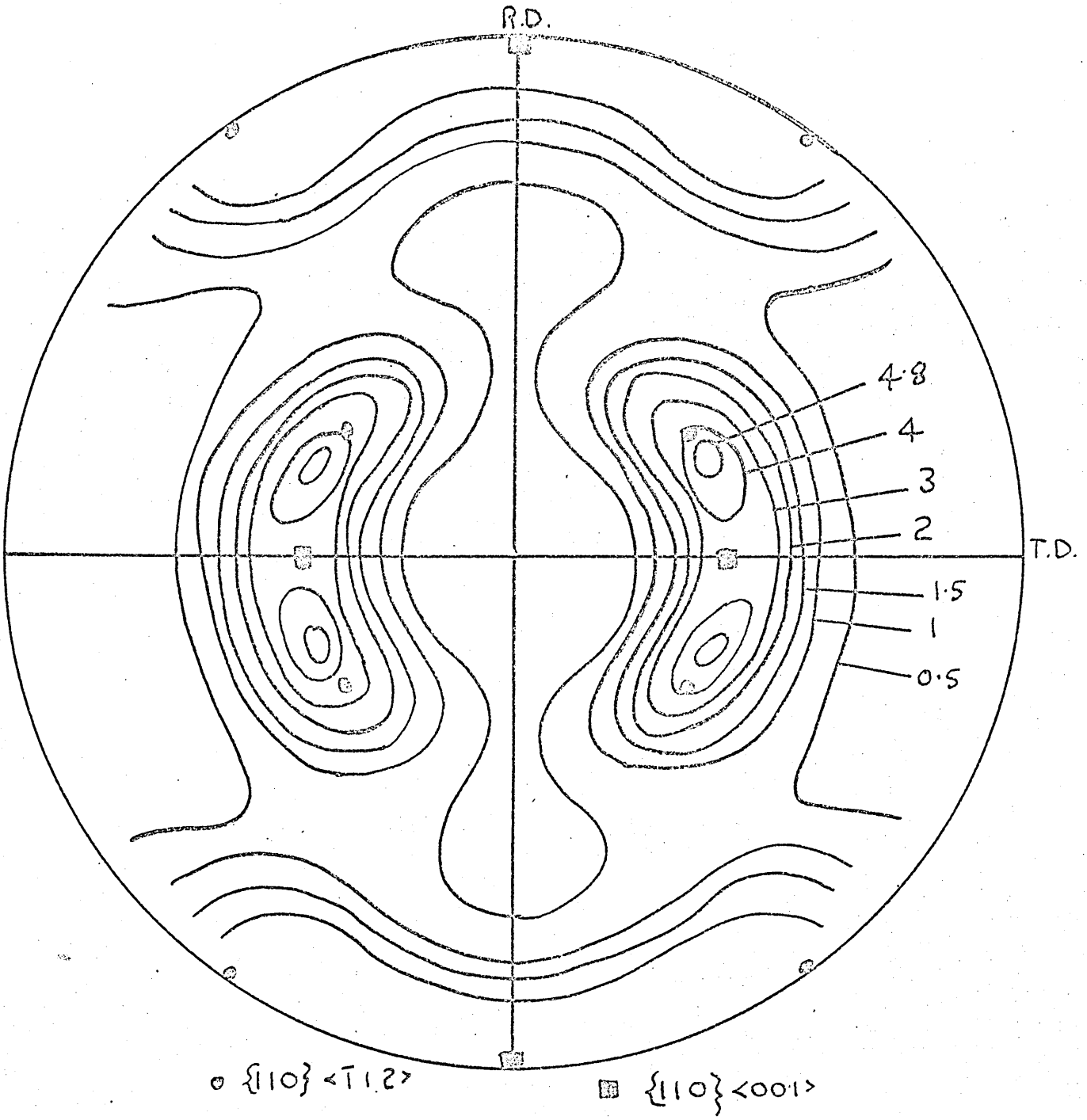

Figure 36

{200}γ pole figure of RF310 steel.
1hr 1050°C. FC, 90% cold rolled.

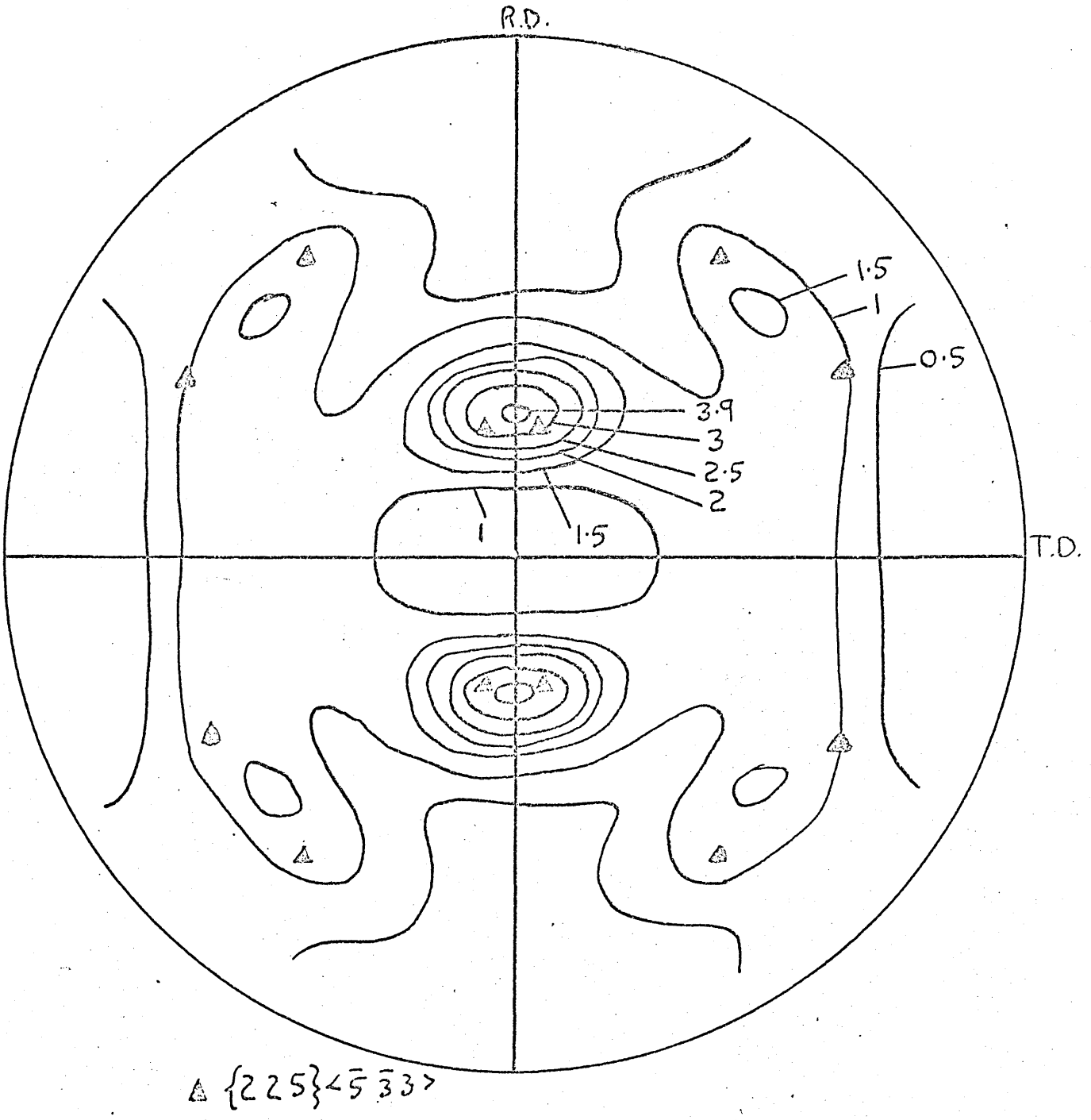

Figure 37

{200}γ pole figure of RF310 steel.
1hr 1050°C. FC, 90% cold rolled + ½hr 900°C.AC.

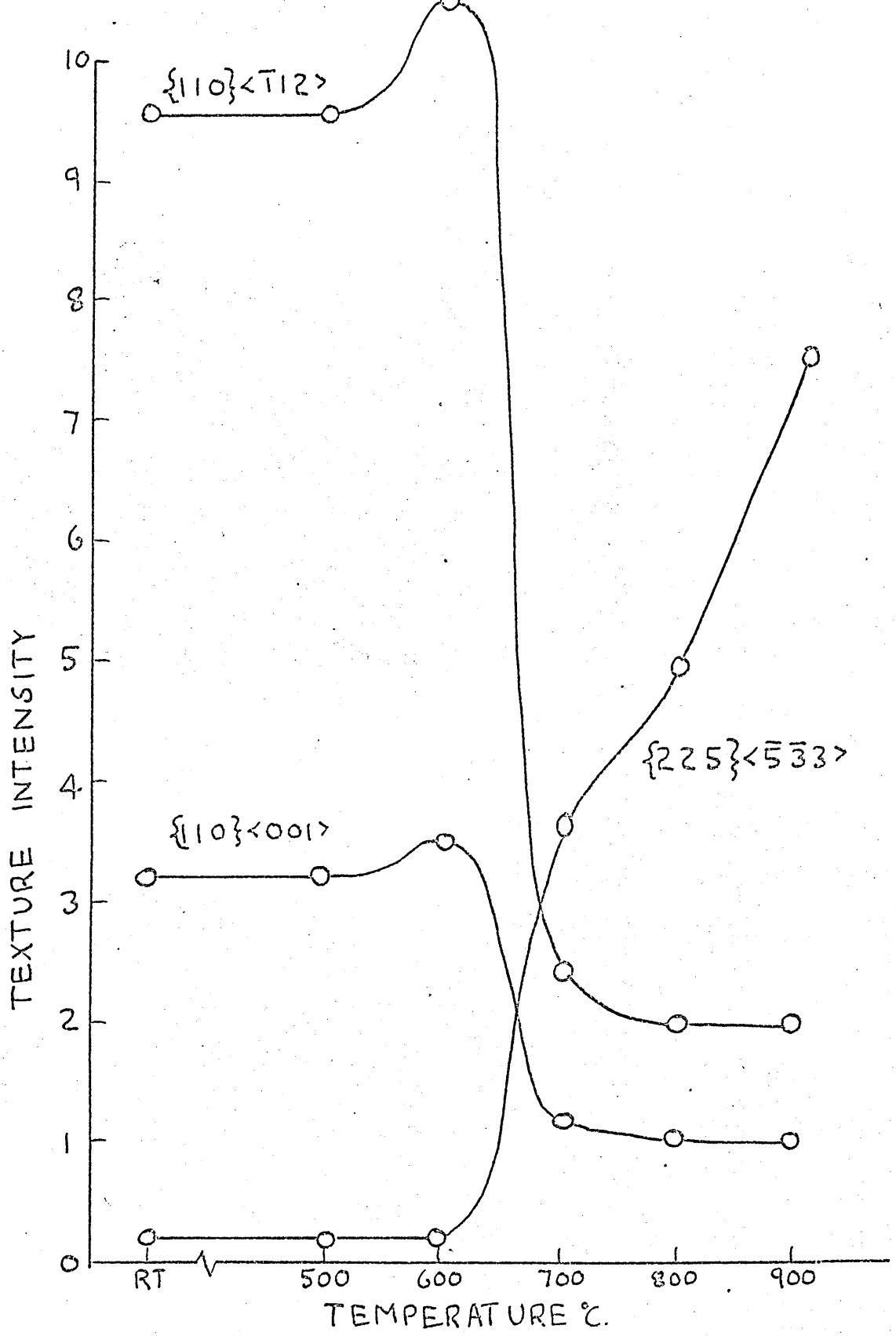

Figure 38

Variation of intensities of γ texture components for RF310 steel. 1hr 1050 °C: FC; 90% cold rolled and annealed.

Figure 39

220γ line profiles for RF310 steel.
1hr 1050°C. FC, 90% cold rolled and annealed.

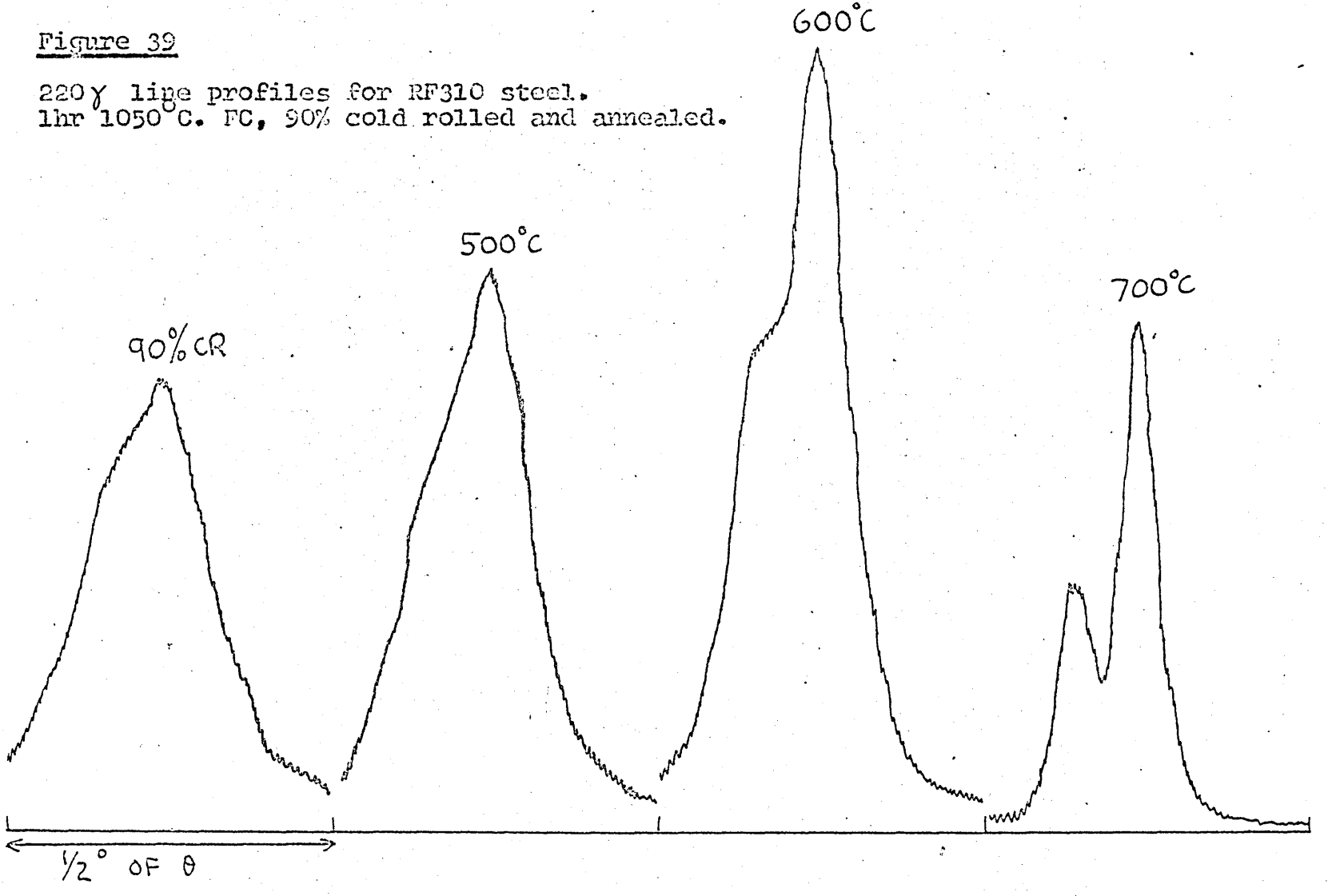

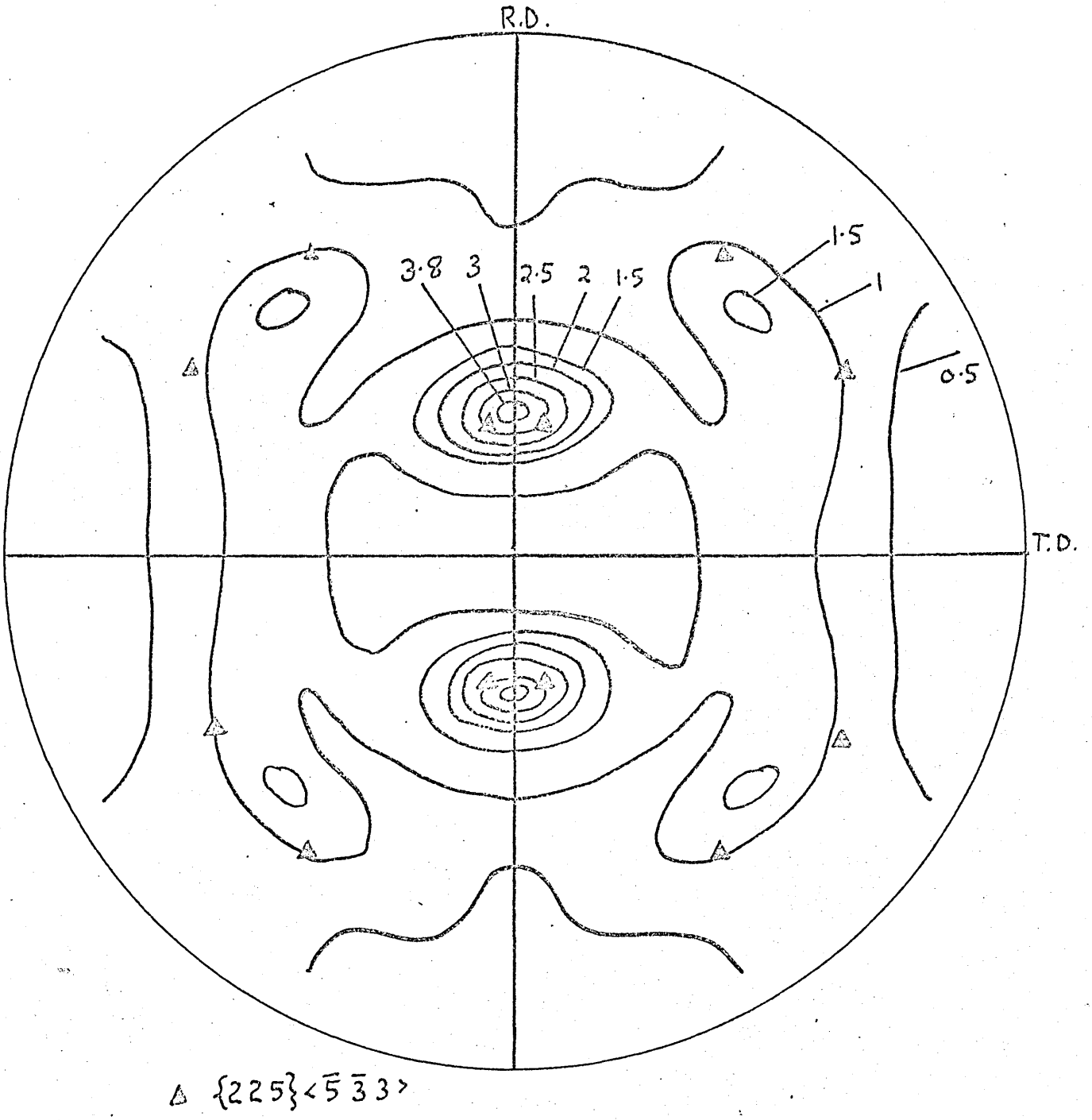

Figure 40

{200}γ pole figure of RF310 steel.
1hr 1050°C. WQ, 90% cold rolled + ½hr 900°C.AC.

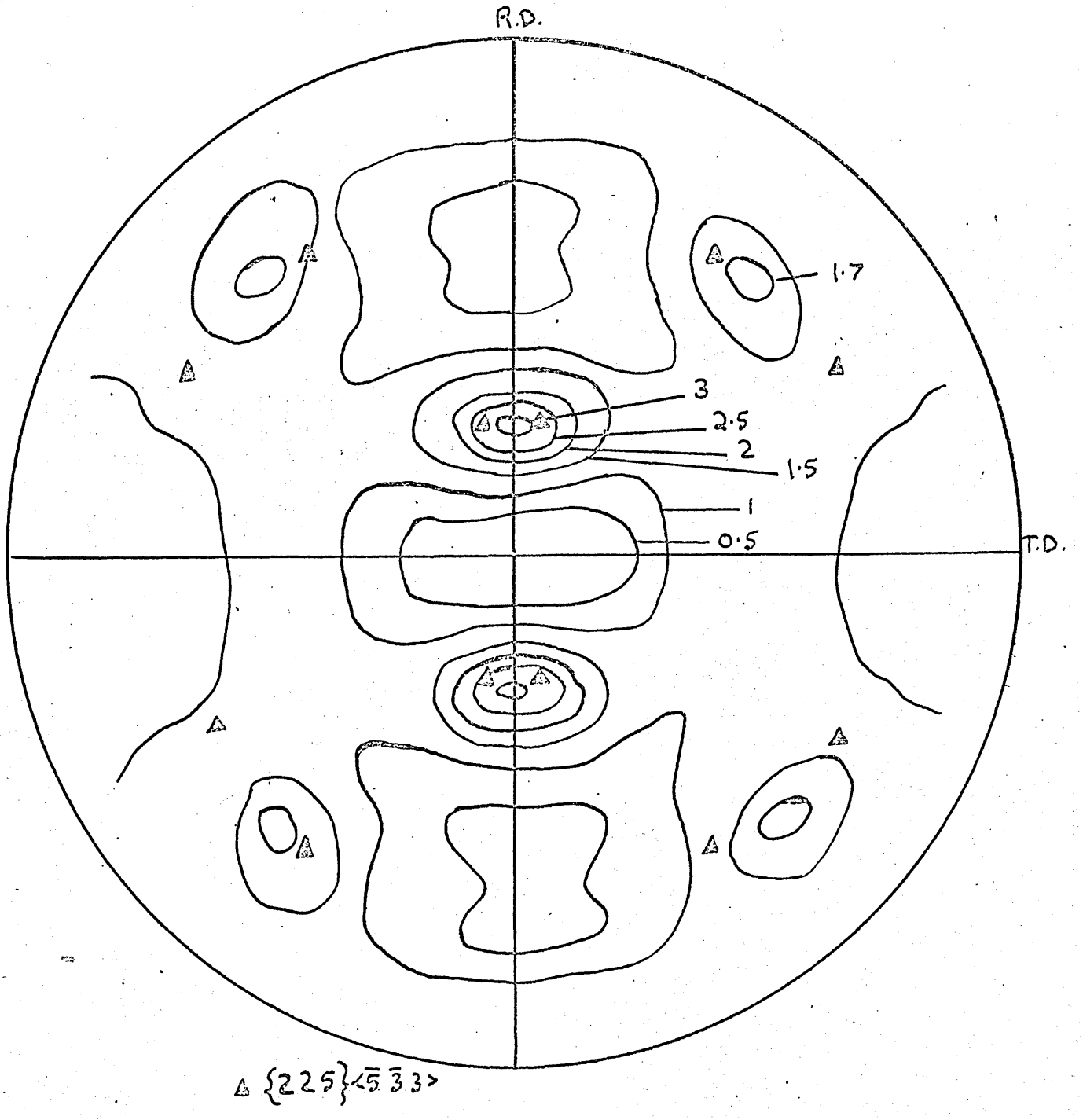

Figure 41

{200}γ pole figure of FST(L) steel.
1hr 1050°C. FC, 90% cold rolled + ½hr 900°C.AC.

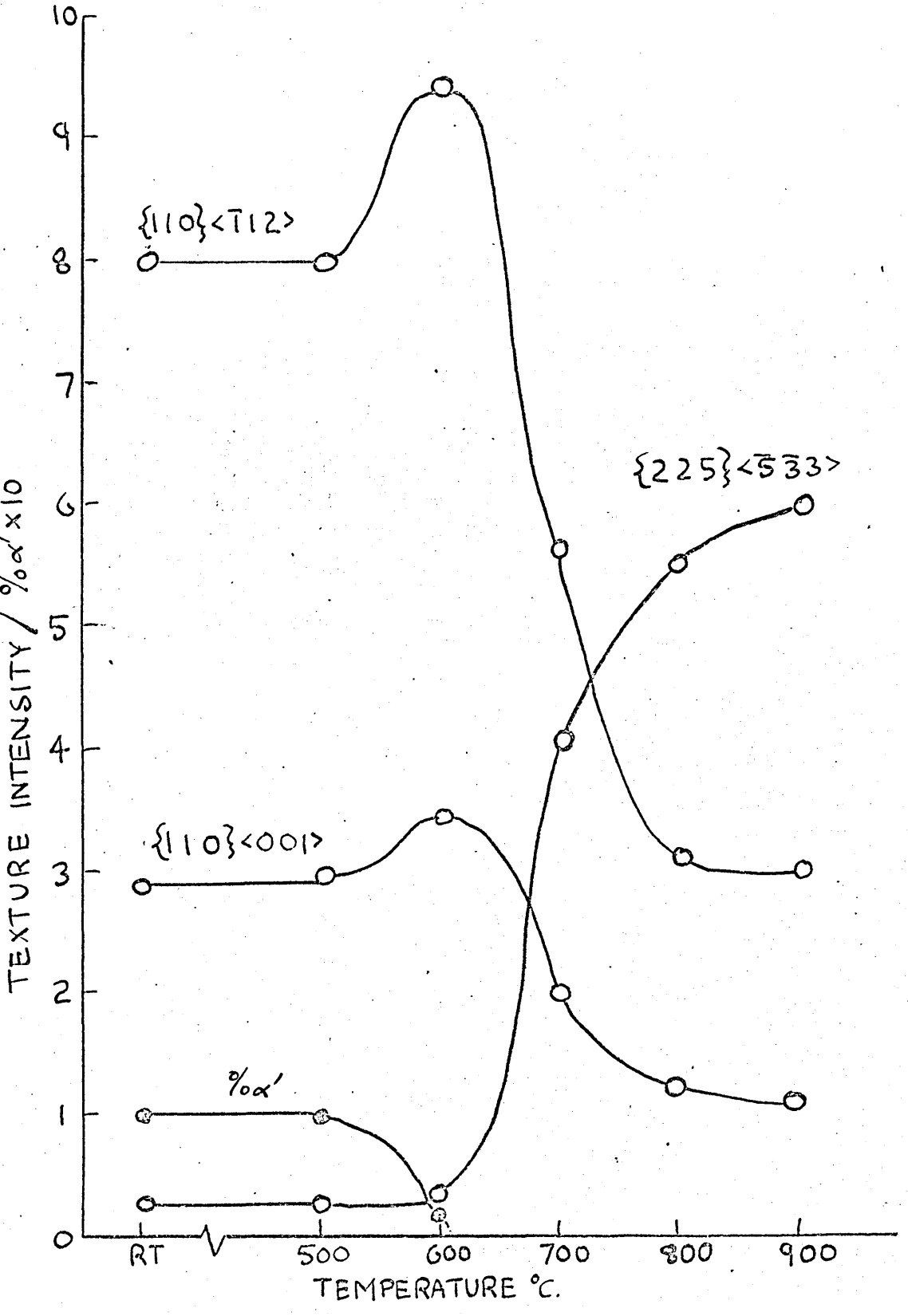

Figure 42

Variation of %α′ and intensities of γ texture components for FST(L) steel. 1hr 1050°C.FC, 90% cold rolled and annealed.

Figure 43

220γ line profiles for FST(L) steel. 1hr 1050°C.FC, 90% cold rolled and annealed.

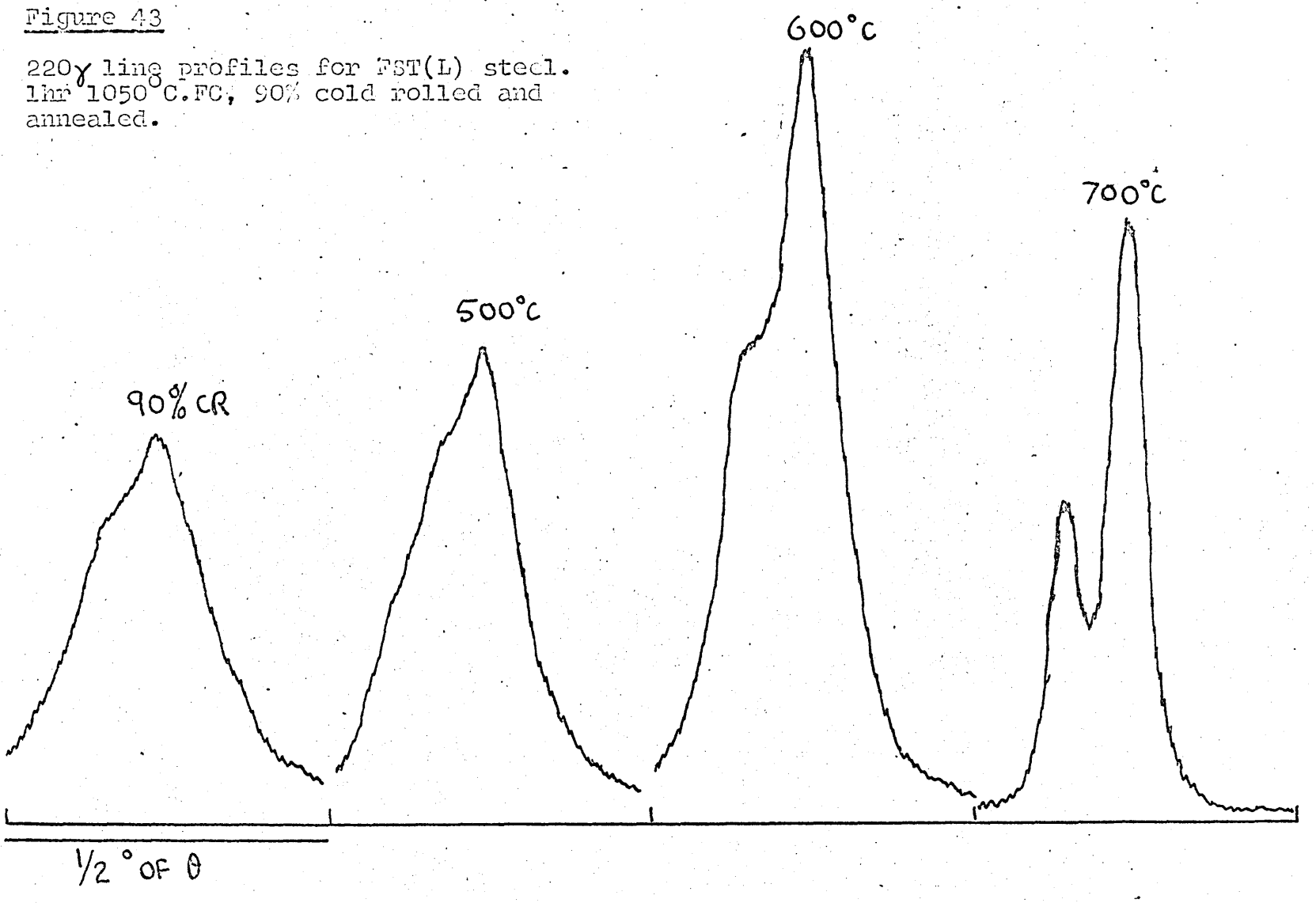

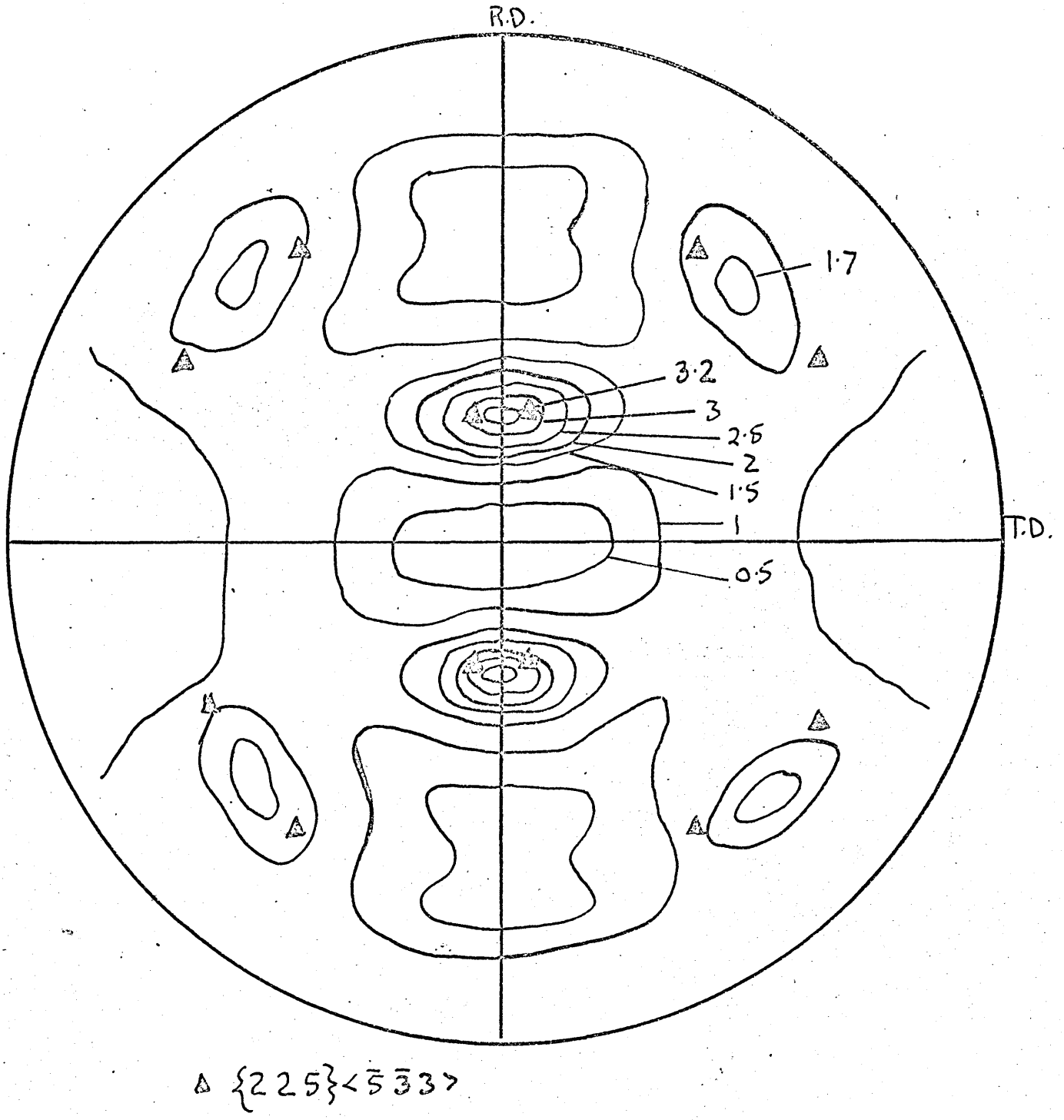

Figure 44

{200}γ pole figure of FST(L) steel.
1hr 1050°C. WQ, 90% cold rolled + ½hr 900°C. AC.

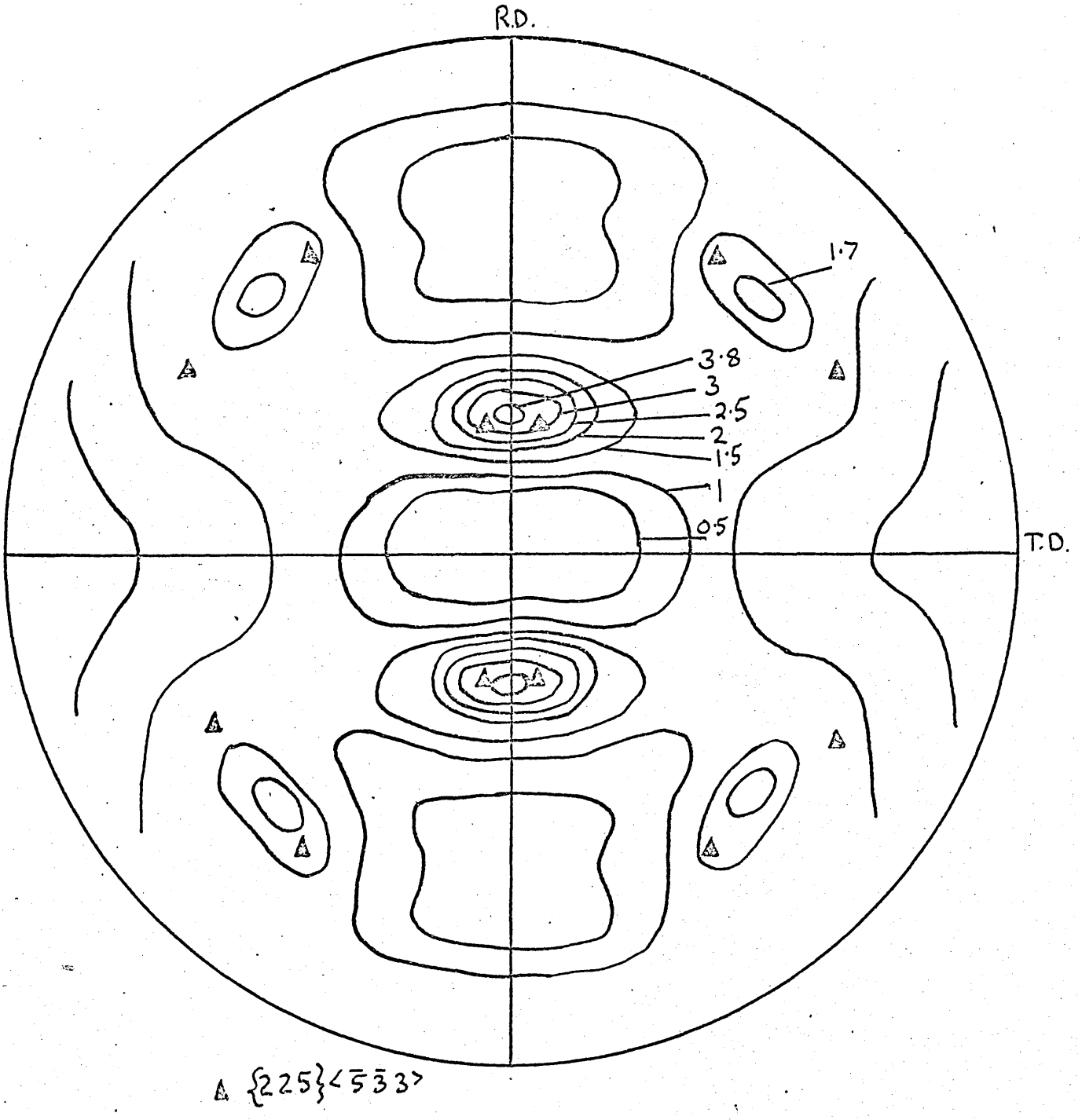

Figure 45

{200}γ pole figure of FSL (L) steel.
1hr 1050°C.FC, 90% cold rolled + ½Hr 900°C.AC.

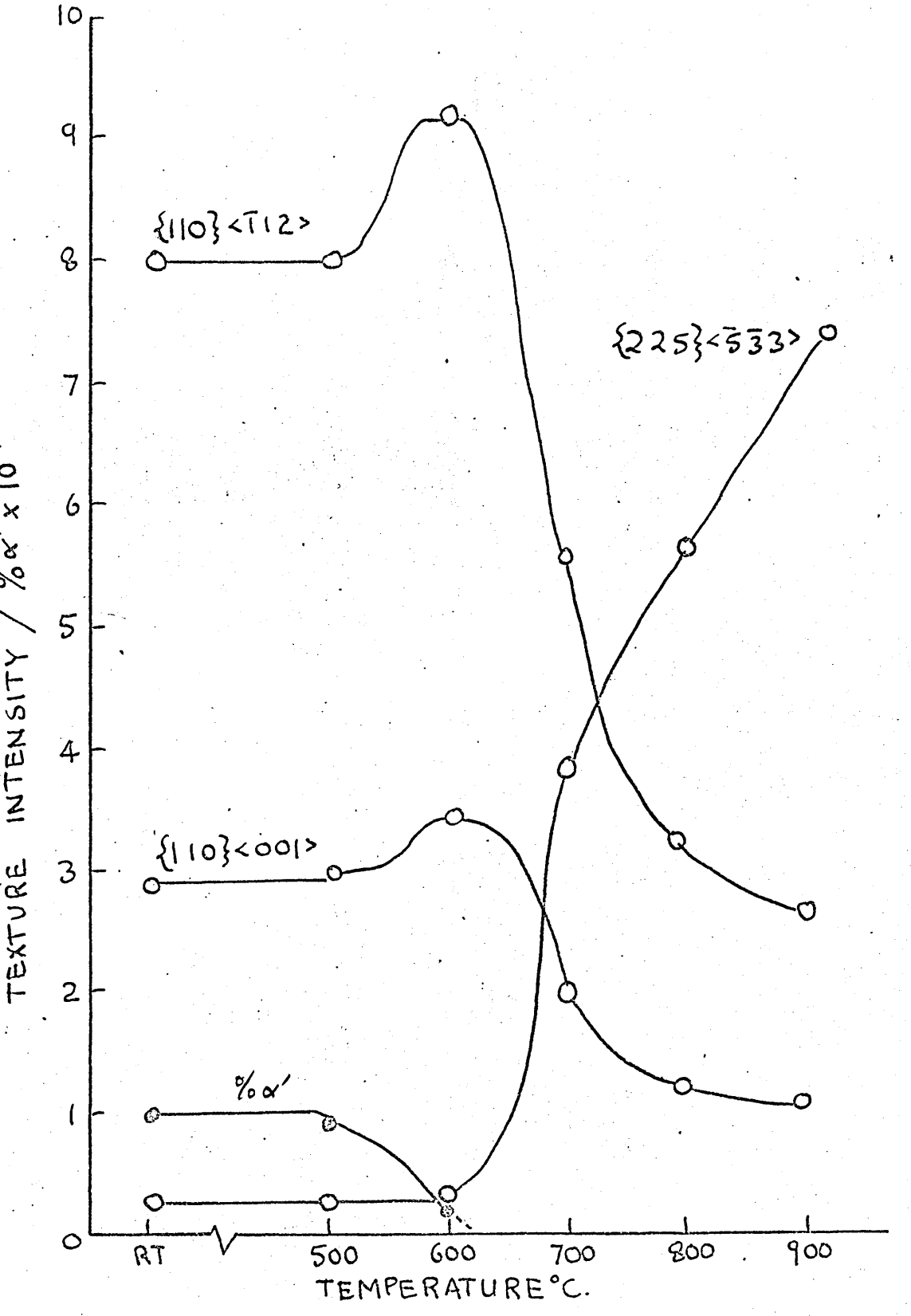

Figure 46

Variation of %α' and intensities of γ texture components for FSL(L) steel.
1hr 1050°C.FC, 90% cold rolled and annealed.

Figure 47

220γ line profiles for FSL(L) steel. 1hr 1050°C. FC, 90% cold rolled and annealed.

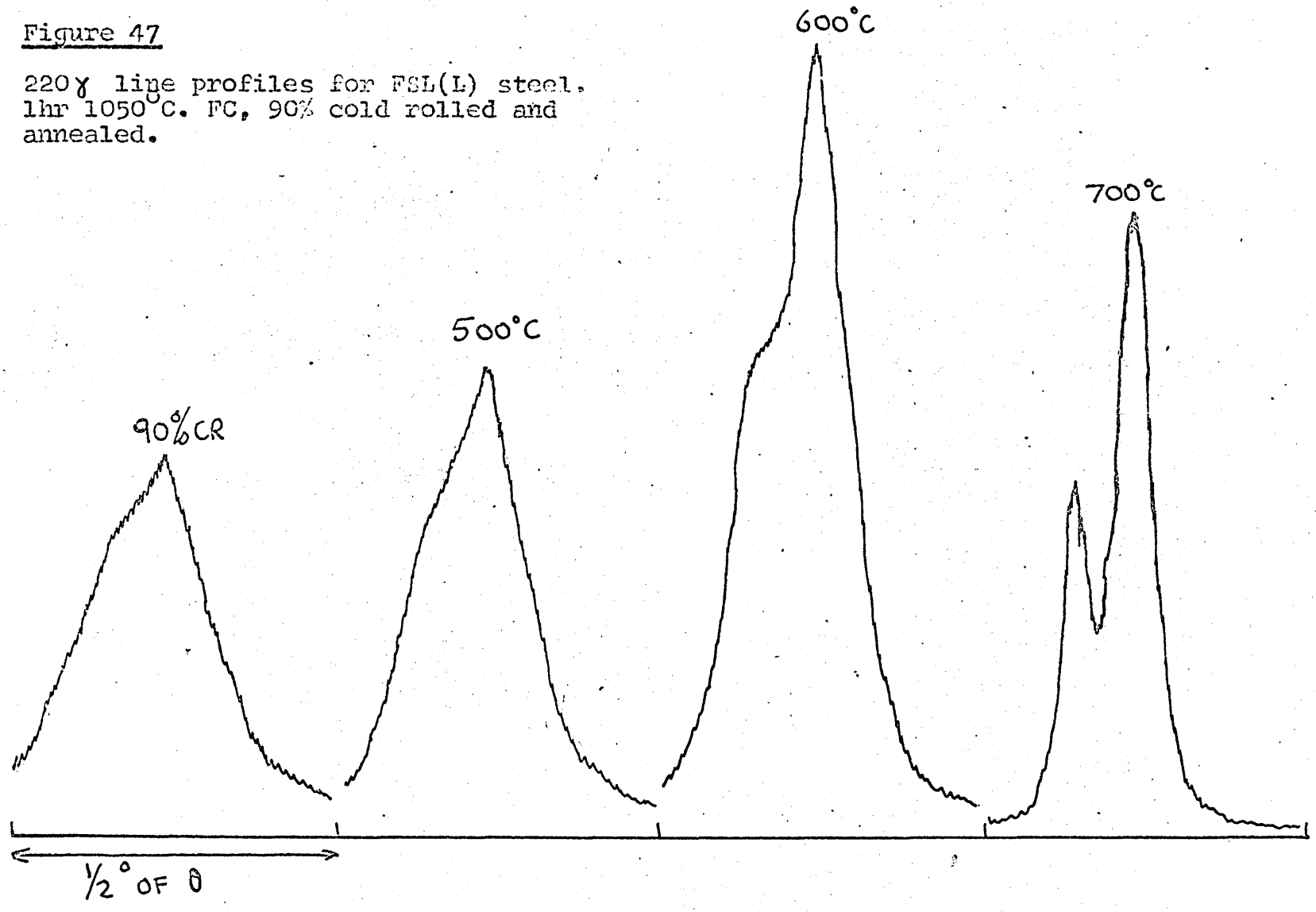

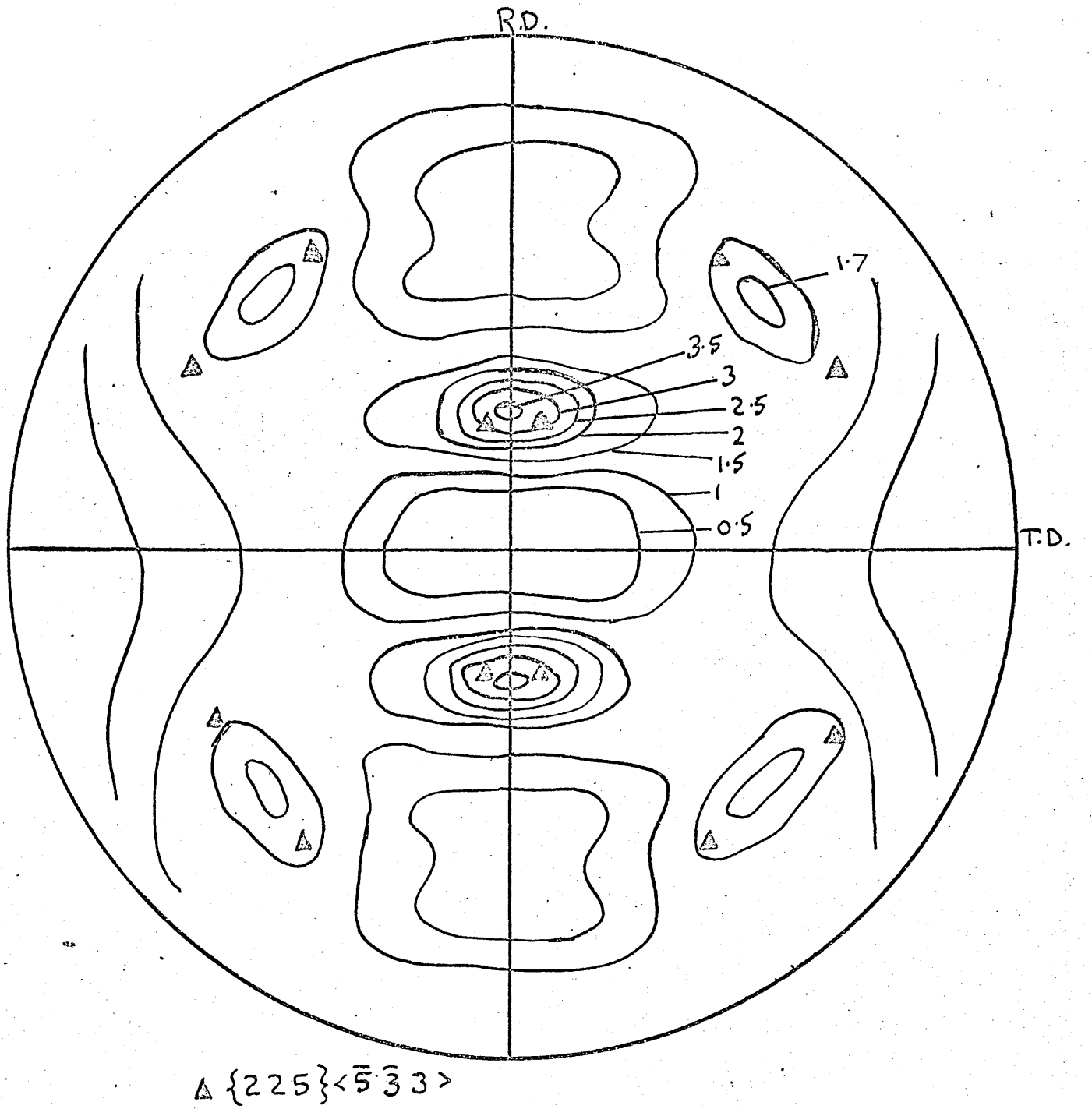

Figure 48

{200}γ pole figure of FSL(L) steel.

1 hr 1050°C. WQ, 90% cold rolled + $\frac{1}{2}$ hr 900°C. AC.

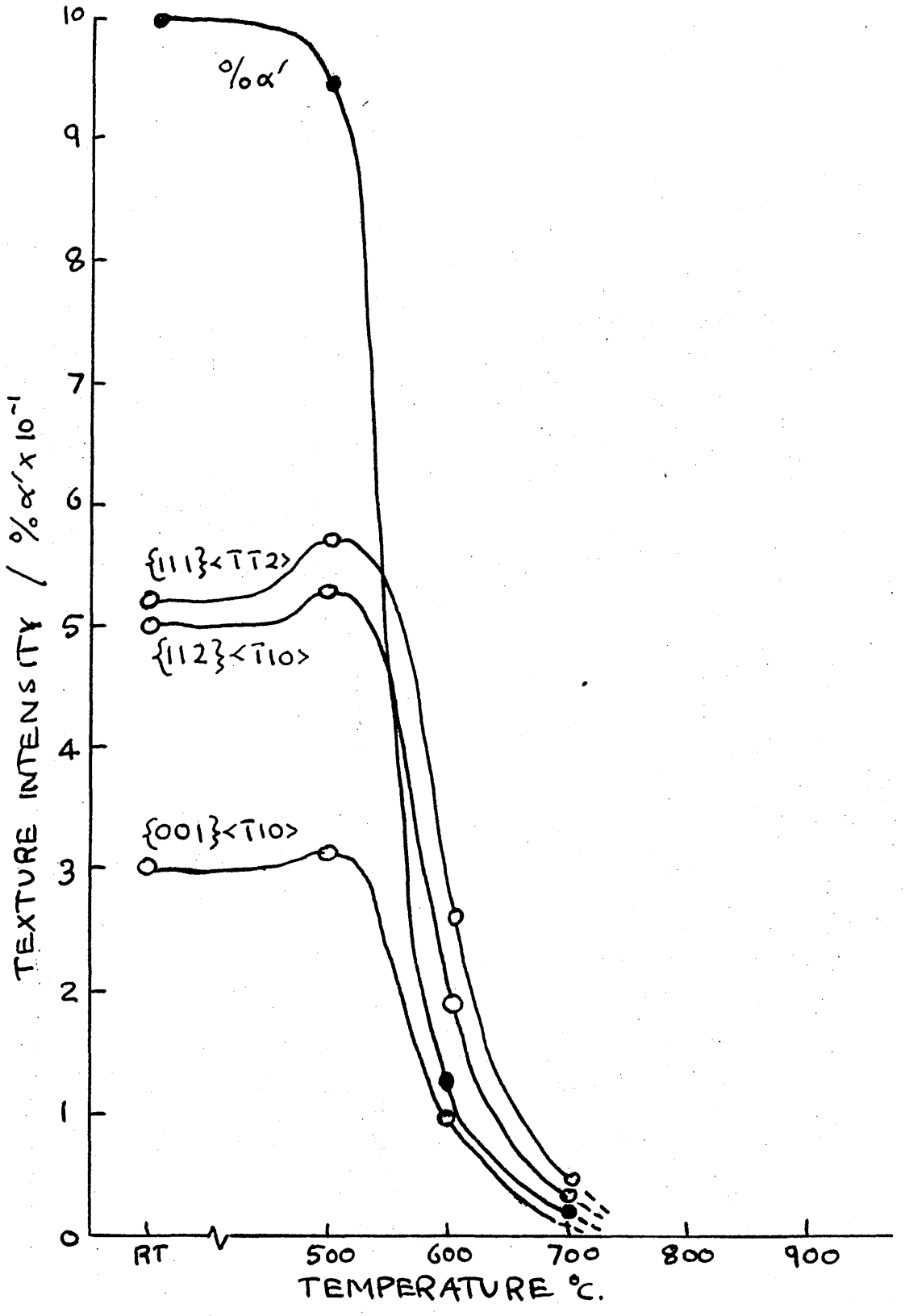

Figure 49

Variation of % α' and intensities of α' texture components for FCB steel.

1 hr 1050°C. FC, 90% cold rolled and annealed.

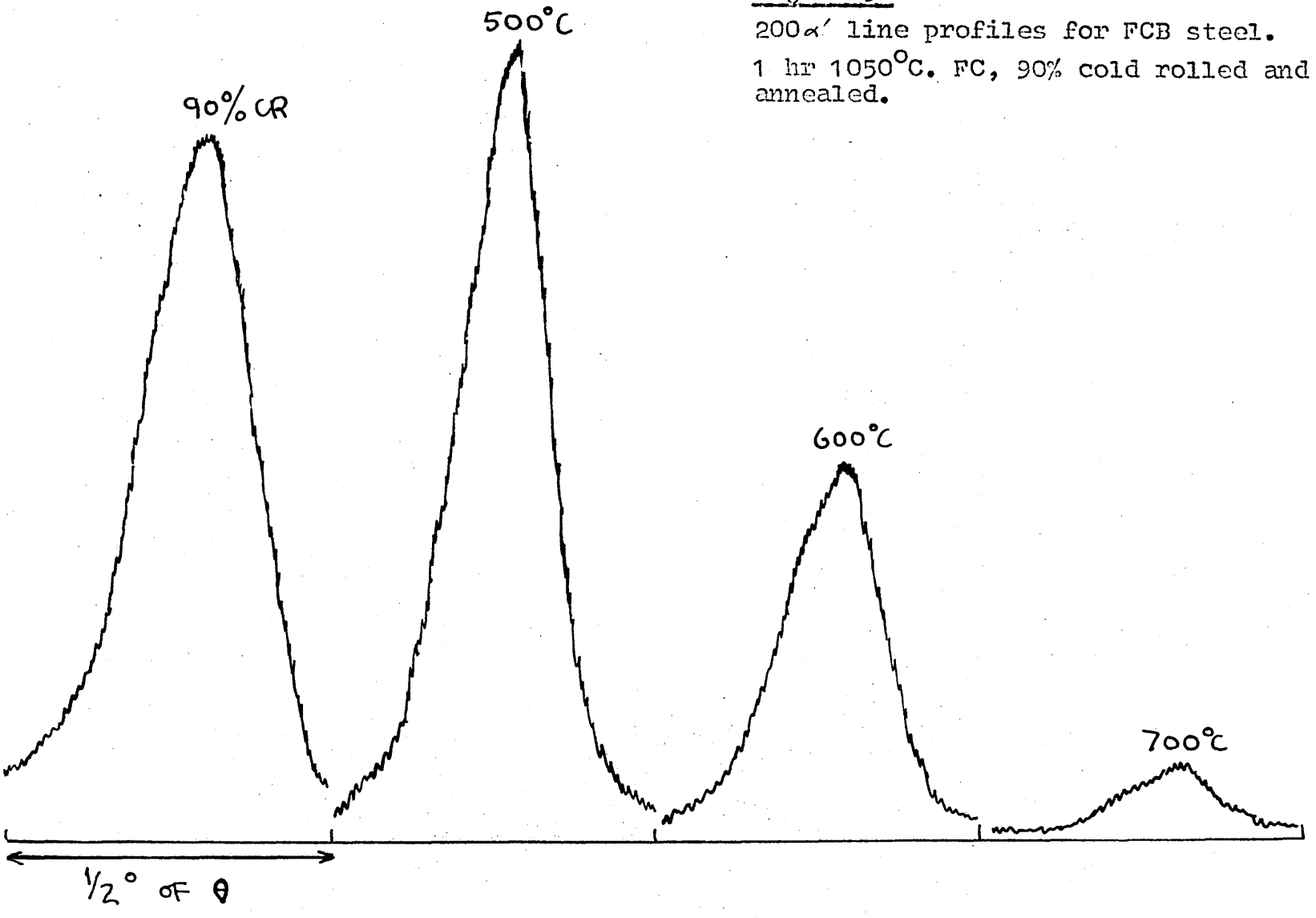

Figure 50

200α' line profiles for FCB steel.

1 hr 1050°C. FC, 90% cold rolled and annealed.

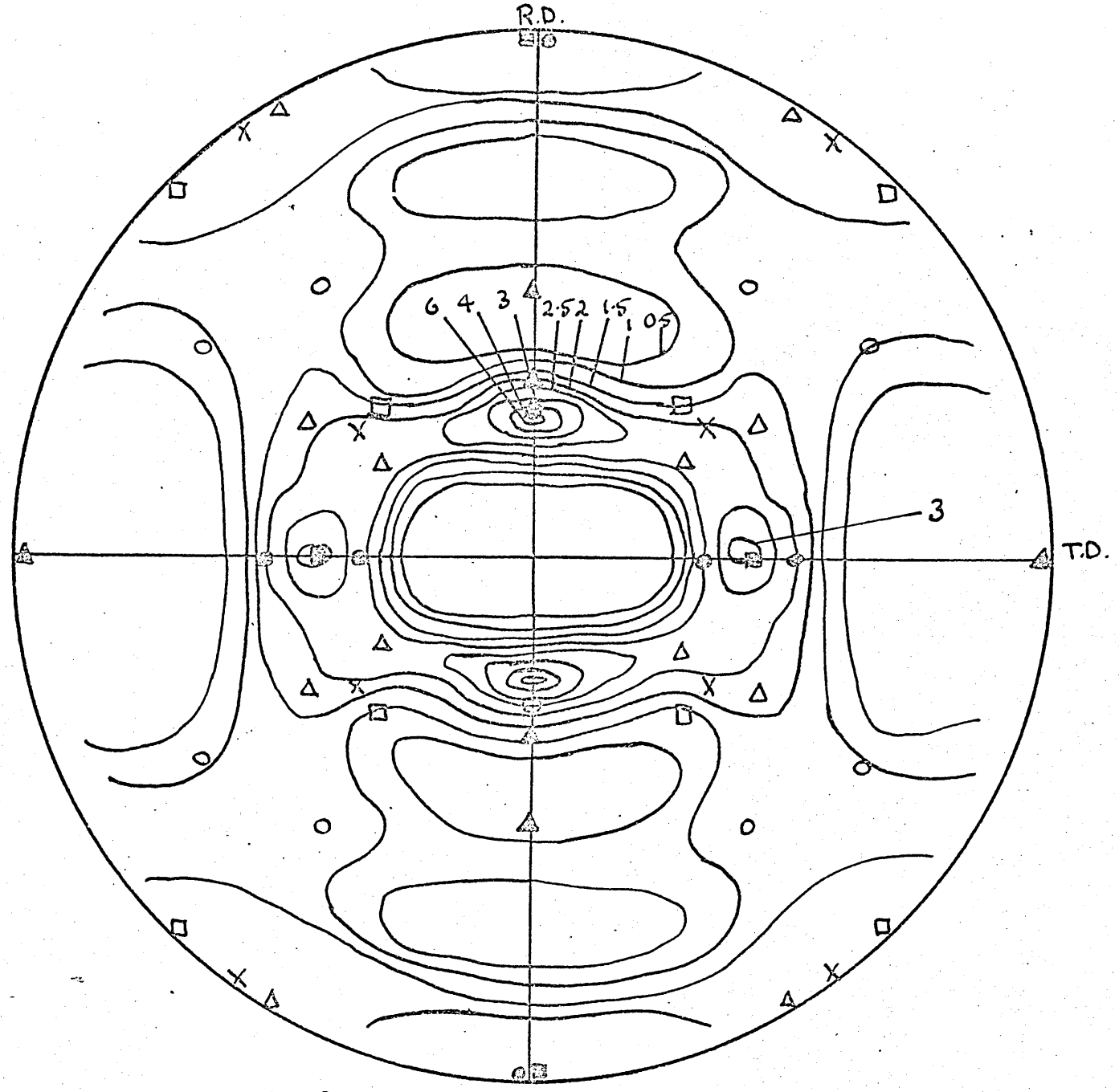

□ {110}<$\bar{5}$57>

△ {430}<$\bar{3}$40>

△ {430}<$\bar{6}$,8,17>

X {110}<$\bar{1}$12>

● {430}<001>

○ {6,8,17}<$\bar{5}\,\bar{7}$5>

▣ {110}<001>

Figure 51

{200}γ pole figure of FCR steel.

1 hr 1050°C. FC, 90% cold rolled + ½ hr 600°C. AC.

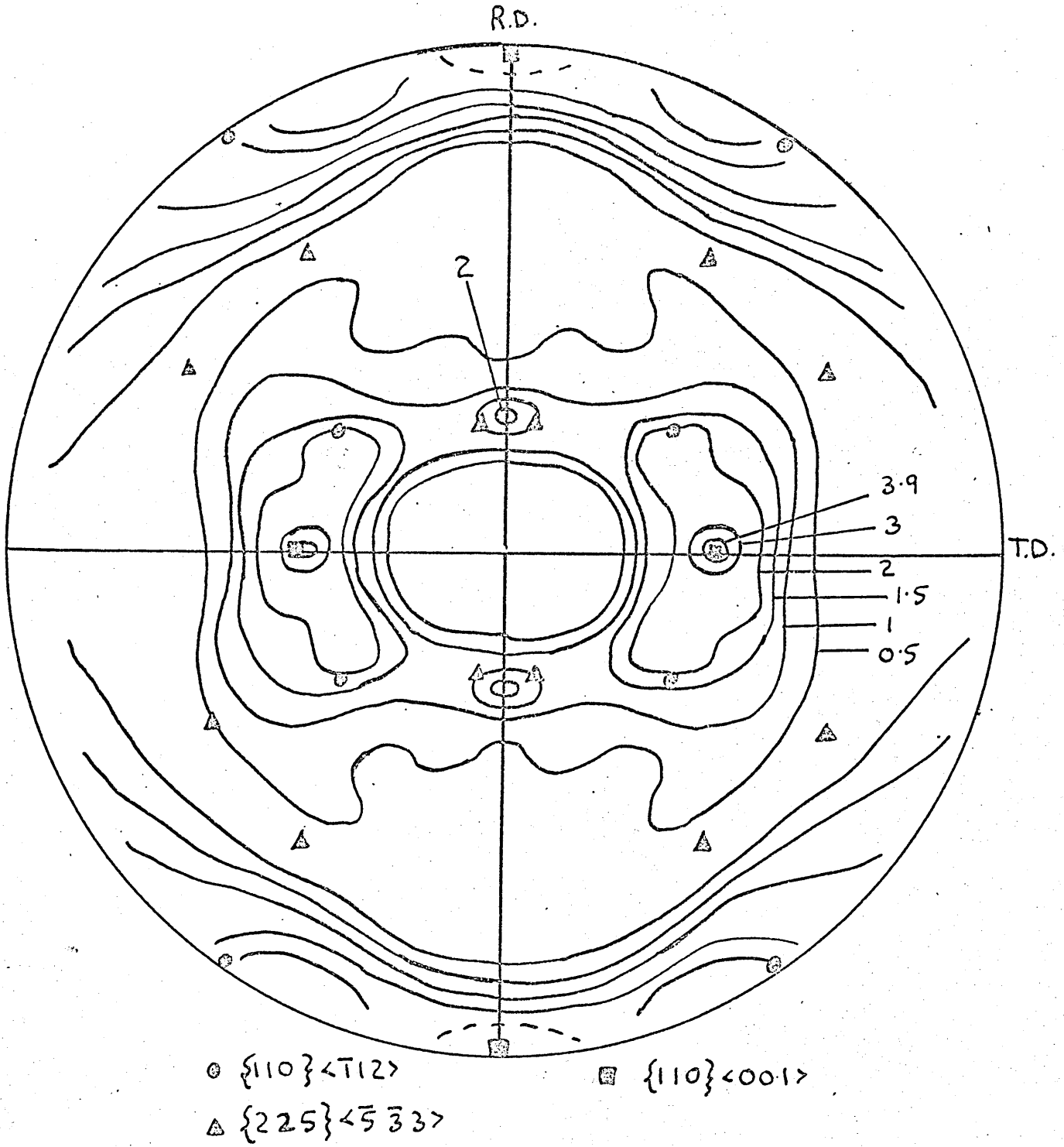

Figure 52

{200}γ pole figure of FCB steel.

1 hr 1050°C. FC, 90% cold rolled + ½ hr 900°C. AC.

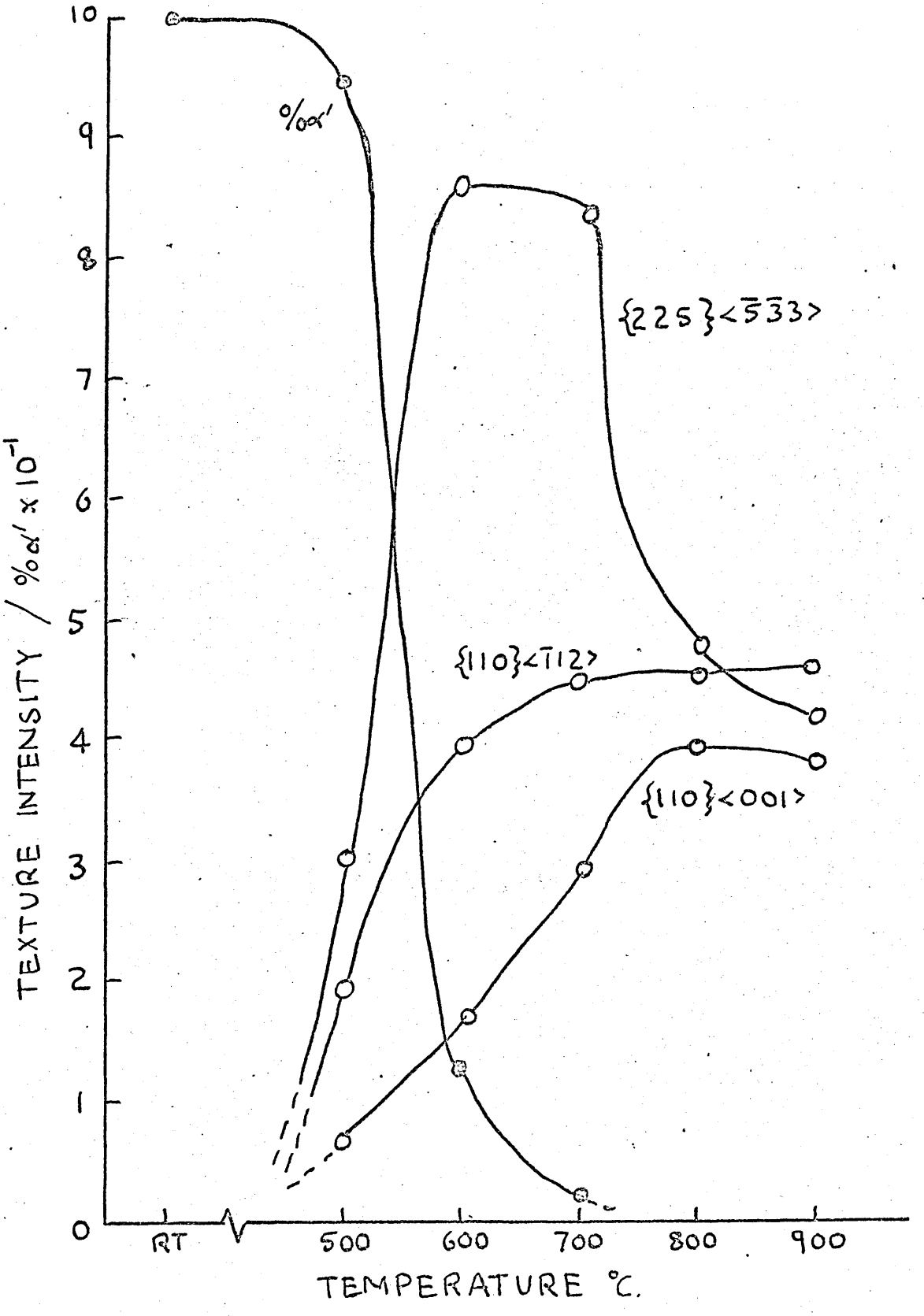

Figure 53

Variation of %α and intensities of γ texture components for FCB steel.

1 hr 1050°C. FC, 90% cold rolled and annealed.

Figure 54

220 γ line profiles for FCB steel.

1 hr 1050°C. FC, 90% cold rolled and annealed.

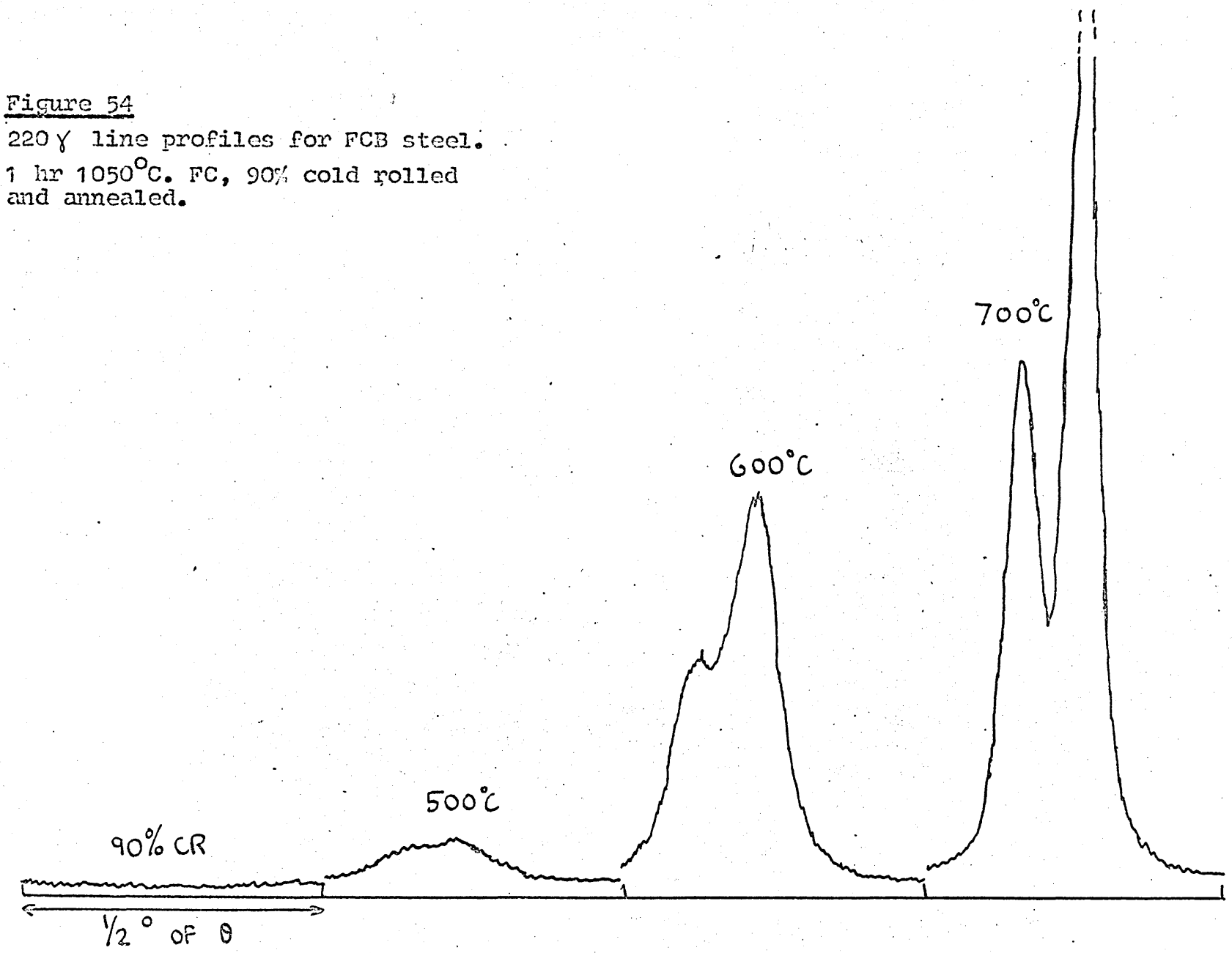

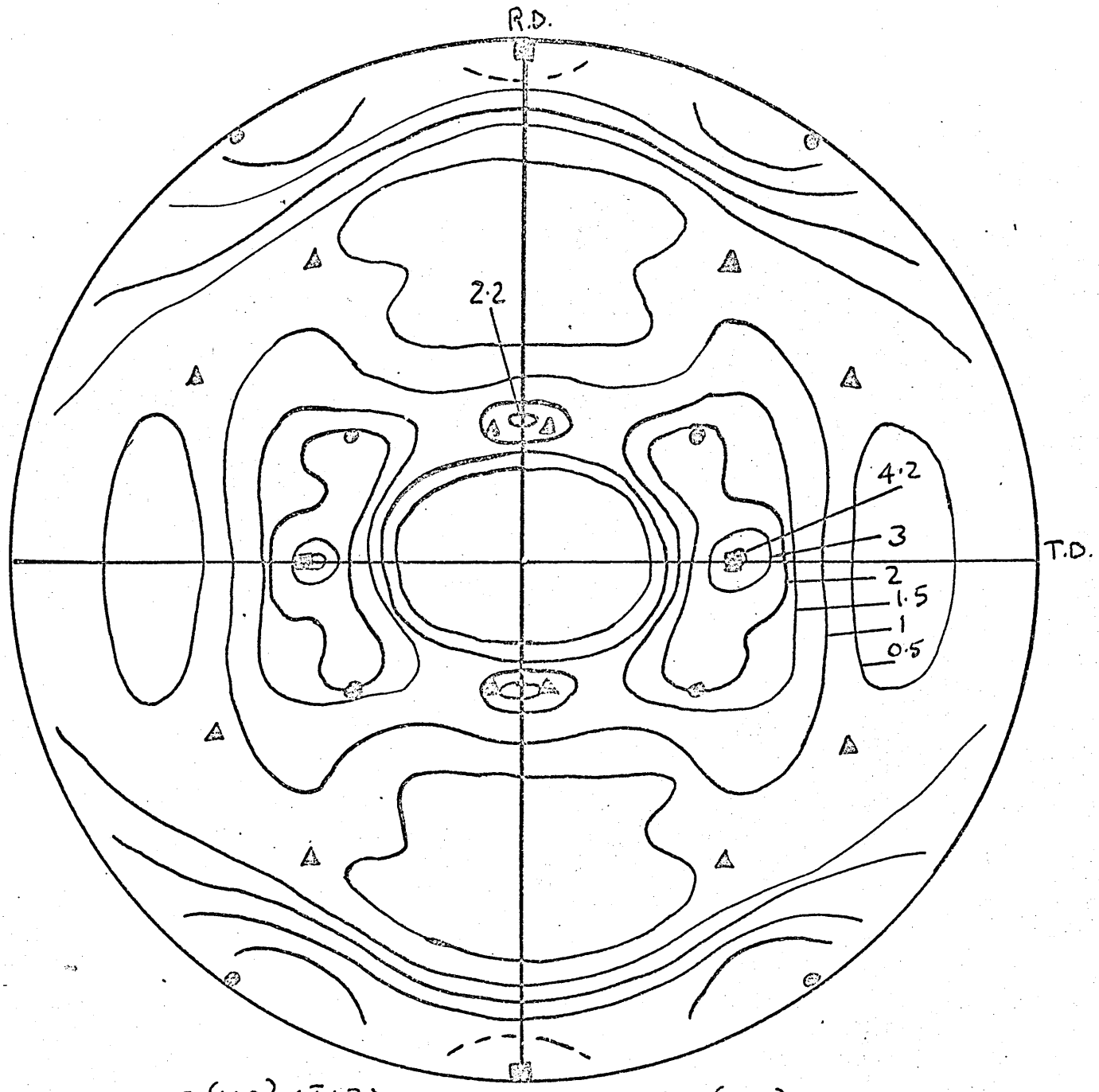

Figure 55

{200}γ pole figure of FCB steel.

1 hr 1050°C. WQ, 90% cold rolled + ½ hr 900°C. AC.

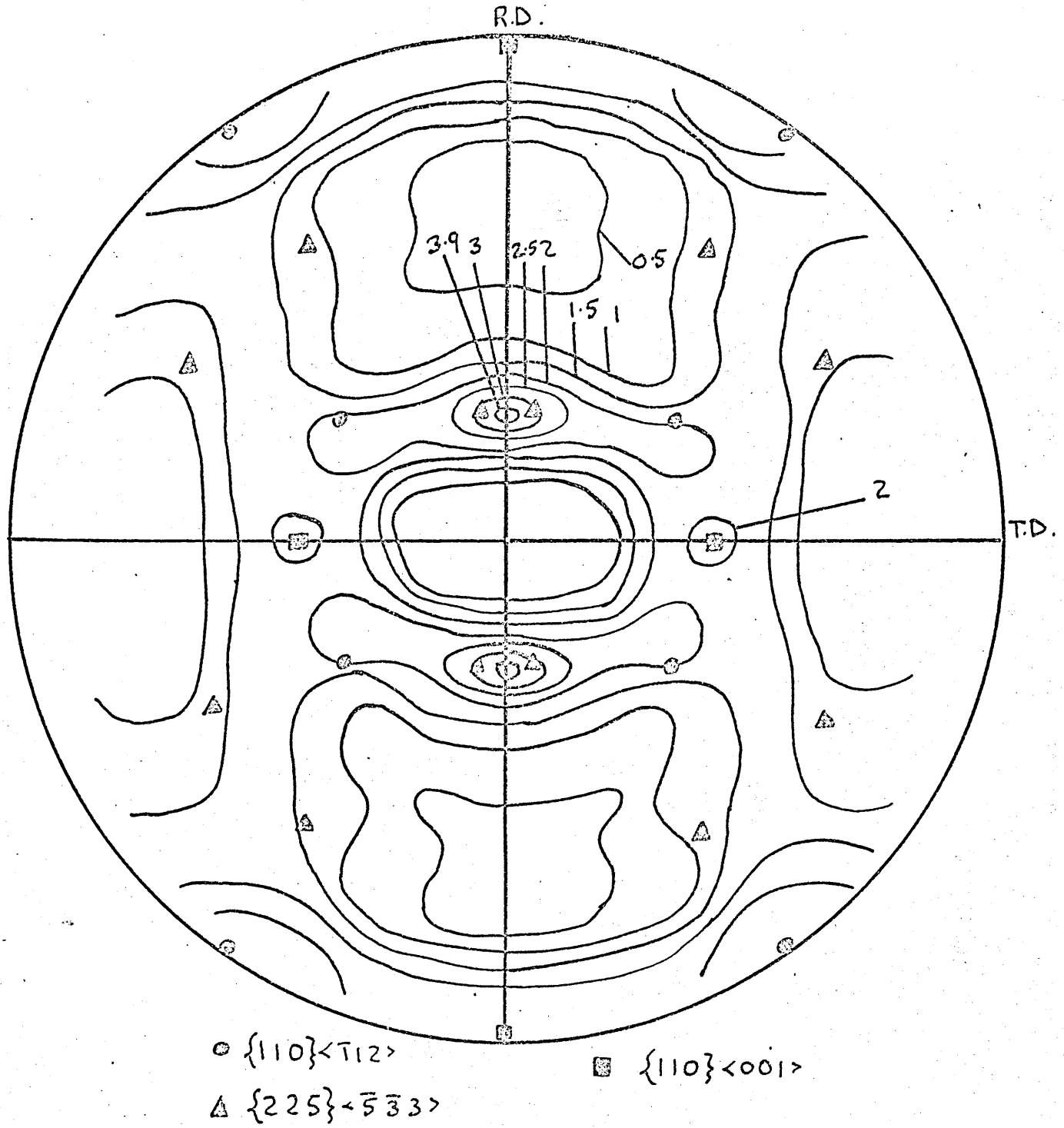

Figure 56

{200}γ pole figure of FCB steel.

15 min 1300°C. FC, 90% cold rolled + $\frac{1}{2}$ hr 900°C. AC.

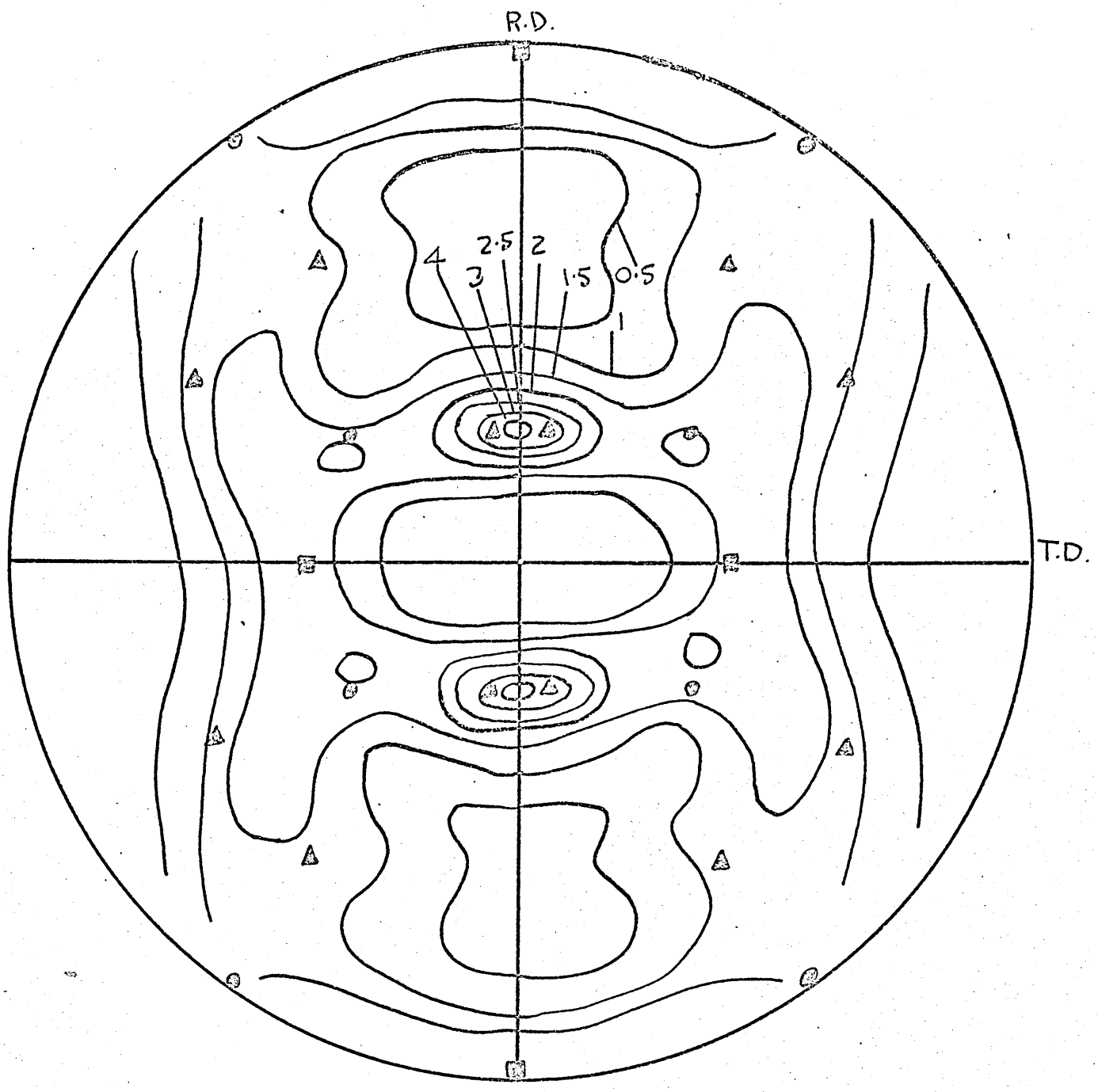

Figure 57

{200}γ pole figure of FCB steel.

15 min 1300°C. WQ, 90% cold rolled + ½ hr 900°C. AC.

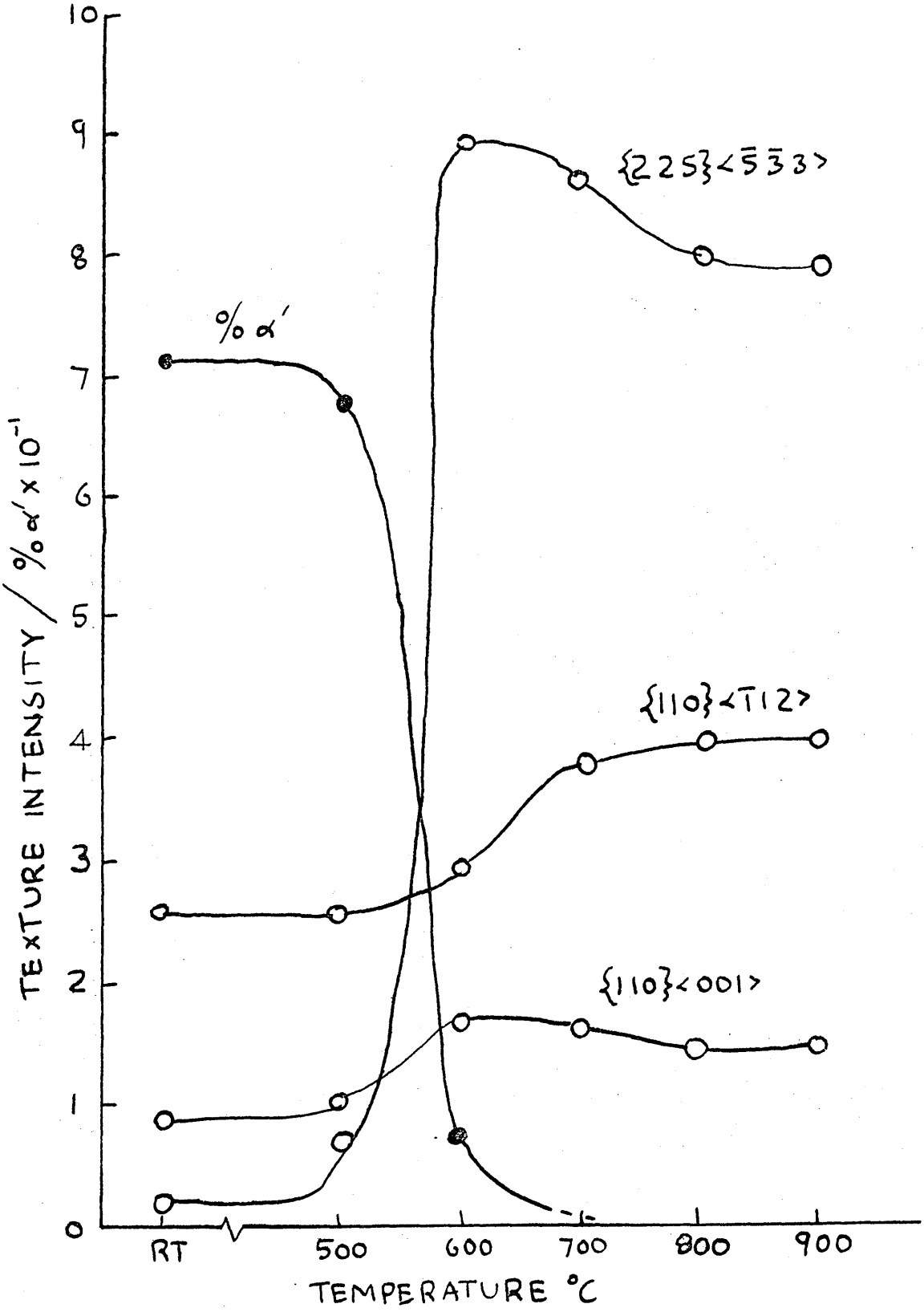

Figure 58

Variation of % α' and intensities of γ texture components for FCB steel.

15 min 1300°C. WQ, 90% cold rolled and annealed.

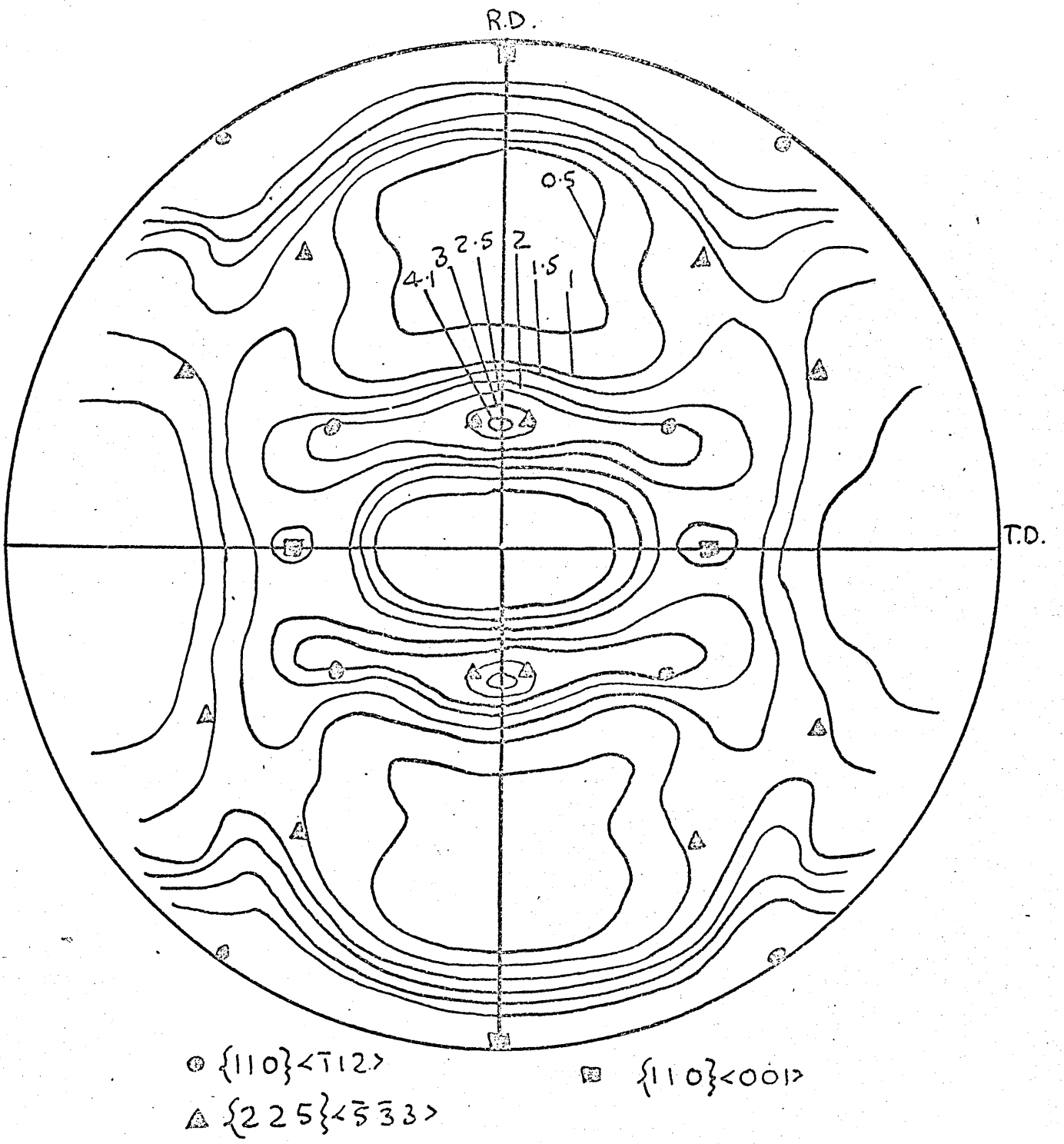

Figure 59

{200}γ pole figure of SF 347 steel.

1 hr 1050°C. FC, 90% cold rolled + ½ hr 900°C. AC.

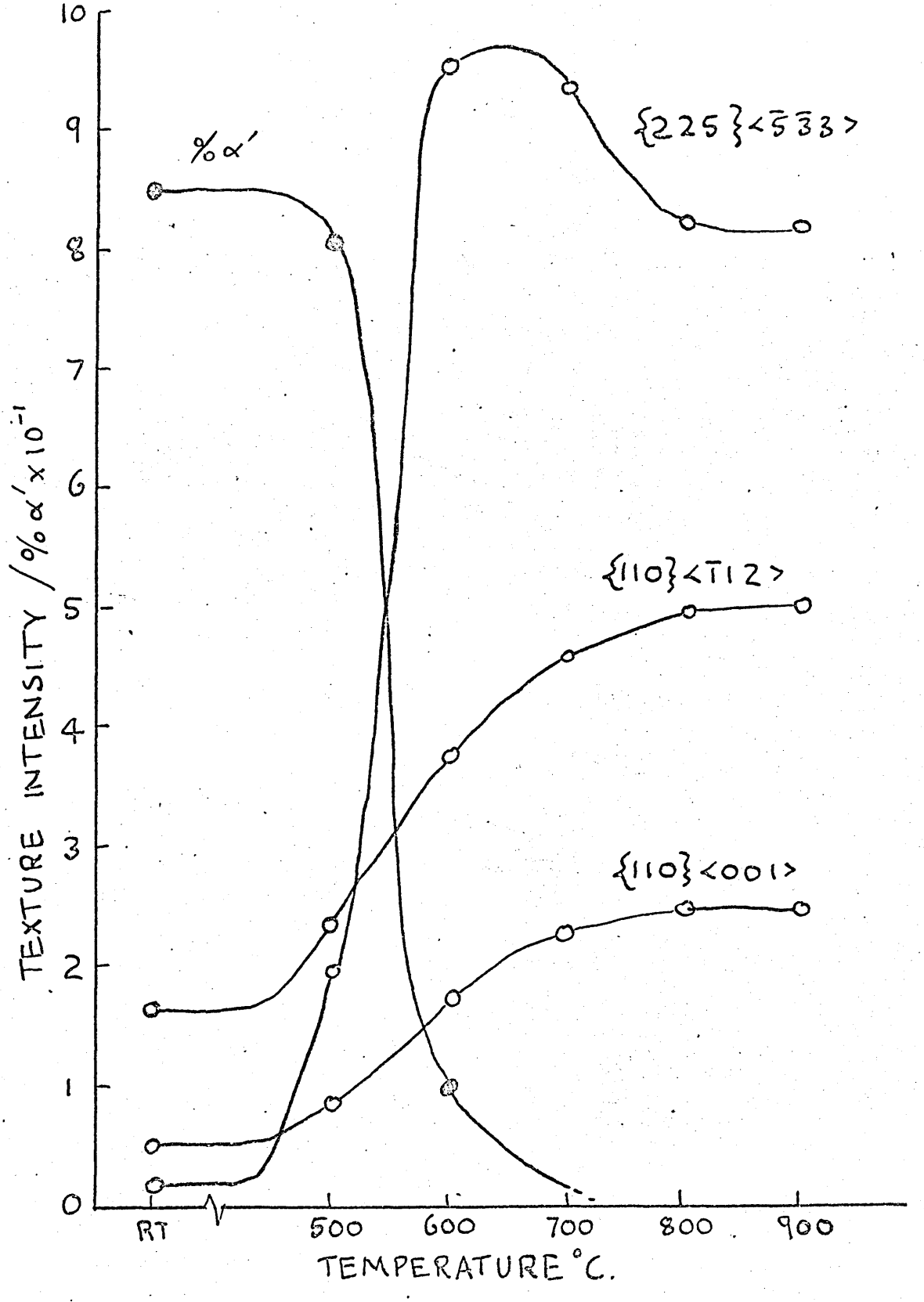

Figure 60

Variation of % α' and intensities of γ texture components for SF 347 steel.

1 hr 1050°C. FC, 90% cold rolled and annealed.

Figure 61

220γ line profiles for SF 347 steel.
1 hr 1050°C. FC, 90% cold rolled and annealed.

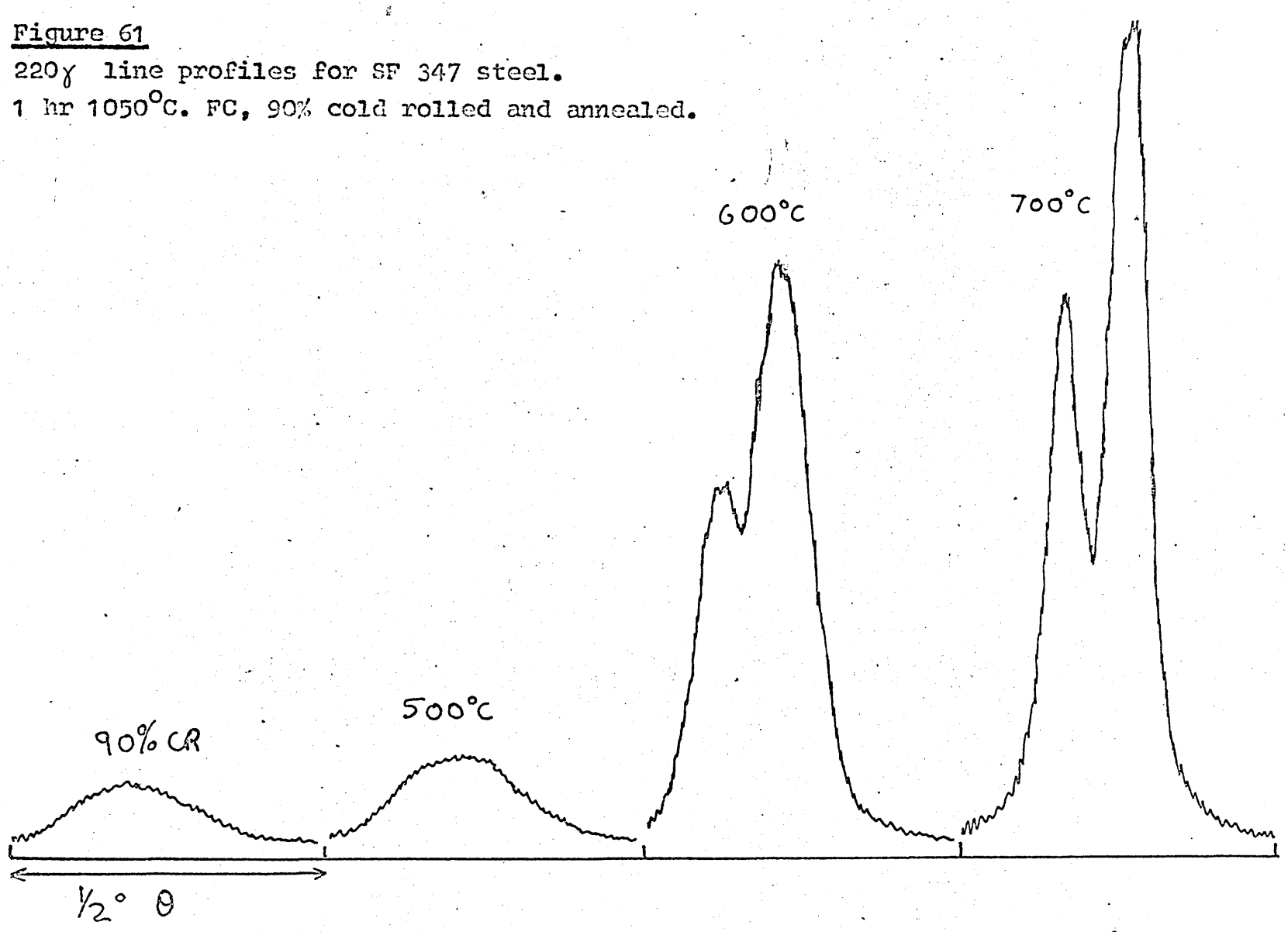

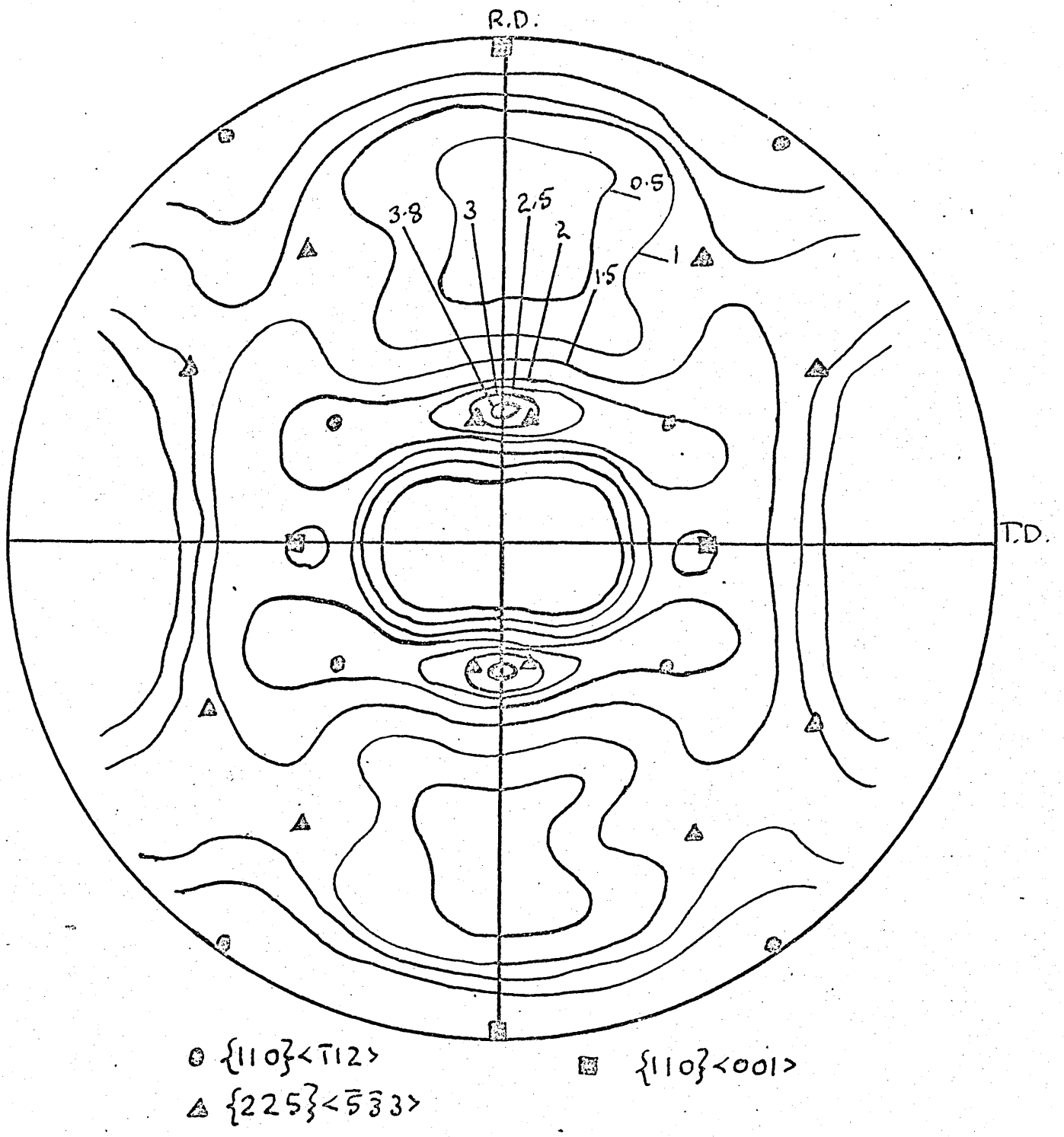

Figure 62

{200}γ pole figure of SF 347 steel.

1 hr 1050°C. WQ, 90% cold rolled + ½ hr 900°C. AC.

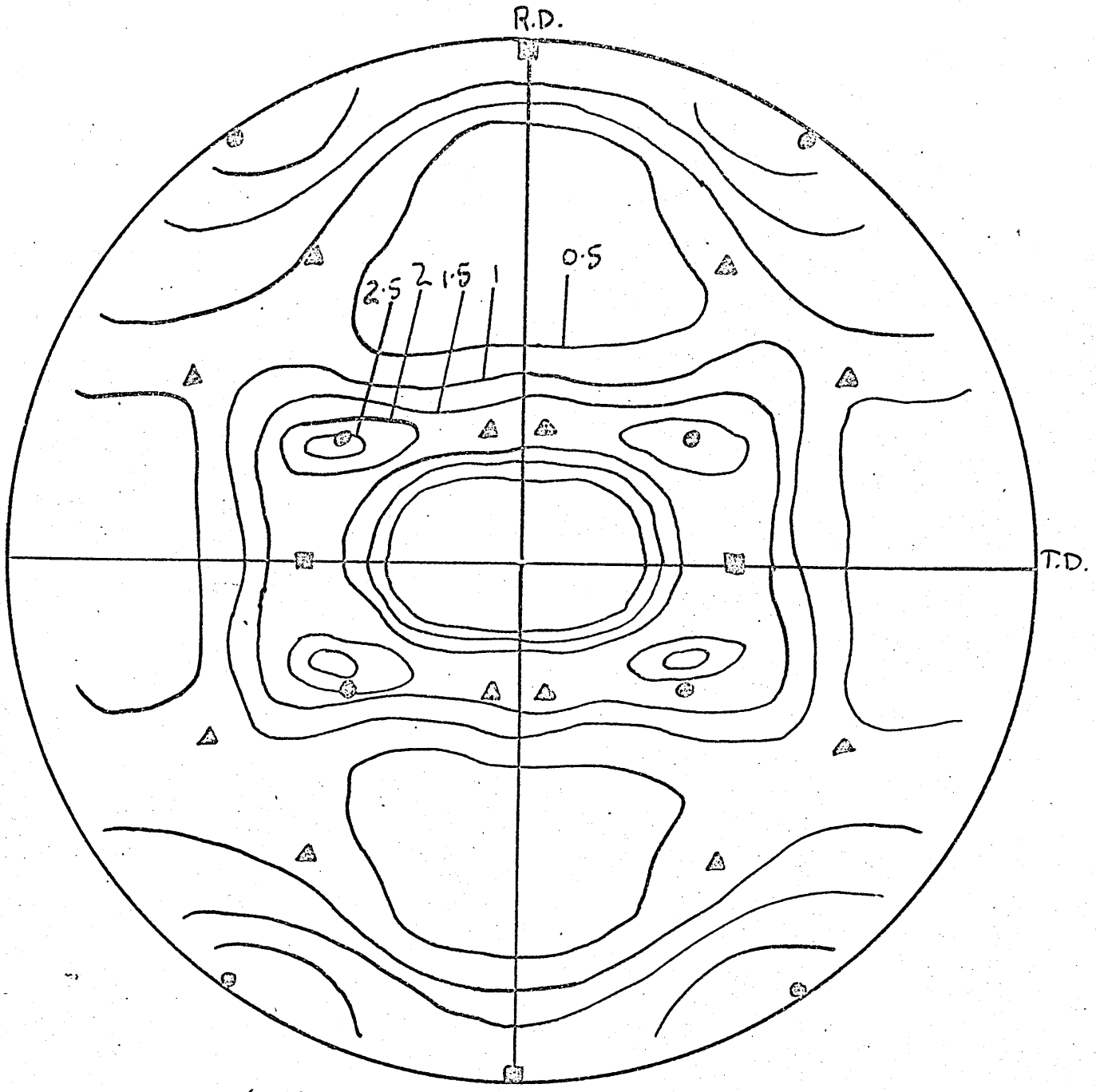

Figure 63

{200}γ pole figure of SF 347 steel.
15 min 1300°C. FC, 90% cold rolled + ½ hr 900°C. AC.

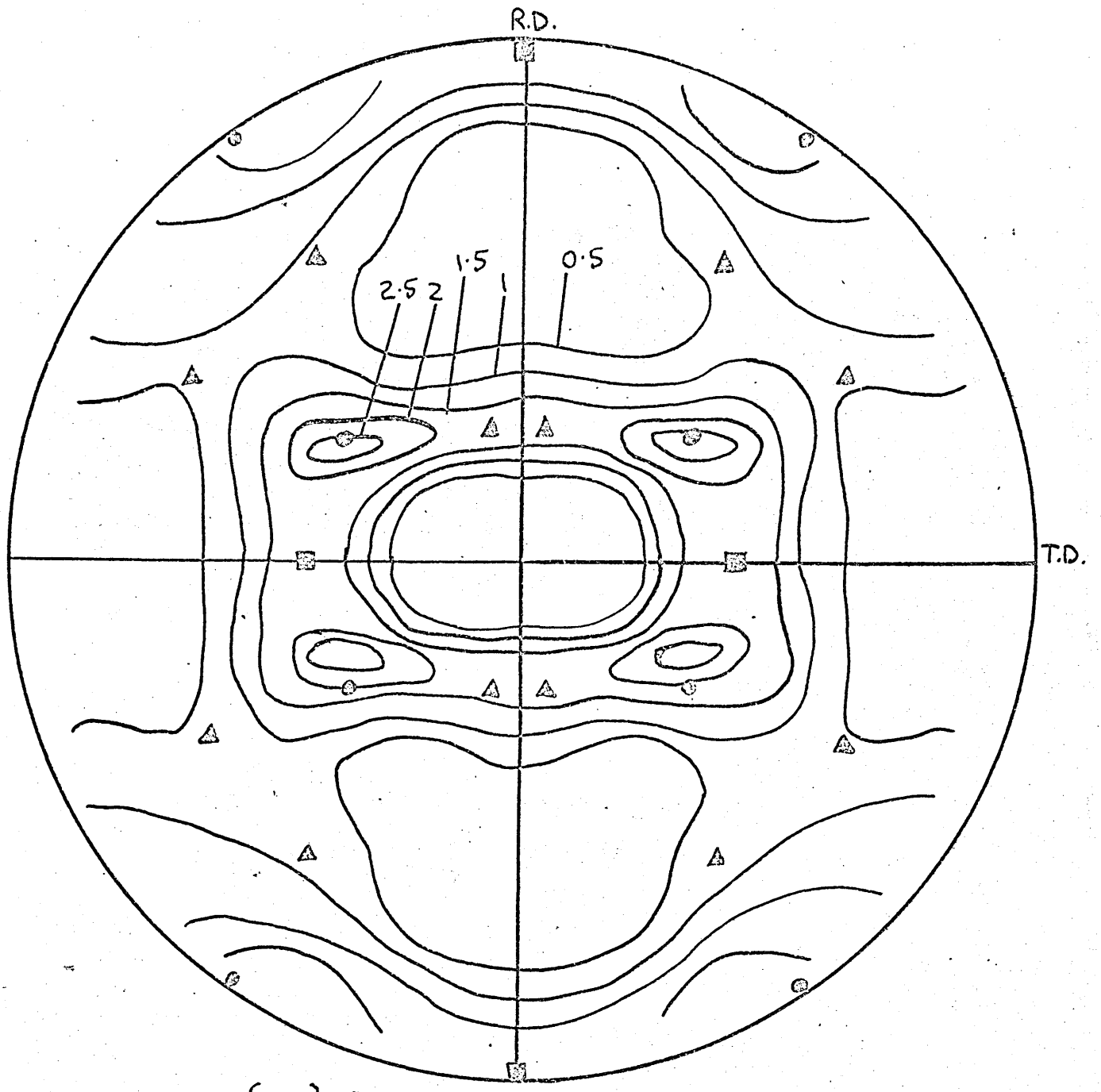

Figure 64

{200}γ pole figure of SF 347 steel.

15 min 1300°C. WQ, 90% cold rolled + ½ hr 900°C. AC.

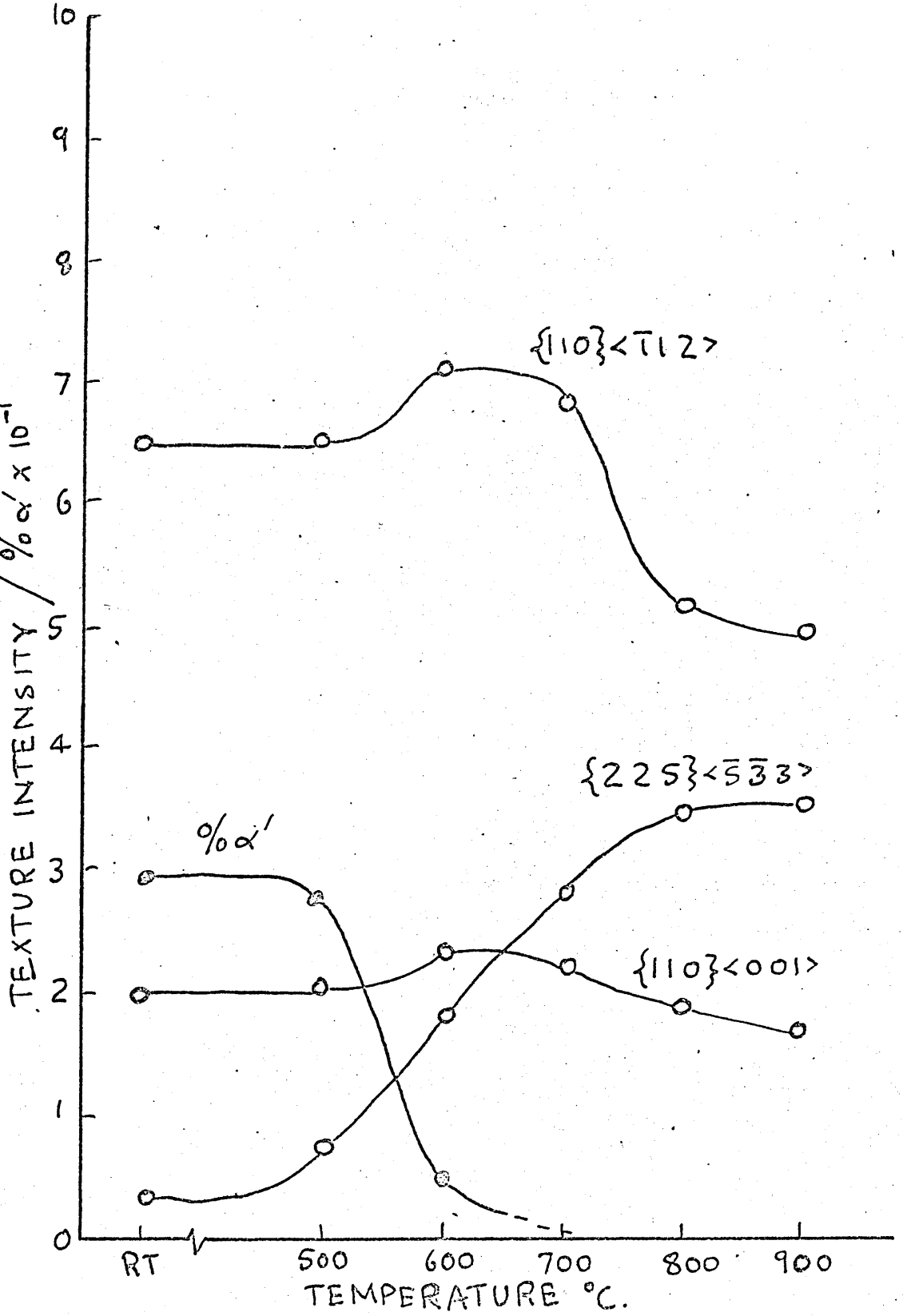

Figure 65

Variation of %α' and intensities of γ texture components for SF 347 steel.

15 min 1300°C. WQ, 90% cold rolled and annealed.

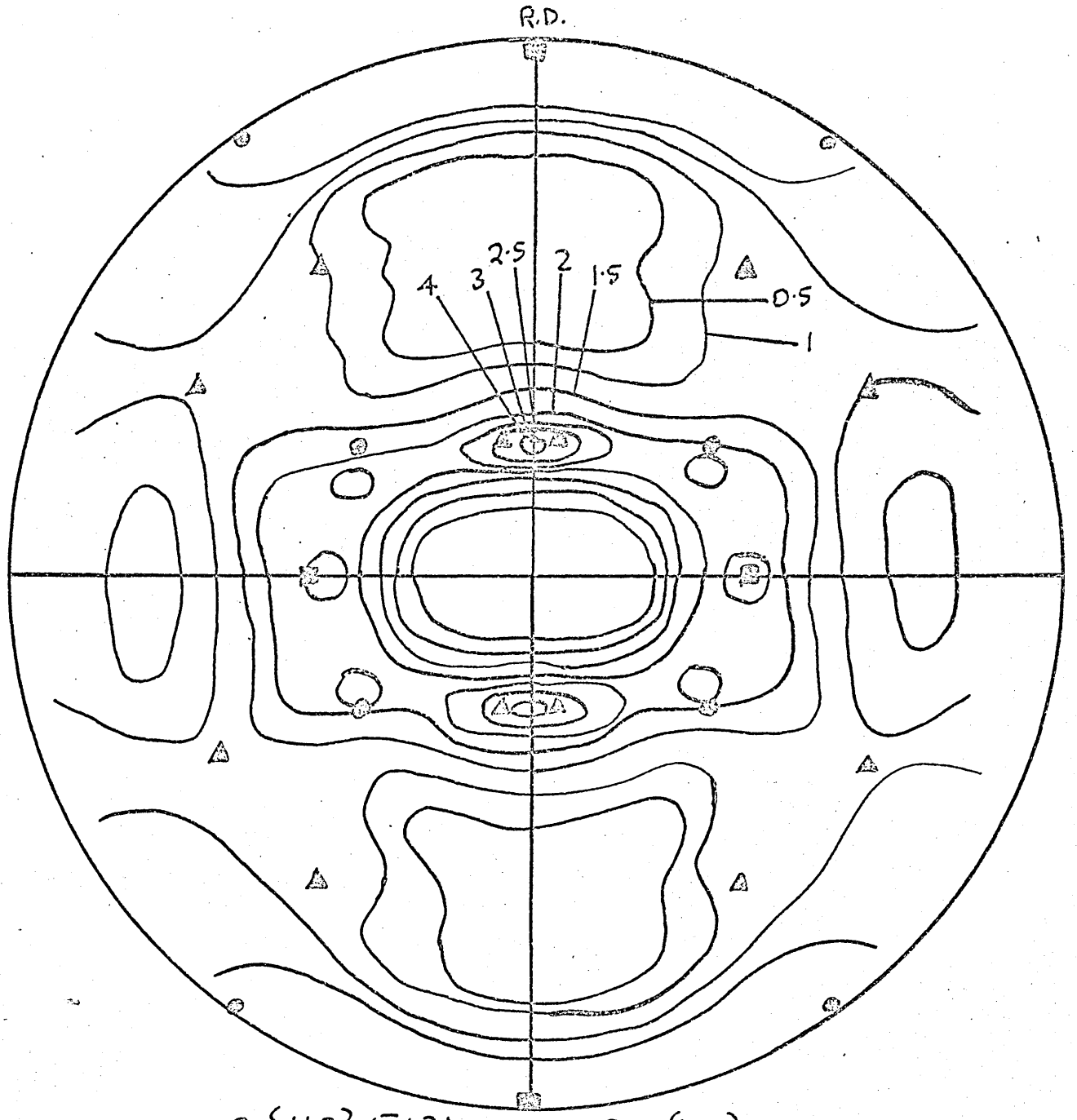

Figure 66

{200}γ pole figure of FDP steel.

1 hr 1050°C. FC, 90% cold rolled + ½ hr 900°C. AC.

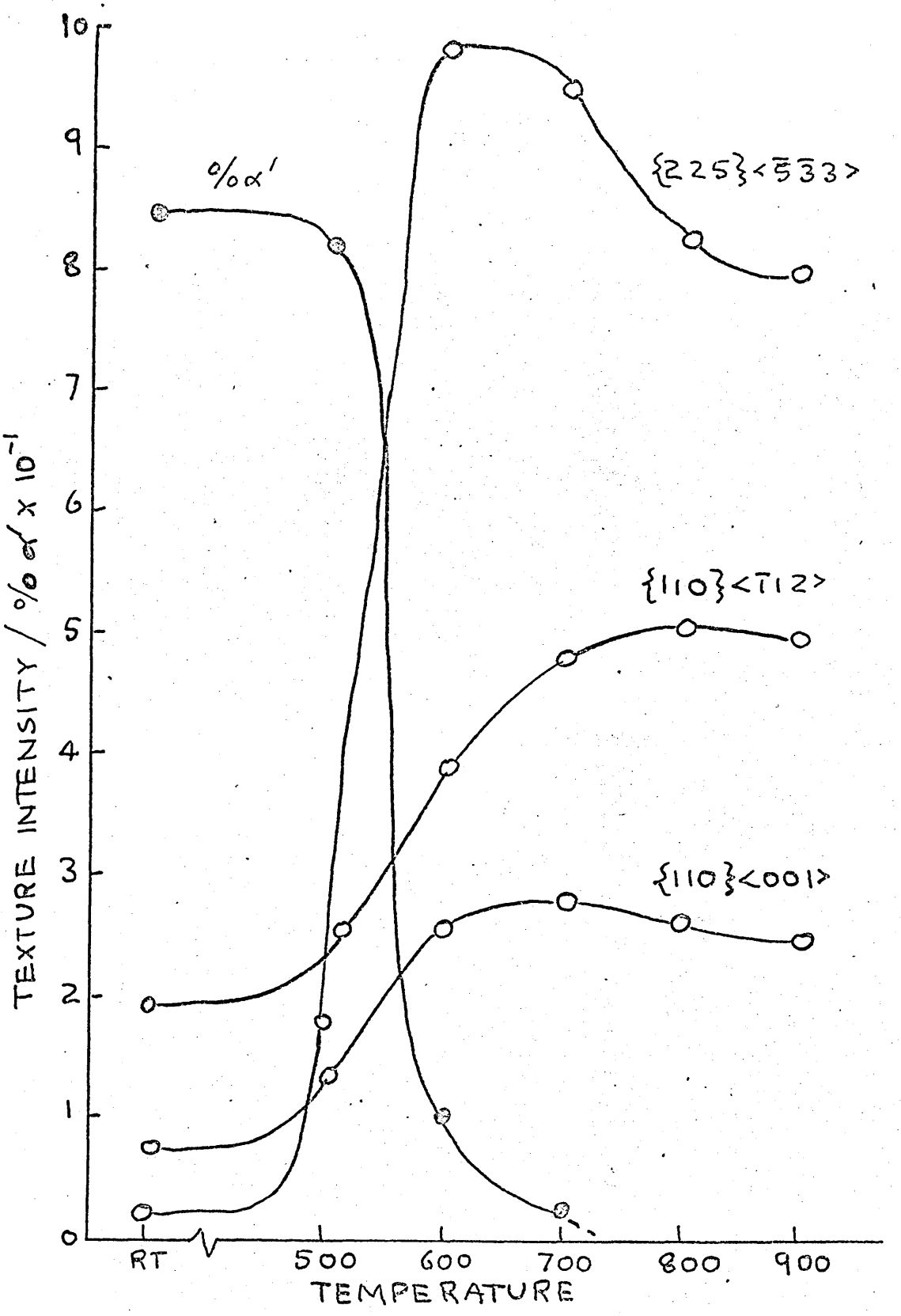

Figure 67

Variation of % α' and intensities of γ texture components for FDP steel.

1 hr 1050°C. FC, 90% cold rolled and annealed.

Figure 68

220γ line profiles for FDP steel.
1 hr 1050°C. FC, 90% cold rolled and annealed.

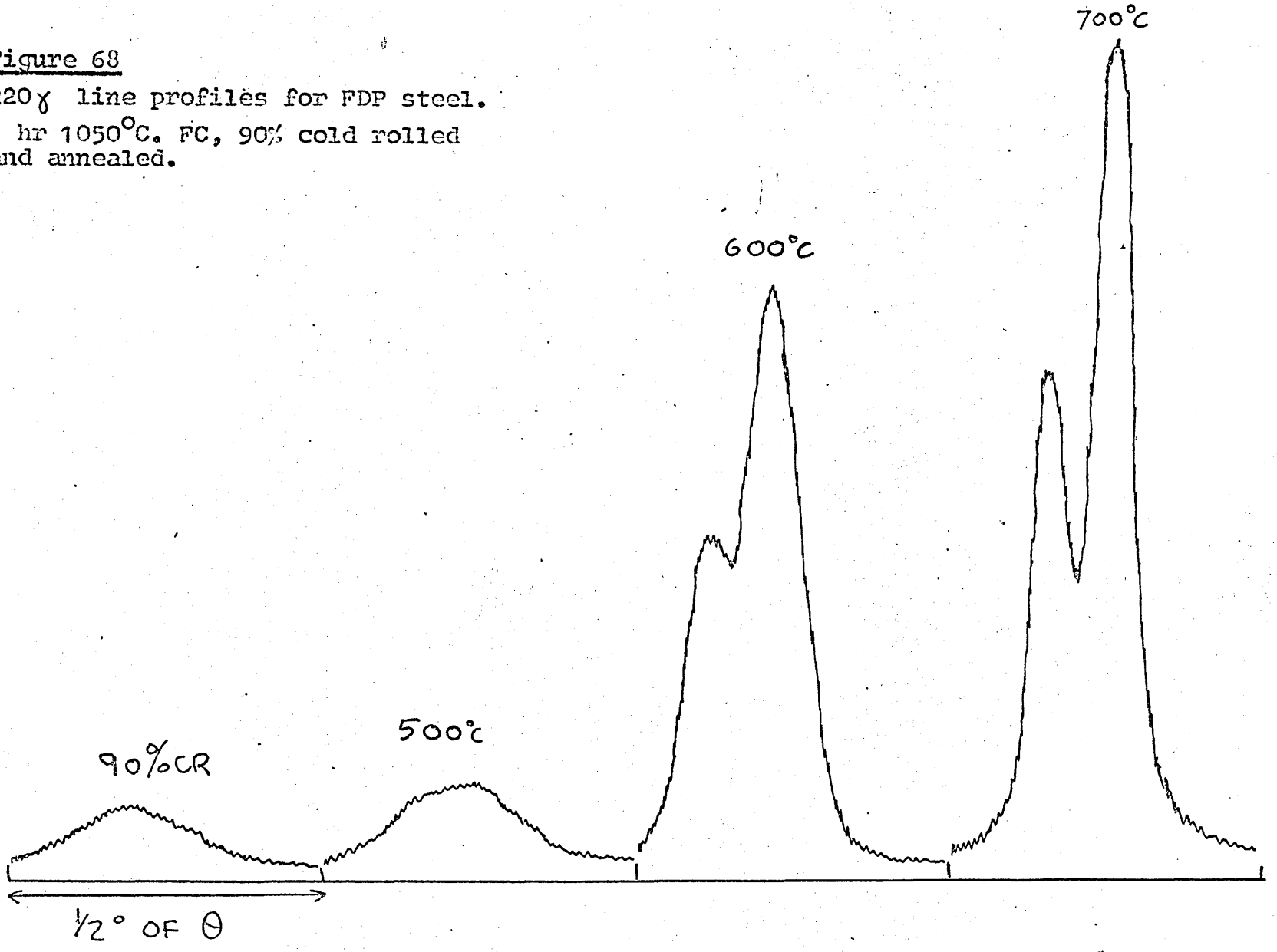

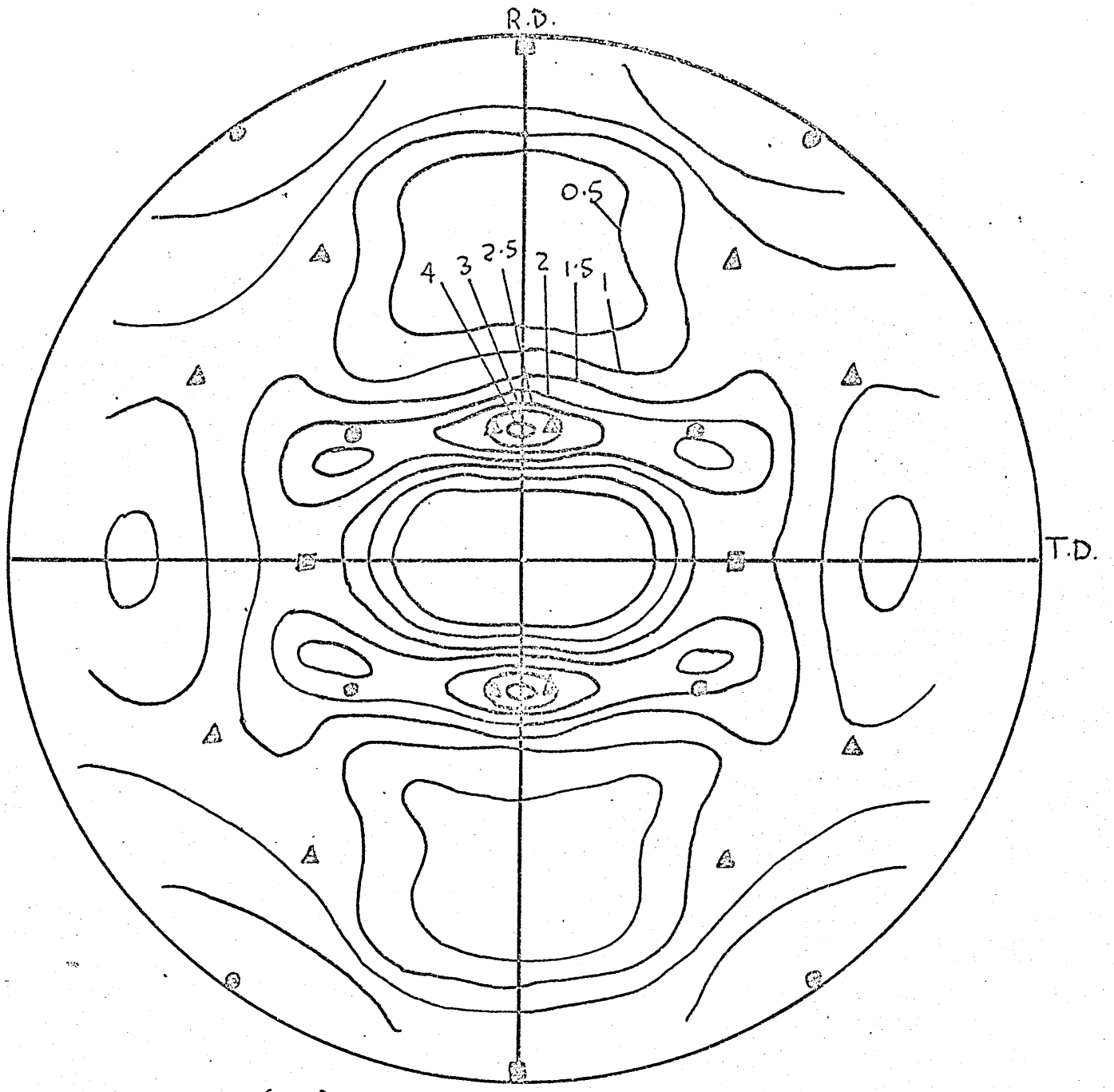
R.D.
T.D.
0.5
4
3
2.5
2
1.5
1
{110}<T12>
{110}<001>
{225}<5̄33>
{200}γ pole figure of FDP steel.
1 hr 1050°C. WQ, 90% cold rolled + ½ hr 900°C. AC.

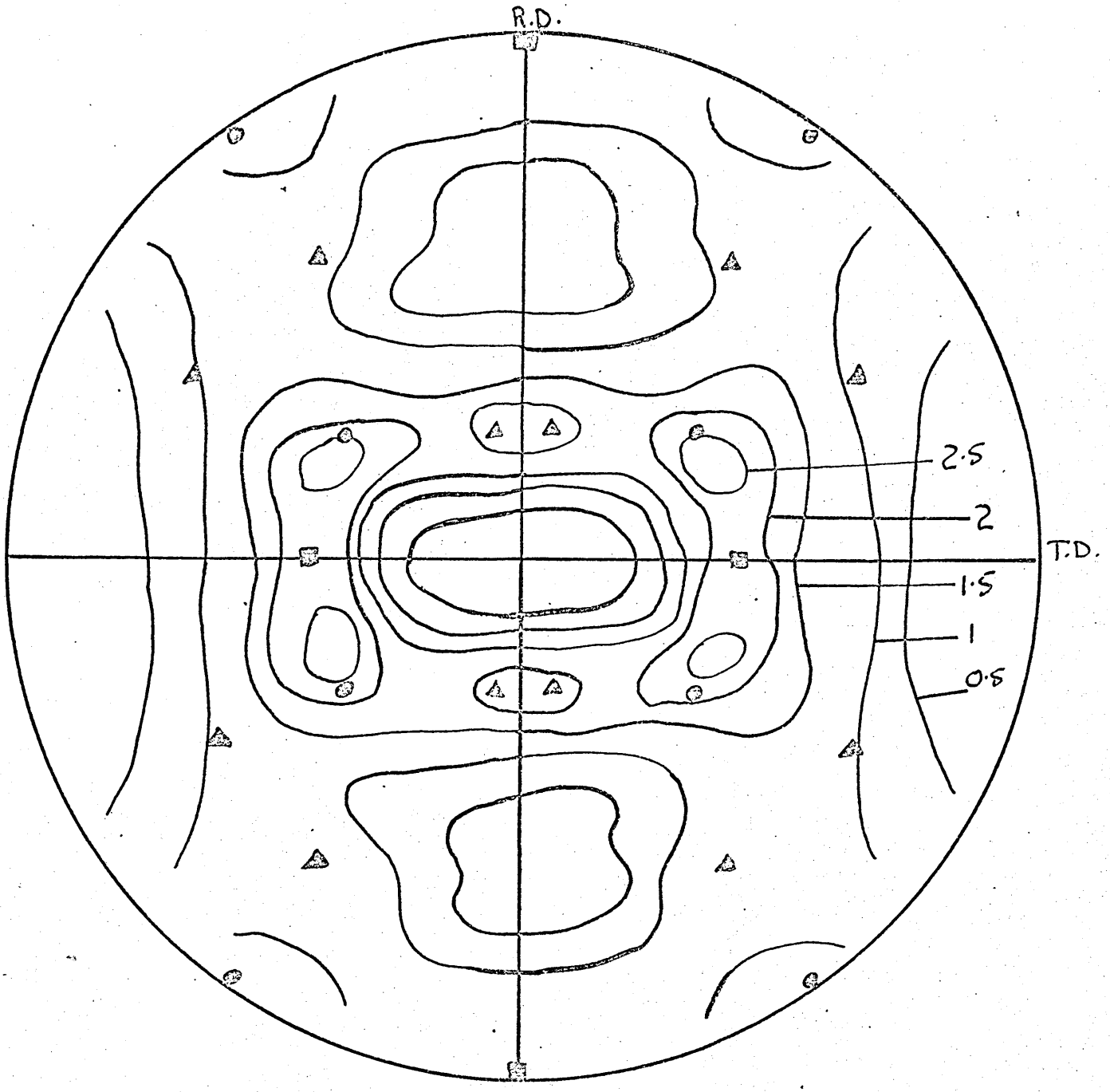

Figure 70

{200}γ pole figure of FDP steel.

15 min 1300°C. FC, 90% cold rolled + ½ hr 900°C. AC.

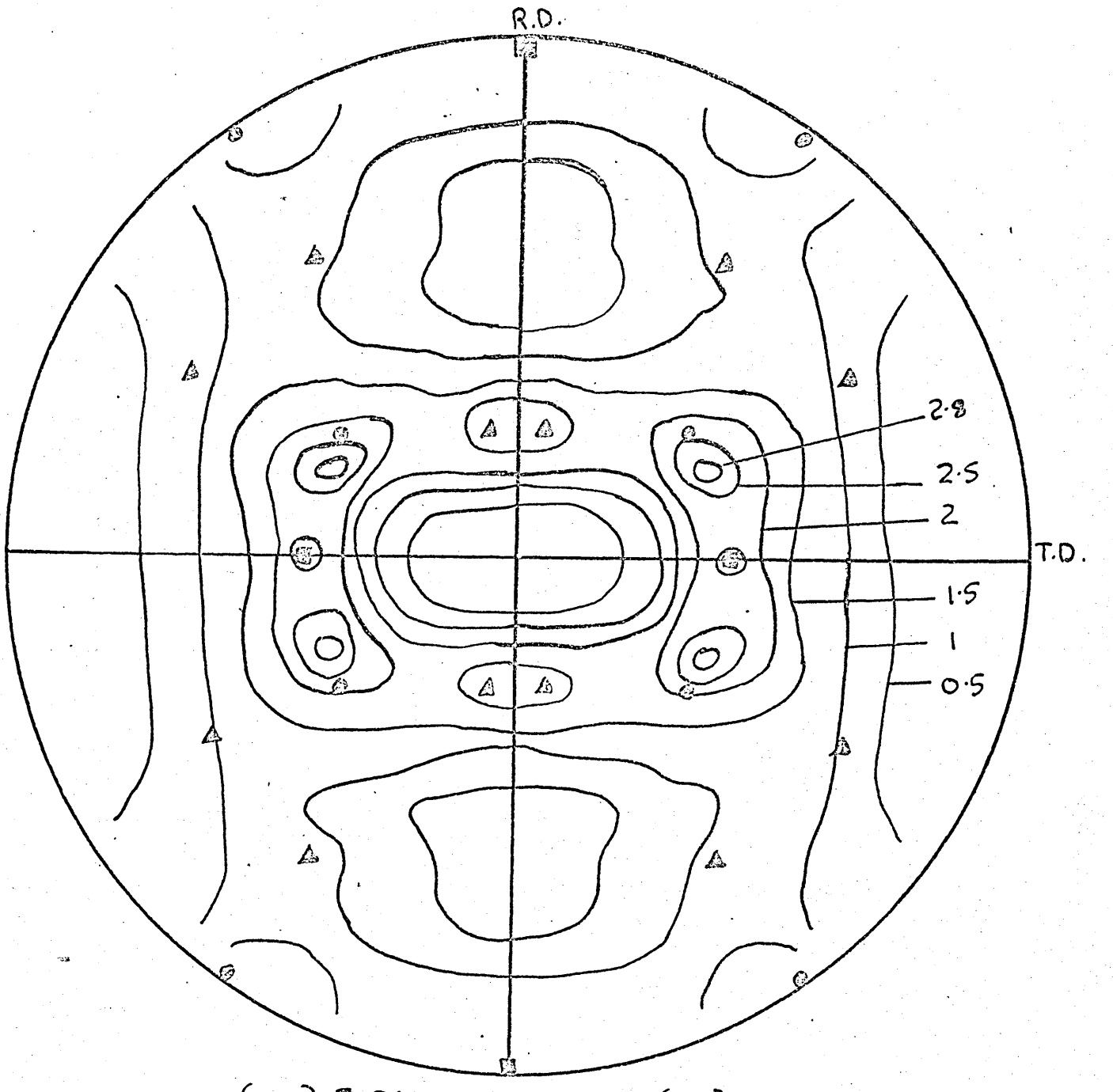

Figure 71

{200}γ pole figure of FDP steel.

15 min 1300°C. WQ, 90% cold rolled + ½ hr 900°C. AC.

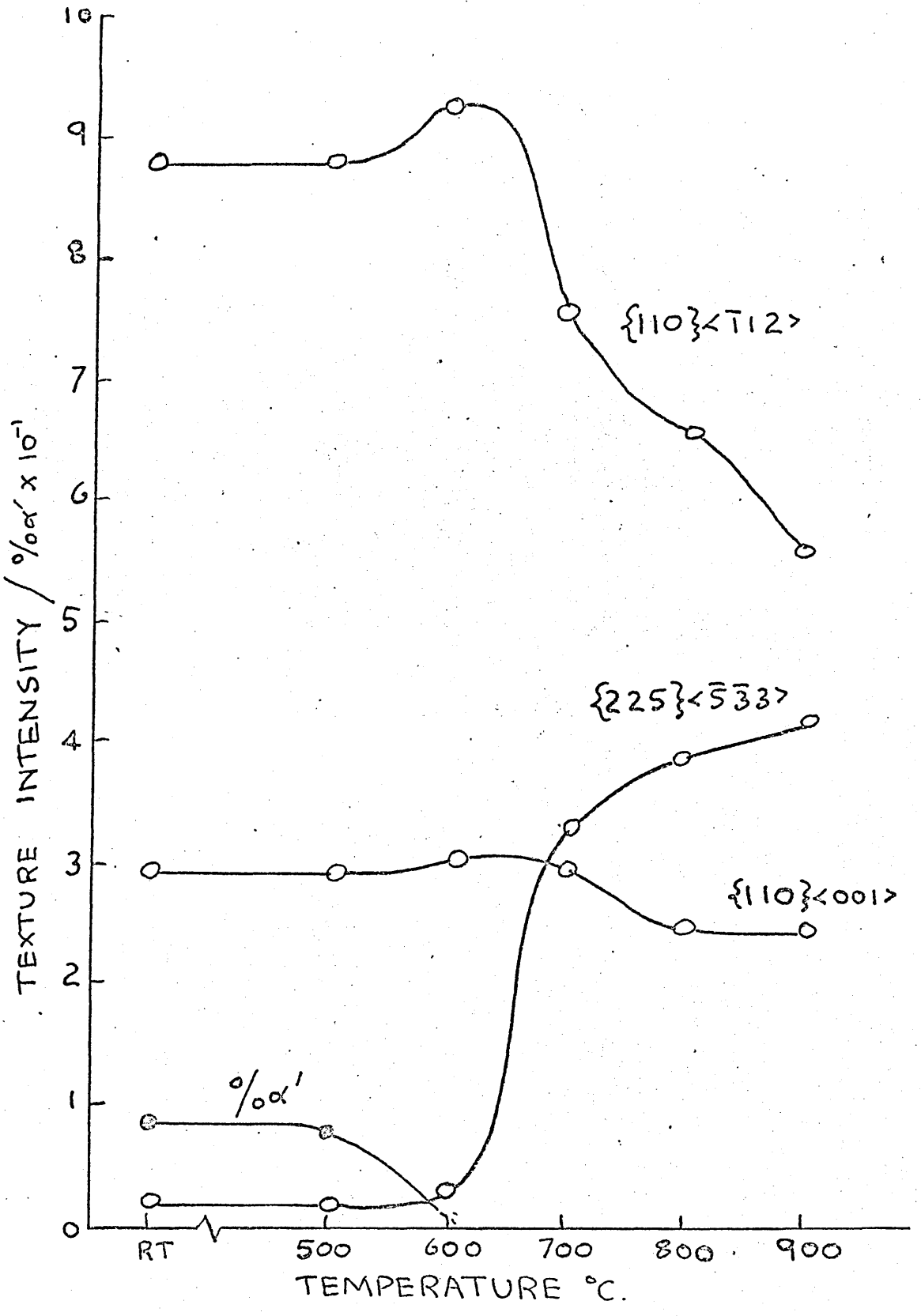

Figure 72

Variation of %α' and intensities of γ texture components for FDP steel.

15 min 1300°C. WQ, 90% cold rolled and annealed.

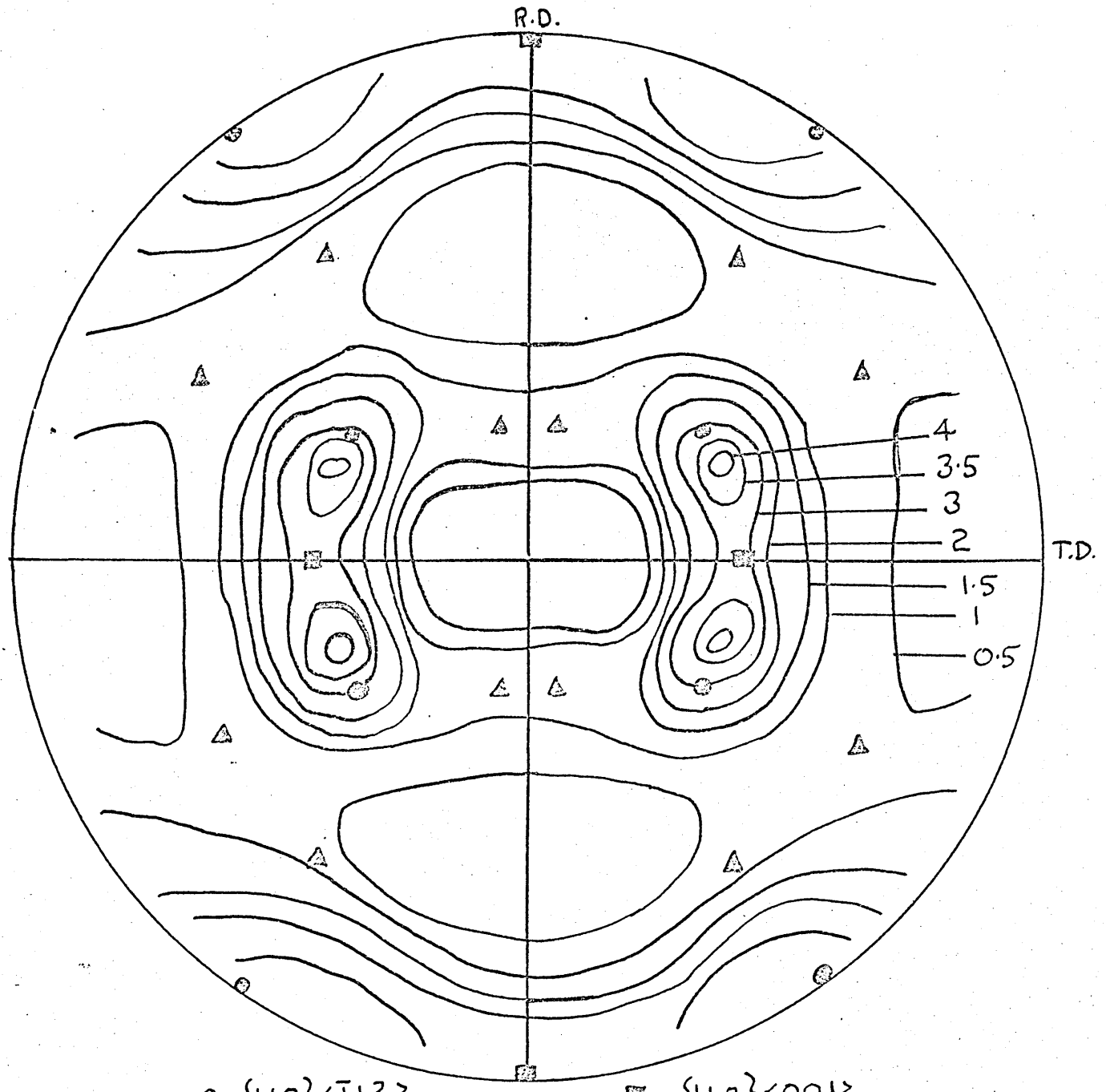

Figure 73

{200}γ pole figure of FMB steel.

1 hr 1050°C. FC, 90% cold rolled + ½ hr 900°C. AC.

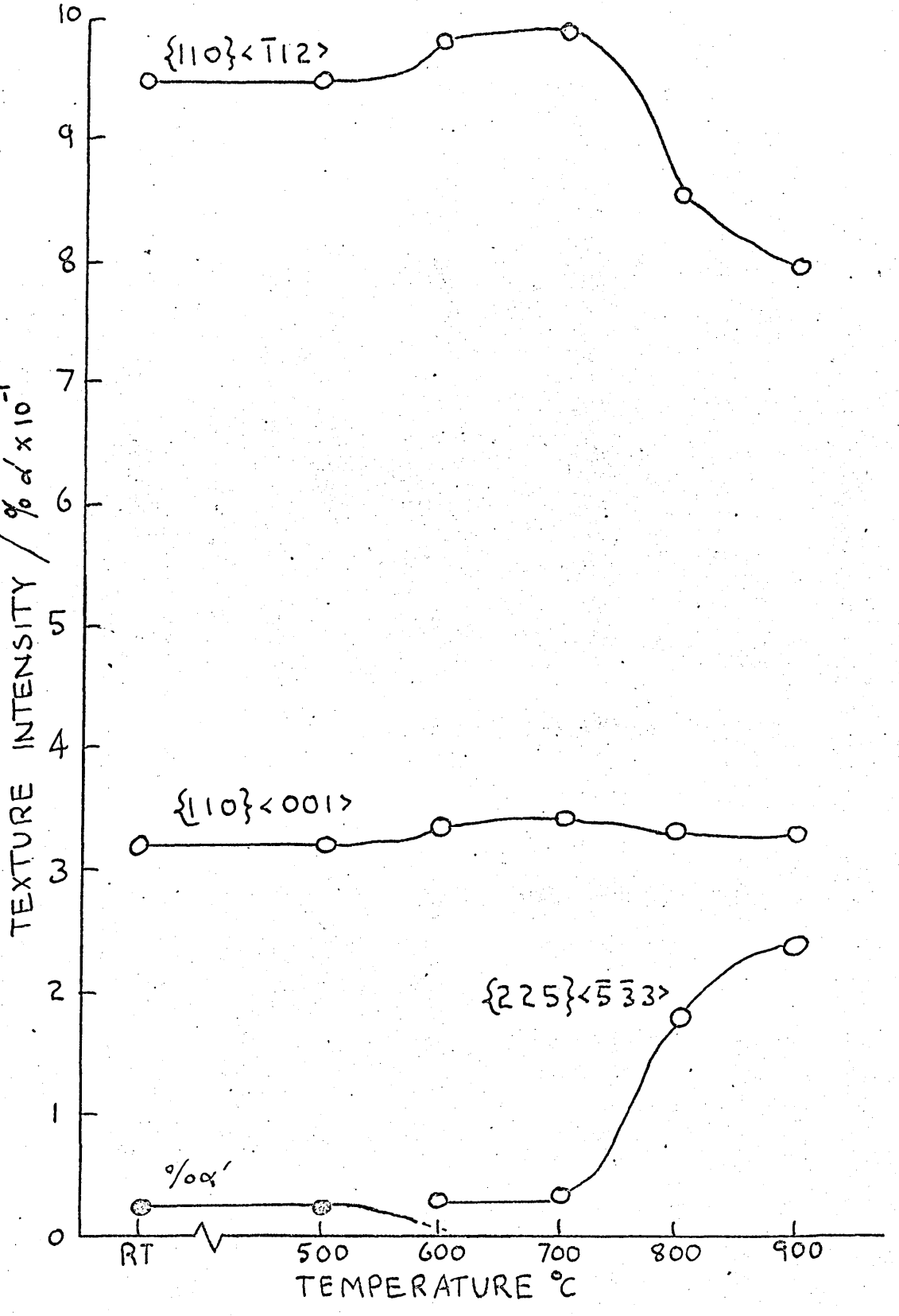

Figure 74

Variation of %α' and intensities of γ texture components for FMB steel.

1 hr 1050°C. FC, 90% cold rolled and annealed.

Figure 75

220γ line profiles for FMB steel.
1 hr 1050°C. FC, 90% cold rolled and annealed.

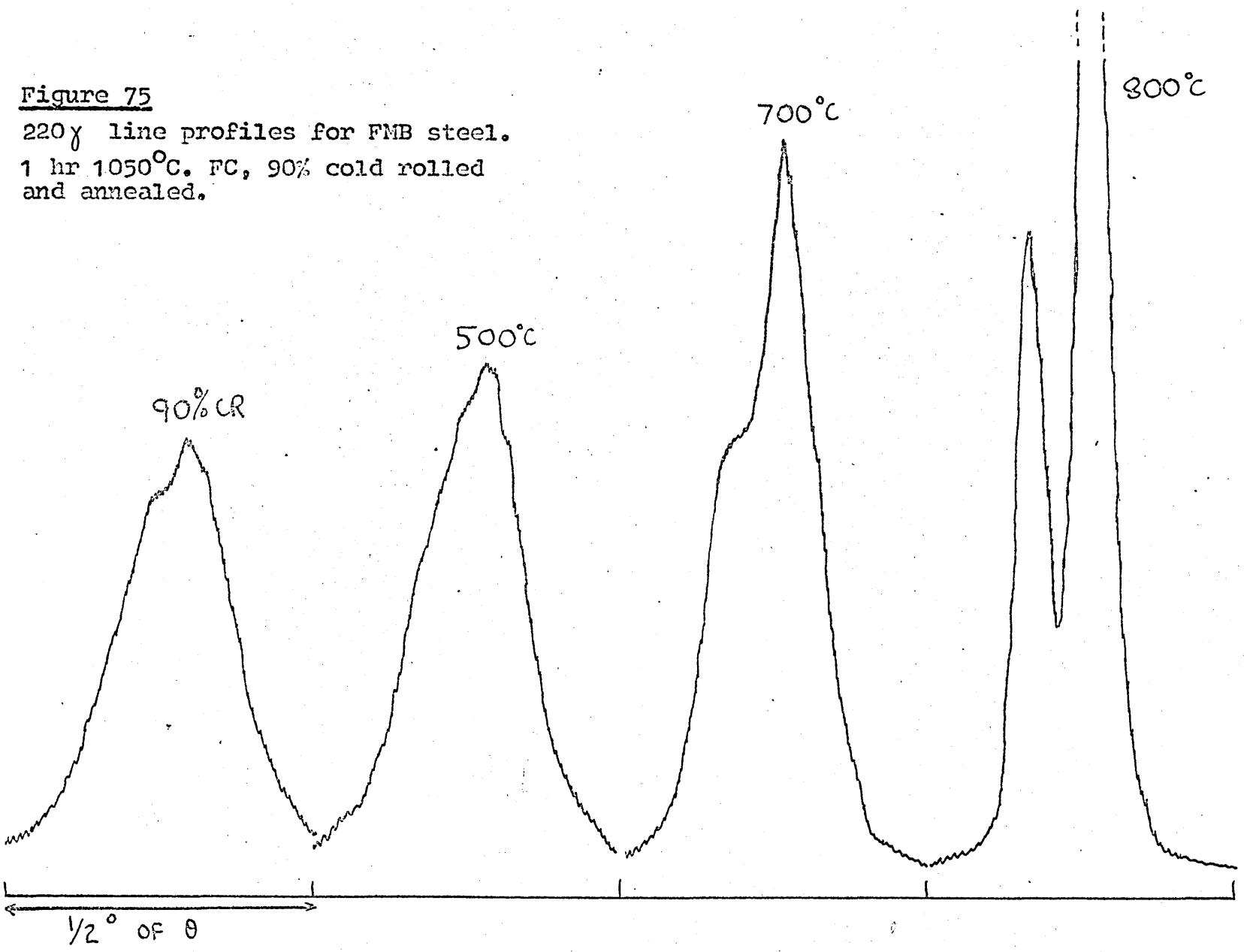

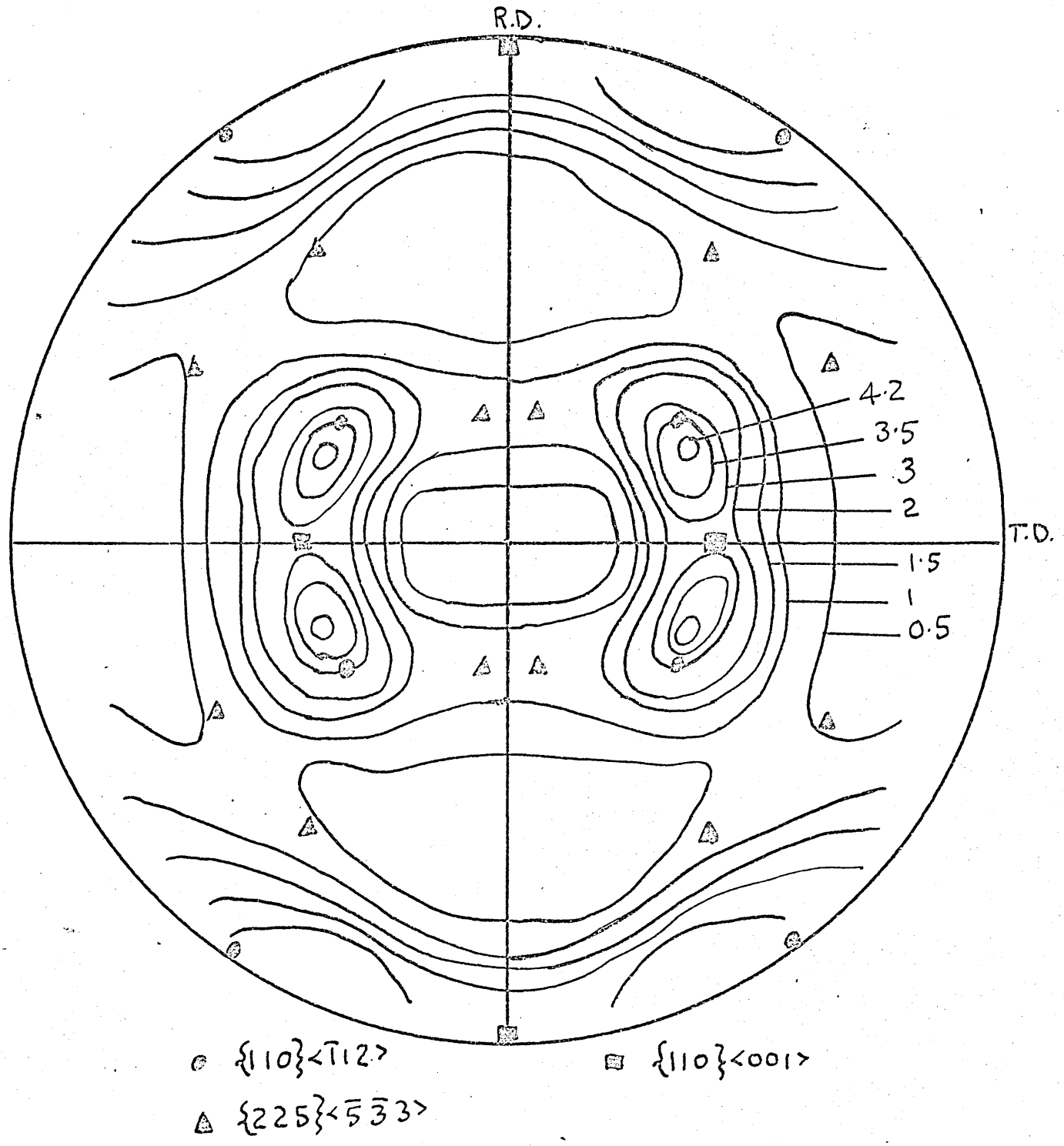

Figure 76

{200}γ pole figure of FMB steel.

1 hr 1050°C. WQ, 90% cold rolled + ½ hr 900°C. AC.

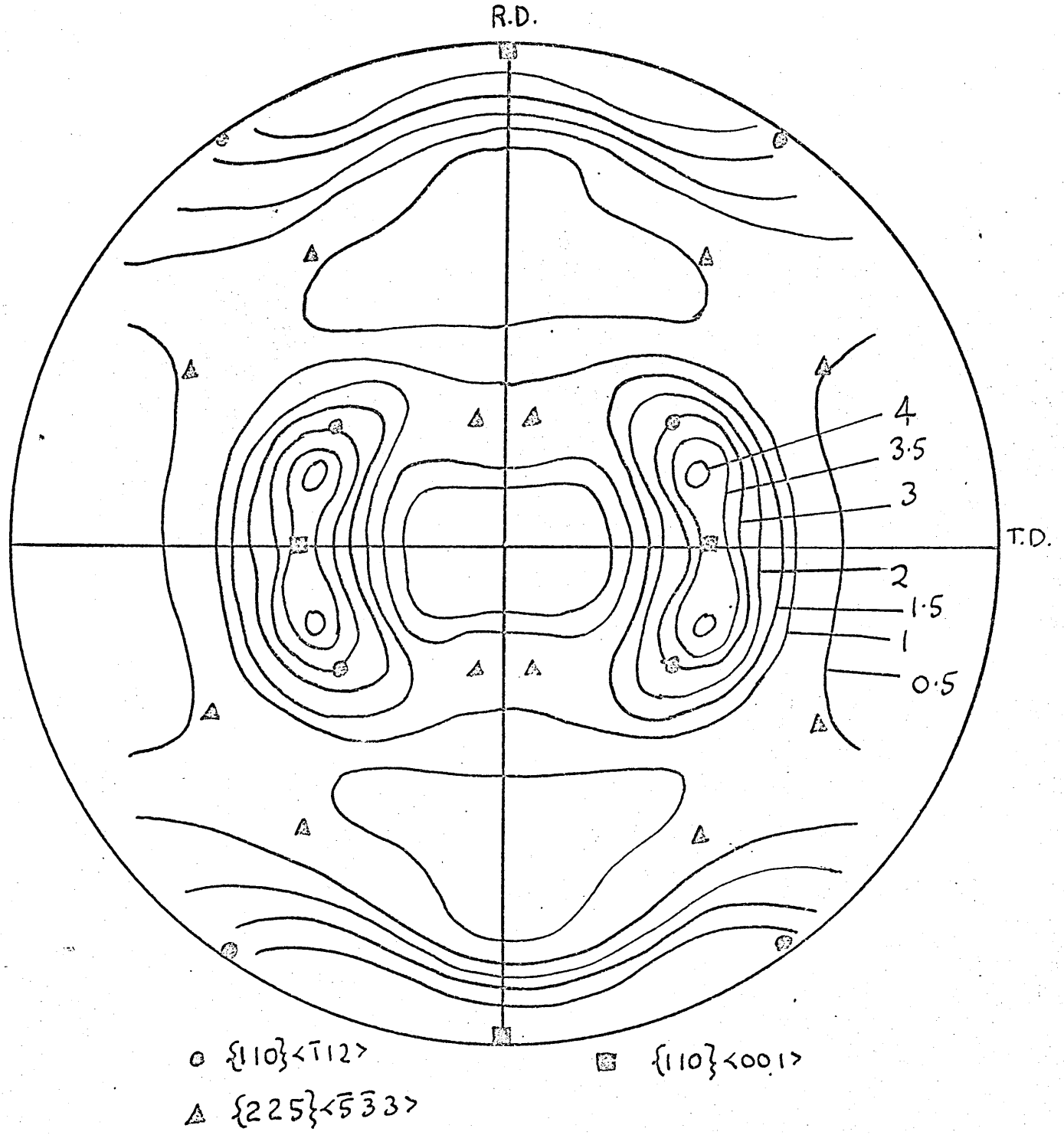

Figure 77

{200}γ pole figure of FMB steel.

15 min 1300°C. FC, 90% cold rolled + ½ hr 900°C. AC.

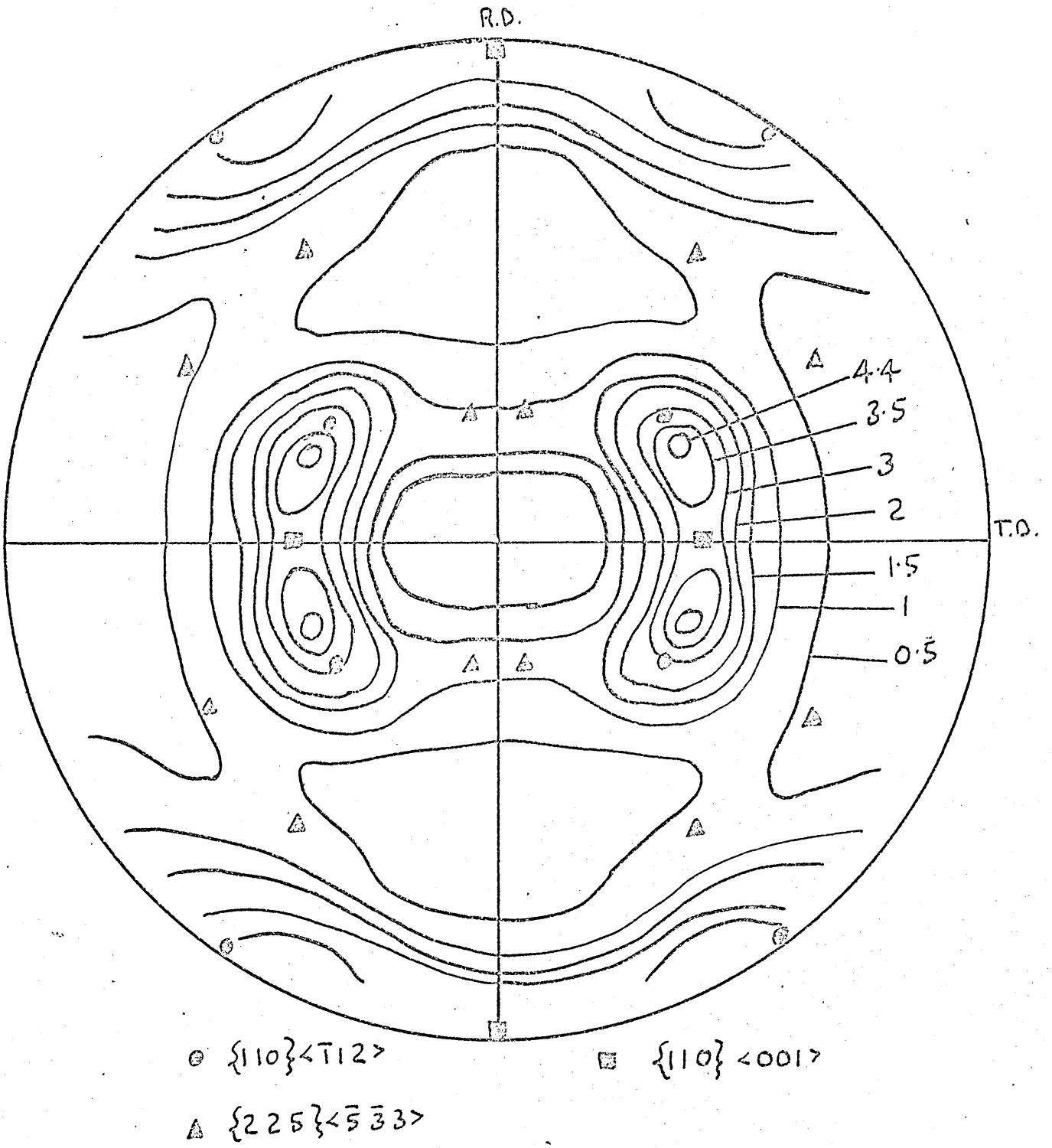

Figure 78

{200}γ pole figure of FMB steel.

15 min 1300°C. WQ, 90% cold rolled + ½ hr 900°C. AC.

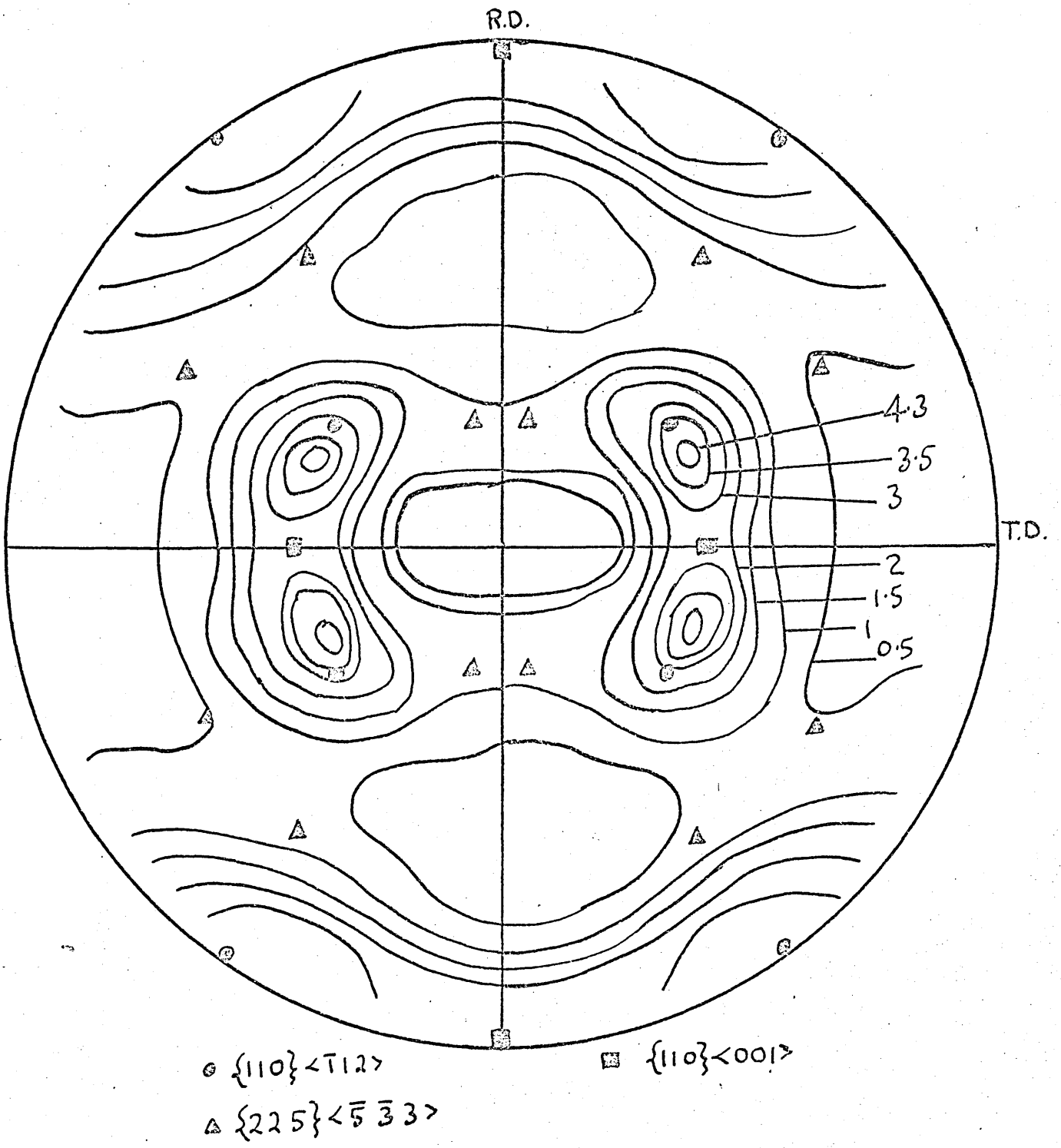

Figure 79

{200}γ pole figure of FMB Ti steel.

1 hr 1050°C. FC, 90% cold rolled + ½ hr 900°C. AC.

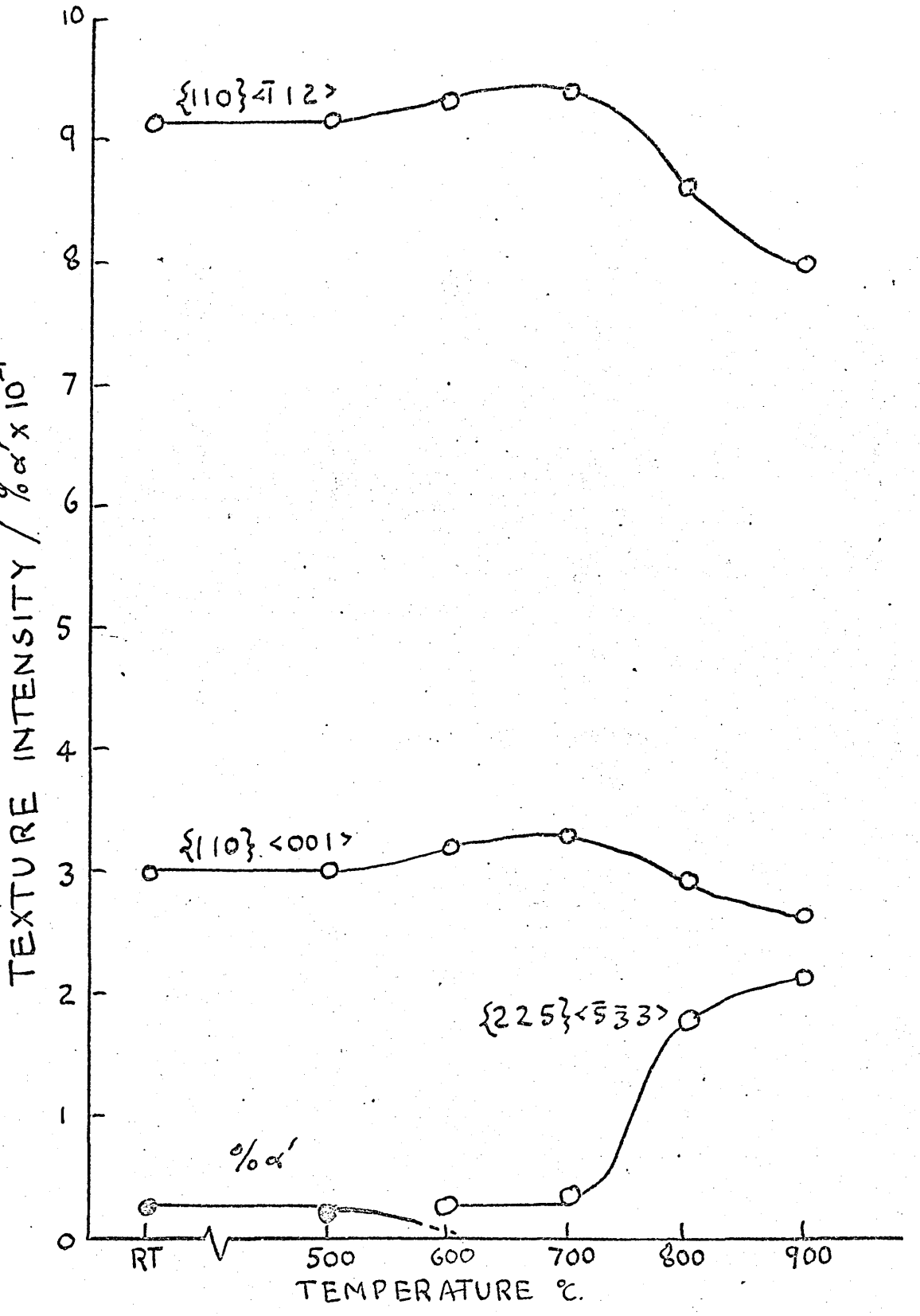

Figure 80

Variation of %α' and intensities of γ texture components for FMB Ti steel.

1 hr 1050°C. FC, 90% cold rolled and annealed.

Figure 81

220 γ line profiles for FMB Ti steel.
1 hr 1050°C. FC, 90% cold rolled and annealed.

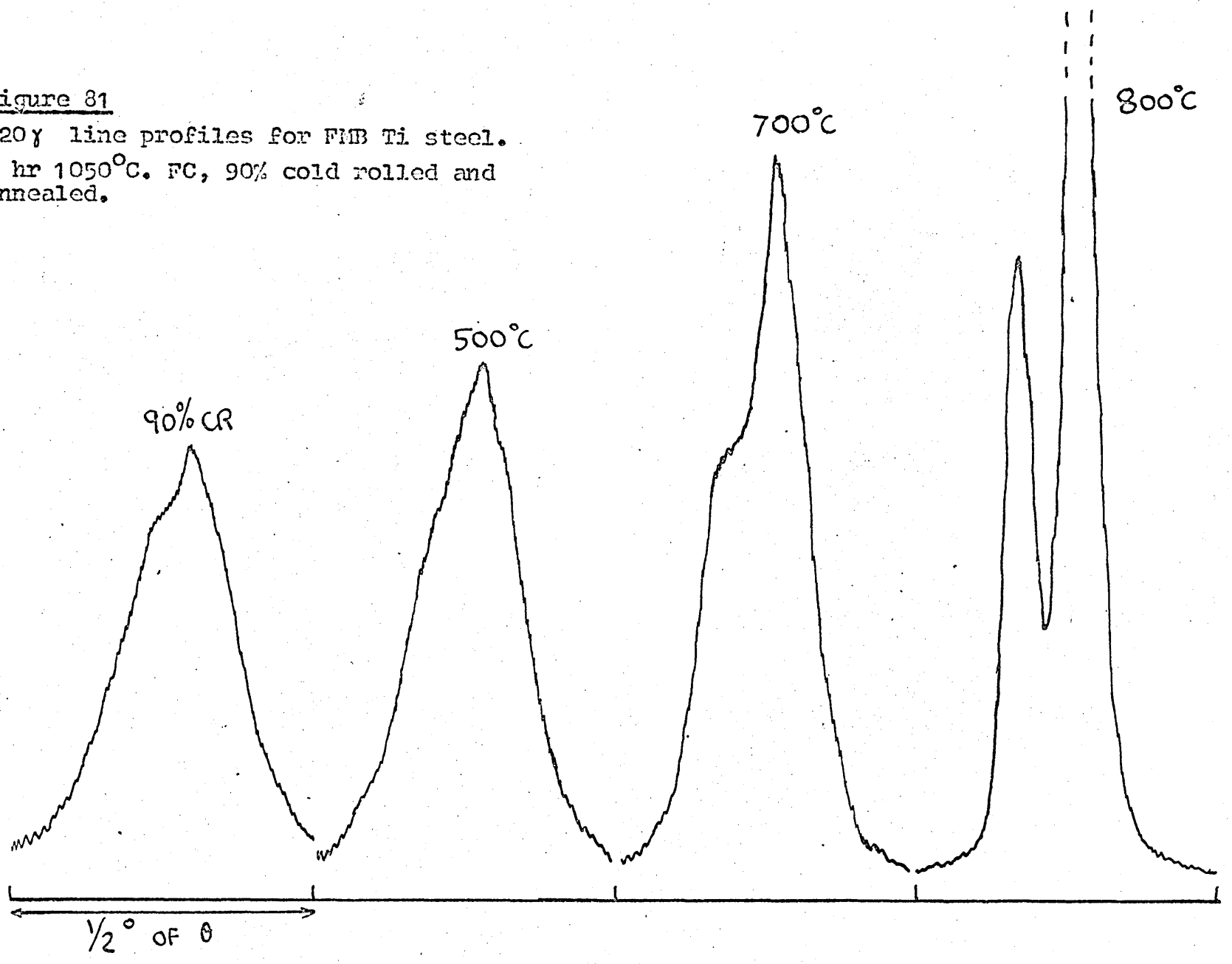

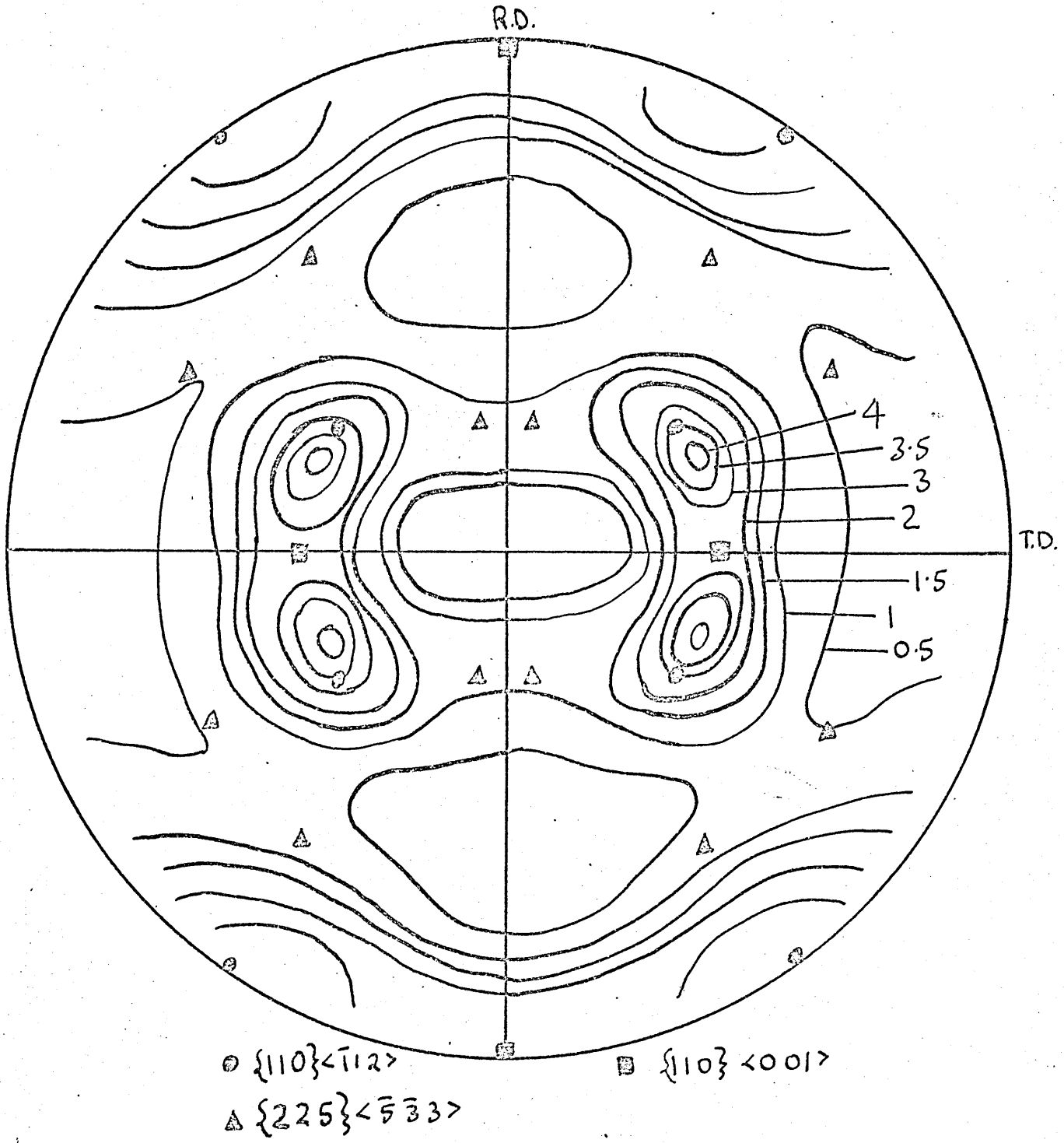

Figure 82

{200}γ pole figure of FMB Ti steel.

1 hr 1050°C. WQ, 90% cold rolled + ½ hr 900°C. AC.

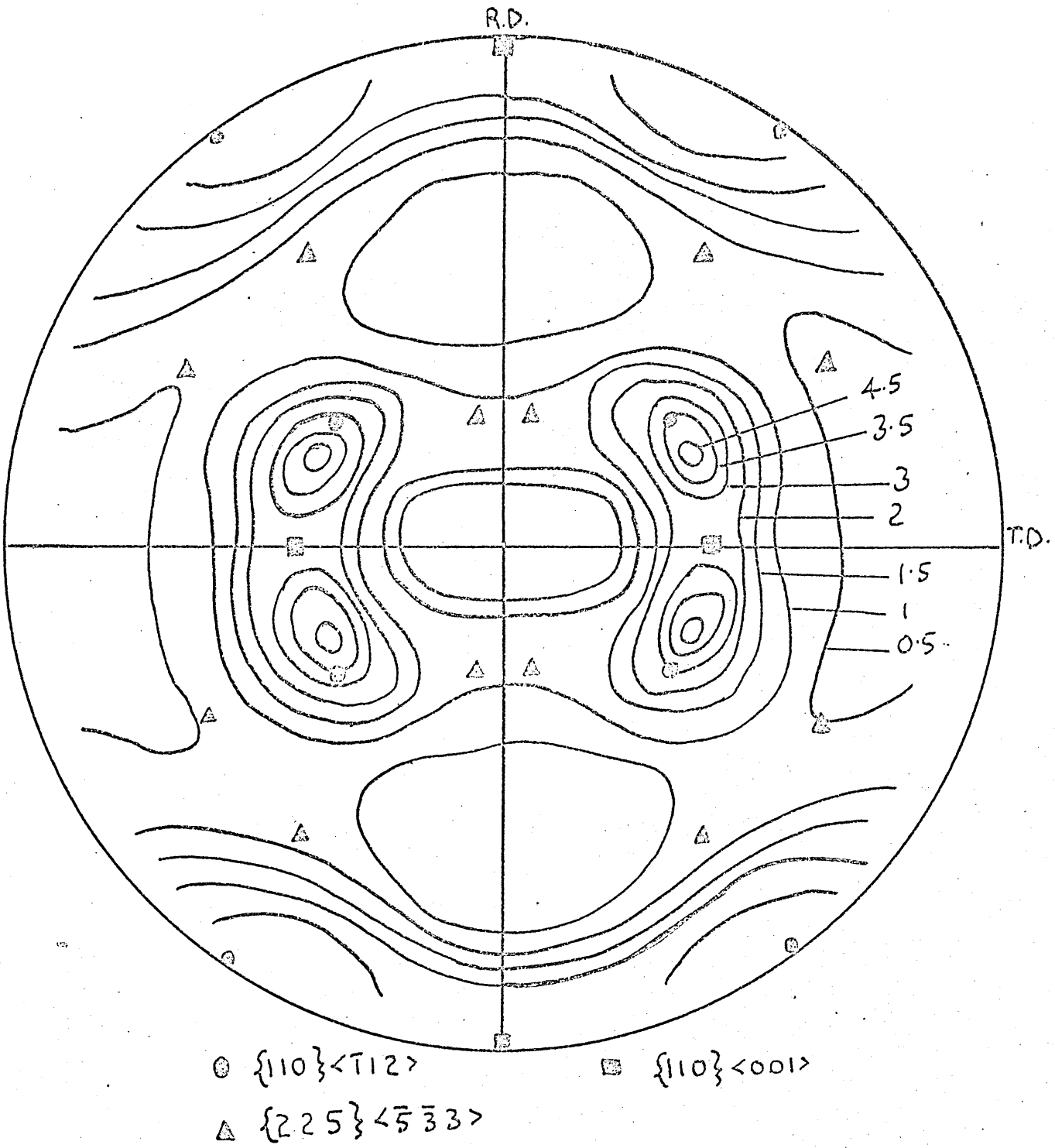

Figure 83

{200}γ pole figure of FMB Ti steel.

15 min 1300°C. FC. 90% coldrolled + ½ hr 900°C. AC.

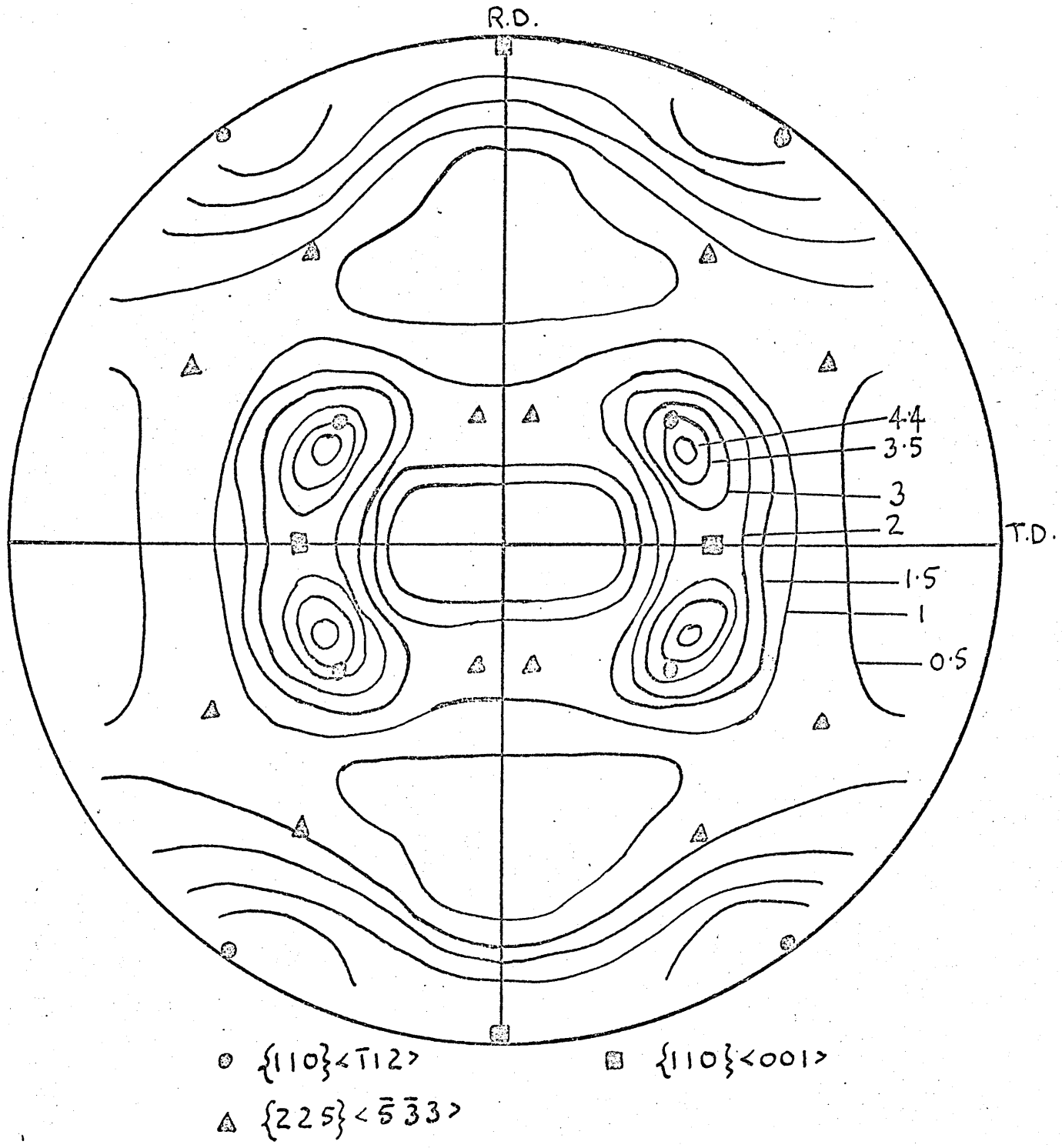
R.D.
T.D.
4·4
3·5
3
2
1·5
1
0·5
{110}<T12>
{110}<001>
{225}<5̄3̄3>
{200}γ pole figure of FMB Ti steel.
15 min 1300°C. WQ, 90% cold rolled + ½ hr 900°C. AC.

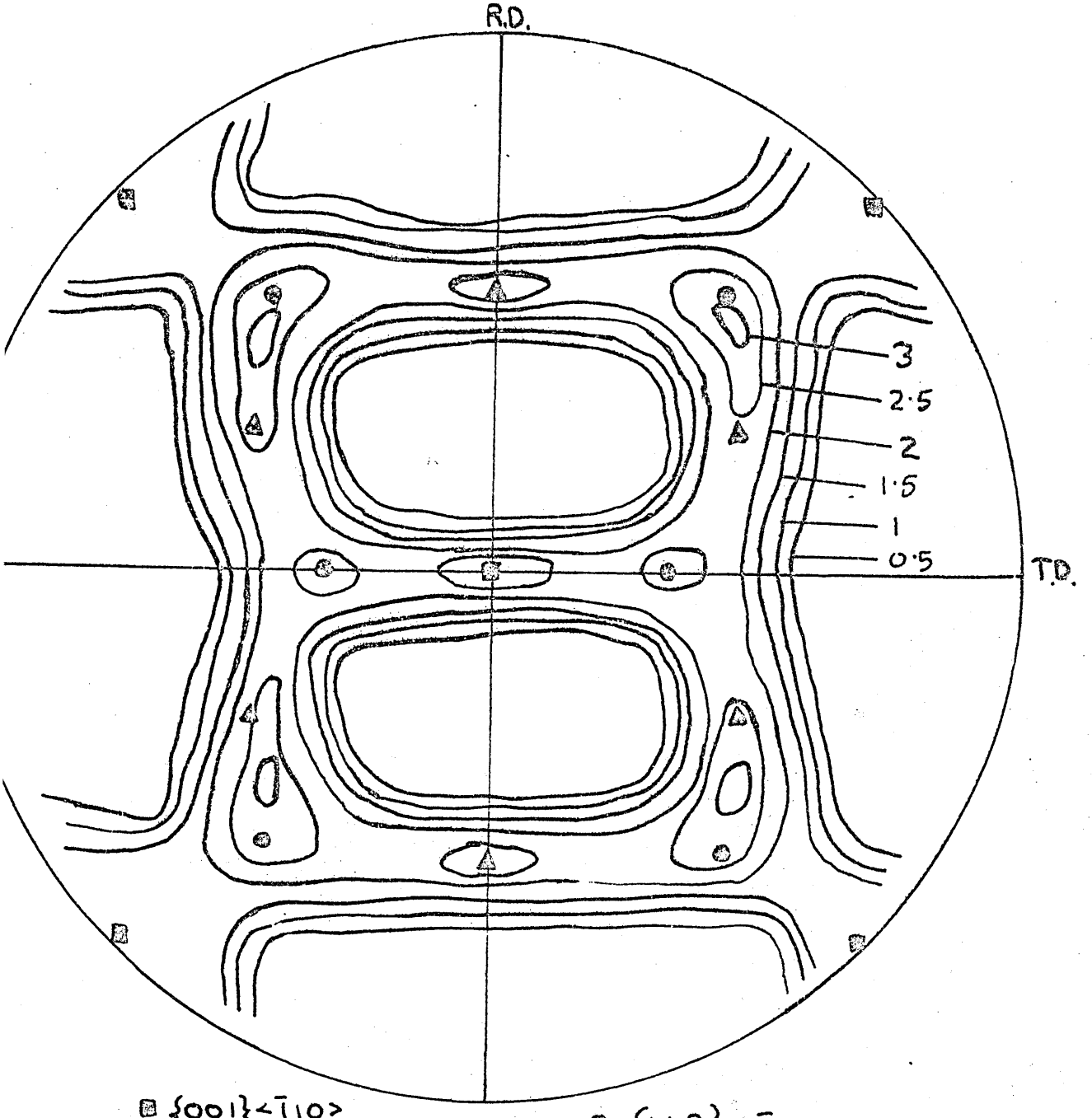

Figure 85

{200}α' pole figure of 18%Cr 10%Ni steel.
1 hr 1050°C. FC, 90% cold rolled at ~ -196°C.

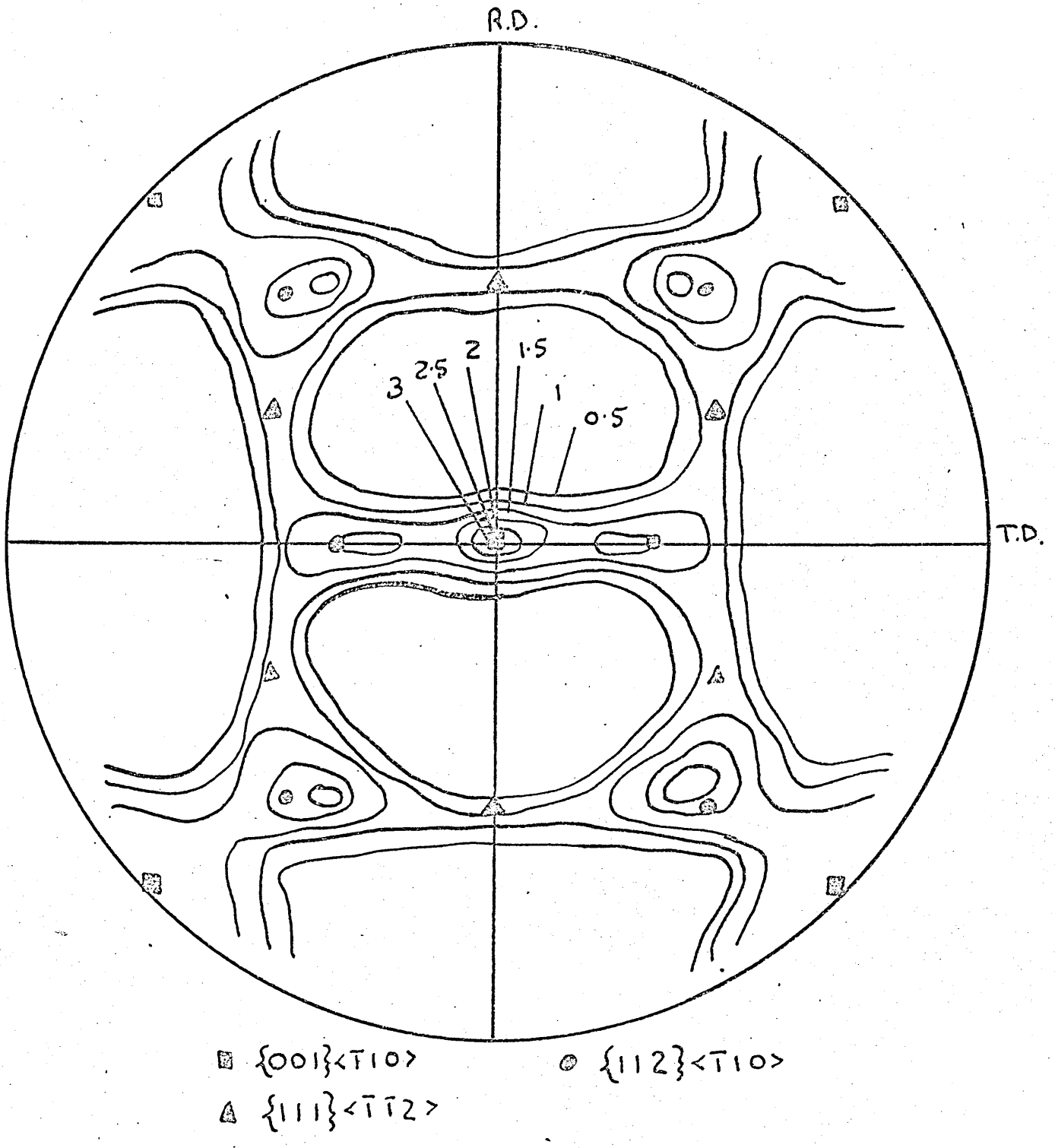

Figure 86

{200}α′ pole figure of FCB steel.

1 hr 1050°C. FC, 90% cold rolled at ~ -196°C.

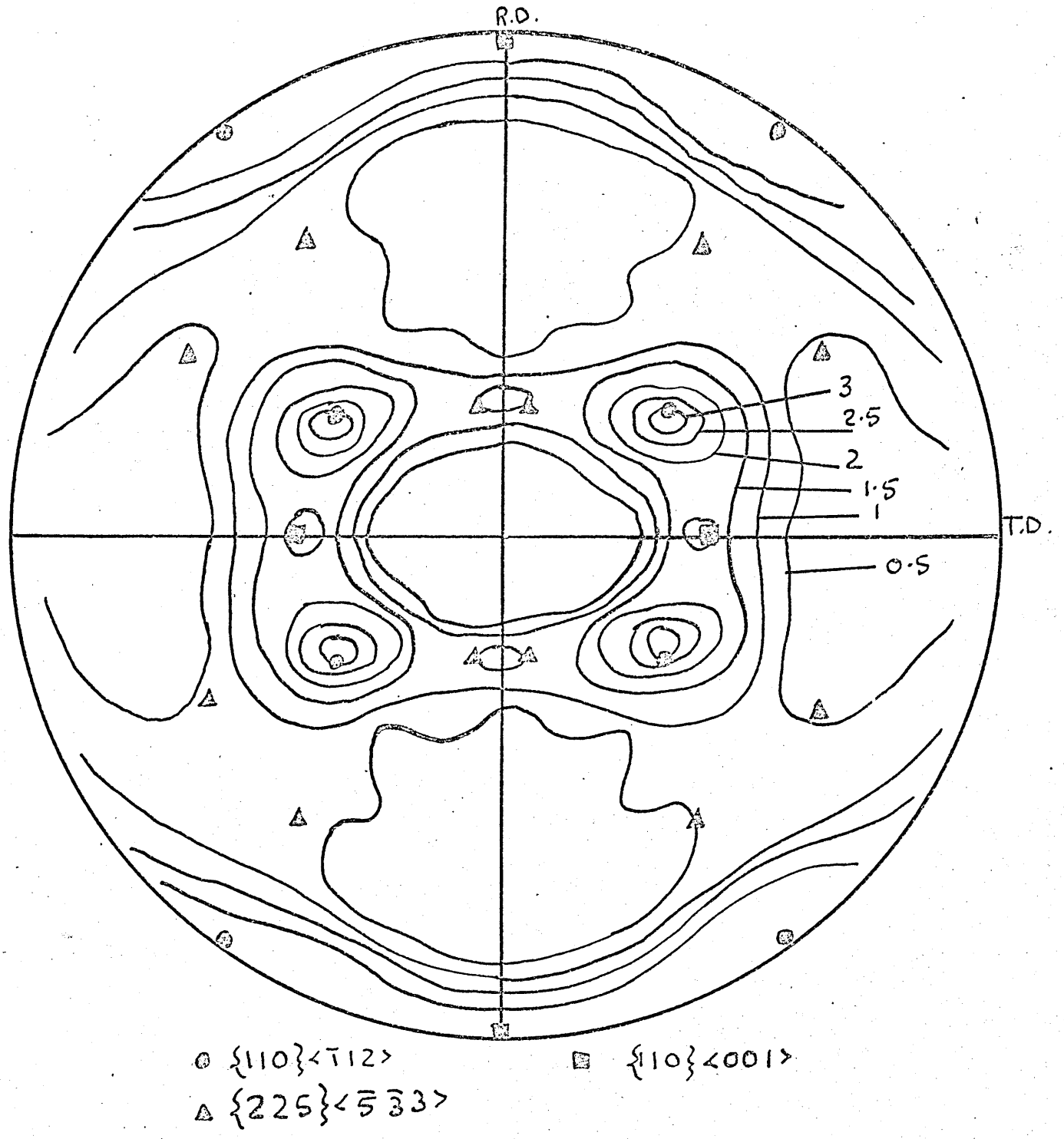

Figure 87

{200}γ pole figure of FCB steel.

1 hr 1050°C. FC, 90% cold rolled at ~ -196°C + ½ hr 900°C. AC.

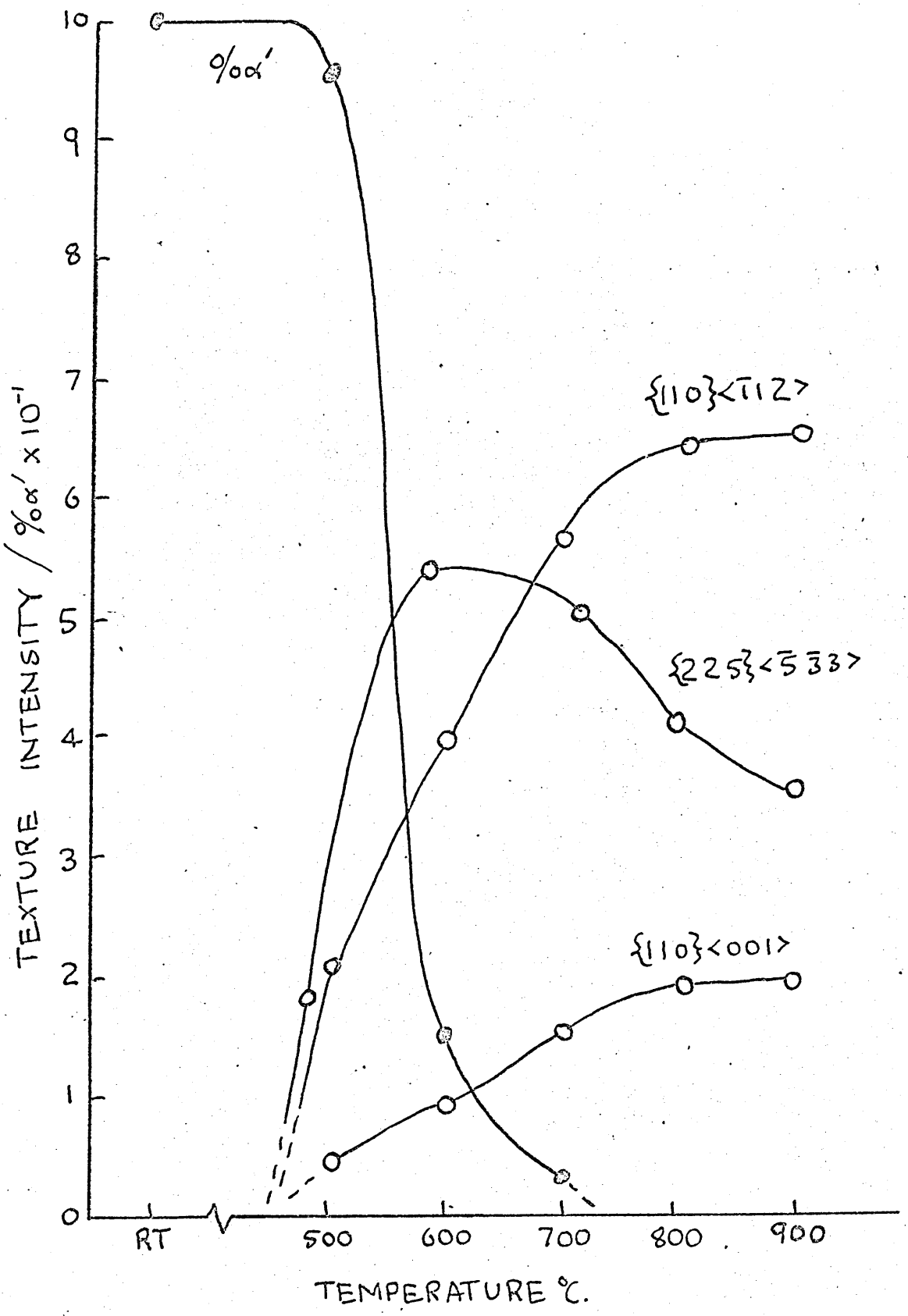

Figure 88

Variation of % α' and intensities of γ texture components for FCB steel.

1 hr 1050°C. FC, 90% cold rolled at ~ -196°C and annealed.

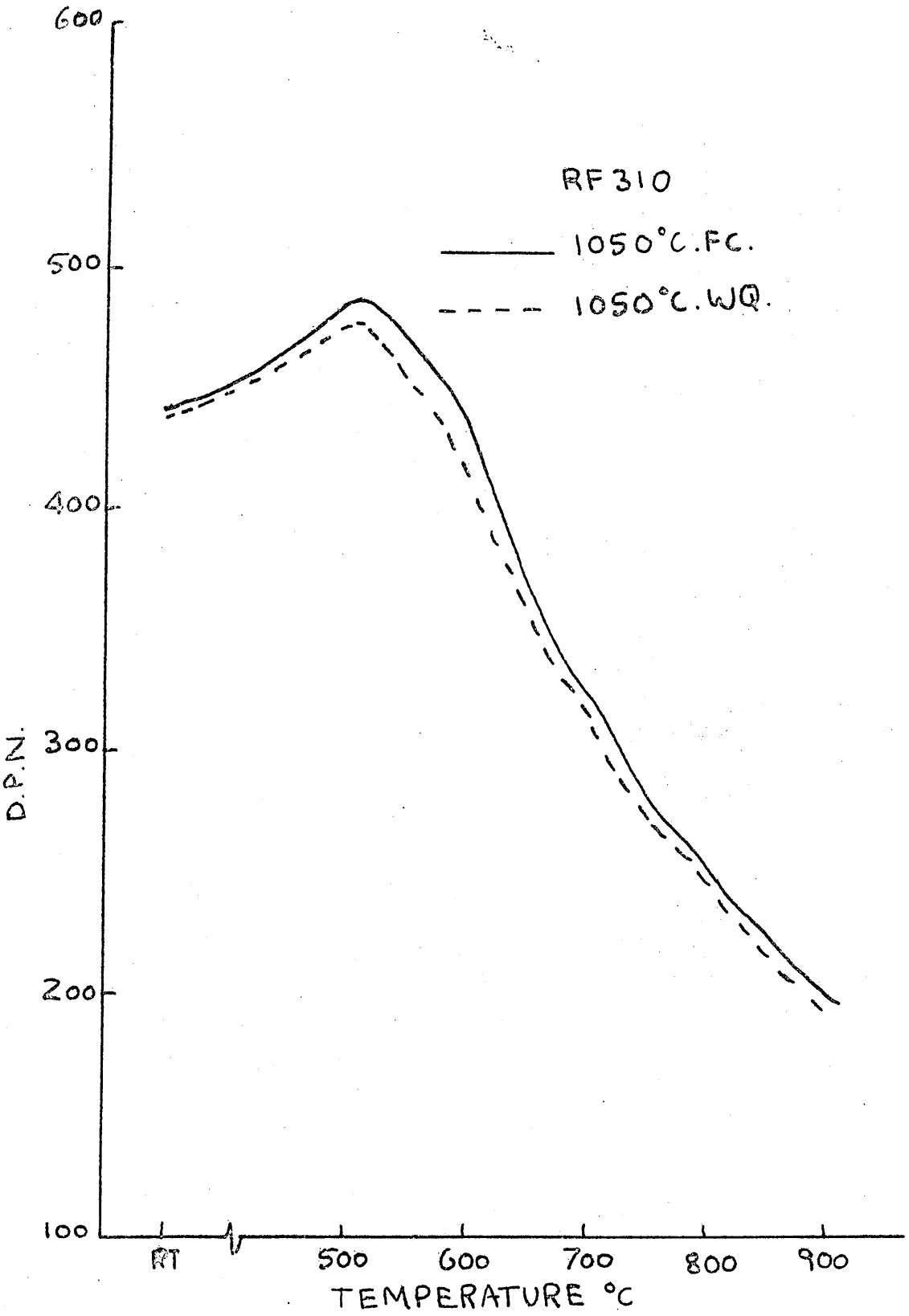

Figure 89

Hardness curves for RF 310 steel.

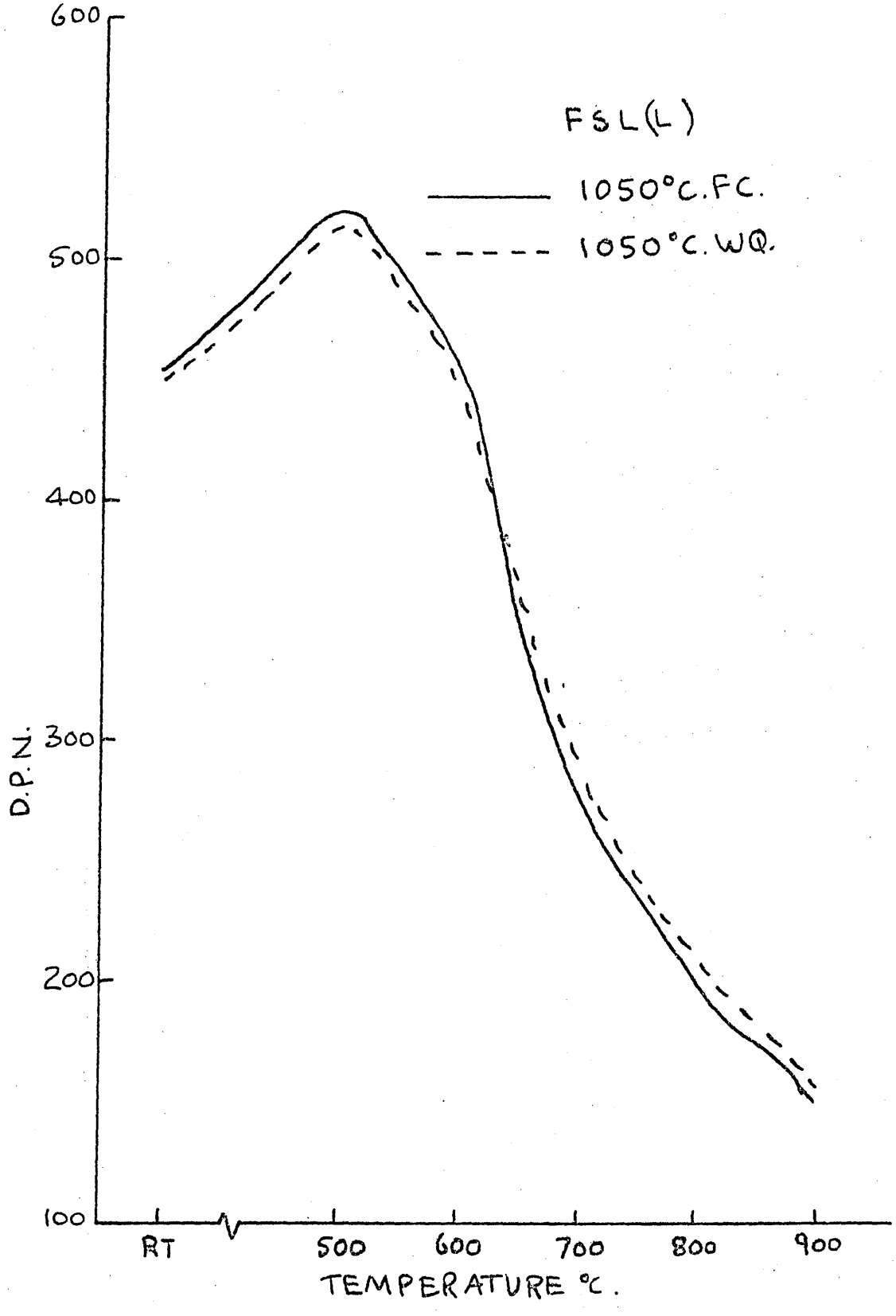

Figure 90

Hardness curves for FSL(L) steel.

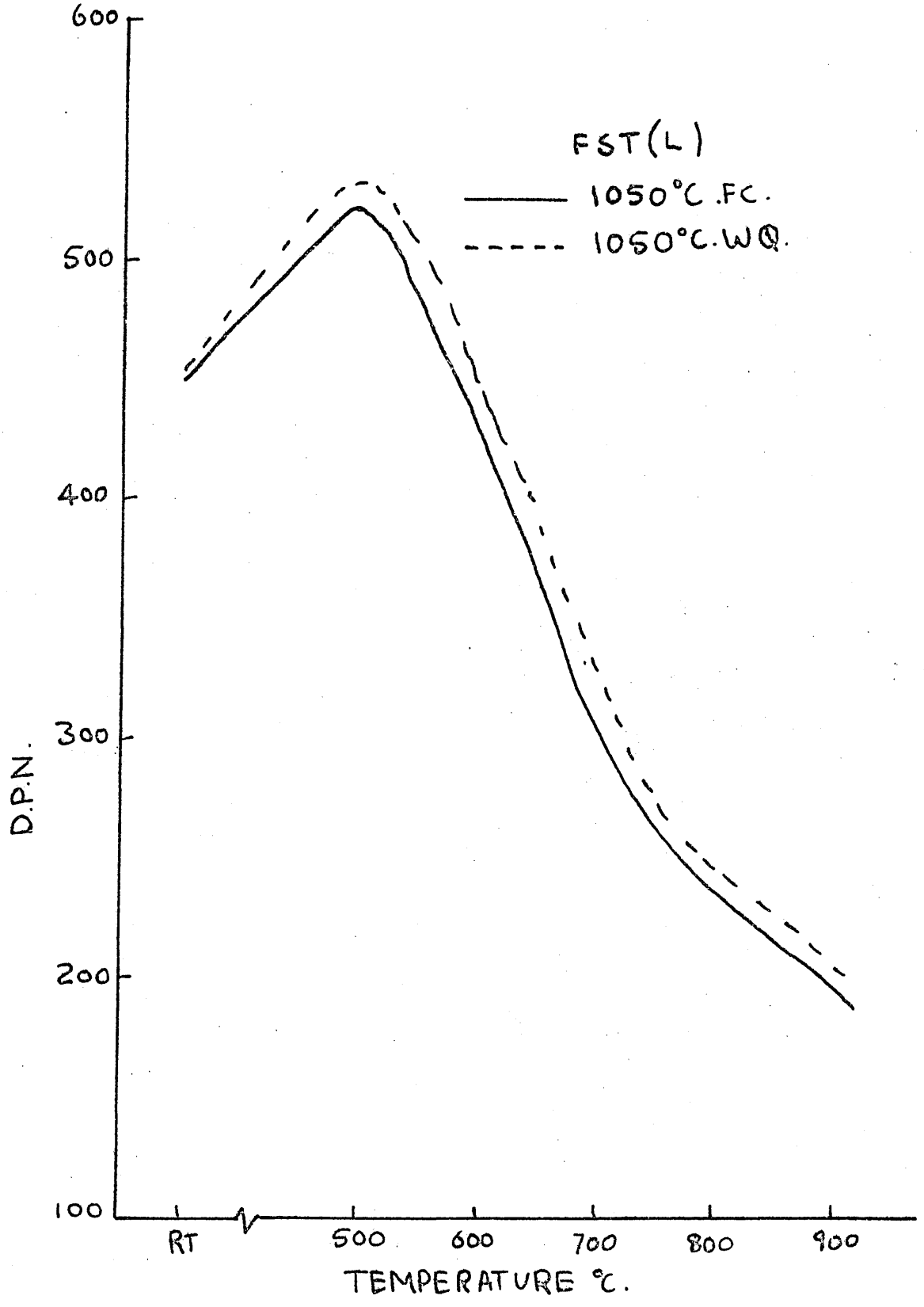

Figure 91

Hardness curves for FST(L) steel.

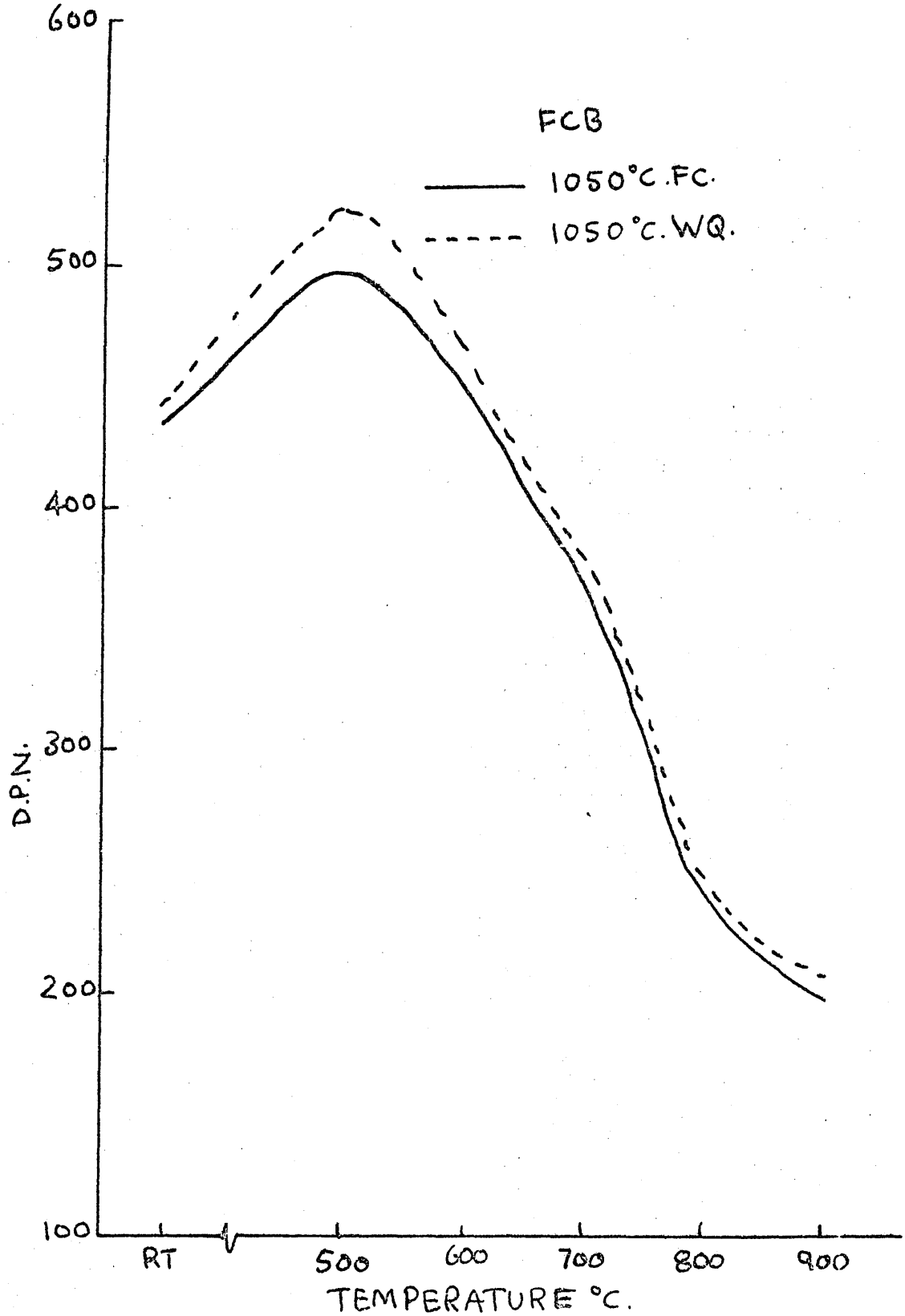

Figure 92(a)
Hardness curves for FCB steel.

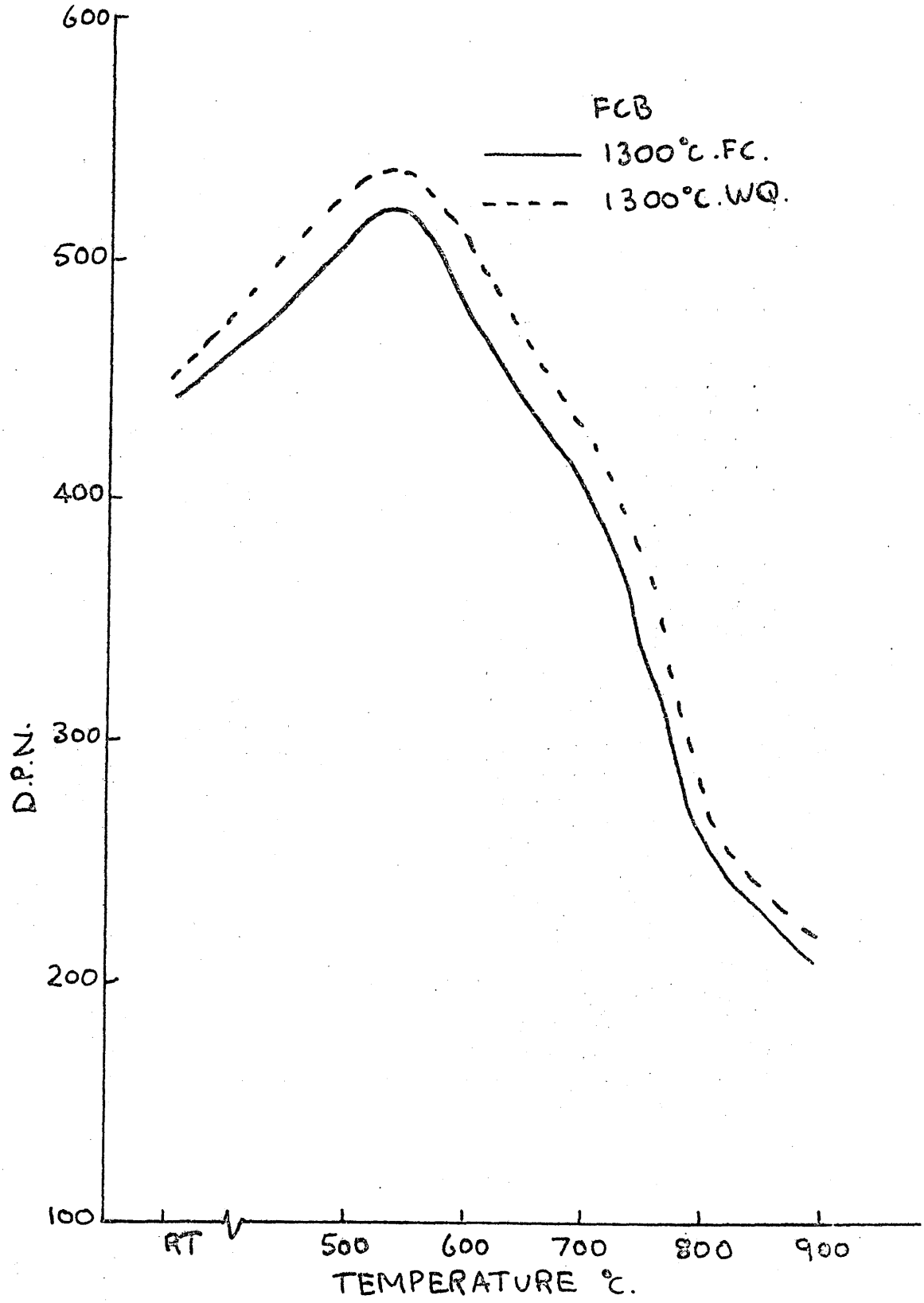

Figure 92(b)

Hardness curves for FCB steel.

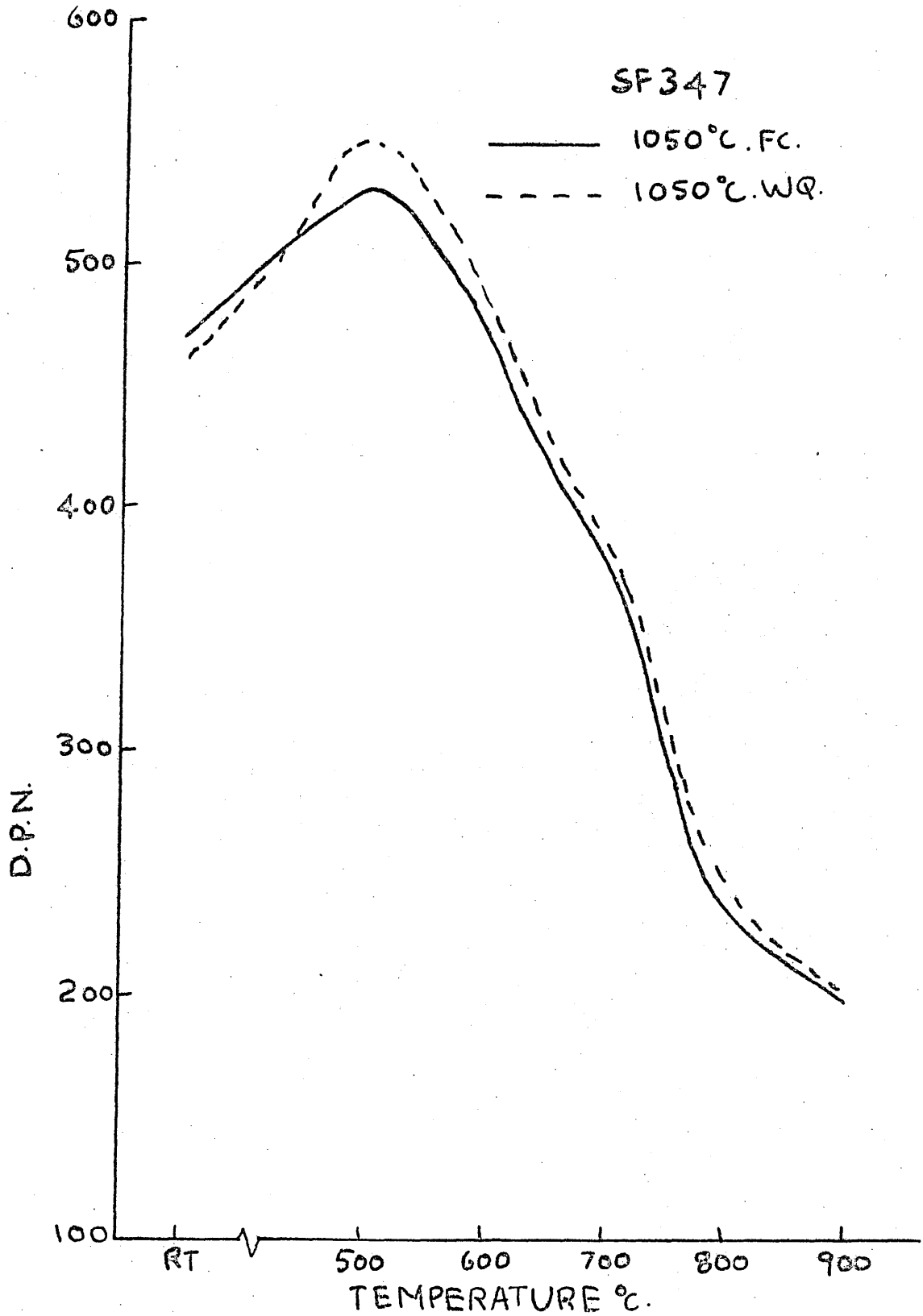

Figure 93(a)
Hardness curves for SF 347 steel.

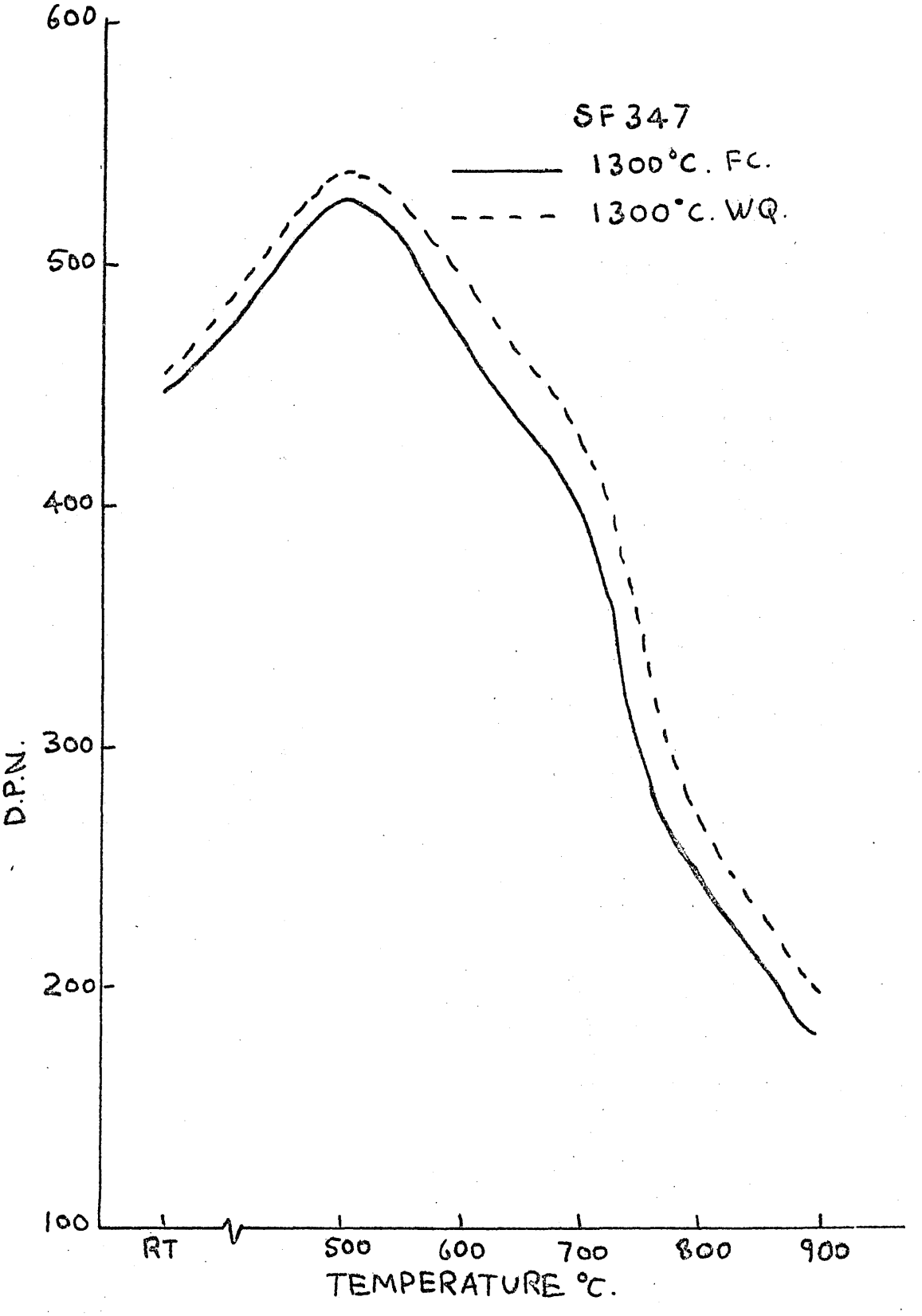

Figure 93(b)
Hardness curves for SF 347 steel.

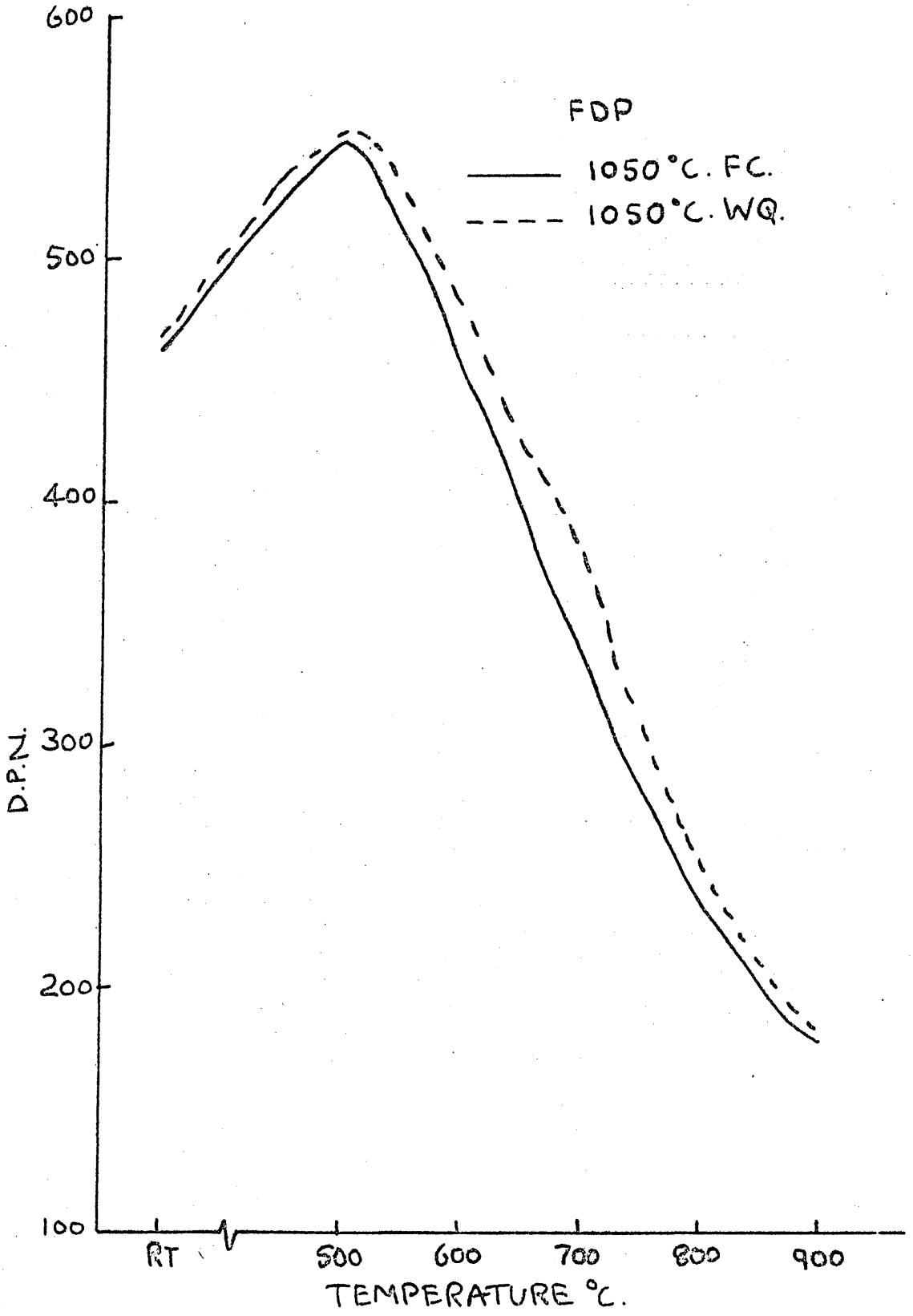

Figure 94(a)
Hardness curves for FDP steel.

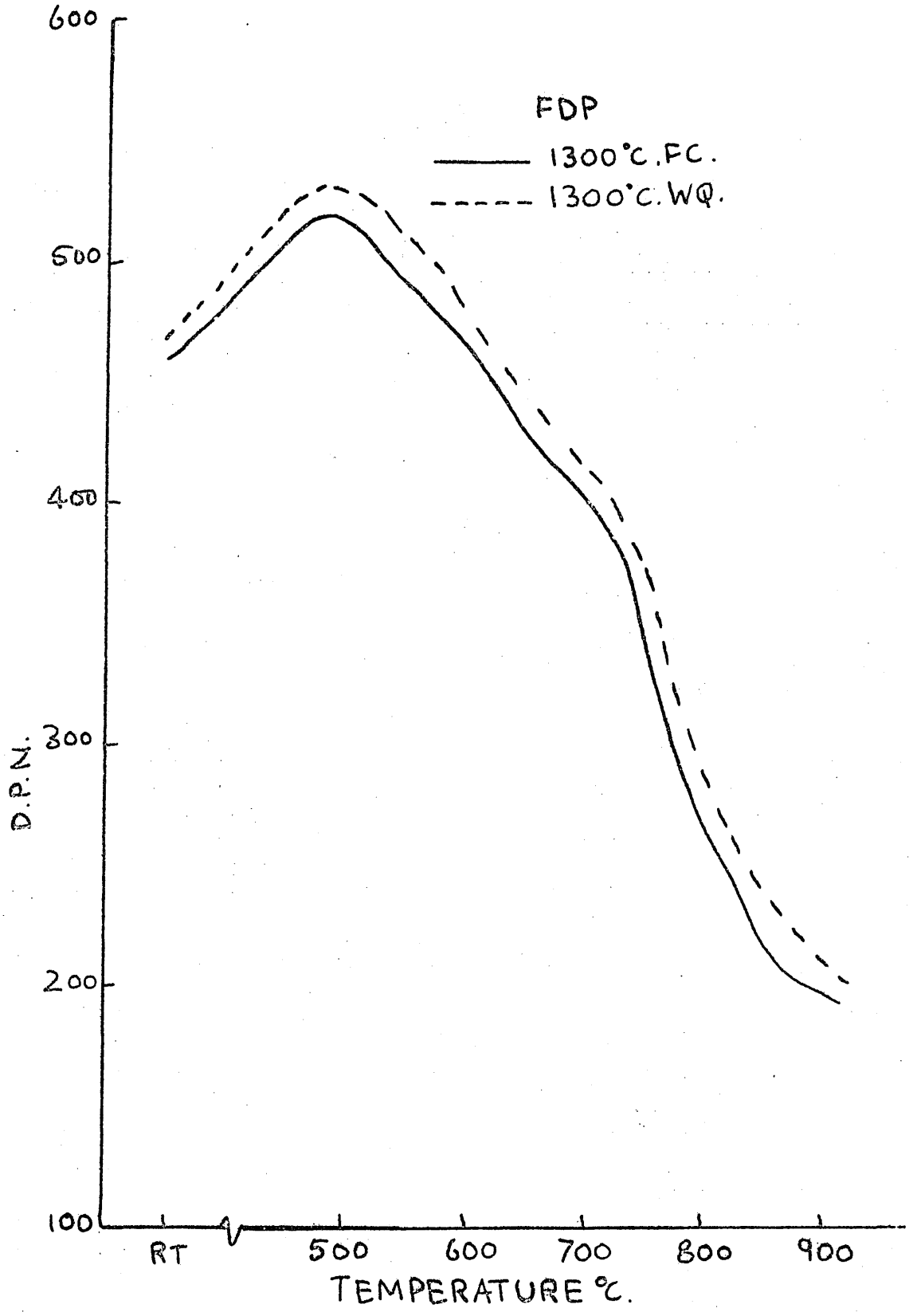

Figure 94(b)

Hardness curves for FDP steel.

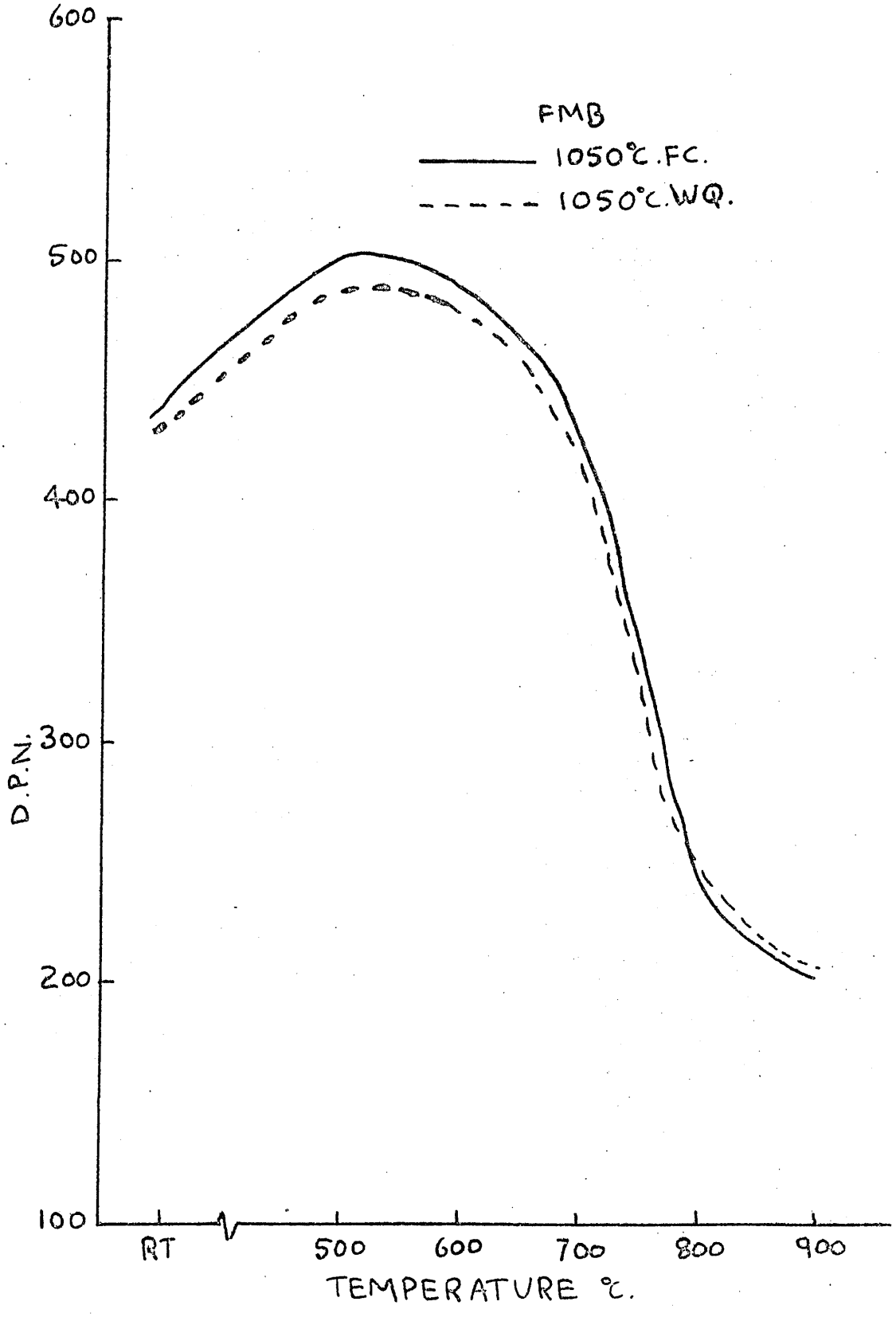

Figure 95(a)
Hardness curves for FMB steel.

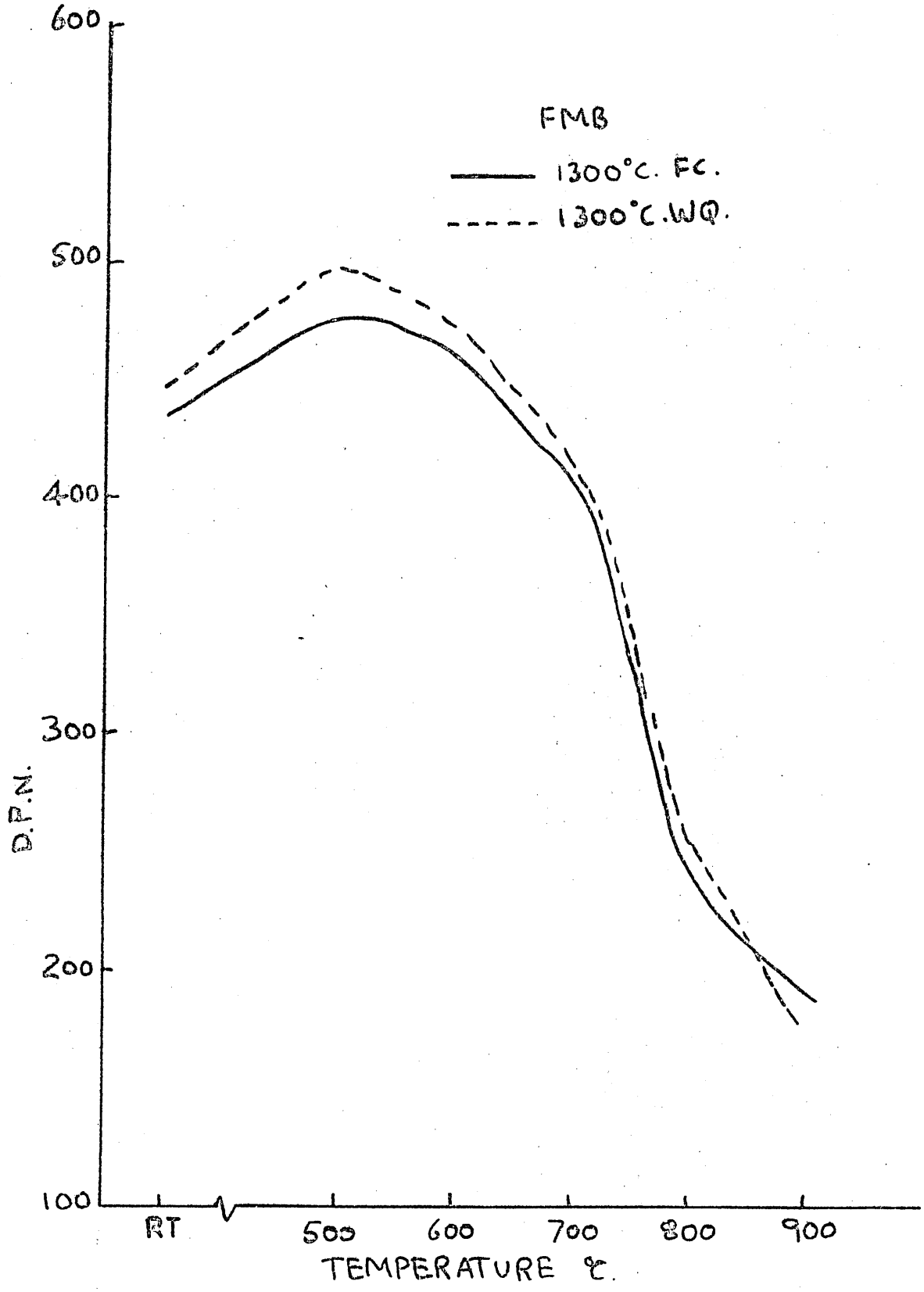

Figure 95(b)
Hardness curves for FMB steel.

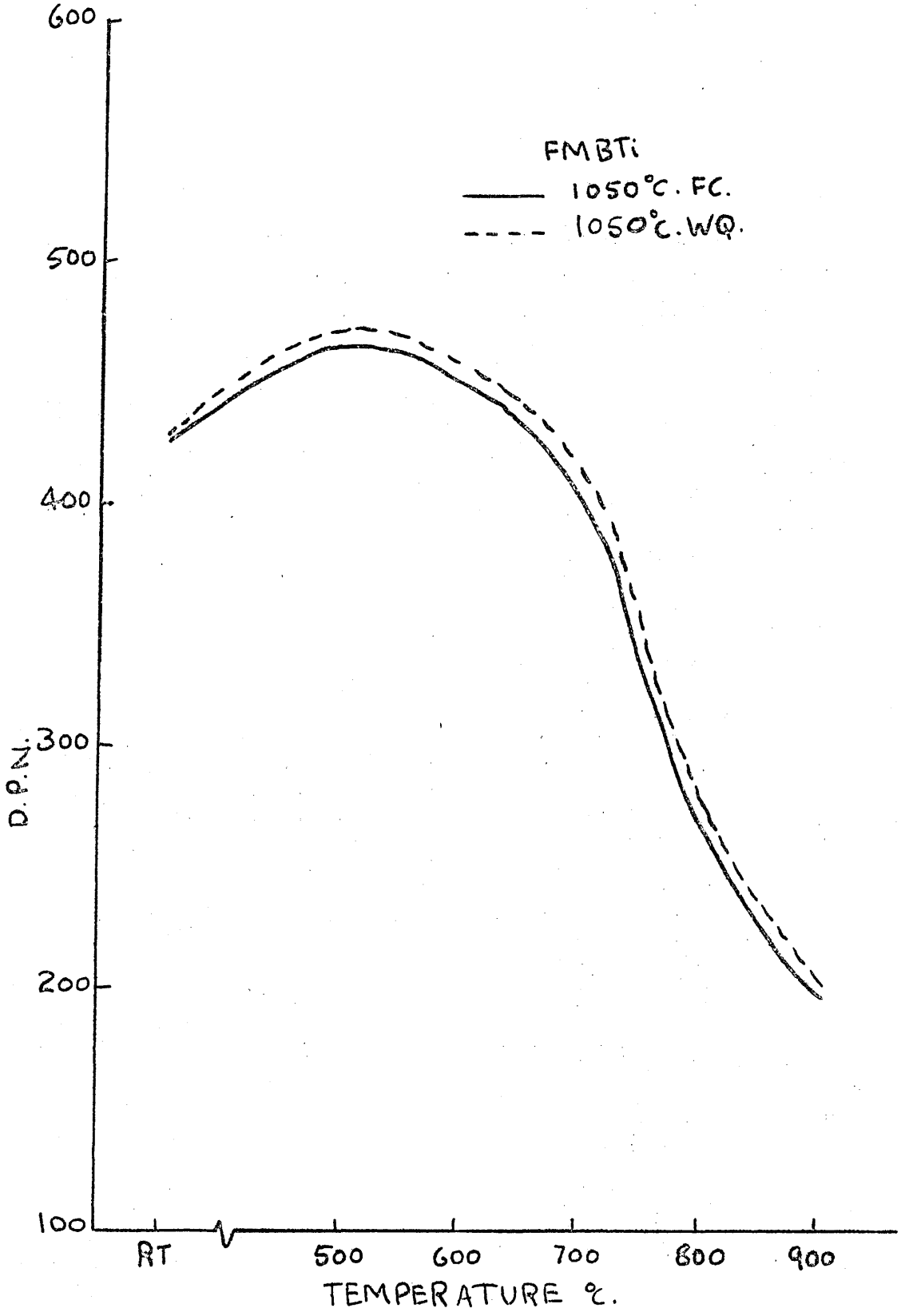

Figure 96(a)
Hardness curves for FMB Ti steel.

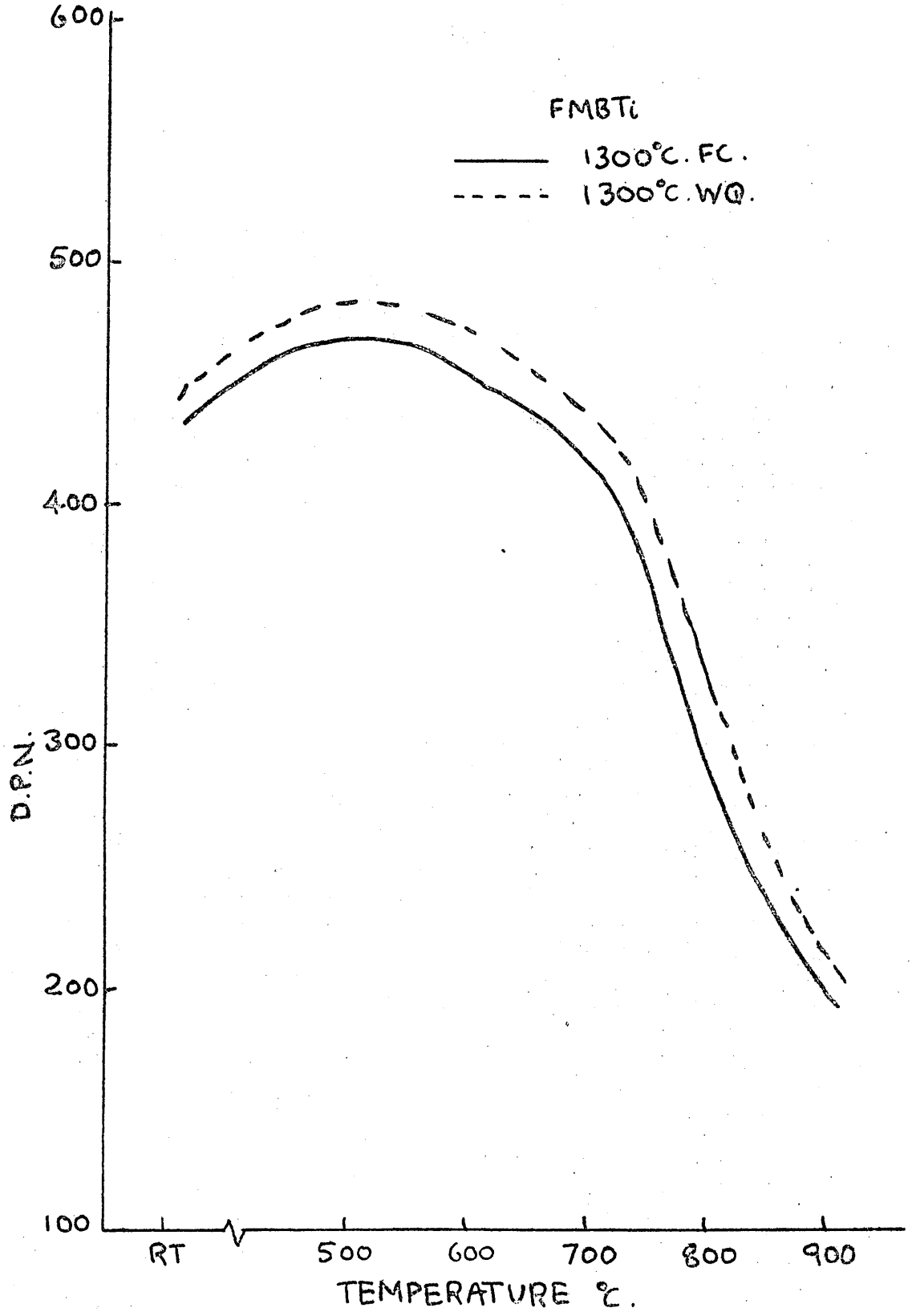

Figure 96(b)

Hardness curves for FMB Ti steel.

Figure 97 Optical micrograph of FSL(L) steel.
1 hr 1050°C. WQ.

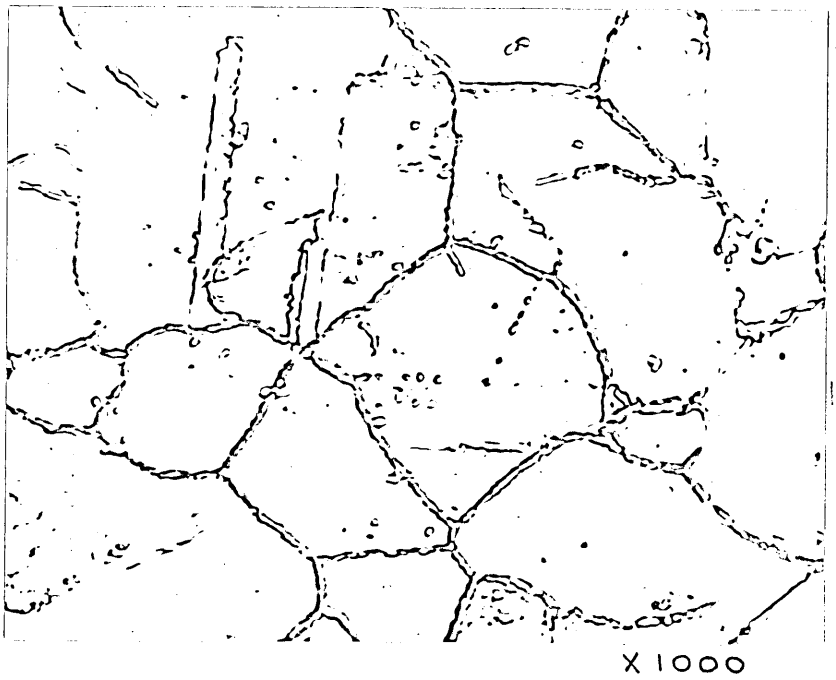

Figure 98 Optical micrograph of FDP steel.
1 hr 1050°C. FC.

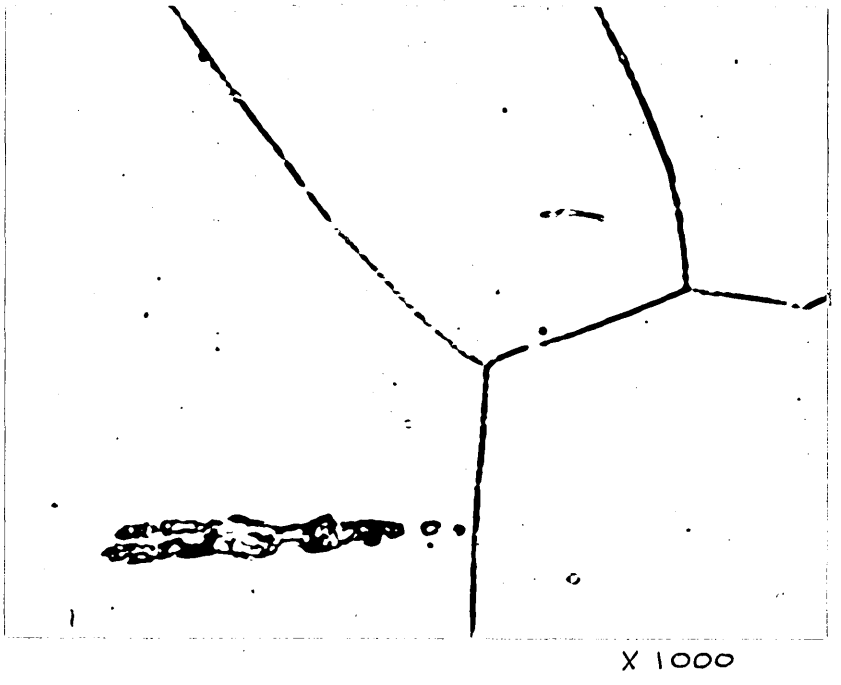

Figure 99 Optical micrograph of FMB steel.
1 hr 1050°C. FC.

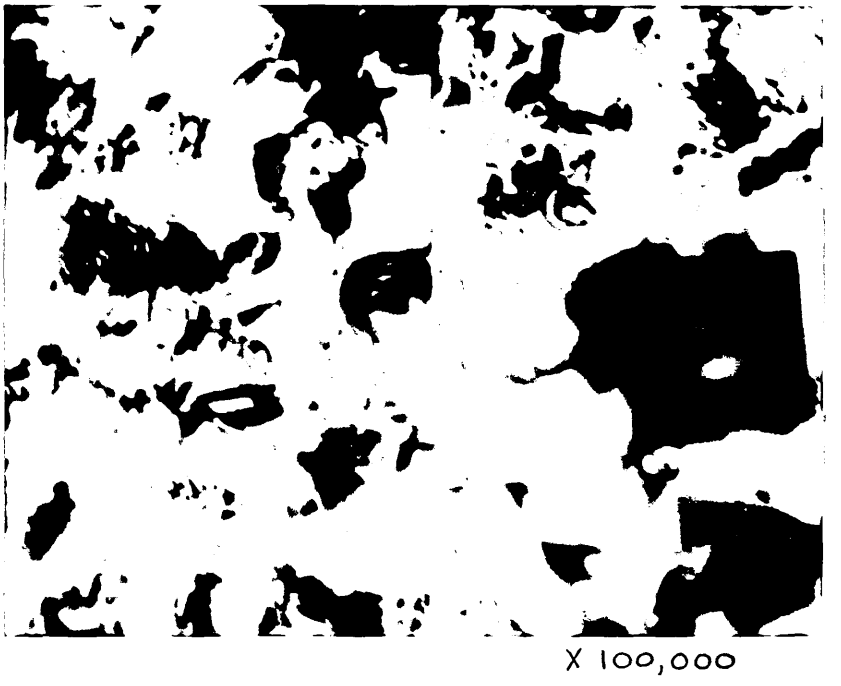

Figure 100 Electron micrograph of RF 310 steel.
1 hr 1050°C. FC, 90%CR + ½ hr 600°C. AC.

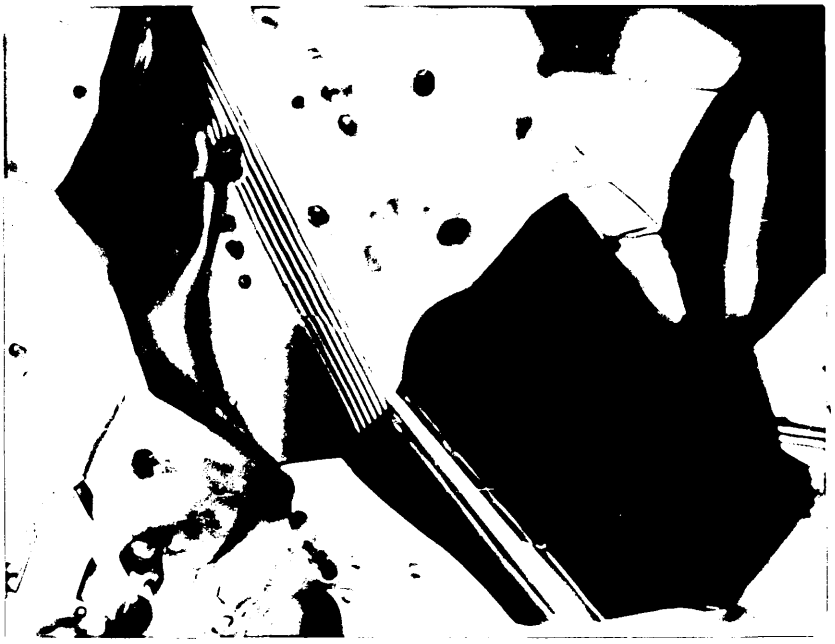

Figure 101 Electron micrograph of RF 310 steel.
1 hr 1050°C. FC, 90%CR + ½ hr 800°C. AC.

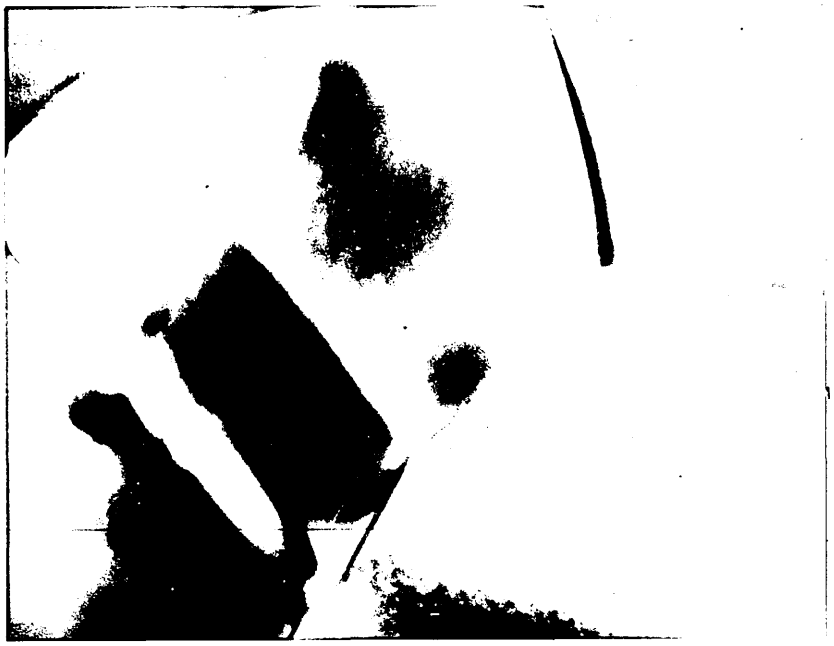

Figure 102 Electron micrograph of RF 310 steel.
1 hr 1050°C. FC, 90%CR + ½ hr 900°C. AC.

Figure 103 Electron micrograph of FCB steel.
1 hr 1050°C. FC, 90%CR + ½ hr 600°C. AC.

Figure 104 Electron micrograph of FCB steel.
1 hr 1050°C. FC, 90%CR + ½ hr 700°C. AC.

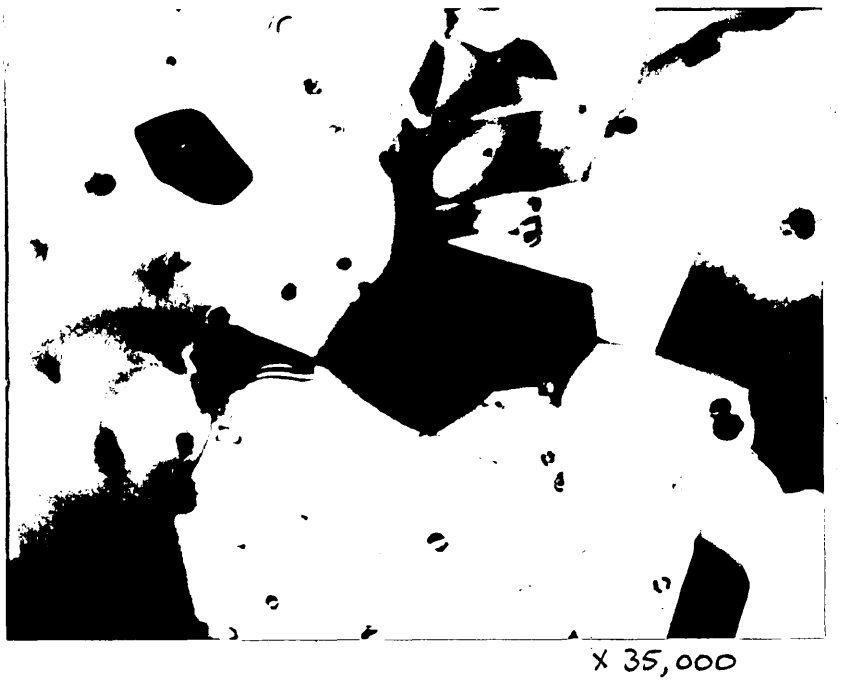

Figure 105 Electron micrograph of FCB steel.
1 hr 1050°C. FC, 90%CR + ½ hr 800°C. AC.

Figure 106 Electron micrograph of FCB steel.
1 hr 1050°C. FC, 90%CR + ½ hr 900°C. AC.

Figure 107 Electron micrograph of FMB steel.
1 hr 1050°C. FC, 90%CR + ½ hr 800°C. AC.

Figure 108 Electron micrograph of FMB steel.
1 hr 1050°C. FC, 90%CR + ½ hr 900°C. AC.

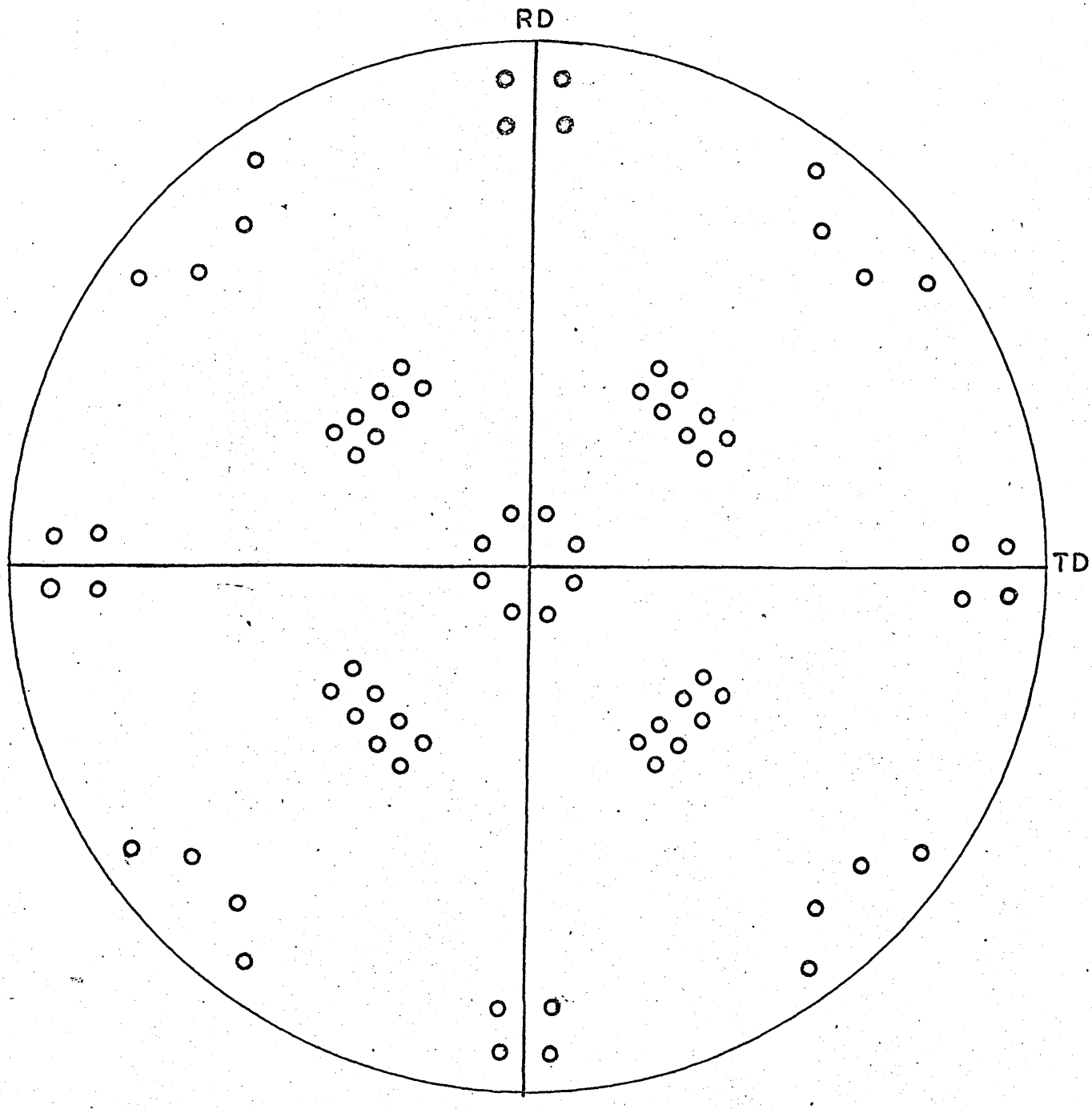

Figure 109

Positions of $\{100\}\gamma$ poles after transformation from $\{001\}<\bar{1}10>\alpha'$ according to the Kurdjumov-Sachs orientation relationship.

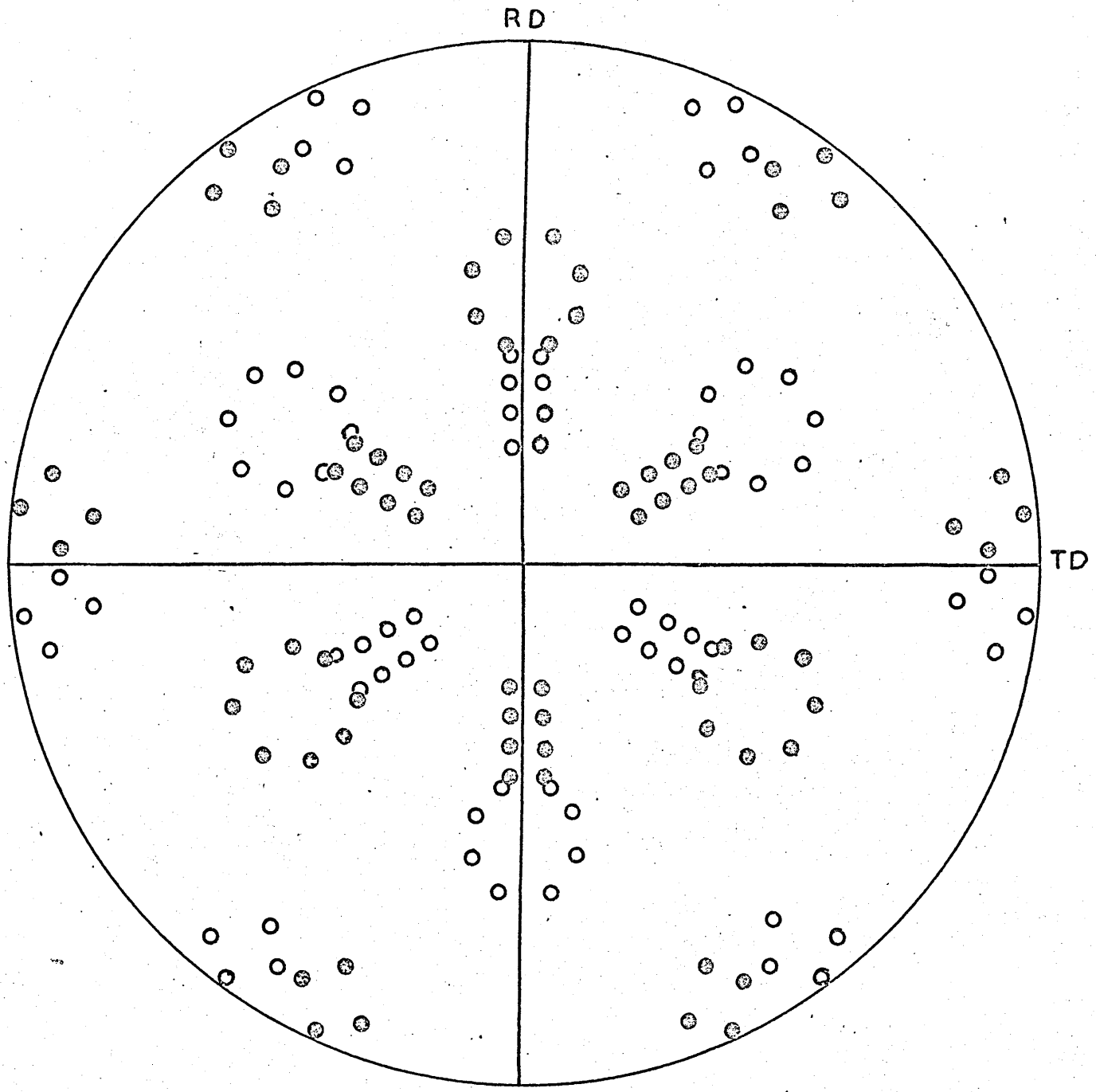

Figure 110

Positions of $\{100\}_\gamma$ poles after transformation from $\{111\}_\alpha \langle \bar{1}\bar{1}2 \rangle_\alpha$ according to the Kurdjumov-Sachs orientation relationship.

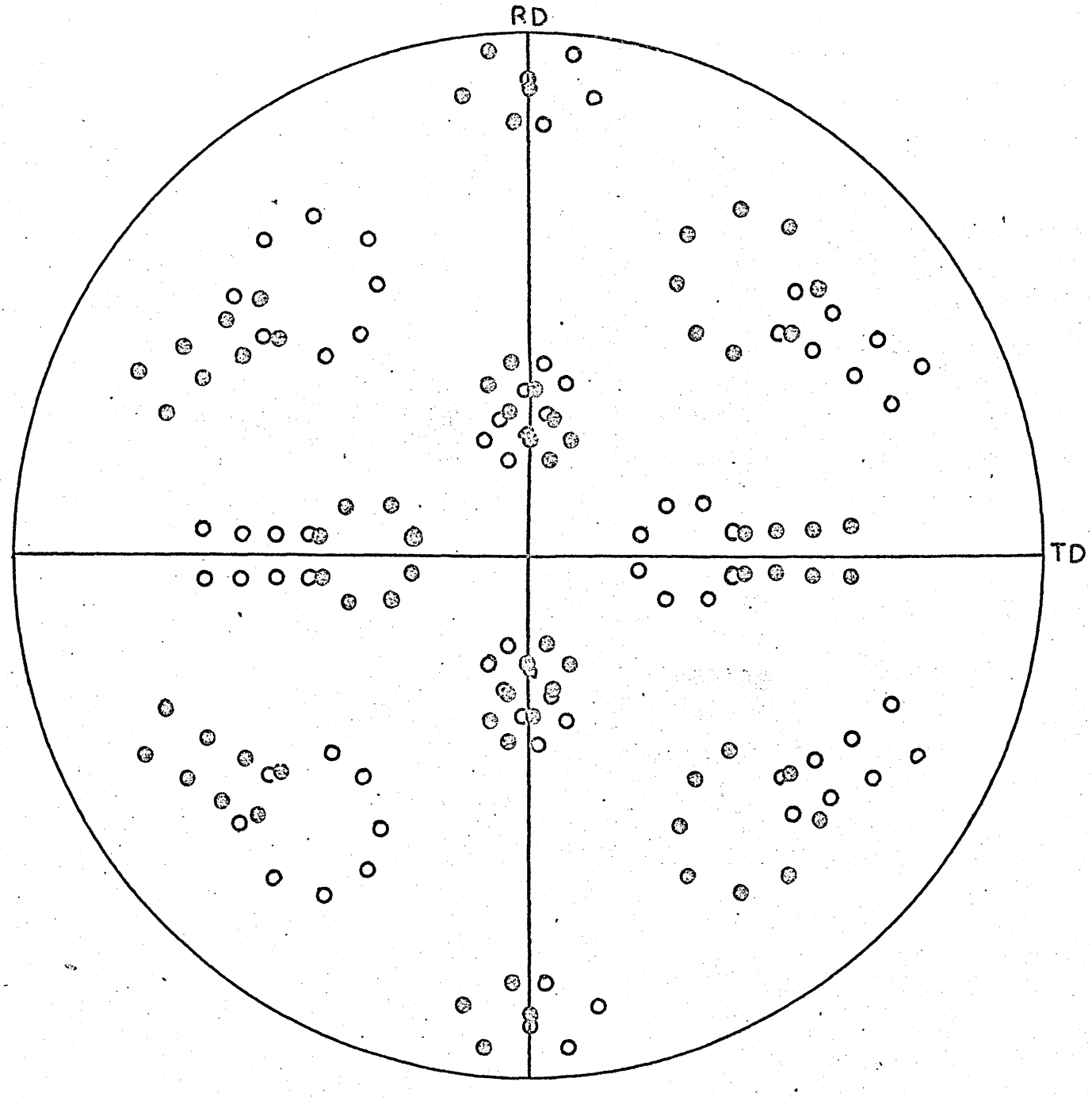

Figure 111
Positions of $\{100\}_\gamma$ poles after transformation from $\{112\}\langle\bar{1}10\rangle_{\alpha'}$ according to the Kurdjumov-Sachs orientation relationship.

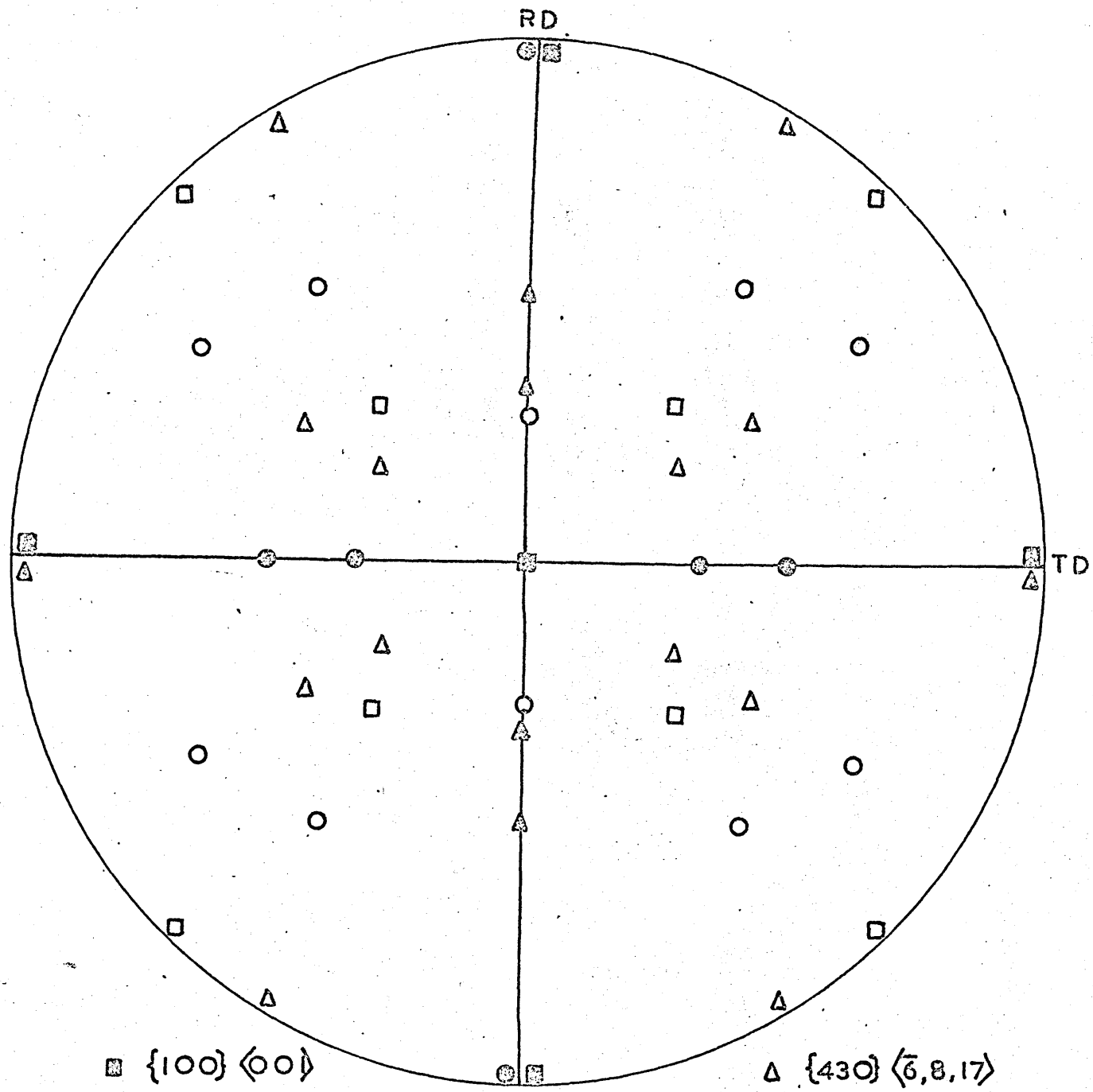

Figure 112
Distribution of $\{100\}_\gamma$ poles represented by ideal orientations.

APPENDIX.

The Significance of Texture Parameters in Phase Analysis by X-ray Diffraction. [J.Appl.Cryst. 2(1969)176].

The theory of the direct comparison X-ray method of phase analysis is extended to correct for preferred orientation effects. Texture parameters are defined to assess the type and intensity of preferred orientation using data from diffractometer patterns. The analysis is illustrated with results obtained on three austenitic stainless steels.

Introduction

In the quantitative phase analysis of polycrystalline materials, a method widely used is that of directly comparing the integrated intensities of diffraction lines from each phase in the mixture. This method has a distinct advantage over other methods in that it does not require a set of calibration samples, and is therefore preferred for conditions where it would be difficult to obtain a series of standards. Details of the method, as applied to randomly oriented polycrystalline specimens, are firmly established, and the present work considers an extension of the theory, to correct for the presence of preferred orientation.

The effects of preferred orientation in phase analysis by this technique have been considered previously (Arnell, 1968; Durnin and Ridal, 1968). These workers considered only relatively low degrees of preferred orientation and their conclusions will be referred to later in this paper. In the present work, the effects of extremely high degrees of preferred orientation, which arise during the heavy cold rolling of metals and alloys, are to be considered. This is important in certain austenitic stainless steels in which cold working can cause strain-induced transformation of face centred cubic austenite (γ) to αmartensite [effectively body centred cubic (Dickson and Green, 1969)], with the result that increasing amount of the martensite phase is accompanied by increasing intensity of preferred orientation in both phases.

The theory of the technique is given with respect to a mixture of two phases, α and γ, but is theoretically valid for any number

of phases, the only limitations being the practical difficulties.

Theory

The intensity diffracted by a single-phase specimen in a diffractometer may be expressed as

$$I = \left(\frac{I_o e^4}{m^2 c^4}\right)\left(\frac{\lambda^3 A}{32\pi r}\right)\left(\frac{1}{V^2}\right)\left[|F|^2 p\left(\frac{1+\cos^2 2\theta}{\sin^2\theta\cos\theta}\right)\right]\left(\frac{e^{-2M}}{2\mu}\right) \qquad (1)$$

where

I = integrated intensity per unit length of diffraction line

I_o = intensity of incident beam

e = charge on the electron

m = mass of the electron

c = velocity of light

λ = wavelength of incident radiation

r = radius of diffractometer circle

A = cross-sectional area of incident beam

V = volume of the unit cell

F = structure factor

p = multiplicity

θ = Bragg angle

e^{-2M} = temperature factor

μ = linear absorption coefficient.

This equation can be applied to a specimen, either a powder compact or a solid, which contains a completely random arrangement of crystals, and is effectively of infinite thickness.

Equation (1) can be re-written as

$$I = \frac{KR}{2\mu} \qquad (2)$$

$$\text{where } K = \left(\frac{I_o e^4}{m^2 c^4}\right)\left(\frac{\lambda^3 A}{32\pi r}\right) \qquad (3)$$

$$\text{and } R = \left(\frac{1}{V^2}\right)\left[|F|^2 p\left(\frac{1+\cos^2 2\theta}{\sin^2\theta\cos\theta}\right)\right]\left(e^{-2M}\right) \qquad (4)$$

K is now a constant which is independent of the nature of the specimen while R is a factor which depends on θ, the reflecting set of planes and the crystal structure of the specimen.

Thus, in a mixture of two phases, α and γ,

$$I_{hkl\alpha} = \frac{K R_{hkl\alpha} \cdot C_\alpha}{2\mu_m} \qquad (5)$$

where C_α is the volume fraction of α phase, $I_{hkl\alpha}$ is the measured integrated intensity, and μ_m is the linear absorption coefficient of the mixture.

Since there will be a similar equation for $I_{hkl\gamma}$, it follows that

$$\frac{I_{hkl\alpha}}{I_{hkl\gamma}} = \frac{R_{hkl\alpha} \cdot C_\alpha}{R_{hkl\gamma} \cdot C_\gamma}$$

$$\text{i.e. } \frac{C_\gamma}{C_\alpha} = \frac{I_{hkl\gamma} \cdot R_{hkl\alpha}}{I_{hkl\alpha} \cdot R_{hkl\gamma}} \qquad (6)$$

Hence by obtaining the integrated intensities of a diffraction line from each phase, C_γ/C_α is obtained, and since $C_\gamma + C_\alpha = 1$,

$$C_\alpha = \frac{1}{(1 + C_\gamma/C_\alpha)} \qquad (7)$$

$$\text{and } C_\gamma = \frac{C_\gamma/C_\alpha}{(1 + C_\gamma/C_\alpha)} \qquad (8)$$

Values of C_γ/C_α obtained from diferent pairs of lines should be constant within the limits of experimental error, and normally an average is calculated. Strictly speaking a direct comparison of integrated intensities in this manner is valid only for a completely random orientation of crystals in each phase. Significant variations in the ratio are a direct indication of anisotropy and the average value of a number of such individual determinations is therefore no longer valid, especially for high degrees of preferred orientation.

The correct equation for summation of intensity ratios from a number of reflections may be deduced as follows:

$$C_\alpha = \frac{2\mu_m \cdot I_{hkl\alpha}}{K \cdot R_{hkl\alpha}}$$

$$= K' \cdot \left(\frac{I_{hkl\alpha}}{R_{hkl\alpha}}\right)$$

$$= K' \cdot \frac{1}{n\alpha} \sum_0^{n\alpha} \left(\frac{I\alpha}{R_\alpha}\right), \qquad (9)$$

where n_α = number of α reflections considered.

$$\text{Hence } \frac{C_\gamma}{C_\alpha} = \frac{\frac{1}{n\gamma} \sum_0^{n\gamma} \left(\frac{I\gamma}{R\gamma}\right)}{\frac{1}{n\alpha} \sum_0^{n\alpha} \left(\frac{I\alpha}{R_\alpha}\right)} \qquad (10)$$

Ideally this summation should be carried out over as large a number of reflections as possible, but in practice the accuracy will depend upon reflections which are available for measurement and on the intensity of preferred orientation, e.g. if there is a high proportion of $\{hkl\}$ planes parallel to the specimen plane and a Bragg reflection is not measurable from these planes, then the omission in equation (10) of data for this set of planes could cause a high error in the value C_γ/C_α. On the other hand, depending on the type of preferred orientation which is present, or with low degrees of preferred orientation, a fairly accurate value of C_γ/C_α may be obtainable from only a few reflections.

To assess the type and intensity of preferred orientation, a texture parameter, P, can be calculated from values of Ihkl and Rhkl. It is defined as

$$P_{hkl_\alpha} = \frac{I_{hkl_\alpha}/R_{hkl\alpha}}{\frac{1}{n_\alpha}\sum_0^{n_\alpha}(I_\alpha/R_\alpha)} \qquad (11)$$

where P >1 shows that the $\{hkl\}$ planes are preferentially oriented parallel th the plane of section.

P < 1 shows that such planes are preferentially avoided

P = 1 corresponds to random orientation.

For $n = \infty$, P_{hkl_α} is proportional to the volume fraction within the α phase of $\{hkl\}_\alpha$ planes which are oriented parallel to the plane of section.

A slightly different texture parameter, P*, may be defined as

$$P^*_{hkl_\alpha} = \frac{I_{hkl_\alpha}/R_{hkl\alpha}}{\frac{1}{n_\alpha}\sum_0^{n_\alpha}(I_\alpha/R_\alpha)+\frac{1}{n_\gamma}\sum_0^{n_\gamma}(I_\gamma/R_\gamma)} \qquad (12)$$

For $n = \infty$, $P^*_{hkl_\alpha}$ is proportional to the volume fraction within the whole specimen of $\{hkl\}_\alpha$ planes which are oriented parallel to the plane of section. For $100\%\alpha$, $P^*_{hkl_\alpha} = P_{hkl_\alpha}$. In equations (11) and (12), finite values of n will not alter the significance of the parameters provided that n is sufficiently large to include all major components of the texture, and also represents a statistical coverage of all possible orientations.

Combining equations (11) and(12) gives

$$\frac{P_{hkl\,\alpha}}{P^*_{hkl\,\alpha}} = \frac{C\gamma}{C\alpha} + 1 \qquad (13)$$

Equation (13) implies that the ratio $\frac{P_{hkl\,\alpha}}{P^*_{hkl\,\alpha}}$ should be constant for all α reflections.

Similarly, for the γ phase,

$$\frac{P_{hkl\,\gamma}}{P^*_{hkl\,\gamma}} = 1 + \frac{C\alpha}{C\gamma} \qquad (14)$$

and from equations (13) and (14)

$$\frac{C\gamma}{C\alpha} = \frac{P^*_{hkl\gamma} \cdot P_{hkl\,\alpha}}{P^*_{hkl\alpha} \cdot P_{hkl\,\gamma}} \qquad (15)$$

The accuracy of results can easily be checked since it can be shown that

$$\sum_{0}^{n\alpha} P_\alpha = n_\alpha \qquad (16)$$

and for $n_\alpha = n_\gamma$,

$$\sum_{0}^{n\alpha+n\gamma} P^* = n_\alpha = n_\gamma \qquad (17)$$

It may be noted that,in equation (11), R_α can be replaced by line intensities measured from a randomly oriented sample, not necessarily of 100%α.This is because $Phkl_\alpha$, as defined by equatien (11), is corrected for non-textural differences, such as grain size and volume fraction of phases between the random sample and the textured sample. However, in equation (12), R_α and R_γ cannot be replaced by experimentally determined random intensities unless the latter are obtained under identical experimental conditions and in the absence of such non-texural differences.

Experimental

The materials used were high purity 18%Cr/10%Ni, 18%Cr/12%Ni and 18%Cr/14%Ni stainless steels which were austenitic after annealing. These compositions cover a range of austenite stability and hence different phase mixtures were obtainable for the same amount of cold rolling. To develop a strong preferred orientation, samples were cold rolled to 93% reduction in thickness.

Preparation of specimens for X-ray examination consisted of grinding to grade 400 silicon carbide paper followed by etching for 1 minute in a boiling solution of 5%HNO_3/30% HCl/65% water.

Automatically recorded diffraction patterns were obtained with MoK_α radiation.

Because of the lattice parametersof the two phases, [a_γ = 3.59 Å, a_α = 2.87 Å (Dickson and Green, 1969)], certain reflections occur at almost the same Bragg angle, i.e. 110_α and 111_γ, 222_α and 331_γ. The relative intensities of these lines were obtained by a peak seperation analysis. The reflections 310_α and 400_γ also overlap, but in each steel after 93% reduction the 400_γ reflection could be eliminated by the absence of the 200_γ reflection.

Results and Discussion

The experimental values of I/R are shown in Table 1, the reflections being numbered in order of increasing Bragg angle. Data for higher order reflections such as 222_γ, 400_γ, 220_α, and 400_α are not included since the information obtainable from these reflections is merely the same as that from the lower orders.

The results clearly demonstrate the inapplicability of equation (6) under the extreme conditions exhibited by these samples: substitution of different I/R values in equation (6) gives results ranging from C_γ=0 to C_γ=100%. The use of reflections which have a high multiplicity factor, e.g. 311_γ and 211_α, still gives C_γ=0 for the 18%Cr/10%Ni and 18%Cr/12%Ni steels. For the 18%Cr/14%Ni steel, C_γ = 21.0% by this method, which is very low when summations are considered. The validity of the assumption made by Durnin and Ridal (1968), that the intensity of such reflections is insignificantly affected by preferred orientation really depends on the type and intensity of preferred orientation in the sample, and large errors could arise by making this assumption without knowing the history of the sample.

Before making any simple comparison of I/R values, it is important to assess the presence or absence of preferred orientation. This can be done by determining a normal pole figure or by calculating texture parameters from I/R values. The parameters may be expressed as an inverse pole figure although this is not necessary.

Calculated texture parameters for the three samples are shown

in Tables 2, 3 and 4 for a range of values of n_α and n_γ. These results illustrate the importance of obtaining data from as large a number of reflections as possible in order to obtain a true picture of the type and intensity of preferred orientation. Provided that n is large enough, there is good agreement between these P values and the texture components determined from normal pole figures (Dickson and Green, 1969). Such agreement may not always be obtained since it depends on there being measurable Bragg reflections which correspond to the main components of the texture.

Arnell (1968) assumed that the first three reflections of austenite and martensite give a representative picture of the effect of preferred orientation. Although this is useful practical assumption for low degrees of preferred orientation, it is not generally true and its validity willdepend entirely on the type and intensity of the preferred orientation. The P values in Tables 2, 3 and 4 illustrate this point, e.g. for the 18%Cr/10%Ni steel, considering n =3 omits data for the 222_α and 331_γ reflections and gives a false set of texture parameters.

Values of P* for n = 7 are also given in Tables 2, 3 and 4 and the ratio P/P* is found to be constant for each phase, according to the theory [equations (13) and (14)].

The parameter P* is more useful when attempting to relate properties to preferred orientation. For the 18%Cr/10%Ni steel for example, the P values indicate a very marked preferred orientation in both phases, but the P* values for the austensite are $\ll 1$, which means that directional properties would be influenced largely by the texture of the martensite. By contrast, the properties of the 18%Cr/14%Ni steel would be influenced largely by the texture of the austenite.

Table 5 shows the calculated values of C_γ (%) for different combinations of n_α and n_γ. Large errors can arise by considering too small a number of reflections or by failing to include data for all major components of the texture. Thus, for all the samples, provided that $n_\alpha = n_\gamma > 4$, C_γ remains constant. The limits of accuracy of the analysis, excluding experimental error, have been assessed

by considering the result for (say) $n_\alpha = n_\gamma = 6$ together with the results for $n_\alpha = 7$, $n_\gamma = 6$ and $n_\alpha = 6$, $n_\gamma = 7$. This gives the following results:

18%Cr/10%Ni steel, $C_\gamma = 13.7\% \pm 2.0\%$

18%Cr/12%Ni steel, $C_\gamma = 67.5\% \pm 3.5\%$

18%Cr/14%Ni steel, $C_\gamma = 95.9\% \pm 0.7\%$

In general, it is simply necessary to use values of n_α and n_γ which include all major components of the texture together with a balance of orientations which are preferentially avoided. In the samples studied, $n_\alpha = n_\gamma = 5$ satisfies this condition, so that C_γ remains constant for $n_\alpha = n_\gamma > 4$. This value of C_γ is the most accurate one obtainable by the analysis. It is useful to note that for the type of preferred orientation which occurs in these steels, considering $n_\alpha = n_\gamma = 3$ gives results which lie within the above limits, and therefore, as a time saving, only these reflections need be considered in phase analysis of samples which exhibit similar textures.

References

Arnell,R.D. (1968) J.I.S.I. 206,1035.

Dickson,M.J. and Green,D. (1969) Mater.Sci.Eng. 4, 304.

Durnin,J. and Ridal,K.A. (1968) J.I.S.I. 206, 669.

Table 1. *Experimental values of I/R*

	18% Cr 10% Ni steel				18% Cr 12% Ni steel				18% Cr 14% Ni steel			
n	hkl_γ	$\frac{I_{hkl\gamma}}{R_{hkl\gamma}}$	hkl_α	$\frac{I_{hkl\alpha}}{R_{hkl\alpha}}$	hkl_γ	$\frac{I_{hkl\gamma}}{R_{hkl\gamma}}$	hkl_α	$\frac{I_{hkl\alpha}}{R_{hkl\alpha}}$	hkl_γ	$\frac{I_{hkl\gamma}}{R_{hkl\gamma}}$	hkl_α	$\frac{I_{hkl\alpha}}{R_{hkl\alpha}}$
1	111	0·290	110	0·296	111	1·086	110	0·114	111	1·802	110	0
2	200	0	200	13·705	200	0	200	0·710	200	0	200	0·254
3	220	3·333	211	11·538	220	5·383	211	1·987	220	7·506	211	0·231
4	311	0	310	0	311	0	310	0	311	0·063	310	0
5	331	4·783	222	27·097	331	0·855	222	0·710	331	2·029	222	0
6	420	0	321	0·114	420	0	321	0	420	0	321	0
7	422	0	411		422	0	411	0	422	0	411	0
			330	0·182			330				330	
8	–	–	420	0	–	–	420	0	–	–	420	0
9	–	–	332	0·435	–	–	332	0	–	–	332	0

Table 2. *Texture parameters for* 18% Cr 10% Ni *steel cold rolled to* 93% *reduction*

Austenite			$P_{hkl\gamma}$						
n_γ	$\sum_0^{n_\gamma}\left(\frac{I_\gamma}{R_\gamma}\right)$	$\frac{1}{n_\gamma}\sum_0^{n_\gamma}\left(\frac{I_\gamma}{R_\gamma}\right)$	111	200	220	311	331	420	422
2	0·290	0·145	2	0					
3	3·623	1·208	0·24	0	2·76				
4	3·623	0·906	0·32	0	3·68	0			
5	8·406	1·681	0·17	0	1·98	0	2·85		
6	8·406	1·401	0·21	0	2·38	0	3·41	0	
7	8·406	1·201	0·24	0	2·78	0	3·98	0	0
			$P^*_{hkl\gamma}$ (for $n_\alpha=n_\gamma=7$)						
7	8·406	1·201	0·03	0	0·38	0	0·55	0	0
	P/P^*		8	0	7·31	0	7·23	0	0

Martensite			$P_{hkl\alpha}$								
n_α	$\sum_0^{n_\alpha}\left(\frac{I_\alpha}{R_\alpha}\right)$	$\frac{1}{n_\alpha}\sum_0^{n_\alpha}\left(\frac{I_\alpha}{R_\alpha}\right)$	110	200	211	310	222	321	411 330	420	332
2	14·001	7·005	0·04	1·96							
3	25·539	8·513	0·03	1·61	1·36						
4	25·539	6·385	0·05	2·14	1·81	0					
5	52·636	10·527	0·03	1·30	1·10	0	2·57				
6	52·750	8·792	0·03	1·56	1·32	0	3·08	0·01			
7	52·932	7·562	0·04	1·82	1·53	0	3·58	0·01	0·02		
8	52·932	6·617	0·04	2·07	1·75	0	4·09	0·02	0·03	0	
9	53·367	5·930	0·05	2·31	1·95	0	4·57	0·02	0·03	0	0·07
			$P^*_{hkl\alpha}$								
7	52·932	7·562	0·03	1·56	1·32	0	3·09	0·01	0·02		
	P/P^*		1·33	1·16	1·16	1·16	1·16	1·00	1·00		

Table 3. *Texture parameters for* 18% Cr 12% Ni *steel cold rolled to* 93% *reduction*

Austenite			$P_{hkl\gamma}$						
n_γ	$\sum_0^{n_\gamma}\left(\frac{I_\gamma}{R_\gamma}\right)$	$\frac{1}{n_\gamma}\sum_0^{n_\gamma}\left(\frac{I_\gamma}{R_\gamma}\right)$	111	200	220	311	331	420	422
2	1·086	0·543	2	0					
3	6·469	2·156	0·50	0	2·50				
4	6·469	1·617	0·67	0	3·33	0			
5	7·324	1·465	0·74	0	3·68	0	0·58		
6	7·324	1·221	0·89	0	4·41	0	0·70	0	
7	7·324	1·046	1·04	0	5·14	0	0·82	0	0
			$P^*_{hkl\gamma}$ (for $n_\alpha=n_\gamma=7$)						
7	7·324	1·046	0·70	0	3·47	0	0·56	0	0
	P/P^*		1·48	0	1·48	0	1·46	0	0

Martensite			$P_{hkl\alpha}$								
n_α	$\sum_0^{n_\alpha}\left(\frac{I_\alpha}{R_\alpha}\right)$	$\frac{1}{n_\alpha}\sum_0^{n_\alpha}\left(\frac{I_\alpha}{R_\alpha}\right)$	110	200	211	310	222	321	411 330	420	332
2	0·824	0·412	0·28	1·72							
3	2·811	0·937	0·12	0·76	2·12						
4	2·811	0·703	0·16	1·01	2·83	0					
5	3·521	0·704	0·16	1·01	2·82	0	1·01				
6	3·521	0·587	0·19	1·21	3·39	0	1·21	0			
7	3·521	0·503	0·23	1·41	3·95	0	1·41	0	0		
8	3·521	0·440	0·26	1·61	4·52	0	1·61	0	0	0	
9	3·521	0·391	0·28	1·82	5·08	0	1·82	0	0	0	0
			$P^*_{hkl\alpha}$								
7	3·521	0·503	0·07	0·46	1·28	0	0·46	0	0		
	P/P^*		3·28	3·06	3·08	0	3·06	0	0		

Table 4. *Texture parameters for* 18% Cr 14% Ni *steel cold rolled to* 93% *reduction*

Austenite			$P_{hkl\gamma}$						
n_γ	$\sum_0^{n_\gamma}\left(\frac{I_\gamma}{R_\gamma}\right)$	$\frac{1}{n_\gamma}\sum_0^{n_\gamma}\left(\frac{I_\gamma}{R_\gamma}\right)$	111	200	220	311	331	420	422
2	1·802	0·901	2	0					
3	9·308	3·103	0·58	0	2·42				
4	9·371	2·343	0·77	0	3·20	0·03			
5	11·40	2·28	0·79	0	3·29	0·03	0·89		
6	11·40	1·90	0·95	0	3·95	0·03	1·07	0	
7	11·40	1·63	1·11	0	4·60	0·04	1·25	0	0
			$P^*_{hkl\gamma}$ (for $n_\alpha=n_\gamma=7$)						
7	11·40	1·63	1·06	0	4·42	0·04	1·19		
	P/P^*		1·05	0	1·04	1	1·05		

Martensite			$P_{hkl\alpha}$								
n_α	$\sum_0^{n_\alpha}\left(\frac{I_\alpha}{R_\alpha}\right)$	$\frac{1}{n_\alpha}\sum_0^{n_\alpha}\left(\frac{I_\alpha}{R_\alpha}\right)$	110	200	211	310	222	321	411 330	420	332
2	0·254	0·127	0	2							
3	0·485	0·1617	0	1·58	1·42						
4	0·485	0·1212	0	2·09	1·91	0					
5	0·485	0·097	0	2·52	2·38	0	0				
6	0·485	0·0808	0	3·14	2·86	0	0	0			
7	0·485	0·0693	0	3·67	3·33	0	0	0	0		
8	0·485	0·0606	0	4·19	3·81	0	0	0	0	0	
9	0·485	0·0539	0	4·71	4·29	0	0	0	0	0	0
			$P^*_{hkl\alpha}$								
	0·485	0·0693	0	0·15	0·14	0	0	0	0		
	P/P^*		0	24·47	23·78	0	0	0	0		

Table 5. Phase analysis results using equation (10)

n_γ	n_α	Volume fraction of austenite (%) 18%Cr10%Ni steel	18%Cr/12%Ni steel	18%Cr/14%Ni steel
2	2	2·0	56·8	87·6
3	3	12·4	69·7	95·0
4	4	12·4	69·7	95·1
5	5	13·8	67·5	95·9
6	6	13·7	67·5	95·9
7	7	13·7	67·5	95·9